2014

Development and feasibility assessment of shallow pressbrake-formed steel tub girders for short-span bridge applications

Gregory K. Michaelson

DEVELOPMENT AND FEASIBILITY ASSESSMENT OF SHALLOW PRESS-BRAKE-FORMED STEEL TUB GIRDERS FOR SHORT-SPAN BRIDGE APPLICATIONS

Gregory K. Michaelson

Disseration submitted to the
Benjamin M. Statler College of Engineering and Mineral Resources
at West Virginia University
in partial fulfillment of the requirements
for the degree of

Doctor of Philosophy
in
Civil and Environmental Engineering

Karl E. Barth, Ph.D., Chair
Hung-Liang "Roger" Chen, Ph.D.
Udaya B. Halabe, Ph.D.
Bruce S. Kang, Ph.D.
Avinash Unnikrishnan, Ph.D.

Department of Civil and Environmental Engineering

Morgantown, West Virginia
2014

Keywords: steel bridge, experimental testing, finite element analysis, cold bending, modular construction, accelerated bridge construction

ABSTRACT

DEVELOPMENT AND FEASIBILITY ASSESSMENT OF SHALLOW PRESS-BRAKE-FORMED STEEL TUB GIRDERS FOR SHORT-SPAN BRIDGE APPLICATIONS

Gregory K. Michaelson

The Short Span Steel Bridge Alliance (SSSBA) is a group of bridge and culvert industry leaders (including steel manufacturers, fabricators, service centers, coaters, researchers, and representatives of related associations and government organizations) who have joined together to provide educational information on the design and construction of short-span steel bridges in installations up to 140 feet in length. From within the SSSBA technical working group, a modular, shallow press-brake-formed steel tub girder was developed. This new technology consists of cold-bending standard mill plate width and thicknesses to form a trapezoidal box girder. The steel plate can either be weathering steel or galvanized steel, each an economical option. Once the plate has been press-brake-formed, shear studs are then welded to the top flanges. A reinforced concrete deck is then cast on the girder in the fabrication shop and allowed to cure, becoming a composite modular unit. The composite tub girder is then shipped to the bridge site, allowing for accelerated construction and reduced traffic interruptions.

The scope of this project was to refine the development of the proposed system. This was performed in five stages. A rational methodology, based on conservative estimates of the system's nominal capacity, was developed to design and proportion the steel tub girder and modular unit. Destructive flexural testing was then performed on representative specimens to assess the ultimate capacity of the system in its composite and noncomposite states. Next, two separate analytical tools utilizing nonlinear finite element methods and strain-compatibility procedures were developed and benchmarked against experimental data. These analytical tools were then employed to perform behavioral studies on the proposed system, resulting in the derivation of expressions which better predict the nominal capacity than those present in AASHTO LRFD Specifications. Finally, feasibility assessments were performed, comparing the economy of the proposed system against traditional short-span bridge solutions. Results of this project demonstrate that the proposed system is an economically competitive alternative for the short-span bridge market.

ACKNOWLEDGEMENTS

First, I would like to express my sincere gratitude to my advisor Dr. Karl Barth for his support during my M.S. and Ph.D. degrees. His encouragement and support throughout my five years in graduate school was invaluable. I cannot imagine having a better advisor and mentor during my time at WVU. Above all, I am honored to consider him a friend and colleague, and look forward to working with him on future endeavors.

I would also like to thank Drs. Roger Chen, Udaya Halabe, Bruce Kang, and Avinash Unnikrishnan for serving as members of my doctoral advisory committee. In addition, I would like to thank Dr. Michael Barker at the University of Wyoming for his countless efforts in the development and promotion of this modular concept.

The development of this project would not have been possible had it not been for the tireless efforts and financial support of the Short Span Steel Bridge Alliance. I salute their efforts, and in particular, the efforts of Daniel Snyder, in this promoting this concept for mainstream use. Also, I would like to thank Nucor-Yamato Steel, SSAB Americas, U.S. Steel, and EVRAZ North America for the donation of steel plate as well as Greiner Industries, American Tank & Fabricating, U.S. Bridge, and AZZ Galvanizing, Inc. for their efforts in fabricating the experimental specimens employed in this project.

The contributions of graduate students Jason Mash, Lindsay Kelly, and Bryan Gallion and undergraduate research assistants Matthew Rector and Eric Roberts were invaluable in this project and are greatly appreciated. I would also like to acknowledge the efforts of Jerry Nestor and Brian Walker at the Major Units Lab, whose assistance in the preparation of experimental specimens was invaluable. In addition, I would like to thank the graduate students who have occupied B-11 with me throughout the five years I have been at WVU. Their encouragement, support, and camaraderie through the good and bad times were invaluable and greatly appreciated.

I would like to acknowledge my friends and family for their endless support during graduate school. In closing, I would like to express my deep appreciation for the countless sacrifices made by my future wife, Rebecca Dale, who has provided continuous support during my time at WVU.

TABLE OF CONTENTS

LIST OF TABLES

LIST OF FIGURES

CHAPTER 1: INTRODUCTION

1.1 BACKGROUND / OVERVIEW

The Short Span Steel Bridge Alliance (SSSBA) is a group of bridge and culvert industry leaders (including steel manufacturers, fabricators, service centers, coaters, researchers, and representatives of related associations and government organizations) who have joined together to provide educational information on the design and construction of short span steel bridges in installations up to 140 feet in length. From within the SSSBA technical working group, a modular, shallow press-brake-formed steel tub girder was developed. This girder is shown in Figure 1.1.

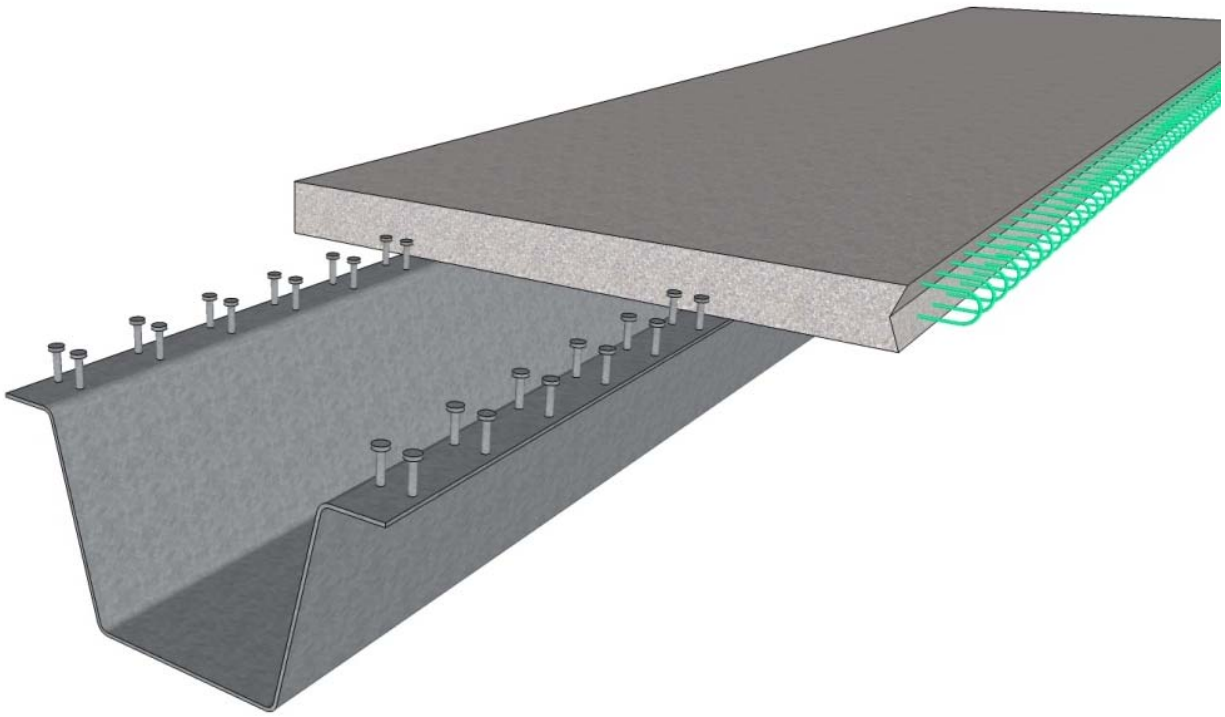

Figure 1.1: Proposed System

This new technology consists of cold-bending standard mill plate width and thicknesses to form a trapezoidal box girder. The steel plate can either be weathering steel or galvanized

steel, each an economical option. Once the plate has been press-brake formed, shear studs are then welded to the top flanges. A reinforced concrete deck is then cast on the girder in the fabrication shop and allowed to cure, becoming a composite modular unit. The composite tub girder is then shipped to the bridge site, allowing for accelerated construction and reducing traffic interruptions. It should be noted that the proposed system should be able to support numerous deck options, including cast-in-place decks and full- or partial-depth precast panels.

1.2 PROJECT SCOPE & OBJECTIVES

The scope of this project was to refine the development of this proposed system. This was achieved by:

- Developing a rational methodology for the design of the proposed system
- Performing destructive flexural testing of representative specimens
- Developing analytical tools for assessing the behavior and capacity of the proposed system
- Conducting behavioral studies in order to assess the applicability of the current AASHTO LRFD Specifications in predicting the capacity of modular press-brake-formed steel tub girders
- Performing economic studies and feasibility assessments to determine the system's competitiveness in the short-span bridge market

1.3 ORGANIZATION

A brief overview of the organization of this dissertation is as follows:

- Chapter 2
  - This chapter summarizes previous research on cold-bent tub girder applications in bridges and using cold-forming to fabricate steel elements. In addition, a comprehensive review of AASHTO provisions for tub girders is provided.
- Chapter 3
  - This chapter briefly summarizes the development of the cross-section for the proposed press-brake tub girder system. Details include sizing girders based on standard mill width plates and the reporting of noncomposite and composite section properties.
- Chapter 4
  - The experimental testing that has been conducted for this research is discussed in this chapter. Testing consisted of the destructive testing of four representative press-brake tub girder specimens. The chapter focuses on the testing program, the test objectives, instrumentation and the test results.
- Chapter 5
  - This chapter describes analytical techniques using a commercial finite element software package and mechanistic strain-compatibility procedures to assess the proposed system. Analysis details, including element selection, material models, and additional finite element considerations are discussed. These analytical procedures are then compared against both previous experimental tests as well as the experiments discussed in Chapter 4.

- Chapter 6
    - This chapter documents the behavioral studies performed on the proposed system in order to assess the validity of employing AASHTO LRFD Specifications to compute the capacity of press-brake-formed steel tub girders.
- Chapter 7
    - This chapter documents feasibility and economic assessments of the proposed system. In addition, based on plate availability, the matrix of girders presented in Chapter 3 is reduced to a set of four modular options for immediate implementation in the short-span bridge market.
- Chapter 8
    - This chapter provides a summary of the scope of work conducted for this study and highlights the key findings. Lastly, this chapter provides recommendations for continued research on the proposed system.
- Appendix A
    - This appendix documents the derivation of flexural and torsional section properties of the proposed system. In addition, an illustrative example is provided to demonstrate the computation of the derived properties.
- Appendix B
    - This appendix documents the MATLAB routines written for this research project. In addition, illustrative examples are provided that demonstrate the computation of the plastic moment capacity and nominal moment capacity using strain-compatibility analysis.
- Appendix C
    - This appendix documents the experimental and analytical data collected during this research. Graphs of experimental and analytical data along with feasibility assessments are presented.

CHAPTER 2: BACKGROUND & LITERATURE REVIEW

2.1 INTRODUCTION

The purpose of this chapter is to discuss previous research findings relating to press-brake-formed tub girders. Since the first appearance of research on press-brake tub girders, minimal efforts have been pursued to explore this type of bridge design. Until recently, when the demands for more economical and rapid construction have been brought to the forefront of design, the press-brake-formed tub girder has once again surfaced as a viable alternative to conventional bridge fabrication and construction. Presented in this section is a comprehensive review of previous studies focused on economical and rapid bridge construction employing various tub girder configurations and current AASHTO Specifications applicable to steel tub girders.

2.2 PREVIOUS IMPLEMENTATIONS OF COLD-BENT STEEL GIRDERS IN BRIDGE APPLICATIONS

Prefabricated steel tub-girder systems have been explored as a potential design solution for the short-span bridge market for a number of years. Many previous research efforts have shown that these types of systems have the potential to be economical and competitive in the short-span range. In recent years, the demands for accelerated bridge construction have been brought to the forefront of design. Presented in this section is a comprehensive review of previous studies focused on economical and rapid bridge construction employing various shallow tub girder configurations.

2.2.1 Prefabricated Press-Formed Steel T-Box Girder Bridge System (Taly & Gangarao, 1979)

Taly and Gangarao (1979) proposed using a press-brake to bend an A36 3/8-inch steel plate to form a tub girder in a short-span modular bridge system. At the time of publication in 1979, The American Association of State Highway and Transportation Officials (AASHTO) Specifications did not provide any criteria for the design of bridge members using a press-brake

to cold form the shape of girders. Therefore, the researchers evaluated their tub girder design in accordance with the 1977 American Iron and Steel Institute (AISI) specifications.

In the proposed design, a prestressed concrete deck would be precast with an embedded shear stud plate, which would, in turn, be shop welded to the steel tub girder's flanges. The total width of the tub girder is 3 feet, and the total width of the prestressed concrete slab is 6 feet. This reduced size permits the complete unit to be fabricated in the shop and shipped to the construction site, greatly decreasing the amount of field labor and construction time. To account for various bridge widths, several prefabricated tub girder units are placed adjacent to one another and joined with a longitudinal closure pour. The system resists lateral loads through shear keys with weld-ties placed at the junction of the prestressed concrete slab flanges. The ends of the tub girder beams are closed off with a 3/8-inch thick steel plate diaphragm that is welded all around the perimeter of the tub girder. To provide additional support, bearing stiffeners are provided at the tub girder ends along with the 3/8-inch thick diaphragm.

In addition, Taly and Gangarao provided an alternative to the concrete-steel composite tub girder bridge system which employed an orthotropic deck. To increase the longitudinal stiffness of the orthotropic deck, WT sections would be shop welded to the steel plate deck. Like the previous design, the composite tub girder unit could be prefabricated in the shop and shipped to the construction site. The tub girder dimensions are highly dependent on the span length, ranging from a 2.5 foot to a 3.5 foot deep tub girder.

The researchers found the tub girder design with the composite concrete deck to be economical for spans of 40 to 100 feet. With the all-steel configurations, the maximum span length would be 65 feet. In addition, the authors note that the tub girders have a greater torsional stiffness then typical I-beam sections due to their closed shape. Furthermore, 95% of the total bridge system would be prefabricated and economy is achieved with the use of a press-brake to cold form the members as opposed to typical fabrication procedures for steel box girders. Also, in addition to rapid construction, the lightweight design of this system (roughly 11 tons for a 65-foot-long girder) allows for low capacity equipment for all phases of construction, including transportation and erection of the tub girders.

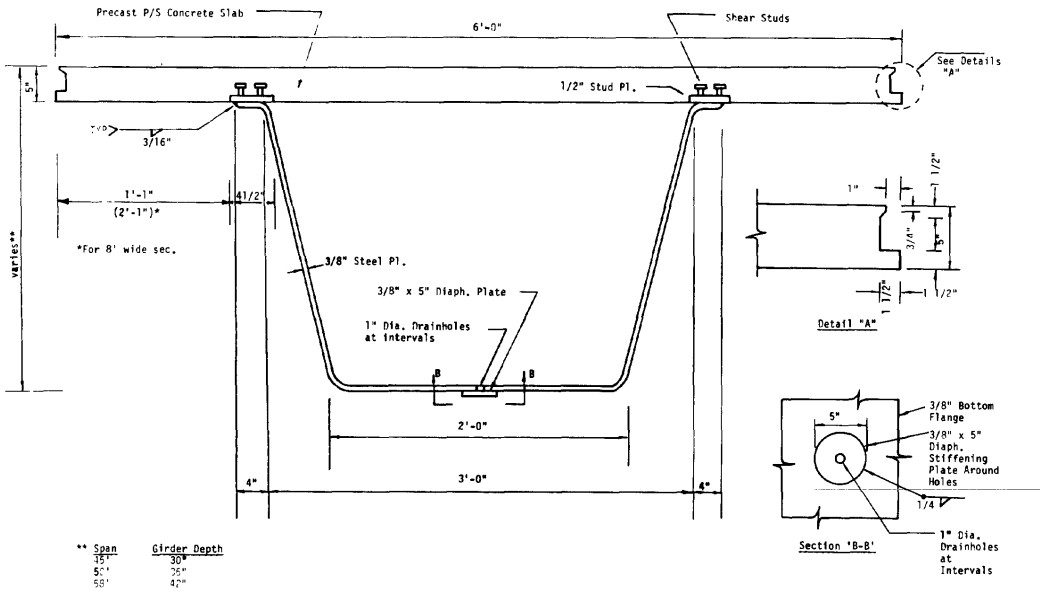

Figure 2.1: Taly and Gangarao's Proposed Bridge System (Taly & Gangarao, 1979)

2.2.2 Composite Girders with Cold-Formed Steel U-sections (Nakamura, 2002)

Similar to Taly and Gangarao's proposed design, Nakamura (2002) proposed a bridge system that utilizes a press-brake to cold form steel tub girders. Nakamura's bridge system includes casting a prestressed concrete slab supported by twin tub girders, forming a composite modular unit. Nakamura envisioned a continuous bridge system with multiple intermediate piers to support the superstructure. To compensate for the potential buckling of the bottom flange at pier locations, Nakamura designed the tub girders to be filled with concrete and prestressed by prestressed concrete (PC) bars, resulting in an increased strength against buckling at the support locations.

The researcher preformed several experimental bending tests on the proposed design. These tests confirmed that the tub girder behaved as a composite beam at the center of the span. Furthermore, at pier regions, the tub girder was shown to behave as a prestressed beam with the prestressed concrete preventing local buckling of the bottom flange. Finally, Nakamura concluded that this bridge system would in fact be practical and feasible since it has adequate bending strength and deformation capacity. A drawback to Nakamura's design is that the tub

girders require more steel than conventional plate girders. However, the cost is offset by decreased fabrication costs, thereby resulting in an economical design.

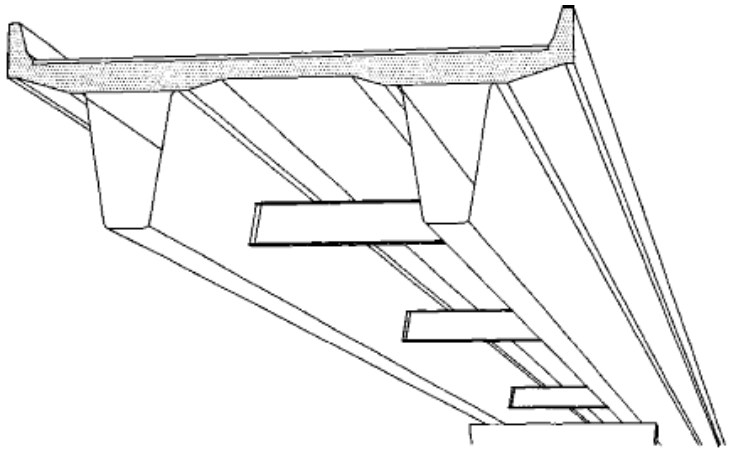

Figure 2.2: Nakamura's Proposed Bridge System (Nakamura, 2002)

2.2.3 Con-Struct Prefabricated Bridge System

Nelson Engineering Services has developed a cold-formed tub girder bridge system similar to previous designs mentioned above (Tricon Precast, 2008). This system, Con-Struct, incorporates a prefabricated composite bridge girder consisting of a shallow steel tub girder and a concrete deck. To increase the service capacity of this system, the steel tub girders are stressed into a camber, and the concrete deck is cast onto the girders in their stressed state. Once the concrete is cured, the steel compressive stress is locked in to provide camber and increase the service capacity of the structure. Employing this system, according to Tricon Precast, designs are valid for spans up to 60 feet.

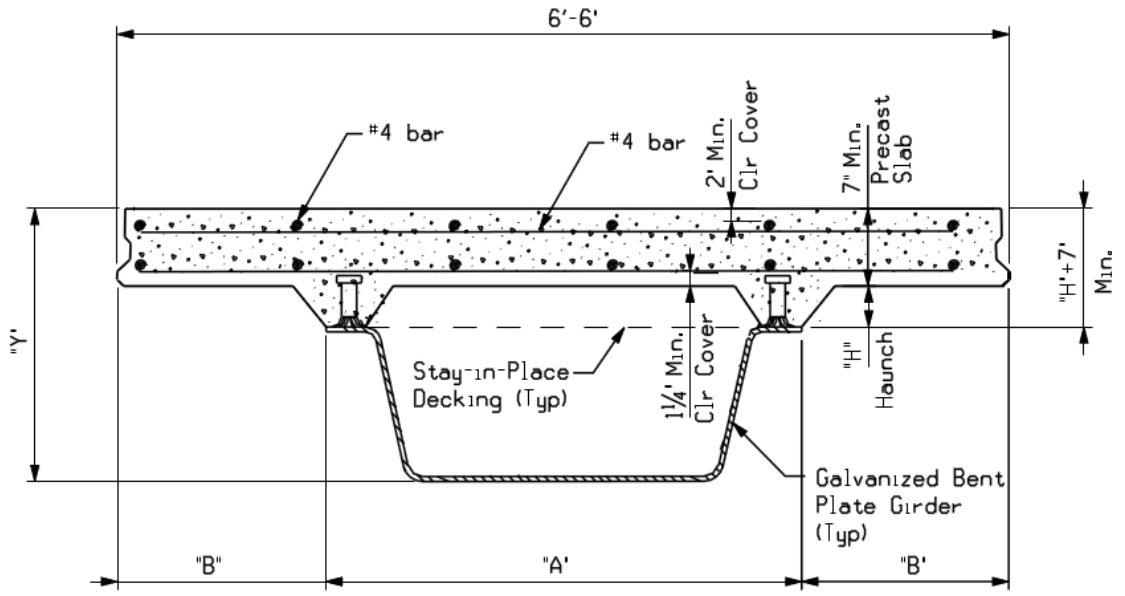

Figure 2.3: Con-Struct Bridge System (Tricon Precast, 2008)

2.2.4 Folded Plate Girders (developed at the University of Nebraska)

The University of Nebraska, Lincoln has also researched cold-bent steel tub girders and developed a composite steel girder system utilizing folded plate girders (Burner, 2010; Glaser, 2010). This system utilizes an inverted tub girder where the flanges of the girder are bent inwards. The concrete deck is then cast on the wider center flange as opposed to previously developed systems, where the deck is cast on the two smaller exterior flanges. An advantage of this system is that the orientation of the girder allows maintenance and ease of inspection of the folded plate girder. Also, the wider top flange resulting from the girder orientation provides a safe work area for construction personnel.

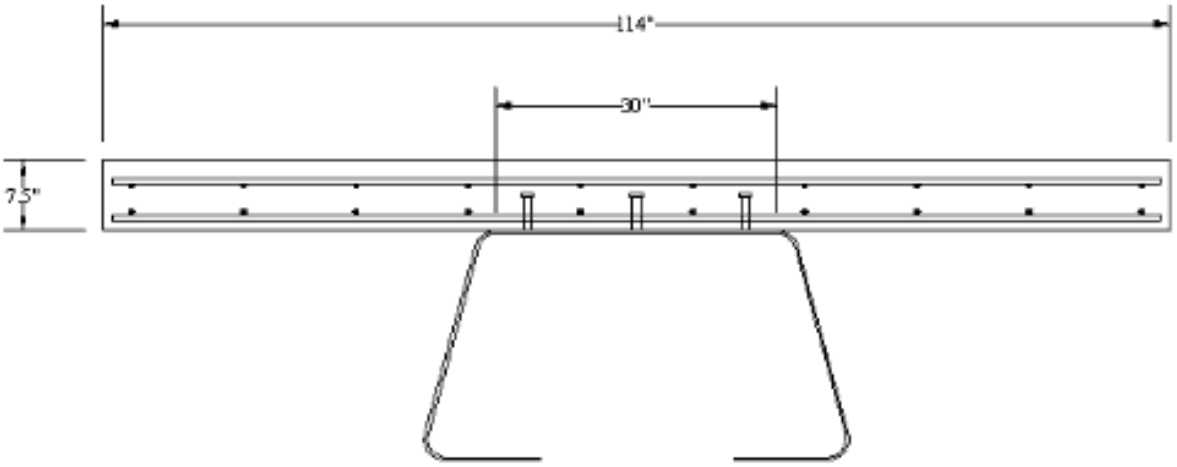

Figure 2.4: System Proposed at the University of Nebraska (Burner, 2010)

2.2.5 TxDOT Rapid Economical Bridge Replacement

In an effort by the Texas Department of Transportation (TxDOT) to create a more shallow bridge superstructure, a bridge system consisting of a shallow steel tub girder was developed (Chandar et. al., 2010). Specifically, the solution was to use a tub girder that consisted of a 5-foot-wide bottom flange width and a 3-foot-deep web. Two rows of shear studs were welded to each top flange, and a reinforced concrete deck was cast.

An application of this concept was completed in August of 2010. The bridge consisted of four simply supported spans of 45 feet, 100 feet, 100 feet, and 65 feet, respectively. The total width of the bridge was 78 feet; as a result, six tub girders were utilized. It should be noted that, in this system, while accelerated bridge construction methods were used, conventionally-fabricated steel tub girders (as opposed to girders formed using cold bending) were employed.

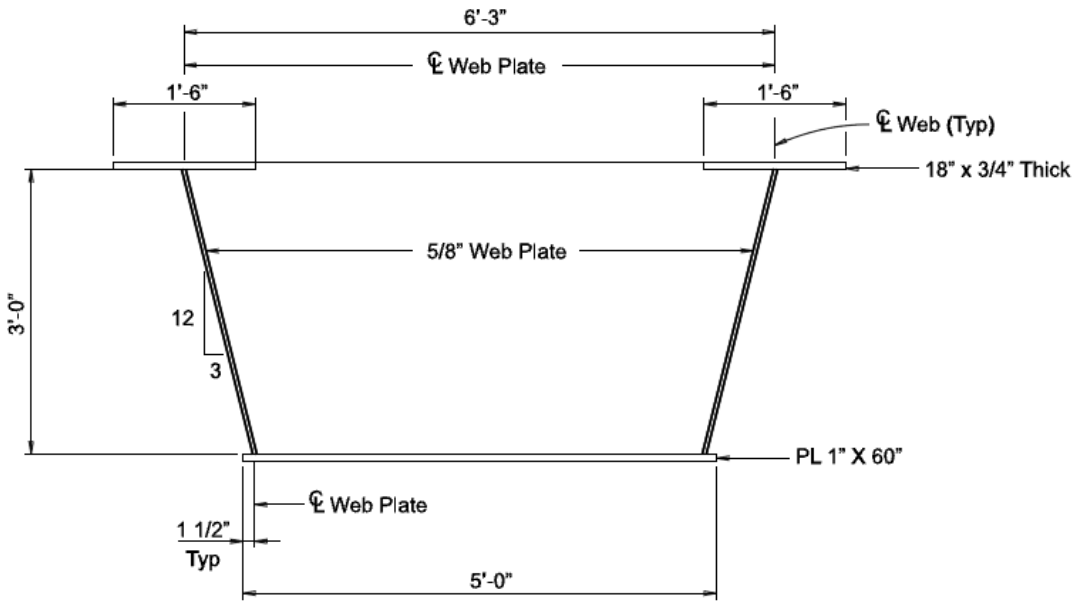

Figure 2.5: TxDOT Tub Girder for Rapid Bridge Replacement (Chandar et. al., 2010)

2.2.6 MDOT Prefabricated Steel Box-Girder Systems for Accelerated Bridge Construction

The Michigan Department of Transportation (MDOT) recognized the need for a prefabricated bridge system to be shipped to the construction site where only placement and post-tensioning were required (Burgueño & Pavlich, 2008). The goal was to create an entirely prefabricated composite bridge which would eliminate the need for lengthy and costly road closures for short-span bridges. In order to accomplish this, a research project was conducted on a shallow, cold-bent tub girder system utilizing a prestressed concrete deck. Specifically, this project focused on the design of individual units which would be joined with longitudinal deck pours. Experimental testing coupled with finite element analyses demonstrated that this system would be competitive in the short-span bridge market.

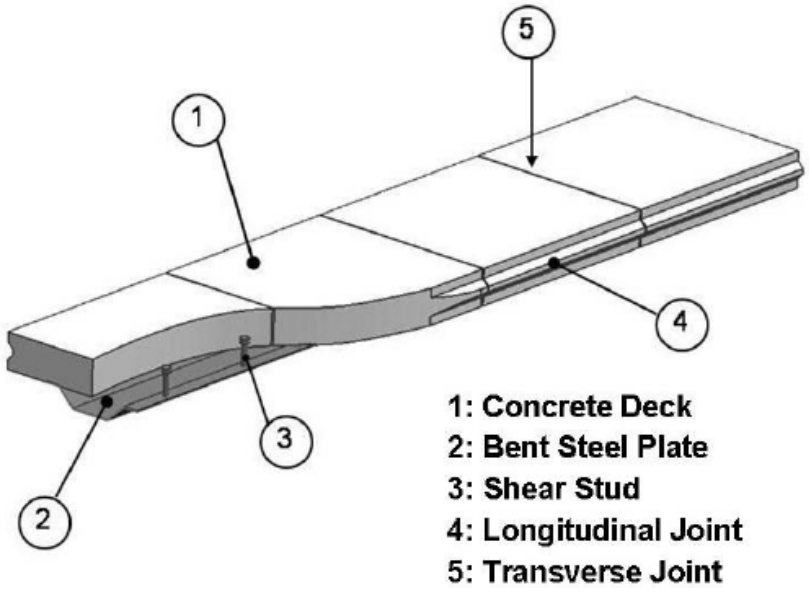

Figure 2.6: MDOT Proposed Bridge System (Burgueno & Pavlich, 2008)

2.2.7 Conclusions

Several researchers over multiple decades have researched the potential economy of prefabricated bridge systems incorporating shallow steel tub girders. Many researchers have found these technologies to be competitive in the short-span bridge market. However, while many of the research conclusions regarding the efficiency and economy of these systems have been promising, many of the systems were hindered by somewhat complex fabricated elements, which would increase the total system cost. In addition, many of these systems did not have industry-wide support, which resulted in their lack of use in mainstream construction of short-span bridges. Therefore, a modular tub girder with simplified details, supported by all levels of the bridge industry, would present a competitive solution for short-span bridges.

2.3 Overview of Current AASHTO Specifications for Tub Girders

The American Association of State Highway and Transportation Officials (AASHTO) publish the AASHTO LRFD Bridge Design Specifications (2010), which governs the design of highway bridges in the United States. Section 6 in this document covers the design of steel structures and more specifically Chapter 6.11 details the specifications for box section (tub girder) flexural members. While these specifications are not directly applicable to cold-bent press-brake-formed tub girders, a review of these provisions is necessary to assess the applicability of the specifications to the proposed system and/or approach the production of specifications for the proposed system.

2.3.1 Structural Loads

Bridge loads are divided into two main categories: permanent loads and transient loads. Permanent loads consist of dead loads and earth loads. Transient loads consist of vehicular live loads and environmental loadings, such as snow, wind, and seismic loads. For the purposes of this review, only dead loads and live loads will be reviewed as they are the chief components of the Strength I, Service II, and Fatigue load combinations (see Section 2.4.2).

Dead loads include the self-weight of all components of the bridge including utilities, wearing surface and planned bridge widenings. If the weights of the dead load components are unknown, AASHTO provides units weights of materials to calculate the total dead load (see Table 2.1). Earth loads include earth pressure, earth surcharge and downdrag loads that act on the bridge over the bridge's design life.

Table 2.1: Unit Weights (AASHTO, 2010)

Material		Unit Weight (kcf)
Aluminum Alloys		0.175
Bituminous Wearing Surfaces		0.140
Cast Iron		0.450
Cinder Filling		0.060
Compacted Sand, Silt, or Clay		0.120
Concrete	Lightweight	0.110
	Sand-Lightweight	0.120
	Normal Weight with $f'_c \leq 5.0$ ksi	0.145
	Normal Weight with $5.0 < f'_c \leq 15.0$ ksi	$0.140 + 0.001 f'_c$
Loose Sand, Silt, or Gravel		0.100
Soft Clay		0.100
Rolled Gravel, Macadam, or Ballast		0.140
Steel		0.490
Stone Masonry		0.170
Wood	Hard	0.060
	Soft	0.050
Water	Fresh	0.0624
	Salt	0.0640
Item		Weight per Unit Length (klf)
Transit Rails, Ties, and Fastening per Track		0.200

Component dead loads are further broken down into non-composite (DC_1) and composite (DC_2 and DW) dead loads. An example of typical DC_1 loads include girder self-weight, the wet concrete deck, stay-in-place metal formwork, concrete haunches, concrete overhang taper and the steel cross frames (i.e. loads applied to the structure before the concrete deck is composite witht he girder). Until the concrete reaches 75 percent of its compressive strength, it is assumed that the load is being supported by only the girders (Morgan, 2010). Once the concrete deck and steel girder become composite, the deck and girder act together to resist DC_2 (weight of the curb, barriers, sidewalks and pedestrian hand railing) and DW (future wearing surface) loads.

The vehicular live load (LL) that is to be applied to the structure is designated as the HL-93, according to AASHTO Specifications. The load model consists of a 0.64 kip/ft lane load in combination with either a design truck or design tandem. The design truck consists of an 8 kip front axle and two 32 kip rear axles (see Figure 2.7). The spacing between the rear 32 kip axles is varied between 14 feet and 30 feet to produce the maximum loading scenario. The design tandem consists of a pair of 25 kip axles that are spaced 4 feet apart. In addition, it is the responsibility of the engineer to determine longitudinal placement of the loads in order to determine the maximum live load response.

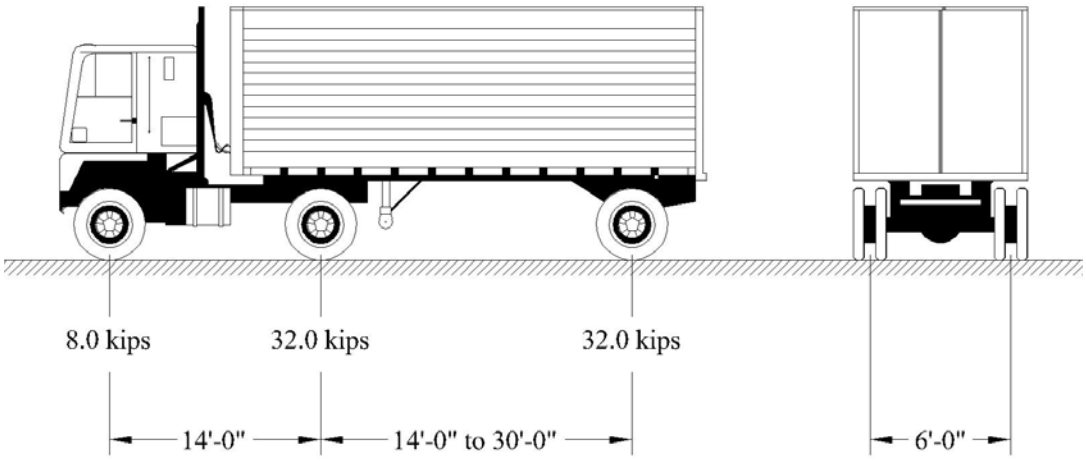

Figure 2.7: HL-93 Vehicular Live Load (AASHTO, 2010)

Dynamic load allowances (IM) account for the dynamic effects of the design vehicle, such as the vehicle's reaction to the driving surface. This effect is accounted for by augmenting the effects of the design truck and design tandem. To account for dynamic load allowances, the vehicular live load is increased by 33% for all limit states except when considering fatigue and when evaluating deck joints. For the fatigue limit state, the live load is increased by 15%, and, for deck joints, the live load is increased by 75%.

In addition to considering loads that are applied to the bridge's finished state, load applied during the construction phase must be evaluated. Examples of construction loads consist of concrete overhangs, overhang deck brackets and formwork, screed rails, railing, construction walkways and the deck finishing machine. In addition, deck casting sequences can provide an additional level of complexity that must be assessed. For multiple span bridges, the deck is cast usually in the positive bending regions first to minimize cracking over the piers.

2.3.2 Limit States Summary

To account for the statistical probability of different loads acting simultaneously at a given time, several load combinations or limit states are employed. The general equation that all limit states must satisfy is as follows:

$$\sum \eta_i \gamma_i Q_i \leq \phi R_n = R_r \qquad \text{Eq. 2.1}$$

Where:

γ_i = load factor: a statically based multiplier applied to force effects

ϕ = resistance factor: a statistically based multiplier applied to nominal resistance

η_i = load modifier: a factor relating to ductility, redundancy and operational classification

Q_i = force effect

R_n = nominal resistance

R_r = factored resistance

To account for ductility, redundancy and operational importance of the bridge, the three load modifiers are multiplied together to calculate the η_i term. The ductility load modifier ensures that visible inelastic deformations occur before failure. The redundancy load modifier safeguards against a catastrophic failure of the entire bridge system if one member fails. Finally, the operational importance load modifier maintains a higher resistance for bridges used in such situations as emergency roadways or that have national security implications. For the majority of cases, the load modifier is to be taken as one.

Strength limit states are used to ensure that strength and stability of both local and global components and connections have the capacity to meet the load combinations the bridge is expected to see over its design life. Both stability and ultimate failure of each structural element is considered. The bridge resistance is considered to be exceeded if any of the components or connections is exceeded in the following limit states:

- Strength I – basic load combination with normal vehicular use, no loads from wind
- Strength II – load combination to account for Owner-specified design vehicles, evaluation permit vehicles, or both, no loads from wind
- Strength III – load combination for bridges exposed to wind velocities exceeding 55 mph
- Strength IV – load combination when dead load to live load force effect ratios is present
- Strength V – load combination for bridges exposed to normal vehicular use with wind velocities of 55 mph

Extreme event limit states account for loads such as earthquakes and vehicle collisions. These loading situations are considered unique occurrences whose return period may be significantly greater than the design life of the bridge. The extreme event limit states are listed below:

- Extreme Event I – load combination to account for earthquake loads
- Extreme Event II – load combination to account for ice loads, collisions, floods and other hydraulic events

To account for excessive stresses, deformations and cracking under regular service conditions, service limit states are employed. These load combinations are derived based on experience, not from strength or statistical calculations, unlike other limit states. The service limit states are listed as follows:

- Service I – load combination for normal use of the bridge with a 55 mph wind, typically used to check for excess bridge deflection and cracking in concrete decks
- Service II – load combination to control yielding of the steel structure and slip of slip-critical connections due to vehicular live load
- Service III – load combination for crack control in prestressed concrete superstructure and girder members
- Service IV – load combination for crack control in prestressed concrete columns

The fatigue and fracture limit state is used to restrict the stress range using a single design truck. These limit states are intended to limit crack growth under repetitive loads and to prevent fracture during the design life of the bridge, and are listed as follows:

- Fatigue I – load combination for infinite load-induced fatigue life
- Fatigue II – load combination related to finite load-induced fatigue life

2.3.3 Structural Analysis Provisions

Multiple presence factors are employed to account for the probability of multiple design lanes being loaded simultaneously. The extreme live load force effect is determined by considering each possible combination of the number of lanes loaded multiplied by the corresponding multiple presence factor. It should be noted that these factors are not to be used when considering the fatigue truck; when assessing fatigue, one design truck is used, regardless of the number of design lanes. AASHTO multiple presence factors are listed in Table 2.2.

Table 2.2: Multiple Presence Factors (AASHTO, 2010)

Number of Loaded Lanes	Multiple Presence Factors, *m*
1	1.20
2	1.00
3	0.85
>3	0.65

In lieu of a complex three-dimensional analysis, live load distribution factors are commonly employed by bridge engineers to simplify the analysis of a bridge system. Specifically, instead of analyzing the three-dimensional bridge system as a whole, these factors allow for a designer or analyst to consider bridge girders individually by determining the maximum number of lanes that may act on a given girder. The applicable distributions factors for both moment and shear for a concrete deck on multiple steel box girders is as follows, regardless of the number of lanes loaded (AASHTO Table 4.6.2.2.2b-1):

$$0.05 + 0.85\frac{N_L}{N_b} + \frac{0.425}{N_L}$$

$$0.5 \le \frac{N_L}{N_b} \le 1.5$$

N_L = number of design lanes as specified in Article 3.6.1.1.1

N_b = number of girders

There are several special restrictions when using the live load distribution factor for bridges containing multiple tub girders. First, the bearing lines shall not be skewed. Second, the inclination of the web plates to a plane normal to the bottom flange shall not exceed a 1 to 4 slope. Third, the cantilever overhang of the concrete deck, including the curb and parapet, shall not be greater than either 60 percent of the average distance between the centers of the top steel flanges of adjacent box sections (see Figure 2.8) or 6.0 feet. Finally, the distance *a* taken at midspan shall neither be greater than 120 percent nor less than 80 percent of the distance center-to-center of the flanges of each adjacent box (see Figure 2.8). If nonparallel box sections are used, the distance center-to-center of the flanges of each adjacent tub girders shall neither be greater than 135 percent nor less than 65 percent.

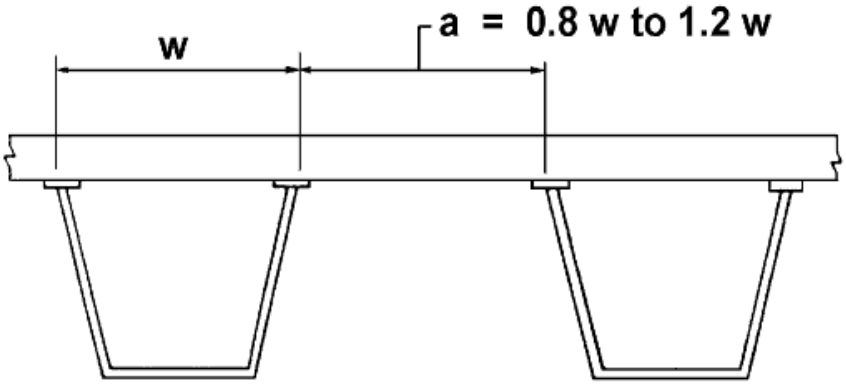

Figure 2.8: Center-to-Center Flange Distance (AASHTO, 2010)

2.3.4 Cross-Section Proportion Limits

In order to prevent transportation and erection issues such as damage during handling and distortion due to welding, cross section proportion limits are used. These limits are based upon years of construction and fabrication experience in addition to research incorporated into the development of the specifications (Morgan, 2010).

The webs must meet the following proportions:

Webs without longitudinal stiffeners:

$$\frac{D}{t_w} \leq 150 \qquad \text{Eq. 2.2}$$

Webs with longitudinal stiffeners:

$$\frac{D}{t_w} \leq 300 \qquad \text{Eq. 2.3}$$

D = depth of the web plate measured along the slope

t_w = web thickness

The top flange must meet the following proportions:

$$\frac{b_f}{2t_f} \leq 12.0 \qquad \text{Eq. 2.4}$$

$$b_f \geq \frac{D}{6} \qquad \text{Eq. 2.5}$$

$$t_f \geq 1.1 t_w \qquad \text{Eq. 2.6}$$

b_f = full width of the widest top flange width within the section under consideration

t_f = flange thickness

t_w = web thickness

D = depth of the web plate measured along the slope

2.3.5 Constructability

In order to provide adequate resistance by the tub girders during construction, Article 6.11.3 of AASHTO (2010) is employed. In addition to Article 6.11.3, Article 3.4.2 is used to determine the appropriate load factors for construction loads. Unlike plate girders where different plate thickness can be employed in different field sections, individual tub girder geometry must be maintained throughout the entire span length. Internal and external cross-frames and diaphragms, and top lateral bracing may be used to control deformations. Finally, the unbraced length is taken as the distance between interior cross-frames or diaphragms.

For tub girders in flexure, the following criteria must be met:

Discretely braced top flanges in compression must meet the following criteria:

$$f_{bu} + f_{\ell} \le \phi_f R_h F_{yc} \qquad \text{Eq. 2.7}$$

$$f_{bu} + \frac{1}{3} f_{\ell} \le \phi_f F_{nc} \qquad \text{Eq. 2.8}$$

$$f_{bu} \le \phi_f F_{crw} \qquad \text{Eq. 2.9}$$

Discretely braced top flanges in tension must meet the following criteria:

$$f_{bu} + f_{\ell} \le \phi_f R_h F_{yt} \qquad \text{Eq. 2.10}$$

Continuously braced top flanges in tension or compression must meet the following criteria:

$$f_{bu} \le \phi_f R_h F_{yf} \qquad \text{Eq. 2.11}$$

For critical stages of construction, non-composite box flanges in compression shall satisfy the following requirements:

$$f_{bu} \le \phi_f F_{nc} \qquad \text{Eq. 2.12}$$

$$f_{bu} \le \phi_f F_{crw} \qquad \text{Eq. 2.13}$$

For critical stages of construction, non-composite box flanges in tension and continuously braced box flanges in tension or compression shall satisfy the following requirements:

$$f_{bu} \le \phi_f R_h F_{yf} \Delta \qquad \text{Eq. 2.14}$$

ϕ_f = resistance factor for flexure specified in Article 6.5.4.2

f_{bu} = longitudinal flange stress due to the factored loads at the section under consideration calculated without consideration of longitudinal warping

f_ℓ = flange lateral bending stress determined as specified in Article 6.10.1.6

F_{crw} = nominal bend-buckling resistance for webs specified in Article 6.10.1.9

F_{nc} = nominal flexural resistance of box flanges in compression determined as specified in Article 6.11.8.2

R_h = hybrid factor specified in Article 6.10.1.10.1

F_{yc} = specified minimum yield strength of the compression flange

F_{yt} = specified minimum yield strength of the tension flange

F_{yf} = specified minimum yield strength of the flange under consideration

$\Delta = \sqrt{1-3\left(\frac{f_v}{F_{yf}}\right)^2}$

f_v = St. Venant torsional shear stress in the flange due to the factored loads at the section under consideration = $\frac{T}{2A_o t_f}$

A_o = enclosed area within the box section

T = internal torque due to the factored loads

For shear requirements, webs shall satisfy the following requirement during critical stages of construction:

$$V_u \le \phi_v V_{cr} \quad \text{Eq. 2.15}$$

$$V_{ui} = \frac{V_u}{\cos(\theta)} \quad \text{Eq. 2.16}$$

ϕ_v = resistance factor for shear specified in Article 6.5.4.2

V_u = vertical shear due the factored loads on one inclined web

V_{cr} = shear buckling resistance determined from Eq. 6.10.9.3.3-1

V_{ui} = shear due to the factored loads along one inclined web

θ = the angle of inclination of the web plate to the vertical

2.3.6 Service Limit State

The function of the service limit state is to ensure the maintainability and durability of the structure. In doing so, it not only provides the user with a higher level of ride ability but also preserves the life of the structure throughout the bridge's service life (Morgan, 2010). The limits specified in this section are related to arresting both elastic and permanent deformations.

To control permanent deformations, several requirements are established. If the concrete deck is assumed to be fully effective in both the negative and positive bending regions, the Service II load combination is applied to both the short-term and long-term composite sections.

The flanges must satisfy the following requirements in order to prevent web yielding and bend-buckling from occurring prior to flange strength development:

For the top steel flange of the composite section, the following requirement must be met:

$$f_f \le 0.95 R_h F_{yf} \quad \text{Eq. 2.17}$$

For the bottom steel flange of the composite section, the following requirement must be met:

$$f_f + \frac{f_\ell}{2} \le 0.95 R_h F_{yf} \qquad \text{Eq. 2.18}$$

For both steel flanges of non-composite section, the following requirement must be met:

$$f_f + \frac{f_\ell}{2} \le 0.80 R_h F_{yf} \qquad \text{Eq. 2.19}$$

f_f = flange stress at the section under consideration due to Service II loads calculated without consideration of lateral flange bending

f_ℓ = lateral flange bending stress at the section under consideration due to the Service II loads determined as specified in Article 6.10.1.6

F_{yf} = specified minimum yield strength of the flange under consideration

R_h = hybrid factor specified in Article 6.10.1.10.1

Article 2.5.2.6 in AASHTO (2010) list suggested limits for elastic live load deflections (see Figure 2.9). When checking live load deflection, the load to be used is the greater of the design truck plus impact or 25% of the design truck with impact plus the design lane load. It is assumed that all of the components of the bridge deflect equally and that all design lanes are to be equally loaded. The short-term composite section is to be used as the stiffness of the structure when computing deflection.

- Vehicular load, general Span/800,
- Vehicular and pedestrian loads Span/1000,
- Vehicular load on cantilever arms..... Span/300, and
- Vehicular and pedestrian loads on cantilever arms Span/375.

Figure 2.9: Live Load Deflection Limits (AASHTO, 2010)

Web bending buckling can cause accelerated deck deteriorating and could possibility lead to rupture from plastic deformations. The following Service II requirements are established so the web has the capacity to resist web bend buckling:

All sections of the web must satisfy:

$$f_c \leq F_{crw} \qquad \text{Eq. 2.20}$$

f_c = compression flange stress at the section under consideration due to the Service II loads calculated without consideration of lateral flange bending

F_{crw} = nominal bend-buckling resistance for the web specified in Article 6.10.1.9

2.3.7 Fatigue & Fracture Limit State

For the fatigue limit state, the design life of the bridge and limits for live load stress ranges are used to prevent fatigue crack growth. Fatigue is generally divided into two categories: load-induced fatigue and distortion-induced fatigue and is outlined in Articles 6.6.1.2 and 6.6.1.3 in AASHTO (2010), respectively. Connections and fabrication details are arranged according to fatigue categories (each with their own respective maximum fatigue threshold stress ranges, ΔF_{th}) and are specified in AASHTO (2010) Table 6.6.1.2.3-1.

For load-induced fatigue, the stress range caused by live loads is computed for flexural members using the short-term composite section. Residual stresses are not considered and fatigue is only considered in regions where permanent loads produce compression if the compression stresses are less than twice the maximum tensile stresses. The maximum tensile stresses are caused by the live loads calculated using the fatigue limit state load combination (Morgan, 2010).

Each detail must satisfy the following for load induced fatigue:

$$\gamma\left(\Delta f\right) \leq \left(\Delta F\right)_n \qquad \text{Eq. 2.21}$$

For the Fatigue I load combination and infinite life, the nominal fatigue resistance is computed as follows:

$$(\Delta F)_n = (\Delta F)_{TH} \qquad \text{Eq. 2.22}$$

For the Fatigue II load combination and finite life, the nominal fatigue resistance is computed as follows:

$$(\Delta F)_n = \left(\frac{A}{N}\right)^{\frac{1}{3}} \qquad \text{Eq. 2.23}$$

N = number of fatigue cycles over the design life of the structure Eq. 2.24

A = constant take from Table 6.6.1.2.5-1

n = number of stress range cycles per truck passage taken from Table 6.6.1.2.5-2

Distortion-induced fatigue is specified in AASHTO (2010) Article 6.6.1.3. Connection details are established to ensure sufficient load paths exist to properly transmit all intended and unintended forces. These forces could be transferred through transverse, lateral and longitudinal members. To establish load paths, the girder compression and tension flanges are bolted or welded at connecting diaphragms, internal or external diaphragms and floor beams or stringers. These diaphragms, floor beams or stringers are attached to transverse connection plates or to transverse stiffeners acting as connection plates. If the load that will act on the welded or bolted connection is unknown, the connection should be able to resist a lateral load of at least 20 kips (Morgan, 2010).

Article 6.6.2 in AASHTO (2010) defines the requirements for fracture. All primary longitudinal superstructure components and connections sustaining stress due to the Strength I Load Combination shall require Charpy V-notch testing. Finally, all structural members that are fracture critical must meet Charpy V-notch toughness requirements (Morgan, 2010).

2.3.8 Strength Limit State

The strength limit state ensures that the bridge has sufficient capacity to safely resist the applied moments and shears that act over the entire life of the bridge. Article 6.11.6 in AASHTO (2010) describes the strength limit state for box girders and is broken down into four main sections.

2.3.8.1 General Requirements

For straight bridges the minimum yield strength of both flanges and the web cannot exceed 70 ksi. The web must satisfy AASHTO (2010) Article 6.11.2.1.2 which is cross section proportion limits; webs without longitudinal stiffeners (see Section 2.5.3).

To check if the web slenderness limit is met, the following equation must be satisfied:

$$\frac{2D_{cp}}{t_w} \le 3.76\sqrt{\frac{E}{F_{yc}}} \qquad \text{Eq. 2.25}$$

D_{cp} = depth of the web in compression at the plastic moment determined as specified in Article D6.3.2

F_{yc} = specified minimum yield strength of the compression flange

E = modulus of elasticity of steel

t_w = web thickness

Compact sections shall satisfy AASHTO (2010) Article 6.11.7.1 (see Section 2.5.9.2). If the section does not satisfy Article 6.11.7.1, the section is considered noncompact and shall meet the requirements of AASHTO (2010) Article 6.11.7.2 (see Section 2.5.9.2).

Compact and noncompact sections shall meet the ductility requirement as follows:

$$D_p \leq 0.42 D_t \qquad \text{Eq. 2.26}$$

D_p = distance from the top of the concrete deck to the neutral axis of the composite section at the plastic moment

D_t = total depth of the composite section

2.3.8.2 Flexural Capacity of Composite Sections

The following provisions apply to compact sections:

At the strength limit state, the section shall satisfy:

$$M_u \leq \phi_f M_n \qquad \text{Eq. 2.27}$$

ϕ_f = resistance factor for flexure specified in Article 6.5.4.2

M_n = nominal flexural resistance of the section determined as specified in Article 6.11.7.1.2

M_u = bending moment about the major axis of the cross section due to the factored loads at the section under consideration

The nominal flexural resistance of simply-supported beams is computed as follows:

If $D_p \leq 0.1\ D_t$ then:

$$M_n = M_p \qquad \text{Eq. 2.28}$$

Otherwise:

$$M_n = M_p\left(1.07 - 0.7\frac{D_p}{D_t}\right) \qquad \text{Eq. 2.29}$$

D_p = distance from the top of the concrete deck to the neutral axis of the composite section at the plastic moment

D_t = total depth of the composite section

M_p = plastic moment of the composite section determined as specified in Article D6.1

M_n = nominal flexural resistance

The nominal flexural resistance of continuous-span beams is limited to:

$$M_n = 1.3R_hM_y \qquad \text{Eq. 2.30}$$

M_n = nominal flexural resistance

M_y = yield moment as specified in Article D6.2

R_h = hybrid factor specified in Article 6.10.1.10.1

The following provisions apply to noncompact sections:

At the strength limit state, compression flanges shall satisfy the following:

$$f_{bu} \le \phi_f F_{nc} \qquad \text{Eq. 2.31}$$

ϕ_f = resistance factor for flexure specified in Article 6.5.4.2

f_{bu} = longitudinal flange stress at the section under consideration calculated without consideration of lateral flange bending or longitudinal warping

F_{nc} = nominal flexural resistance of the compression flange as specified in Article 6.11.7.2.2

The nominal resistance of compression flanges is computed as follows:

$$F_{nc} = R_b R_h F_{yc} \qquad \text{Eq. 2.32}$$

F_{nc} = nominal flexural resistance of the compression flange as specified in Article 6.11.7.2.2

R_b = web load shedding factor determined as specified in Article 6.10.1.10.2

R_h = hybrid factor specified in Article 6.10.1.10.1

F_{yc} = specified minimum yield strength of the compression flange

2.3.8.3 Flexural Capacity of Noncomposite Sections

The following provisions are applied to noncomposite sections:

At the strength limit state, the following requirement shall be satisfied for flanges in compression:

$$f_{bu} \le \phi_f F_{nc} \qquad \text{Eq. 2.33}$$

ϕ_f = resistance factor for flexure specified in Article 6.5.4.2

f_{bu} = longitudinal flange stress at the section due to the factored loads at the section under consideration calculated without consideration of longitudinal warping

F_{nc} = nominal flexural resistance of the compression flange as specified in Article 6.11.8.2

At the strength limit state, the following requirement shall be satisfied for flanges in tension:

$$f_{bu} \le \phi_f F_{nt} \qquad \text{Eq. 2.34}$$

ϕ_f = resistance factor for flexure specified in Article 6.5.4.2

f_{bu} = longitudinal flange stress at the section due to the factored loads at the section under consideration calculated without consideration of longitudinal warping

F_{nt} = nominal flexural resistance of the flange determined as specified in Article 6.11.8.3

The flexural resistance of unstiffened flanges in compression is computed as follows:

If $\lambda_f \le R_1\sqrt{\frac{kE}{F_{yc}}}$ then:

$$F_{nc} = R_h R_h F_{yc}\Delta \qquad \text{Eq. 2.35}$$

If $R_1\sqrt{\frac{kE}{F_{yc}}} < \lambda_f \le R_2\sqrt{\frac{kE}{F_{yc}}}$ then:

$$F_{nc} = R_b R_h F_{yc}\left[\Delta - \left(\Delta - \frac{F_{yr}}{R_h F_{yc}}\right)\left\{1 - \sin\left(\frac{\pi}{2}\left(\frac{R_2 - \frac{b_{fc}}{t_{fc}}\sqrt{\frac{F_{yc}}{kE}}}{R_2 - R_1}\right)\right)\right\}\right] \qquad \text{Eq. 2.36}$$

If $\lambda_f > R_2\sqrt{\frac{kE}{F_{yc}}}$ then:

$$F_{nc} = \frac{0.9ER_b k}{\left(\frac{b_{fc}}{t_{fc}}\right)^2} - \frac{R_b f_v^{\,2} k}{0.9Ek_s^{\,2}}\left(\frac{b_{fc}}{t_{fc}}\right)^2 \qquad \text{Eq. 2.37}$$

$$\lambda_f = \frac{b_{fc}}{t_{fc}} \qquad \text{Eq. 2.38}$$

$$\Delta = \sqrt{1 - 3\left(\frac{f_v}{F_{yc}}\right)^2} \qquad \text{Eq. 2.39}$$

$$f_v = \frac{T}{2A_o t_{fc}} \qquad \text{Eq. 2.40}$$

$$F_{yr} = \left(\Delta - 0.4\right)F_{yc} \le F_{yw} \qquad \text{Eq. 2.41}$$

k = plate buckling coefficient for uniform normal stress = 4.0

k_s = plate buckling coefficient for shear stress = 5.34

$$R_1 = \frac{0.57}{\sqrt{\frac{1}{2}\left(\Delta + \sqrt{\Delta^2 + 4\left(\frac{f_v}{F_{yc}}\right)^2\left(\frac{k}{k_s}\right)^2}\right)}} \qquad \text{Eq. 2.42}$$

$$R_2 = \frac{1.23}{\sqrt{\frac{1}{1.2}\left(\frac{F_{yr}}{F_{yc}} + \sqrt{\left(\frac{F_{yr}}{F_{yc}}\right)^2 + 4\left(\frac{f_v}{F_{yc}}\right)^2\left(\frac{k}{k_s}\right)^2}\right)}} \qquad \text{Eq. 2.43}$$

b_{fc} = compression flange width between webs

A_o = enclosed area within the box section

R_b = web load shedding factor determined as specified in Article 6.10.1.10.2

R_h = hybrid factor specified in Article 6.10.1.10.1

T = internal torque due to the factored loads

E = modulus of elasticity of steel

F_{yc} = specified minimum yield strength of the compression flanges

F_{nc} = nominal flexural resistance of the compression flanges as specified in Article 6.11.8.2

t_{fc} = thickness of the compression flanges

The flexural resistance of longitudinally stiffened flanges in compression is computed in the same fashion as for unstiffened flanges, with the following substitutions:

- w shall be substituted for b_{fc}
- k shall be taken as follows:
  - If $n = 1$, then:

$$k = \left(\frac{8I_s}{wt_{fc}^3} \right)^{\frac{1}{3}} \qquad \text{Eq. 2.44}$$

  - If $n = 2$ then:

$$k = \left(\frac{0.894I_s}{wt_{fc}^3} \right)^{\frac{1}{3}} \qquad \text{Eq. 2.45}$$

$$1.0 \le k \le 4.0$$

- $$k_s = \frac{5.34 + 2.84\left(\frac{I_s}{wt_{fc}^3} \right)^{\frac{1}{3}}}{(n+1)^2} \le 5.34 \qquad \text{Eq. 2.46}$$

I_s = moment of inertia of a single longitudinal flange stiffener about an axis parallel to the flange and taken at the base of the stiffener

n = number of equally spaced longitudinal flange stiffeners

w = larger of the width of the flange between longitudinal flange stiffeners or the distance from a web to the nearest longitudinal flange stiffener

t_{fc} = thickness of the compression flanges

The flexural resistance of flanges in tension is computed as follows:

$$F_{nt} = R_h F_{yt} \qquad \text{Eq. 2.47}$$

R_h = hybrid factor specified in Article 6.10.1.10.1

F_{yt} = specified minimum yield strength of the tension flanges

F_{nt} = nominal flexural resistance of the tension flanges

2.3.8.4 Shear Capacity

The provisions for addressing shear concerns are as follows:

At the strength limit state, straight and curved web panels shall satisfy:

$$V_u \le \phi_v V_n \qquad \text{Eq. 2.48}$$

ϕ_v = resistance factor for shear specified in Article 6.5.4.2

V_n = nominal shear resistance determined as specified in Articles 6.10.9.2 and 6.10.9.3 for unstiffened and stiffened webs, respectively

V_u = $V_{ui}\cos(\theta)$

V_{ui} = vertical shear due to the factored loads on the inclined web

θ = the angle of inclination of the web plate to the vertical

The nominal shear resistance of unstiffened webs shall be taken as:

$$V_n = V_{cr} = CV_p \qquad \text{Eq. 2.49}$$

C = Eq. 2.53, Eq. 2.54 and Eq. 2.55 are applicable with $k = 5.0$

V_p = $0.58F_{yw}Dt_w$

V_{cr} = shear buckling resistance

F_{yw} = specified minimum yield stress of the web

D = web depth

t_w = web thickness

For interior panels, the provisions are as follows:

The interior web panel with section along the entire panel proportioned such that:

$$\frac{2Dt_w}{b_{fc}t_{fc} + b_{ft}t_{ft}} \le 2.5 \qquad \text{Eq. 2.50}$$

If Eq. 2.50 is satisfied, the nominal shear resistance of an interior web shall be taken as:

$$V_n = V_p \left[C + \frac{0.87(1-C)}{\sqrt{1+\left(\frac{d_o}{D}\right)^2}} \right] \qquad \text{Eq. 2.51}$$

If Eq. 2.50 is not satisfied, the nominal shear resistance of an interior web shall be:

$$V_n = V_p \left[C + \frac{0.87(1-C)}{\sqrt{1+\left(\frac{d_o}{D}\right)^2 + \frac{d_o}{D}}} \right] \qquad \text{Eq. 2.52}$$

$V_p =$ $0.58F_{yw}Dt_w$

$F_{yw} =$ specified minimum yield stress of the web

$D =$ web depth

$t_w =$ web thickness

$d_o =$ transverse stiffener spacing

$V_n =$ nominal shear resistance of the web panel

C shall be determined as follows:

- If $\frac{D}{t_w} \le 1.12\sqrt{\frac{Ek}{F_{yw}}}$ then:
  - $C = 1.0$ Eq. 2.53
- If $1.12\sqrt{\frac{Ek}{F_{yw}}} < \frac{D}{t_w} \le 1.40\sqrt{\frac{Ek}{F_{yw}}}$ then:
  - $C = \frac{1.12}{\frac{D}{t_w}}\sqrt{\frac{Ek}{F_{yw}}}$ Eq. 2.54
- If $\frac{D}{t_w} > 1.40\sqrt{\frac{Ek}{F_{yw}}}$ then:
  - $C = \frac{1.57}{\left(\frac{D}{t_w}\right)^2}\left(\frac{Ek}{F_{yw}}\right)$ Eq. 2.55

The plate buckling coefficient is computed as follows:

$$k = 5 + \frac{5}{\left(\frac{d_o}{D}\right)^2} \quad \text{Eq. 2.56}$$

D = web depth

t_w = web thickness

F_{yw} = specified minimum yield stress of the web

E = modulus of elasticity of steel

For end panels, the resistance is computed as follows:

$$V_n = V_{cr} = CV_p \qquad \text{Eq. 2.57}$$

C = Eq. 2.51, Eq. 2.52 and Eq. 2.53 are applicable

V_p = $0.58F_{yw}Dt_w$

F_{yw} = specified minimum yield stress of the web

D = web depth

t_w = web thickness

V_{cr} = shear buckling resistance

2.3.9 AASHTO Equation References

Table 2.3 details a summary of the equations referenced in this chapter along with their respective AASHTO equation references and page numbers.

Table 2.3: Equation Legend (AASHTO, 2010)

Chapter 2	AASHTO 5th Edition	AASHTO 5th Edition Page Number
Equation 2.1	Equation 1.3.2.1-1	1-3
Equation 2.2	Equation 6.11.2.1.2-1	6-179
Equation 2.3	Equation 6.11.2.1.3-1	6-179
Equation 2.4	Equation 6.11.2.2-1	6-180
Equation 2.5	Equation 6.11.2.2-2	6-180
Equation 2.6	Equation 6.11.2.2-3	6-180
Equation 2.7	Equation 6.10.3.2.1-1	6-120
Equation 2.8	Equation 6.10.3.2.1-2	6-120
Equation 2.9	Equation 6.10.3.2.1-3	6-120
Equation 2.10	Equation 6.10.3.2.2-1	6-122
Equation 2.11	Equation 6.10.3.2.3-2	6-122
Equation 2.12	Equation 6.11.3.2-1	6-181
Equation 2.13	Equation 6.11.3.2-2	6-181
Equation 2.14	Equation 6.11.3.2-3	6-182
Equation 2.15	Equation 6.11.3.3-1	6-123
Equation 2.16	Equation 6.11.8.3-1	6-196
Equation 2.17	Equation 6.10.4.2.2-1	6-127
Equation 2.18	Equation 6.10.4.2.2-2	6-127
Equation 2.19	Equation 6.10.4.2.2-3	6-127
Equation 2.20	Equation 6.10.4.2.2-4	6-127
Equation 2.21	Equation 6.6.1.2.2-1	6-33
Equation 2.22	Equation 6.6.1.2.5-1	6-43
Equation 2.23	Equation 6.6.1.2.5-2	6-44
Equation 2.24	Equation 6.6.1.2.5-3	6-44
Equation 2.25	Equation 6.11.6.2.2-1	6-188

Table 2.3 (cont'd)

Chapter 2	AASHTO 5th Edition	AASHTO 5th Edition Page Number
Equation 2.26	Equation 6.10.7.3-1	6-140
Equation 2.27	Equation 6.11.7.1.1-1	6-189
Equation 2.28	Equation 6.10.7.1.2-1	6-137
Equation 2.29	Equation 6.10.7.1.2-2	6-137
Equation 2.30	Equation 6.10.7.1.2-3	6-137
Equation 2.31	Equation 6.11.7.2.1-1	6-189
Equation 2.32	Equation 6.11.7.2.2-1	6-190
Equation 2.33	Equation 6.11.8.1.1-1	6-191
Equation 2.34	Equation 6.11.8.1.2-1	6-192
Equation 2.35	Equation 6.11.8.2.2-1	6-193
Equation 2.36	Equation 6.11.8.2.2-2	6-193
Equation 2.37	Equation 6.11.8.2.2-3	6-193
Equation 2.38	Equation 6.11.8.2.2-4	6-193
Equation 2.39	Equation 6.11.8.2.2-5	6-193
Equation 2.40	Equation 6.11.8.2.2-6	6-194
Equation 2.41	Equation 6.11.8.2.2-7	6-194
Equation 2.42	Equation 6.11.8.2.2-8	6-194
Equation 2.43	Equation 6.11.8.2.2-9	6-194
Equation 2.44	Equation 6.11.8.2.3-1	6-195
Equation 2.45	Equation 6.11.8.2.3-2	6-195
Equation 2.46	Equation 6.11.8.2.3-3	6-195
Equation 2.47	Equation 6.11.8.3-1	6-196
Equation 2.48	Equation 6.10.9.1-1	6-151
Equation 2.49	Equation 6.10.9.2-1	6-152
Equation 2.50	Equation 6.10.9.3.2-1	6-153
Equation 2.51	Equation 6.10.9.3.2-2	6-153
Equation 2.52	Equation 6.10.9.3.2-8	6-154
Equation 2.53	Equation 6.10.9.3.2-4	6-154
Equation 2.54	Equation 6.10.9.3.2-5	6-154
Equation 2.55	Equation 6.10.9.3.2-6	6-154
Equation 2.56	Equation 6.10.9.3.2-7	6-154
Equation 2.57	Equation 6.10.9.3.3-1	6-154
Figure 2.7	Figure 3.6.1.2.2-1	3-24
Figure 2.8	Figure 6.11.2.3-1	6-180
Figure 2.9	---	2-12

Table 2.3 (cont'd)

Chapter 2	AASHTO 5th Edition	AASHTO 5th Edition Page Number
Table 2.1	Table 3.5.1-1	3-17
Table 2.2	Table 3.6.1.1.2-1	3-18

2.4 CONCLUSION

This chapter summarized past research projects and implementations of cold-bent tub girders in bridge applications, the mechanics of cold bending of steel, and AASHTO specifications that are applicable to tub girders. Several research projects in the past have attempted to use cold bending of steel to construct a bridge using accelerated bridge technology. Based on the findings of this chapter (and the needs of the current short-span highway bridge market), a more refined press-brake-formed tub girder is developed in the following chapters with the focus of implementing the proposed system using accelerated bridge construction methods.

CHAPTER 3: DESIGN METHODOLOGY

3.1 INTRODUCTION

The following chapter details the design methodology of the proposed press-brake steel tub girder system for short-span bridges. Design iterations were performed for a suite of girders employing standard mill plates, and girder proportions were selected based on the composite yield moment. Cross-sectional properties of both the noncomposite and composite sections are also summarized in this chapter.

3.2 DESIGN METHODOLOGY

Design of the proposed system was completed in two stages. First, a spreadsheet was developed to compute the section properties of any configuration of tub girder (for a discussion of the derivation of section properties, the reader is referred to Appendix A). Next, design iterations were performed based on conservative estimates of press-brake tub girder capacity (essentially, limiting the capacity of the composite girders to the yield moment).

For this effort, three different plate thicknesses were evaluated (7/16”, 1/2”, and 5/8") and six different standard mill plate widths were evaluated (60”, 72”, 84”, 96”, 108”, and 120”). All plates were assumed for design purposes to have a yield stress, F_y = 50 ksi. For each standard mill plate, a design study was performed by investigating different variations of the girder dimensions in order to obtain an optimum girder configuration. For this study, the slope of the webs was kept at a constant 1:4 slope, and the inside bend radii of the girders was kept at a constant value of five times the respective plate thickness, and the top flange width was kept at a constant value of 6 inches. The dimensions of the concrete deck of the composite unit were kept at 7.5’ wide by 8” thick. Normal-weight concrete was assumed with a modular ratio, n = 8 and a compressive strength, f_c' = 4 ksi.

3.3 PARAMETRIC MATRIX OF GIRDERS

Figures 3.1 through 3.6 show the results of these design assessments for the suite of standard mill plates chosen for design. From these plots, it is clear that, for each plate, an optimum depth is seen at the point of maximum yield moment. In lieu of selecting an optimum depth for each individual plate, plates with common standard mill widths were grouped together, and an optimum depth was selected for each group. This chosen depth is indicated by the vertical line present in each plot.

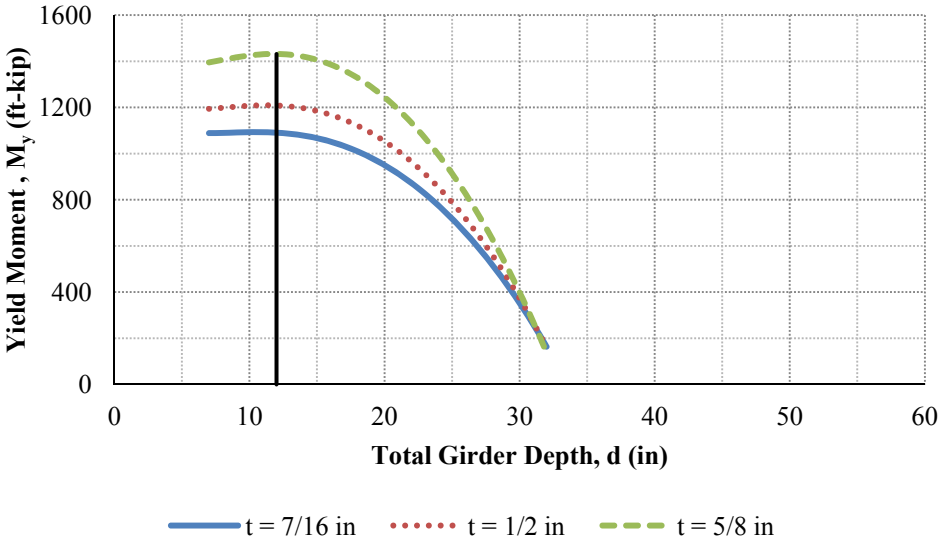

Figure 3.1: Design Comparisons (60" Wide Standard Mill Plates)

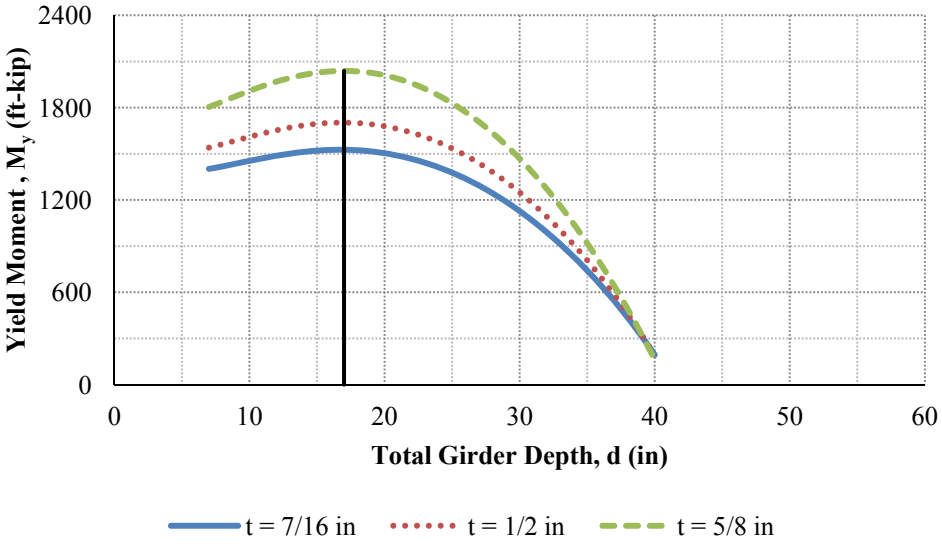

Figure 3.2: Design Comparisons (72" Wide Standard Mill Plates)

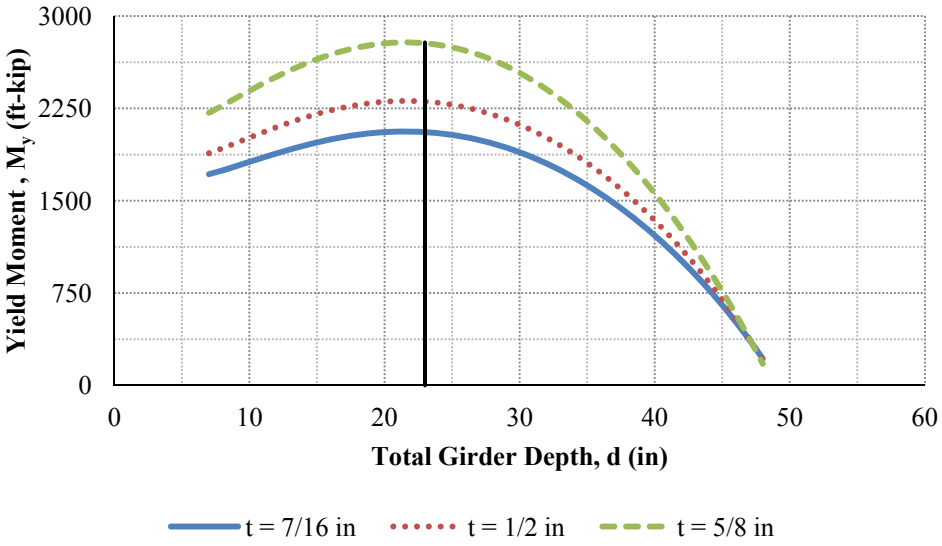

Figure 3.3: Design Comparisons (84" Wide Standard Mill Plates)

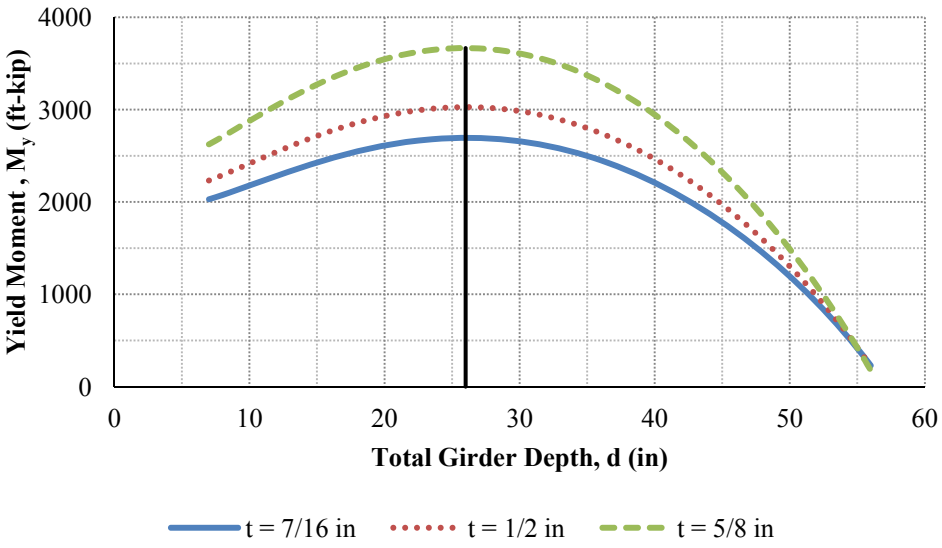

Figure 3.4: Design Comparisons (96" Wide Standard Mill Plates)

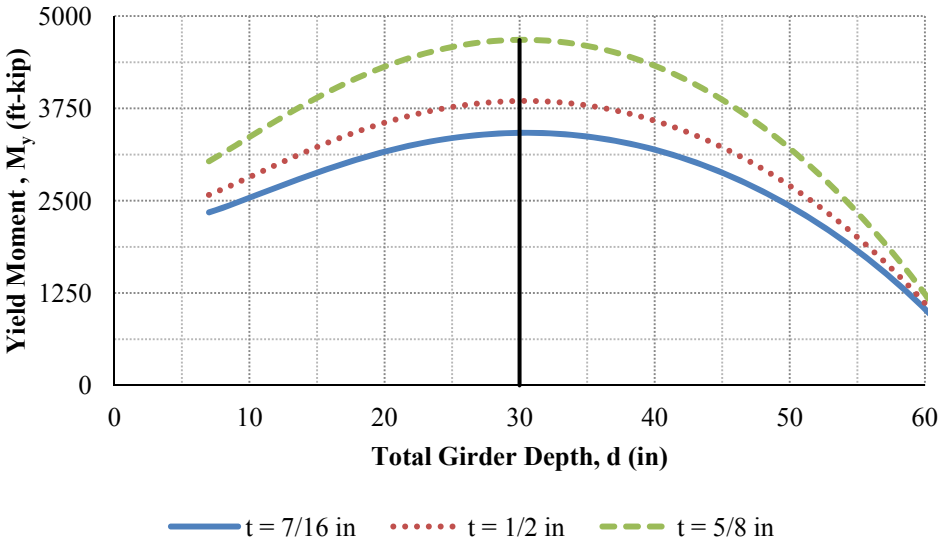

Figure 3.5: Design Comparisons (108" Wide Standard Mill Plates)

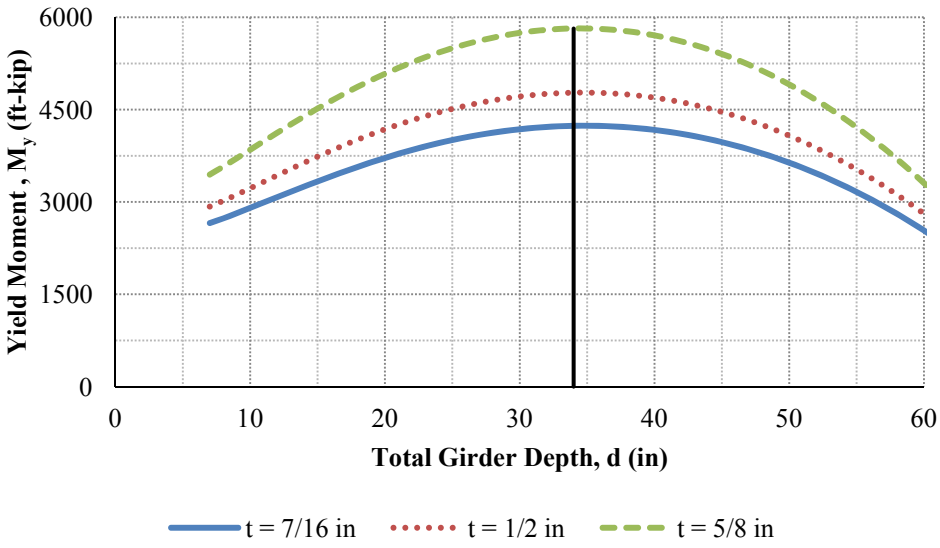

Figure 3.6: Design Comparisons (120" Wide Standard Mill Plates)

The resulting matrix of girders, along with their respective noncomposite and composite section properties, are summarized in Tables 3.1 and 3.2. Note that both the center-or-gravity, $\bar{y}$, and the shear center, Y_o, for each girder are expressed with respect to the bottom of the steel girder (taken positive if the distance is measured above the bottom of the girder). In addition, for all composite girders, the plastic moment capacity, M_p, along with the depth to the plastic neutral axis, D_p (for a discussion regarding the computation of these composite properties, the reader is referred to Appendix B.)

Table 3.1: Noncomposite Section Properties of Parametric Matrix of Girders

Girder	w (in)	d (in)	t (in)	b_{bf} (in)	D (in)	A (in^2)	$\bar{y}$ (in)	I_x (in^4)	I_y (in^4)	Y_o (in)	J (in^4)	C_w (in^6)	β_x (in)
1			7/16	18.917	8.1609	26.250	5.3335	627.27	4284.6	-4.0359	1.6748	25442	5.1891
2	60	12	1/2	18.297	7.5597	30.000	5.3966	710.77	4956.6	-3.8840	2.5000	28229	5.9100
3			5/8	17.056	6.3572	37.500	5.5208	871.53	6355.5	-3.5677	4.8828	33297	7.4696
4			7/16	20.610	13.315	31.500	7.5098	1437.4	6246.4	-6.0295	2.0098	69754	-6.3935
5	72	17	1/2	19.989	12.714	36.000	7.5846	1635.1	7204.0	-5.8669	3.0000	78041	-5.9021
6			5/8	18.748	11.511	45.000	7.7327	2021.9	9179.2	-5.5247	5.8594	93727	-4.8274
7			7/16	20.240	19.499	36.750	10.393	2893.1	8049.6	-8.0792	2.3447	139952	-19.704
8	84	23	1/2	19.620	18.898	42.000	10.480	3296.6	9267.1	-7.8955	3.5000	158281	-19.336
9			5/8	18.378	17.696	52.500	10.650	4092.1	11765	-7.5078	6.8359	194534	-18.521
10			7/16	26.056	22.592	42.000	11.129	4189.0	12693	-9.8140	2.6797	310587	-20.647
11	96	26	1/2	25.435	21.991	48.000	11.216	4780.6	14584	-9.6645	4.0000	347898	-20.363
12			5/8	24.194	20.788	60.000	11.388	5953.5	18437	-9.3462	7.8125	418495	-19.719
13			7/16	29.809	26.715	47.250	12.563	6142.6	17741	-11.579	3.0146	590336	-25.132
14	108	30	1/2	29.189	26.114	54.000	12.652	7016.0	20359	-11.444	4.5000	660933	-24.915
15			5/8	27.948	24.911	67.500	12.831	8753.5	25674	-11.156	8.7891	793522	-24.411
16			7/16	33.563	30.838	52.500	13.985	8605.4	24011	-13.306	3.3496	1049543	-29.419
17	120	34	1/2	32.943	30.237	60.000	14.077	9834.5	27531	-13.184	5.0000	1175747	-29.257
18			5/8	31.701	29.034	75.000	14.260	12285	34655	-12.923	9.7656	1412339	-28.870

Table 3.2: Composite Section Properties of Parametric Matrix of Girders

Girder	w (in)	d (in)	t (in)	$\bar{y}$ (in)	I_x (in^4)	M_y (ft-kip)	D_p (in)	D_p / D_t	M_p (ft-kip)
1			7/16	13.591	3419.5	1048.3	4.2892	0.2145	1369.6
2	60	12	1/2	13.349	3720.5	1161.3	4.9020	0.2451	1519.1
3			5/8	12.918	4258.4	1373.5	6.1275	0.3064	1783.7
4			7/16	17.503	6163.8	1467.4	5.1471	0.2059	1957.8
5	72	17	1/2	17.167	6743.0	1636.6	5.8824	0.2353	2171.1
6			5/8	16.578	7782.6	1956.1	7.3529	0.2941	2548.3
7			7/16	22.185	10569	1985.1	6.0049	0.1937	2695.6
8	84	23	1/2	21.743	11592	2221.4	6.8627	0.2214	2990.6
9			5/8	20.976	13435	2668.7	8.1406	0.2626	3518.5
10			7/16	23.995	14867	2581.6	6.8627	0.2018	3402.0
11	96	26	1/2	23.466	16306	2895.4	7.8431	0.2307	3772.6
12			5/8	22.555	18904	3492.1	8.3844	0.2466	4461.2
13			7/16	26.620	20862	3265.3	7.7206	0.2032	4248.0
14	108	30	1/2	25.995	22876	3666.9	8.1852	0.2154	4722.8
15			5/8	24.928	26518	4432.5	8.6336	0.2272	5613.6
16			7/16	29.152	28209	4031.8	8.1312	0.1936	5190.0
17	120	34	1/2	28.431	30918	4531.2	8.4084	0.2002	5805.8
18			5/8	27.209	35821	5485.4	10.735	0.2556	6897.7

3.4 CONCLUSION

The preceding chapter detailed the design methodology of the proposed press-brake steel tub girder system for short-span bridges. However, the design evaluations and determination of cross-section dimensions were based on conservative estimates of press-brake tub girder capacity. The following chapters discuss experimental testing, analytical modeling, behavioral studies, and feasibility assessments of this system in order to better define its behavior and capacity.

CHAPTER 4: EXPERIMENTAL TESTING PROGRAM

4.1 INTRODUCTION

Contained in this chapter is an overview of the physical investigation completed to assess proposed press-brake-formed shallow steel tub girder. A brief description of the composite and noncomposite specimens tested is provided along with an overview of the test procedure, the equipment used, and the results of testing efforts.

4.2 OVERVIEW OF TESTING PROGRAM

In order to verify the performance and capacity of this newly-developed modular tub girder, physical flexural testing was conducted at the Major Units Laboratory at West Virginia University. Flexural testing was conducted on simply-supported composite and noncomposite press-brake tub girder specimens in three-point bending, according to Figures 4.1 and 4.2.

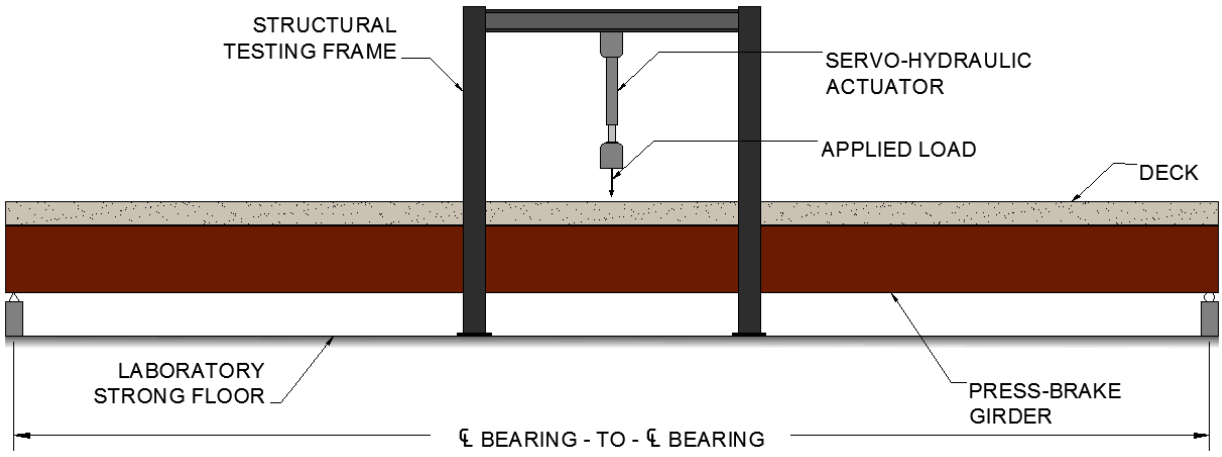

Figure 4.1: Typical Test Setup Schematic

Figure 4.2: Isometric View of Typical Test Setup

Simply-supported boundary conditions were simulated by using bearing plates fabricated with 2-inch-diameter round bar (shown in Figures 4.3 and 4.4), which act as the beam supports. One of the bearing plates was fabricated with the round bar welded to the bearing plate (simulating a "pinned" boundary condition) whereas the other was fabricated with a small groove, allowing the round bar to freely displace longitudinally (simulating a "roller" boundary condition). In addition, to prevent unintentional rotation at support reactions and increase the safety of the test conditions, lateral bracing was provided at support locations by equal-leg angles, connecting the flexural specimen to a lateral-resisting steel frame. Connection plates were welded to the outside webs of the testing specimen to connect the specimen to the bracing elements.

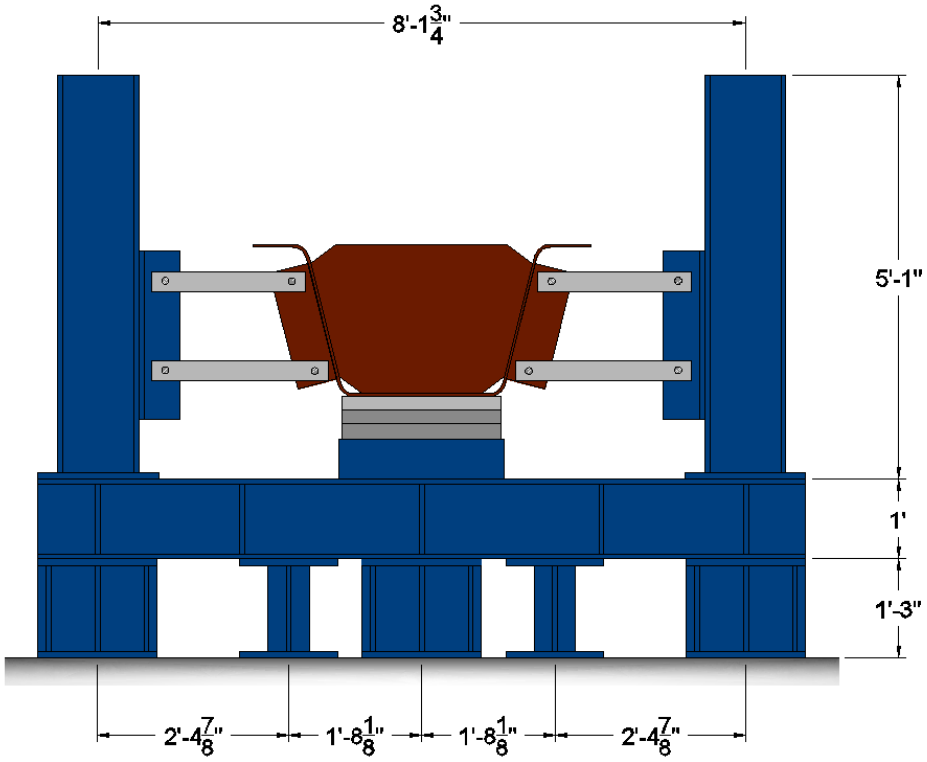

Figure 4.3: Typical Support Schematic

Figure 4.4: In-Place View of Typical Support Conditions

4.3 SPECIMEN DESCRIPTIONS

Four specimens were tested for this research effort:

- Two of the specimens (Experiments 1 and 2) consisted of a single tub girder specimen (comprised of HPS-50 steel) with a composite cast-in-place concrete deck.
- The remaining two specimens consisted of the noncomposite steel section alone.
    - The plate used for Experiment 3 consisted of HPS-50W weathering steel
    - The plate used for Experiment 4 consisted of HPS-50 steel. The girder was galvanized (hot-dipped) at AZZ Galvanizing Service (located in Canton, OH) prior to its arrival at the Major Units Lab.

The steel employed for each specimen was an 84" × 7/16" × 480" plate. Fabrication was performed by Greiner Industries, Inc. (located in Mt. Joy, PA) and American Tank & Fabricating (located in Cleveland, OH). Utilizing a standard plate, the tub girder was fabricated using a large capacity press-brake. Plates were aligned in the press-brake, and cold bent to achieve target bend radii. Coupons were taken from appropriate locations on the steel sections and tested by Turner-Fairbank's Highway Research Center to obtain material properties. Figure 4.5 shows the large-capacity press brake being used to form the testing specimen.

(a) (b)

Figure 4.5: Forming Process, (a) Press Brake, (b) Bending of Specimen's Top Flange.

Using the design studies discussed in Chapter 3, the optimum section using an 84" × 7/16" plate was found to have a top flange width of 6 inches and a total girder depth of 23

inches. Figure 4.6 shows a cross-section view of the press-brake tub girder design that was used for experimental testing. Two rows of 7/8" × 4" shear studs were welded on each top flange. End bearing plates were also utilized to prevent potential premature bearing failure during flexural testing (see Figure 4.7). A reinforced concrete deck was also cast on the top flanges of composite specimens as shown in Figure 4.8; it should be noted that the reinforcement pattern was designed according to the empirical deck method presented in Article 9.7.2 of AASHTO LRFD Specifications (AASHTO 2010).

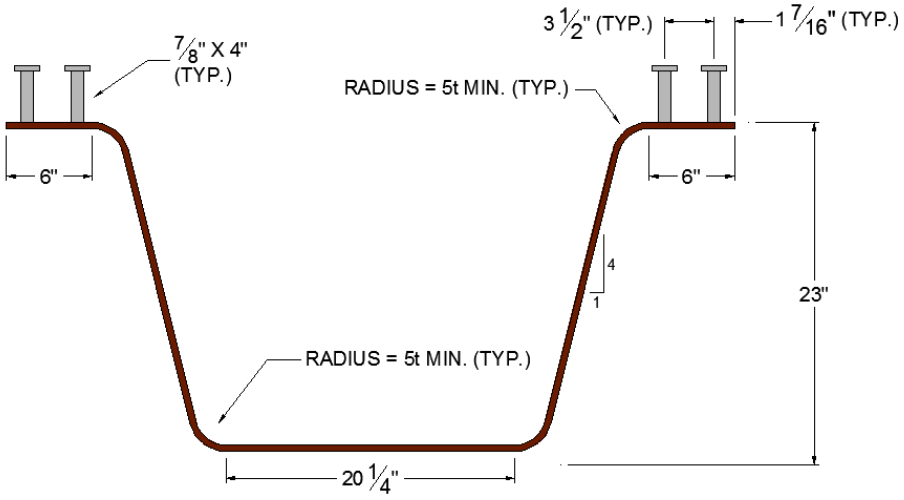

Figure 4.6: Testing Specimen Dimensions

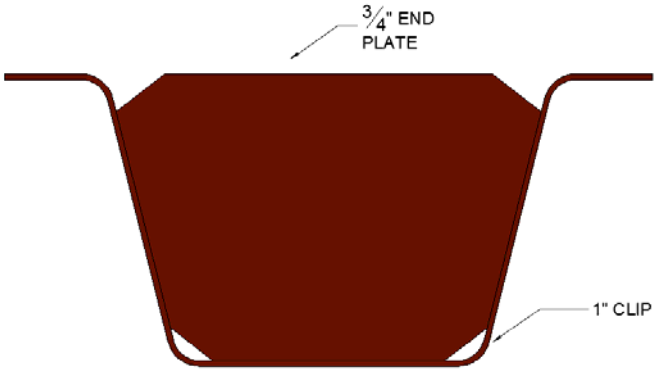

Figure 4.7: Bearing Plate

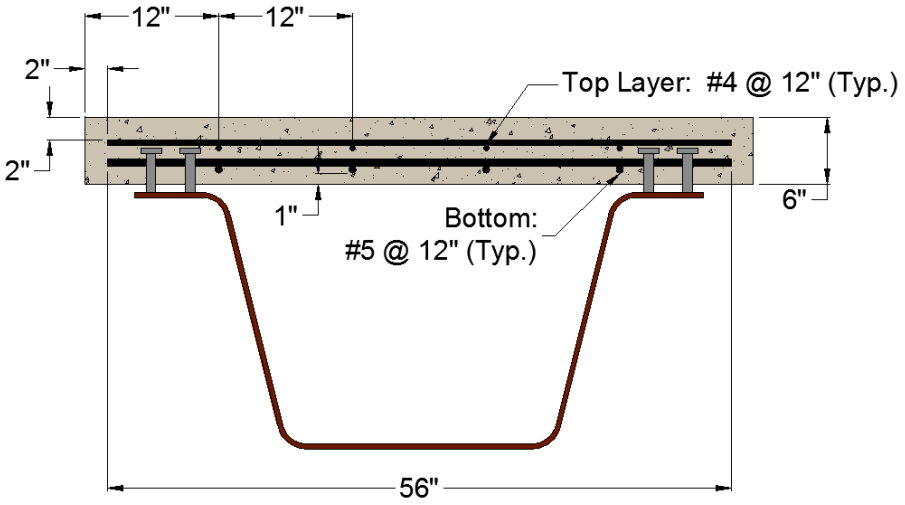

Figure 4.8: Deck Reinforcement for Composite Specimens

Once the steel girders were fitted in the testing frame, a system of deck forms was constructed around those specimens that were to be tested with a composite concrete deck. Figures 4.9 through 4.11 show a typical view of these forms, which were intended to support the weight of the uncured concrete deck, reinforcement and construction loads on the girder overhang.

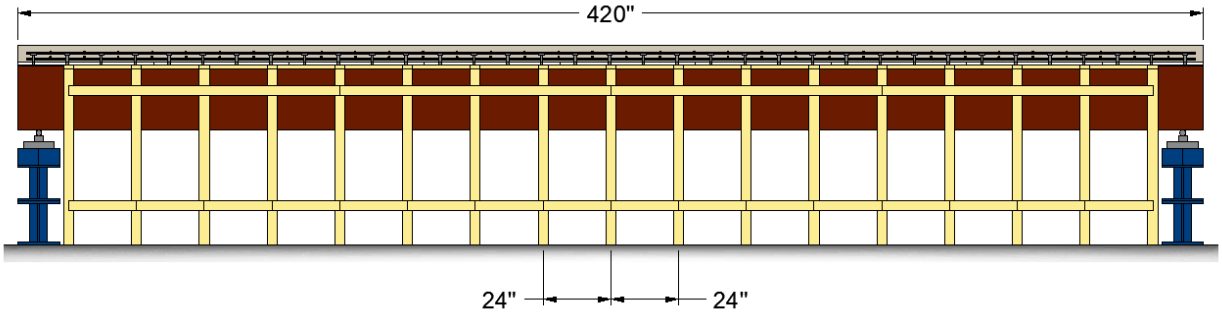

Figure 4.9: Elevation View Schematic of Deck Forms

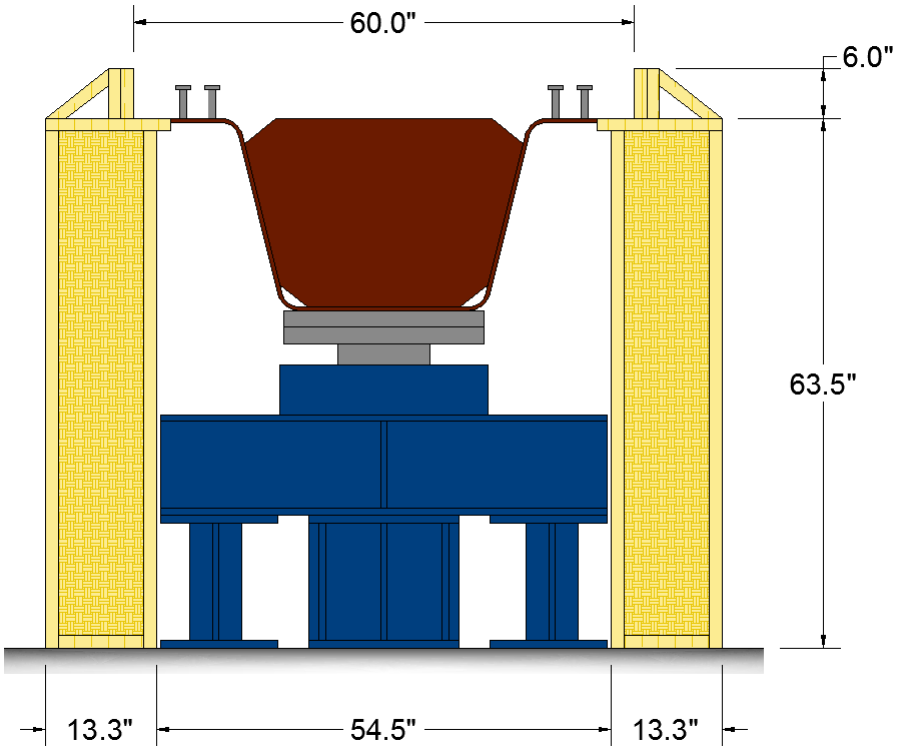

Figure 4.10: Section View Schematic of Deck Forms

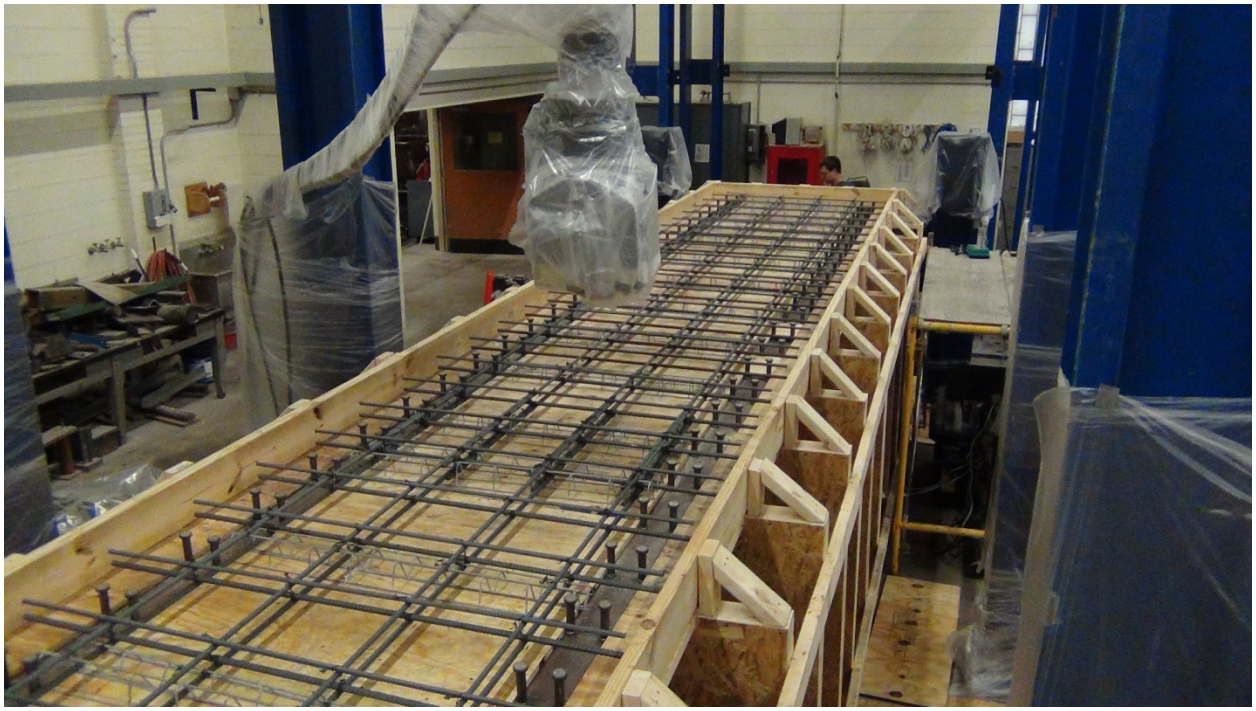

Figure 4.11: Isometric View of Deck Forms

Concrete was placed using a three-quarter yard concrete bucket (see Figure 4.12). After casting, the concrete deck was allowed to cure for 28 days before flexural testing.

Figure 4.12: Concrete Bucket Used for Deck Placement

4.3 INSTRUMENTATION

4.3.1 Instruments

Vertical deflections were determined by means of linear variable displacement transducers (LVDTs), each with a total range of 6 inches. In addition, two types of foil-resistor strain gages were employed: uniaxial strain gages were installed along the bottom flange of the girder, and rectangular rosettes were installed along the web of the girder. The load was applied using an MTS 330-kip servo hydraulic actuator.

The data was recorded using StrainSmart software (Micro-Measurements, Inc., 2010) in conjunction with a Micro-Measurements Model 5100 Scanner. This data acquisition system was also used to obtain the deflection data from the installed LVDTs.

4.3.2 Instrumentation Plan

A total of 18 strain gages were employed during flexural testing as shown in Figure 4.13. Six of these gages were uniaxial gages, placed along the bottom flange to capture tensile strains in the steel girder. The remaining gages were rectangular rosettes, placed along quarter points along the flat portion of the web to capture bending and shear strains. All of these strain gages were placed along a cross section 46 inches (or 2 × steel girder depth) away from the point of load application to avoid strain concentration effects.

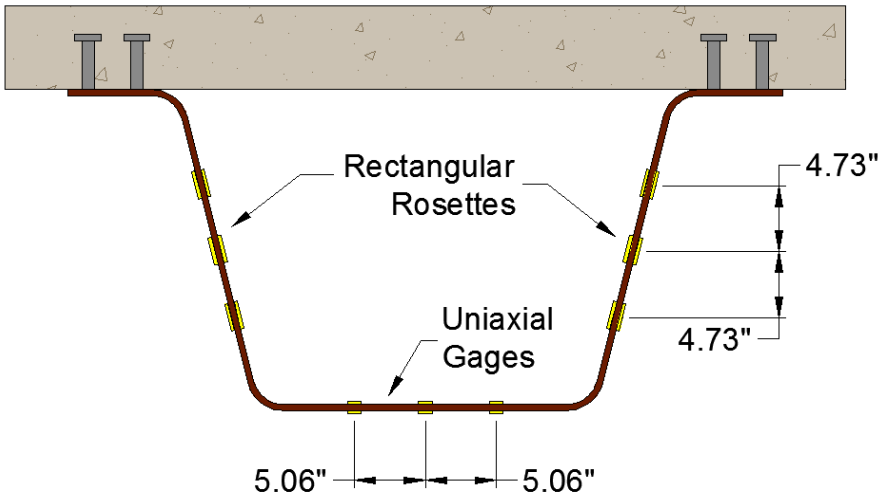

Figure 4.13: Typical Strain Gage Layout

Four LVDTs were placed along the girder to measure vertical deflections. Specifically, two LVDTs were placed at 0.50*L* (one on the edge of each top flange) and two were placed at 0.25*L*, where *L* is the span length. To prevent possible damage to the instruments, equal-leg angles were welded to the top flange to allow access to the LVDTs. These LVDT measurements were subsequently averaged to obtain vertical deflections at respective locations along the span of the specimen.

Figure 4.14: LVDTs Measuring Vertical Deflection

4.4 MATERIAL TESTING

Both the steel and concrete samples were tested to obtain material properties for use in subsequent finite element modeling and strain compatibility assessments of these members.

4.4.1 Steel Material Properties

Tensile coupons were taken from appropriate locations during the press-brake operation on the steel sections and tested by Turner-Fairbank's Highway Research Center. Specifically, five coupons were obtained (both in the longitudinal and transverse directions of rolling). Figure 4.15 shows the coupon test results from Turner-Fairbank's tensile testing. This data was subsequently used in analytical studies discussed in Chapter 5.

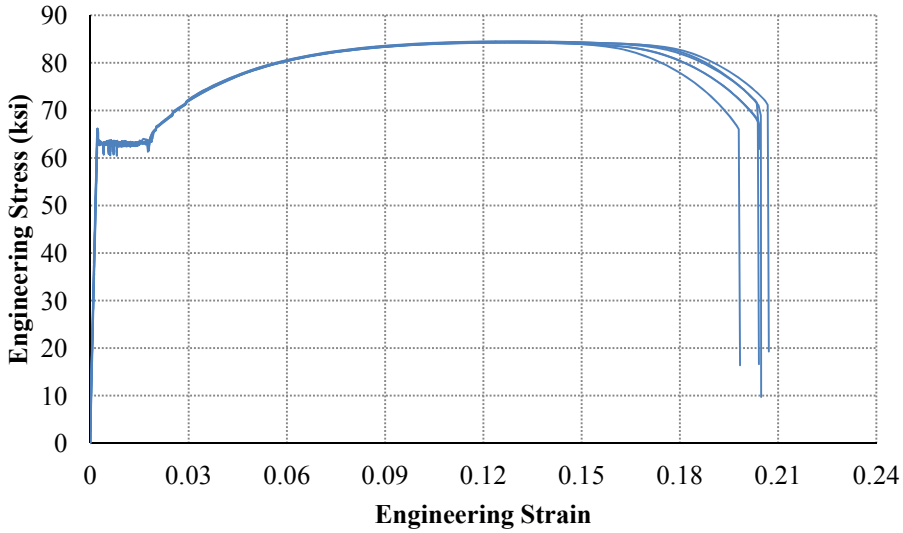

Figure 4.15: Results from Tensile Testing of Steel Coupons

4.4.2 Concrete Material Properties

For this test, six concrete cylinders were cast during deck placement. Cylinders were tested 28 days after casting to obtain in-place compressive strength of the flexural specimen. These compressive strengths were then averaged to obtain the compressive strength used in the analytical and mechanistic models. After testing, an average compressive stress of 4.1 ksi was found.

4.5 FLEXURAL TESTING

Once specimens were installed in the testing frame and instrumented (and, if applicable, the composite concrete deck was allowed to cure), load was applied until each specimen reached failure. During each test, readings were recorded from strain gages and LVDTs; these readings are summarized in Appendix C.

4.5.1 Testing Procedure

As previously stated, the test load was applied at midspan using a servo-hydraulic actuator which was mounted to a large structural reaction frame. To minimize bearing effects, for composite specimens load was applied through a steel spreader beam placed on top of an elastomeric bearing pad. For noncomposite tests, a WT section was fabricated to be bolted between top flanges; the steel spreader beam and elastomeric pad was then placed on top of the spreader for load application.

For safety and accurate data collection, each specimen was loaded in the stroke control. Each load step consisted of the application of a small increment of displacement (typically between 0.05 and 0.10 in.). Allowing for stabilization of the applied load, the following load step was applied after a time period of approximately 5 minutes had elapsed.

4.5.2 Composite Specimen Testing Results

Figure 4.16 shows the failure mode for a typical composite specimen. As shown, the failure modes of these specimens are governed by the section's ductility, exhibited by crushing of the concrete deck.

Figure 4.16: Typical Failure Mode for Composite Specimens

Midspan load-deflection results for the two composite specimens tested are shown in Figure 4.17. Both girders experienced a maximum deflection of approximately 3.1 inches and an average maximum applied load of approximately 304 kips at the moment of failure.

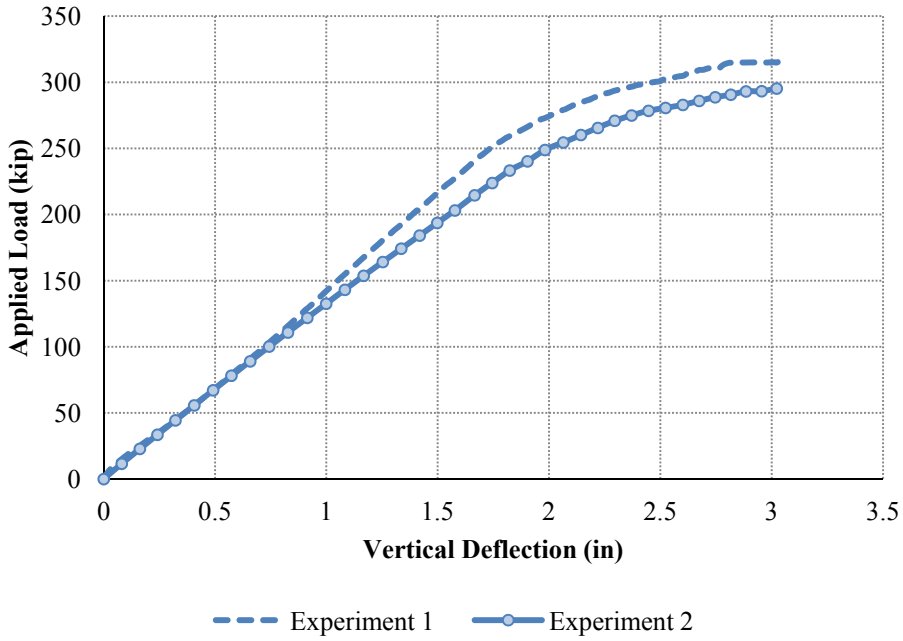

Figure 4.17: Load-Deflection Data from Flexural Testing of Composite Specimens

4.5.2 Noncomposite Specimen Testing Results

Figure 4.18 shows the failure mode for a typical noncomposite specimen. As shown, the failure modes of these specimens are governed by the section's stability, exhibited by excessive lateral deflection and twist.

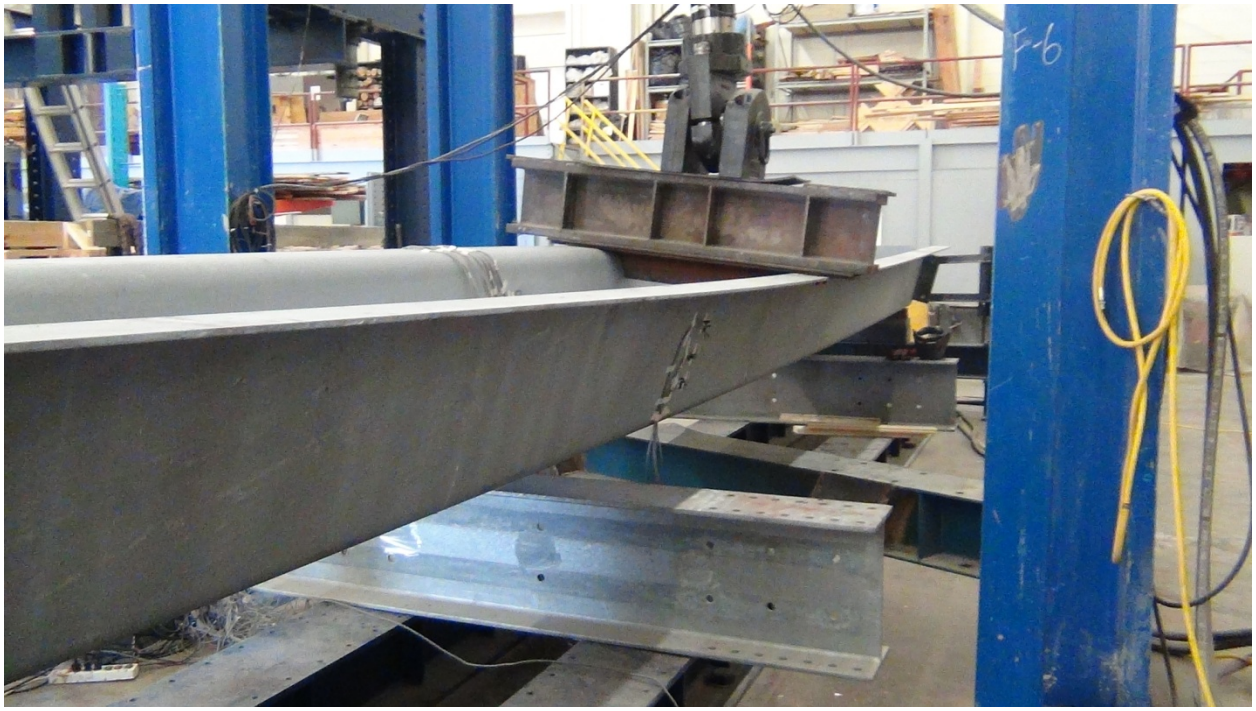

Figure 4.18: Typical Failure Mode for Noncomposite Specimens

Midspan load-deflection results for the two composite specimens tested are shown in Figure 4.17. Both girders exhibited linear behavior until failure. It should be noted that noncomposite testing was terminated when the girders exhibited excessive lateral deflection and twist. This behavior of the noncomposite is discussed further in Chapter 6.

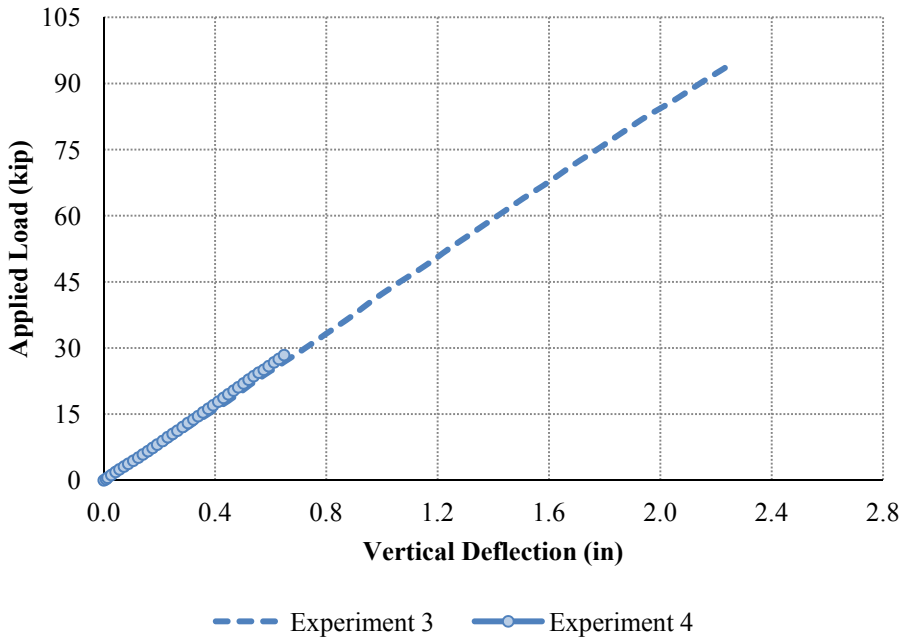

Figure 4.19: Load-Deflection Data from Flexural Testing of Noncomposite Specimens

4.6 CONCLUSION

The preceding chapter discussed flexural testing conducted on representative shallow steel press-brake-formed tub girder specimens. This data will be used to validate analytical studies on this system, discussed in Chapter 5.

CHAPTER 5: ANALYTICAL MODELING TECHNIQUES

5.1 INTRODUCTION

The following chapter details two separate analytical tools developed to accurately assess the behavior and capacity of the proposed press-brake tub girder system. The first is a three-dimensional nonlinear finite element modeling procedure for capturing the behavior and ultimate capacity of both noncomposite and composite press-brake tub girders. The second is a strain-compatibility approach developed to quickly determine the nominal flexural capacity of a composite press-brake-formed tub girder.

5.2 FINITE ELEMENT MODELING PROCEDURES

Finite element analysis was conducted in this study using the commercial finite element software package Abaqus/CAE (Dassault Systèmes, 2010). Modeling results were also benchmarked against experimental data to assess their validity and accuracy.

5.2.1 Element Selection

Abaqus is a commercial finite element software package which provides the user with a large library of elements for three-dimensional stress analysis. Therefore, it is necessary to initially investigate the suitability of a selected element type for a given problem. As shown by several researchers (Barth, 1996; Yang, 2004; Roberts, 2004; Righman, 2005), S4R shell elements are quite accurate in modeling the physical behavior of both noncomposite and composite steel plate girders. The S4R element is a 4-node general-purpose shell element intended to provide robust, accurate solutions for both thin and thick shells, using classical (Kirchhoff) shell theory when appropriate for relatively thin shells and thick (Mindlin) shell theory as the shell thickness increases. These elements allow for finite membrane strains and rotations of the shell. Therefore, they are suitable for large-strain analysis involving inelastic

deformation of materials. These elements also allow for change in shell thickness as a function of the membrane strain. In addition, consideration of transverse shear deformation is also included.

S4R elements employ "reduced" integration schemes; that is, for a four-noded element, only one Gauss integration point is used to form the element stiffness matrix. This integration scheme yields several advantages over traditional shell elements. For example, reduced integration computes strains and stresses at the locations known to provide optimal accuracy; thus, reduced integration usually produces more accurate results, provided the elements are not disturbed or loaded in in-plane bending. The use of fewer integration points also benefits the user by resulting in reduced computing time and storage requirements. The primary disadvantage of using reduced integration is that deformation modes that cause no strain at the integration points may develop. This may lead to inaccurate results if these zero-energy modes propagate through the structure in a phenomenon commonly known as hourglassing. However, this can be prevented by the user by introducing a small artificial stiffness associated with zero-energy deformation modes using the *SECTION CONTROLS command in an Abaqus input file.

5.2.2 Material Modeling

5.2.2.1 Structural Steel

Elements simulating steel in this study were modeled using an elastic-plastic constitutive law including strain hardening effects. Specifically, the steel was modeled using the *PLASTIC command in the Abaqus input file, which designates a material with a material with a standard von Mises yield surface, an associated plastic flow rule (Chen & Han, 1988), and isotropic work hardening. This type of material model has been found to be suitable to represent rate-independent behavior of a metal subjected to a relatively monotonic loading where creep effects are non-critical (Barth, 1996; Yang, 2004).

A multilinear relationship (Galindez, 2009) was used to represent the stress-strain characteristics used in the material modeling. This material model is shown in Figure 5.1, and the expressions employed to compute the curve are listed in Table 5.1. The values used to define key points in the nonlinear region of the curve are based on the coupon testing of samples discussed in Chapter 4 and are listed in Table 5.2. The stress-strain relationship described is then

converted into terms of true stress and true plastic strain (Chen & Han, 1988), as required for input into an Abaqus input file.

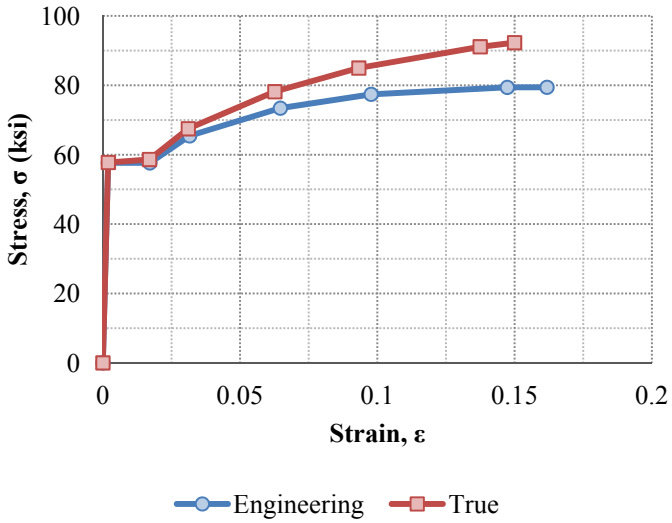

Figure 5.1: Multilinear Stress-Strain Curve

Table 5.1: Expressions for Computing Steel Stress-Strain Behavior (Galindez, 2009)

Point	Strain	Stress
1	$\varepsilon_1 = \frac{\sigma_y}{E}$	$\sigma_1 = \sigma_y$
2	$\varepsilon_2 = \varepsilon_{st}$	$\sigma_2 = \sigma_y$
3	$\varepsilon_3 = \frac{1}{10}(\varepsilon_u - \varepsilon_{st}) + \varepsilon_{st}$	$\sigma_3 = \frac{E_{st}}{10}(\varepsilon_u - \varepsilon_{st}) + \sigma_y$
4	$\varepsilon_4 = \frac{2}{7}(\varepsilon_6 - \varepsilon_3) + \varepsilon_3$	$\sigma_4 = \frac{4}{7}(\sigma_6 - \sigma_3) + \sigma_3$
5	$\varepsilon_5 = \frac{2}{7}(\varepsilon_6 - \varepsilon_3) + \varepsilon_4$	$\sigma_5 = \frac{2}{7}(\sigma_6 - \sigma_3) + \sigma_4$
6	$\varepsilon_6 = \varepsilon_u - \frac{1}{10}(\varepsilon_u - \varepsilon_{st})$	$\sigma_6 = \left(\frac{\sigma_y}{\sigma_{0.2\%}}\right)\sigma_u - \frac{100}{E_{st}}(\varepsilon_u - \varepsilon_{st})$
7	$\varepsilon_7 = \varepsilon_u$	$\sigma_7 = \left(\frac{\sigma_y}{\sigma_{0.2\%}}\right)\sigma_u$

Table 5.2: Average Steel Plate Properties

Property	Average Value
Modulus of Elasticity, E (ksi)	29559
Static Yield Stress, σ_y (ksi)	60.962
Offset Yield Stress, $\sigma_{0.2\%}$ (ksi)	63.050
Strain at the Onset on Strain Hardening, ε_{st} (%)	1.7883
Strain Hardening Modulus, E_{st} (ksi)	1033.5
Tensile Stress, σ_u (ksi)	84.382
Strain at the Tensile Stress, ε_u (%)	13.165

5.2.2.2 Reinforced Concrete

Elements modeling reinforced concrete in this study are modeled using a smeared crack concrete model in conjunction with reinforcement definitions for appropriate elements. Specifically, the concrete is modeled using the *CONCRETE and *TENSION STIFFENING commands in the Abaqus input file. The concrete model is a smeared crack model in the sense that it does not track individual "macro" cracks. Constitutive calculations are performed independently at each integration point of the finite element model. The presence of cracks enters into these calculations by the way in which the cracks affect the stress and material stiffness associated with the integration point. Cracks are irrecoverable: they remain for the rest of the calculation (but may open and close). Following crack detection, the crack affects the calculations because a damaged elasticity model is used (Dassault Systèmes, 2010). This type of material model has been found to be suitable to represent rate-independent behavior of reinforced concrete subjected to a relatively monotonic loading where creep effects are not important (Roberts, 2004).

The Comitè Europèen du Bèton (CEB) concrete model (Roberts, 2004) was chosen to represent the compressive concrete properties used in the analyses in this work. Previous research by Roberts has shown that the CEB model (see Equation 5.1) successfully captures the compressive behavior of the type of decks studied in this work. Figure 5.2 shows the CEB compressive model for a compressive strength of 4.1 ksi (equal to the average compressive stress

found in the cylinder samples discussed in Chapter 4), with a concrete crushing strain of 0.003. Tension behavior is modeled using a simple bi-linear constitutive model as shown in Figure 5.3.

$$\sigma_c(\varepsilon_c) = \frac{0.85 f_c' (a - 206000\varepsilon_c)\varepsilon_c}{1 + b\varepsilon_c} \qquad \text{Eq. 5.1}$$

where: σ_c = concrete compressive stress (ksi)

ε_c = concrete compressive strain

f_c' = concrete compressive strength (ksi)

$$a = 6193.6\left(0.85 f_c' + 1.015\right)^{-0.953}$$

$$b = 8074.1\left(0.85 f_c' + 1.450\right)^{-1.085} - 850$$

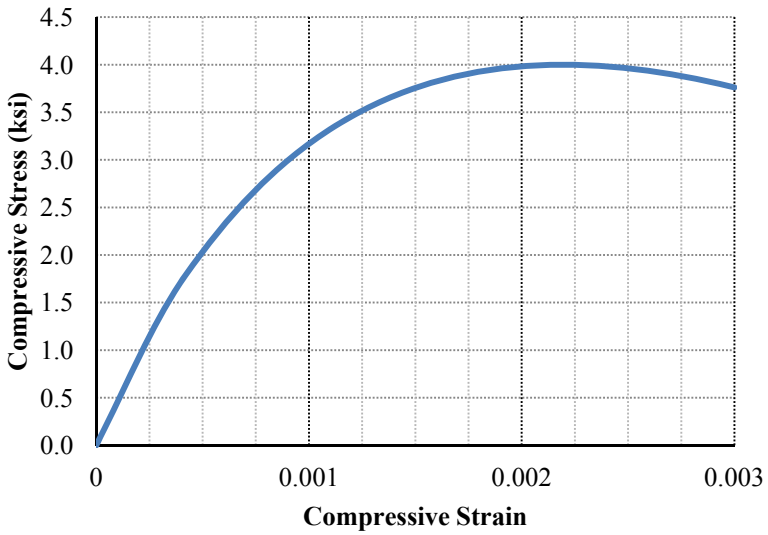

Figure 5.2: Stress-Strain Curve for Reinforced Concrete (Compression Region)

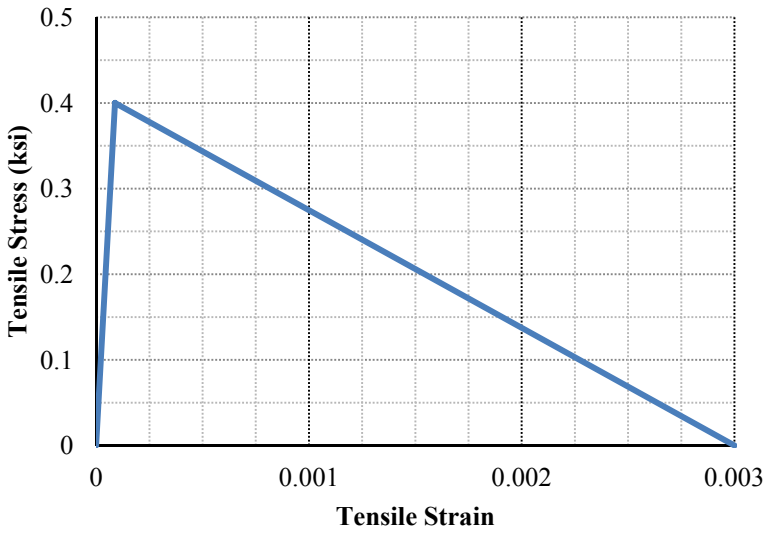

Figure 5.3: Stress-Strain Curve for Reinforced Concrete (Tension Region)

The modeling of elements simulating concrete also incorporates steel reinforcement within the deck. This is included by using the *REBAR option in the Abaqus input file and is represented by a smeared layer of reinforcement at the specified location within the deck. The material model for steel reinforcement is essentially the same as for structural steel, as discussed in Section 5.2.2.1. The stress-strain curve utilized for rebar is taken from Roberts (2004) and simulates steel with a modulus of elasticity of 29000 ksi and a yield stress of 60 ksi.

5.2.3 Additional Modeling Considerations

Composite steel girders undergoing flexure predominately experience failure due to either yielding of steel elements in tension or loss of stiffness of concrete components due to excessive compressive stress or cracking. However, in noncomposite steel girders, because elements in compression are not restrained by the concrete deck, the girder can experience a variety of buckling modes, such as lateral torsional buckling, local flange buckling, and local web buckling. Therefore, when modeling noncomposite steel girders in flexure, additional considerations, such as the incorporation of geometric imperfections of the girder during fabrication and residual stresses due to flame cutting and welding, must be taken to ensure accurate modeling of structural behavior of steel flexural elements.

5.2.3.1 Application of Geometric Imperfections

The nonlinearity in response due to the presence of initial imperfections of the girder has a measurable impact on girder response under flexural loads due to the girder's susceptibility to various buckling modes. Furthermore, from the numerical analysis point of view, the modified Riks method of analysis (as discussed in Section 5.2.4) used in this work is a type of post-buckling analysis. Thus, a continuous response is required as opposed to bifurcation. This can be accomplished by introducing a geometric imperfection pattern in the "perfect" geometry so that some degree of amplification occurs before the critical load is reached, as would occur in actual girders. Therefore, introduction of geometric imperfections is a critical step in this type of analysis.

In welded plate girders, initial geometric imperfections are generally generated during the welding process and result in initial out-of-flatness of the long steel plates. Three types of geometric imperfections are considered in this work in order to capture these characteristics: an out-of-flatness of the web, a tilt of the compression flange, and a lateral sweep of the compression flange. These imperfections are illustrated in Figure 5.4.

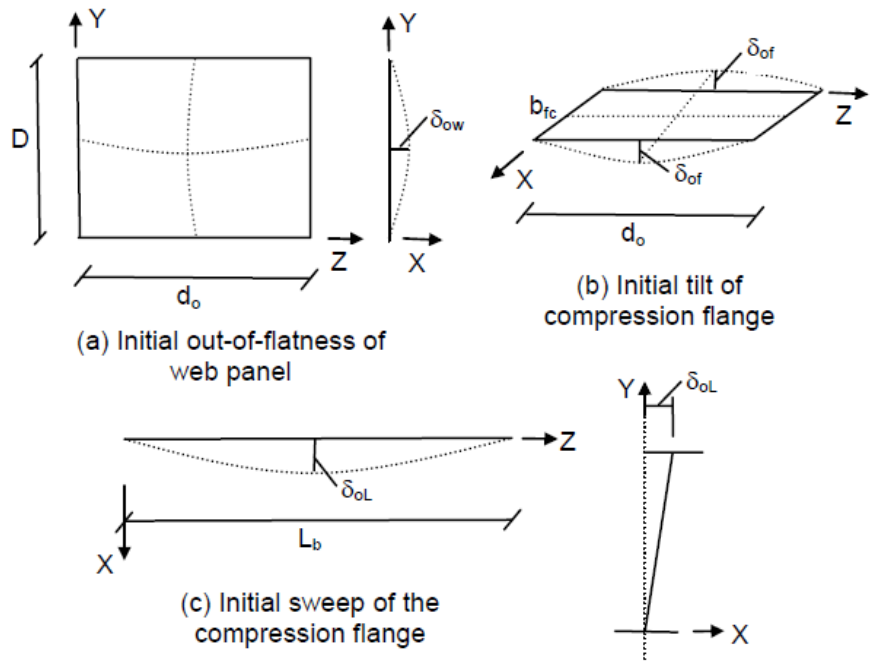

Figure 5.4: Initial Geometric Imperfections Patterns (Yang, 2004)

The values prescribed for these three types of imperfections are based on maximum allowable tolerances specified by the American Welding Society (AWS) and engineering judgment (Yang, 2004). For example, AWS specifies alternative tolerances for the initial out-of-flatness of the web, depending on if the girder is stiffened. For girders with one-sided transverse stiffeners, the maximum allowable initial out-of-flatness of the web, δ_{ow}, is d / 67, where d is the minimum panel dimension, either the web depth (D) or distance between stiffeners (d_o). Alternatively, the maximum allowable value is D / 150 for unstiffened girders. In this study δ_{ow} is prescribed to be equal to d / 100, which is chosen to represent a midpoint between the above two requirements. This maximum value of distortion occurs at the center of each web panel and the amount of out-of-flatness at all other locations in the web panel decreases in a half sine wave pattern, in both the X and Y-directions. Furthermore, the direction of δ_{ow} alternates in adjacent web panels.

The maximum allowable tilt of the flanges, δ_{of}, specified by AWS is equal to b_f / 100 or 0.25 in., whichever is greater. However, it is felt that it is unlikely that the distortion of the flange would be this severe in girders with relatively short panel lengths. Therefore, δ_{of} is assigned to be the lesser value of b_{fc} / 150 or $0.3d_o$ / 150 = d_o / 500. This results in values slightly less than that permitted by AWS for girders with long panel lengths (i.e., $b_{fc} < 0.3d_o$), while for short panels, δ_{of} may be significantly less than AWS tolerances. The maximum value of δ_{of} occurs at the horizontal center of each web panel along the flange edge. The value of δ_{of} decreases in a sine-wave pattern along the length of the girder and also decreases linearly along the width of the flange. The direction of δ_{of} also alternates in adjacent panels.

AWS limits the variation in straightness of welded girders to 1/960th of the girder length. In this work, a lateral sweep of the compression flange (δ_{oL}) is specified to be somewhat less than this limit, with a maximum value equal to L_b / 1500, where L_b is the distance between lateral bracing. This value is prescribed at the center of the lateral bracing segment at the web-compression flange junction. The value of δ_{oL} varies in a sine wave pattern along the longitudinal direction of the girder and varies linearly along the depth of the girder. As with the other imperfections, the direction of δ_{oL} alternates in adjacent lateral bracing segments. Furthermore, δ_{oL} and δ_{ow} are prescribed in the same direction within each web panel so that the effects of these two imperfections are cumulative.

5.2.3.2 Application of Residual Stresses

The longitudinal residual stresses in welded I-girders are primarily caused by flame cutting of the plates and longitudinal welding between the flanges and the web. Typically, the tensile residual stresses are essentially equal to the yield stress of the material within a small area, termed the heat affected zones, while a smaller, near-constant self-equilibrating compression stress is developed within the other regions of the plates. The residual stress distribution may be idealized by assuming that when the section is free of external forces, the residual stresses over the entire cross-section must satisfy equilibrium and sum to zero.

In this study, residual stress effects are represented by specifying initial stress conditions at the beginning of the analysis through a user-defined sub-routine, which automatically applies a prescribed magnitude of initial (residual) stress to each element depending on the elements location in the girder. When initial stresses are given, the initial stress state may not be in exact equilibrium for the finite element matrix. Therefore, an initial step is included to allow Abaqus to check for equilibrium and iterate, if necessary, to achieve equilibrium. Specifically, a *STATIC step, where girder dead load is also applied, is implemented before the Riks analysis to insure that equilibrium is satisfied once residual stresses have been included.

The residual stress pattern that is used in this study is shown in Figure 5.5. This stress distribution is considered a reasonable approximation of the actual residual stresses induced by welding and flame cutting in typical plate girders (Righman, 2005).

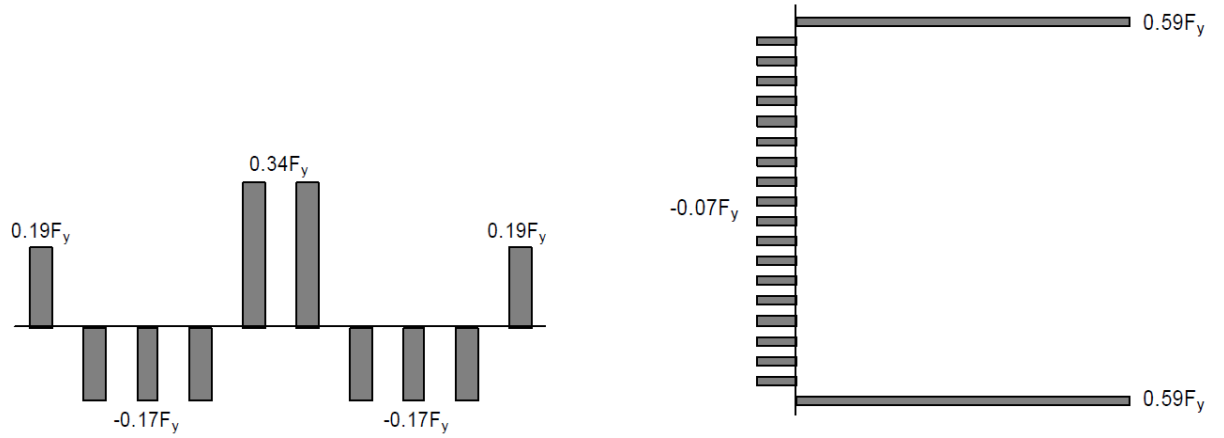

(a) Residual Stress Pattern for Flanges (b) Residual Stress Pattern for Webs

Figure 5.5: Gauss Ppoint Residual Stresses (Righman, 2005)

5.2.4 Solution Algorithm

To capture the load-deflection response of the finite element models, unstable collapse and post-buckling analysis procedures were needed to trace the complete nonlinear load-deflection behavior. Specifically, a modified Riks algorithm available in Abaqus, shown in Figure 5.6, was used to analyze the girders.

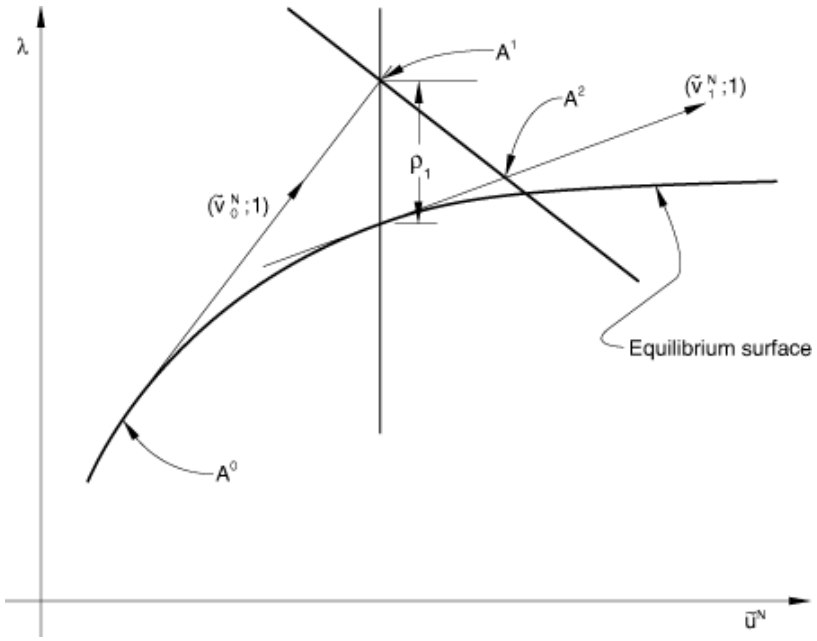

Figure 5.6: Modified Riks Algorithm (Dassault Systèmes, 2010)

Assuming the loading is proportional (i.e., all load magnitudes vary with a single scalar parameter) and that the response is reasonably smooth (sudden bifurcations do not occur), the modified Riks method uses the load magnitude as an additional unknown and solves simultaneously for loads and displacements. Because the progress of the solution is independent of the load increment, Abaqus uses the "arc length," which is the distance along the static equilibrium path in load-displacement space, to control the increment size. The "arc length" value is initially set by the users and is later adjusted by the Abaqus automatic load increment algorithm based on the convergence rate. The fundamental nature of the method is that the solution is viewed as the discovery of a single equilibrium path in a space defined by the nodal variables and the loading parameter (Dassault Systèmes, 2010).

Development of the solution requires navigation of this path as far as required. The basic algorithm remains the Newton method; therefore, at any time there will be a finite radius of convergence. During each increment, the solution is found by moving a given distance along the tangent line to the current solution point and then searching for equilibrium in the plane that not only passes through the point obtained, but also is orthogonal to the same tangent line. The total path length traversed is determined by the load magnitudes supplied by the user in the loading options. The number of increments is determined by the user-specified time increment data, assisted by Abaqus automatic incrementation scheme, if chosen.

Also important to note is that the number of Gauss integration points through the slab thickness has been changed from 5 points (the Abaqus default value) to 7 points and a linear search technique by changing the load level during iteration is used. These changes have been well established to better capture the crushing and cracking of the concrete and speed of convergence (Barth & Wu, 2006).

5.3 VERIFICATION OF FINITE ELEMENT MODELING

In order to assess the validity of these modeling techniques, experimental data from previous laboratory experiments were employed as a benchmark. Discussed herein are the benchmark tests utilized and results from comparisons between experimental and analytical results.

5.3.1 Benchmark Analysis #1: Schilling and Morcos (1988)

In 1988, Schilling and Morcos tested three steel plate girders in order to determine moment-rotation characteristics of steel girders with ultra-compact flanges. These three girders (denoted "S" for shallow, "M" for medium depth, and "D" for deep) were tested in three-point bending and loaded until failure. Figure 5.7 shows the details of the "D" girder, which was used for benchmarking.

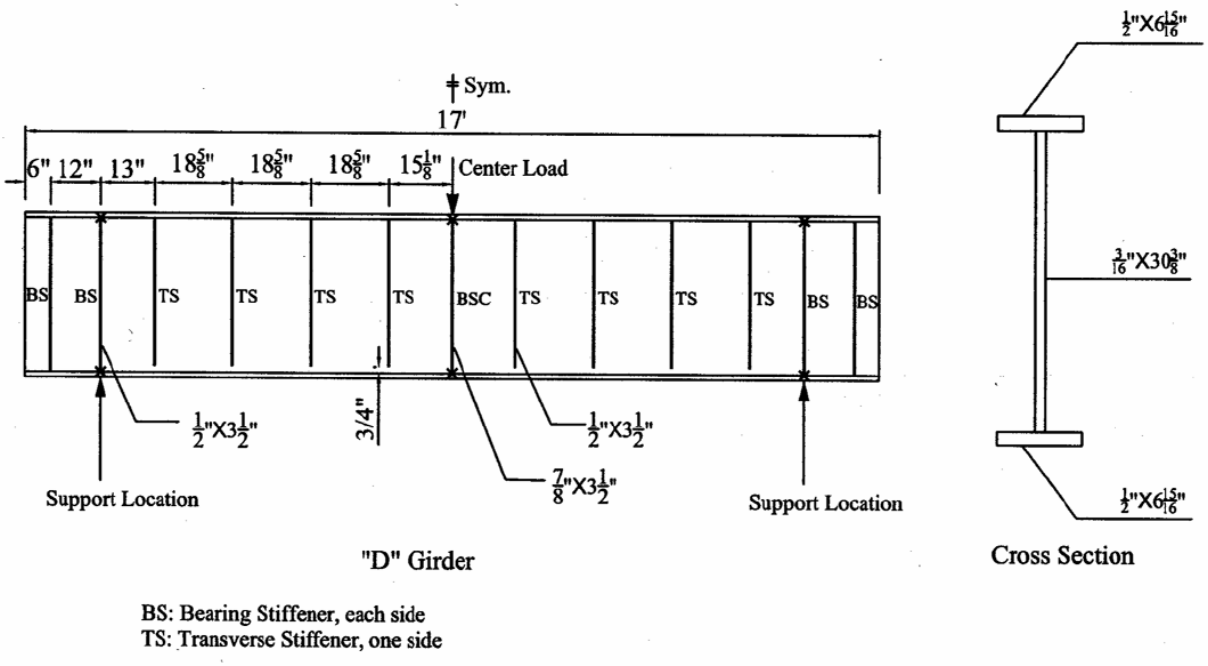

Figure 5.7: "D" girder from Schilling and Morcos (1988).

The selection of relatively large elements will result in unrealistically low predicted strengths due to the effects of stress concentrations, while relatively small elements can cause an overestimation of the energy dissipation capacity (Righman, 2005). By selecting the appropriate mesh density, these situations will be avoided, and accurate results can be obtained. Previous research by Yang (2004) has evaluated the ideal mesh density for steel I-girders of the type investigated in this study. This assessment included an evaluation of the accuracy and processing time for models with three different mesh densities: a relatively course mesh with 4 elements across the width of each flange and 6 elements throughout the height of the web, an intermediate mesh density with 6 elements across the width of the flange and 10 elements throughout the height of the web, and a fine mesh density with 10 elements across the flange width and 20 elements through the web height. Yang concluded that the ideal mesh density was the combination of 10 elements across the flange width and 20 elements throughout the web height, which resulted in less than 1% error compared to selected experimental results. Thus, this same element size for this evaluation.

Furthermore, the aspect ratio is minimized (made closest to 1) to the extent possible. Using the mesh density discussed above, there are twice as many elements in the web as there are in each flange. However, the web height is typically three to four times the width of the

compression flange. Because it is desirable for the web and flange elements to have equal lengths so that these elements will share coincident nodes, it is not possible to choose the element length so that the web and flange will both have an aspect ratio of 1. Instead, an element length is selected that gives an equal aspect ratio in the compression flange and the web, which typically results in an aspect ratio of approximately 1.4 for all elements.

A finite element model was created using the aforementioned modeling technique to model the "D" girder. The load-deflection curve from experimental testing was plotted and compared with finite element analysis results, and is shown in Figure 5.8. As shown, the proposed modeling technique is efficient in capturing the nonlinear behavior of this experimental test.

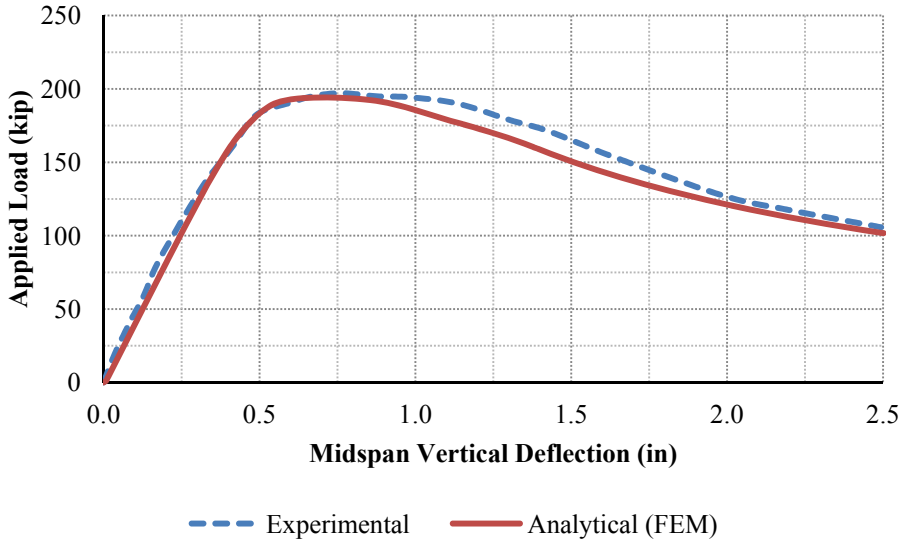

Figure 5.8: Comparison of Schilling and Morcos (1988) "D" Girder Test and FEA Results

5.3.2 Benchmark Analysis #2: Lay et al. (1964)

In 1964, Lay et. al. tested numerous steel elements to failure to assess the impacts of utilizing plastic design procedures for structural steel. For this benchmark assessment, test "HT-29," a uniform bending test on a rolled W10×25 was selected. Figure 5.9 shows the details of the HT-29 laboratory test.

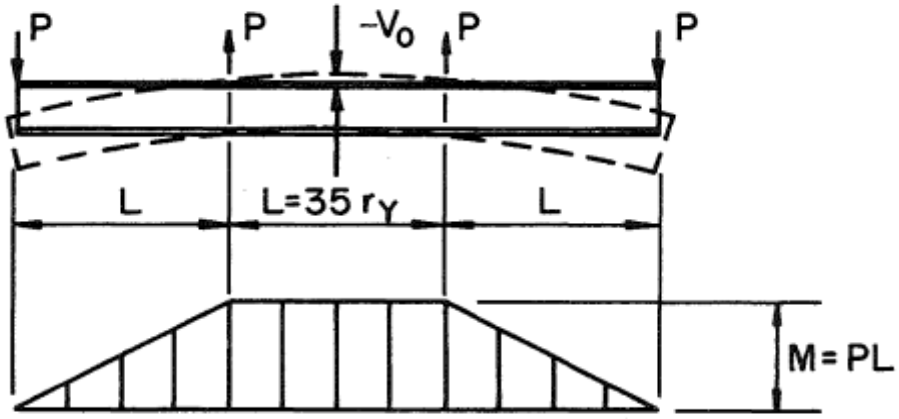

Figure 5.9: "HT-29" Girder Test Schematic (Lay et. al. 1964)

A finite element model was created using the aforementioned modeling technique (incorporating the same target mesh density as discussed in Section 5.3.1) to model the "HT-29" girder. The load-deflection curve from experimental testing was plotted and compared with finite element analysis results, and is shown in Figure 5.8. As shown, the proposed modeling technique is efficient in capturing the nonlinear behavior of this experimental test.

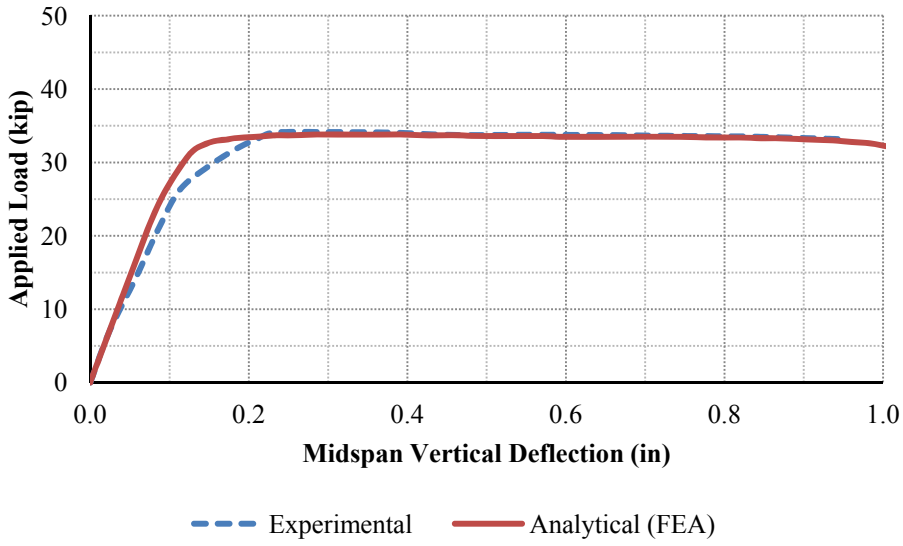

Figure 5.10: Comparison of Lay et. al. (1964) "HT-29" Girder Test and FEA Results

5.3.4 Modeling of Press-Brake Tub Girder Flexural Tests

Figure 5.11 illustrates a finite element mesh of a composite press-brake-formed tub girder specimen. As shown, shell elements are employed to simulate the behavior of the steel and concrete components of the girder. A nonlinear analysis utilizing this mesh is compared against the experimental tests discussed in Chapter 4 (additional comparisons for individual gages and instruments are shown in Appendix C). As shown in Figure 5.12, the model is shown to accurately capture the behavior of the system until failure.

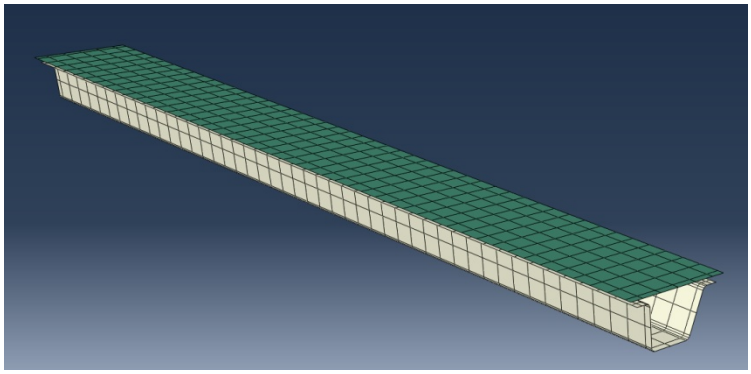

Figure 5.11: Finite Element Model of Composite Press-Brake-Formed Steel Tub Girder

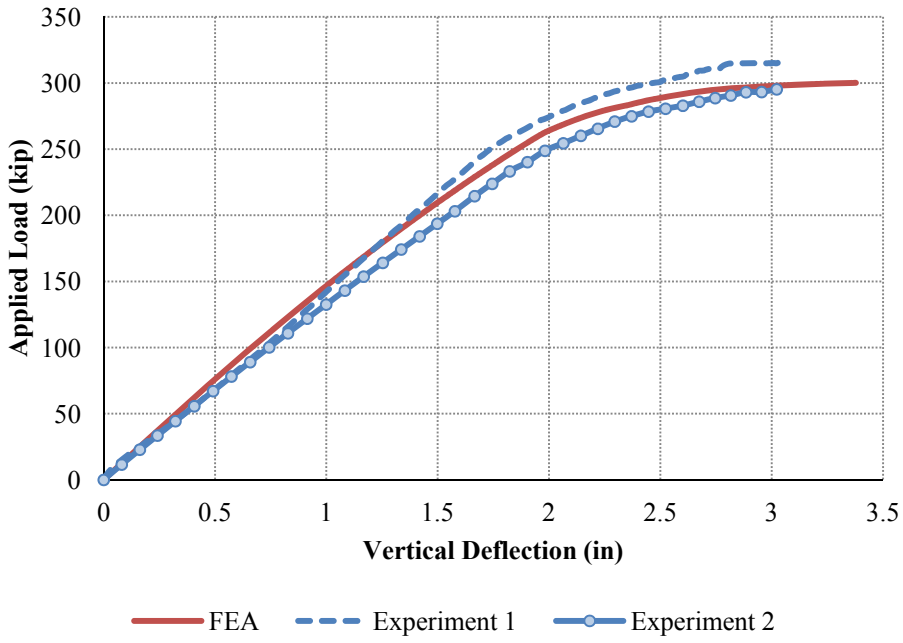

Figure 5.12: Comparison of Experimental and Analytical Results (Composite Tests)

Figure 5.13 illustrates a finite element mesh of a non composite press-brake-formed tub girder specimen. As shown, shell elements are employed to simulate the behavior of the girder and WT section (utilized for load application). A linear analysis utilizing this mesh is compared against the experimental tests discussed in Chapter 4 (additional comparisons for individual gages and instruments are shown in Appendix C). As shown in Figure 5.14, the model is shown to accurately capture the behavior of the system.

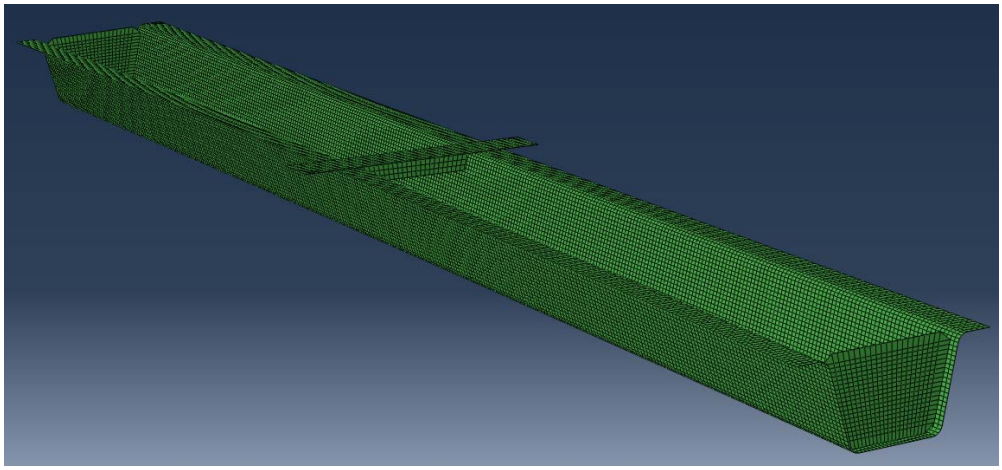

Figure 5.13: Finite Element Model of Noncomposite Press-Brake-Formed Steel Tub Girder

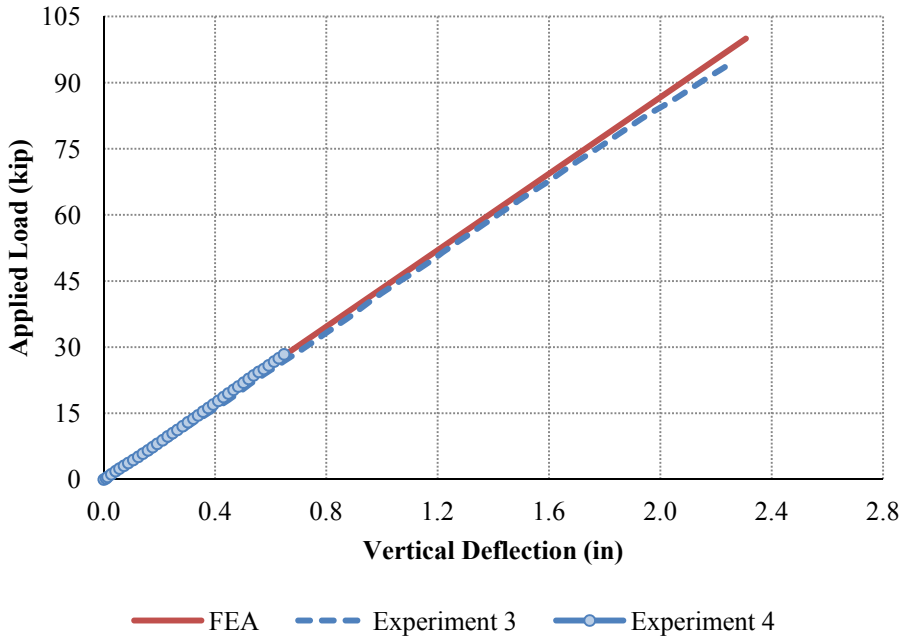

Figure 5.14: Comparison of Experimental and Analytical Results (Noncomposite Tests)

5.4 STRAIN-COMPATIBILITY ASSESSMENT

To assess the flexural capacity of press-brake tub girders, a strain compatibility based analysis procedure was developed using MATLAB (The Mathworks, Inc., 2010). The results of this assessment are used to determine a reasonable estimate of ultimate flexural capacity for design purposes. Subsequent verification of this procedure through refined FEA modeling as previously discussed. For more information and illustrative examples utilizing this procedure, the reader is referred to Appendix B.

5.4.1 Initial Assumptions

Using the mechanistic strain compatibility procedure, it was possible to determine the ultimate flexural capacity of a given cross-section defined by geometric and material properties. By assuming a ratio M_{DL} / M_y of the dead load moment acting on the non-composite steel girder (M_{DL}), the initial strains present on the section before deck casting could be determined as a percentage of the non-composite yield moment (M_y). Assuming this ratio allowed for the dead load effects to be accounted for in strain-compatibility analyses.

5.4.2 Iterative Procedure

Assuming a concrete strain of 0.003 at crushing and a linear strain distribution, the ultimate capacity of a typical composite press-brake tub girder girder in positive flexure can be predicted using the following iterative procedure (a MATLAB m-file was employed to perform these iterative calculations):

1. Compute the yield moment of the non-composite steel section
2. Use the assumed ratio of the non-composite dead load to the yield moment of the non-composite section, M_{DL} / M_y, to compute a dead load moment.
3. Assume a concrete crushing strain at the top of the deck equal to 0.003 and a subsequent linear strain distribution
4. Choose an assumed value to the depth of the neutral axis from the top of the deck
5. Using the linear strain distribution and superimposing the strains induced by dead load effects on the non-composite steel girder, the final strain profile is determined
6. The cross-section of the composite press-brake tub girder is divided into transverse slices; the number of slices is chosen to be large (for this study, the depth of each slice is chosen to be 0.1 inches) to attain acceptable accuracy
    - For a given slice, the out-to-out width of the girder at the mid-depth of the slice is computed.
    - The slice is then assumed to be rectangular in shape (with the width equal to the calculated out-to-out width of the girder and the thickness equal to the slice depth)
7. Compute the stress in each slice
    - For steel slices, the stress is assumed to be the minimum of E × the strain or the yield stress, F_y.
    - For concrete slices, the stress is assumed to be 0.85 f_c' for slices in compression and zero for slices in tension.
8. Compute the force in each slice by multiplying the stress in each slice by the area of each slice (it should be noted that, since each slice is assumed to be rectangular in shape, the area of each slice is simply the width of a slice multiplied by its thickness)
9. Sum the forces of each slice; if the calculated sum is not equal to zero, adjust the value of the assumed neutral-axis depth and repeat steps 4-8

10. Once the depth of neutral axis is determined, the nominal moment capacity may be determined by summing the moments produced by the forces in each slice about the neutral axis.

5.4.3 Results of Strain-Compatibility Analysis

Figure 5.15 shows a comparison of the analytical (FEA) and strain-compatibility results. As shown, the strain compatibility analysis proves quite well in predicting the ultimate capacity of the composite press-brake tub girder specimen.

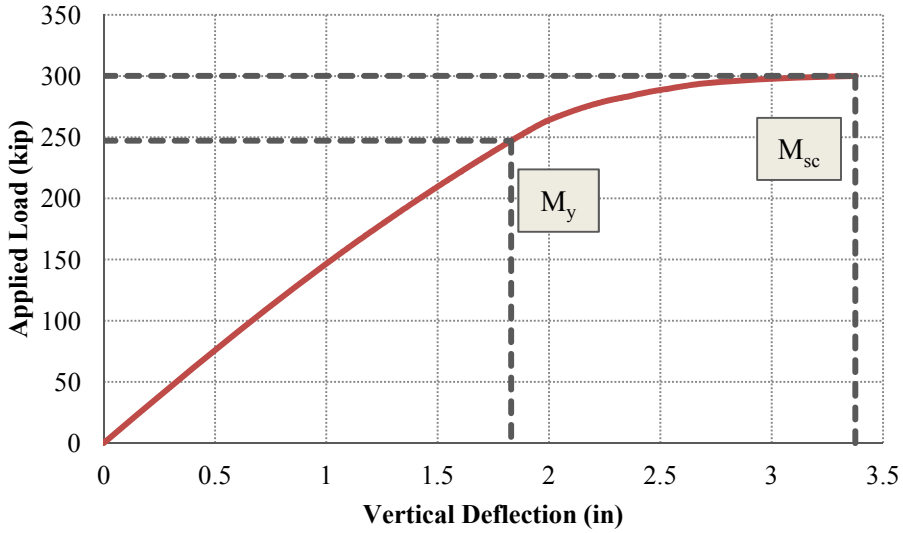

Figure 5.15: Comparison of Analytical (FEA) and Strain-Compatibility Results

5.5 CONCLUSION

The contents of this chapter have detailed two separate analytical tools for assessing the proposed press-brake tub girder system. The accuracy of these tools has been benchmarked against previous tests as well as the experimental investigations discussed in Chapter 4. The results of these assessments show that the proposed analytical tools accurately capture the behavior of the proposed press-brake-formed tub girder system. These tools will be used in the following chapter to further assess the behavior of the proposed system.

CHAPTER 6: BEHAVIORAL STUDIES

6.1 INTRODUCTION

The purpose of this chapter is to present several studies focused on assessing the behavior of the proposed system. The goal of these studies was to determine the applicability of AASHTO LRFD Specifications for the proposed system. Specifically, the capacity of the modular composite unit and the stability of the noncomposite press-brake-formed steel girder was assessed.

6.2 ASSESSMENT OF COMPOSITE UNIT CAPACITY

Utilizing the analytical procedures discussed in Chapter 5, a comprehensive study was conducted evaluating the applicability of AASHTO LRFD Specifications for computing the nominal flexural of composite press-brake-formed tub girders. Presented in this section are the results of this study, along with recommended expressions for computing the nominal flexural capacity of compact composite units.

6.2.1 AASHTO Requirements for Compact Composite Girders

AASHTO (2010) outlines a series of conditions must be met in order for a composite box girder to be considered compact. The first of these conditions is that the yield strength of the flanges must not exceed 70 ksi; this condition is easily met by simply choosing a standard mill plate that falls within this requirement. The second is that the web slenderness ratio, D / t_w, not exceed 150. Table 6.1 lists the web slenderness values for the parametric matrix of girders presented in Chapter 3. As shown, this requirement is met by all of the proposed girders.

Table 6.1: Web Slenderness Values for Parametric Matrix of Girders

Girder	w (in)	d (in)	t (in)	D (in)	D / t_w
1			7/16	8.1609	18.653
2	60	12	1/2	7.5597	15.119
3			5/8	6.3572	10.172
4			7/16	13.315	30.434
5	72	17	1/2	12.714	25.427
6			5/8	11.511	18.418
7			7/16	19.499	44.570
8	84	23	1/2	18.898	37.796
9			5/8	17.696	28.313
10			7/16	22.592	51.638
11	96	26	1/2	21.991	43.981
12			5/8	20.788	33.261
13			7/16	26.715	61.062
14	108	30	1/2	26.114	52.227
15			5/8	24.911	39.858
16			7/16	30.838	70.487
17	120	34	1/2	30.237	60.473
18			5/8	29.034	46.455

The third requirement is that Eq. 6.1 be satisfied, where D_{cp} is the depth of the web in compression at the plastic moment:

$$\frac{2D_{cp}}{t_w} \le 3.76\sqrt{\frac{E}{F_{yc}}} \qquad \text{Eq. 6.1}$$

To evaluate this limit, the plastic moment capacity and the resulting $2D_{cp} / t_w$ value was computed for a suite of composite girders. For this assessment, F_y was taken to equal 70 ksi and f_c' was taken to equal 4 ksi in order to generate the most conservative results. A total of 25 concrete deck options were evaluated: five concrete deck thicknesses ranging from 7 inches to 11 inches in 1-inch increments and five deck widths. The provisions of Articles 6.11.2.3 and

Article 6.11.6.2.2 (AASHTO, 2010) were employed to compute the corresponding deck widths, which state that, for a composite box girder to be considered compact, the distance center-to-center of flanges of adjacent boxes, a, shall neither be greater than 120 percent nor less than 80 percent of the distance center-to-center of the flanges of each adjacent box, w. Therefore, the five deck widths employed ranged from 1.8w to 2.2w in 0.1w increments. These deck options were employed with each of the proposed 18 steel girders, resulting in 450 individual assessments. Figure 6.1 illustrates the results of this assessment; as shown the proposed system easily meets this limit. D_{cp} was taken as the length of the flat portion of the web in compression at the plastic moment. It should therefore be noted that, for many cases, the plastic neutral axis lied in either the concrete deck or the top flange; in those cases, D_{cp} was equal to zero (only 22 cases in total resulted in nonzero values of D_{cp}).

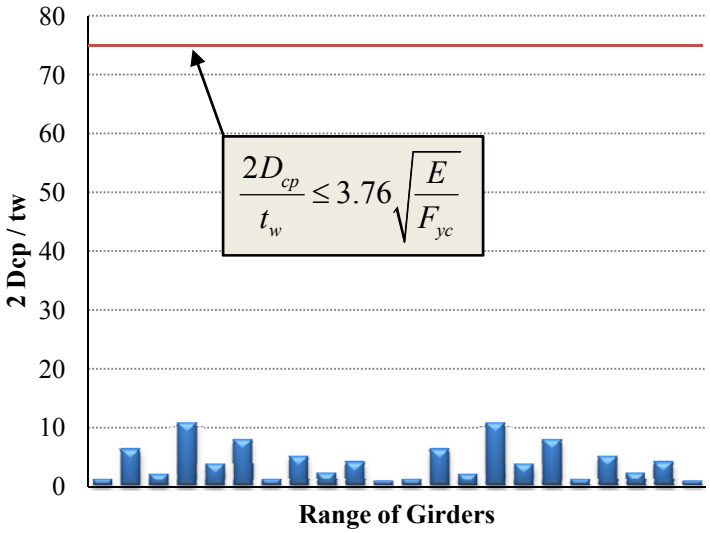

Figure 6.1: Evaluation of Eq. 6.1

6.2.2 AASHTO Definition of M_n for Compact Composite Girders

From the previous section, it was deemed that the proposed composite girders meet the AASHTO LRFD Specifications requirements for compactness in composite box girders. If a composite box girder qualifies as compact, the flexural capacity of the compact girder is defined by AASHTO by Eq. 6.2.

$$M_n = \begin{cases} M_p & D_p \le 0.1D_t \\ M_p\left(1.07 - 0.7\frac{D_p}{D_t}\right) & 0.1D_t < D_p \le 0.42D_t \end{cases} \qquad \text{Eq. 6.2}$$

To evaluate the applicability of AASHTO's nominal moment capacity prediction equation on the proposed system, strain-compatibility assessments were performed on the aforementioned suite of 450 girders. This suite of girders was augmented to include both 50 ksi and 70 ksi yield strengths and two cases of noncomposite dead load, resulting in a matrix of 1800 girders. Specifically, cases with no dead load (i.e. $M_{DL} = 0$) and $M_{DL} = 0.50\ M_y$ were assessed to account for different means of casting the deck (i.e. shored vs. unshored). Upon completion of strain-compatibility assessments, 26 girders were eliminated from the matrix as they violated the $D_p / D_t \le 0.42$ limit required by AASHTO; this was deemed appropriate as these girders utilized relatively thin deck sizes and large girder proportions (it should also be noted that only girders with $F_y = 70$ ksi exhibited failure of this limit) .

Figure 6.2 illustrates the accuracy of the Eq. 6.2 for the proposed system. As shown, employing Eq. 6.2 would result in a somewhat overconservative estimate of capacity of the proposed system. Therefore, Eq. 6.3 is proposed to provide a more accurate estimate of girder capacity. This equation was derived by curve fitting a straight line to the 95th percentile of the strain-compatibility results with respect to D_p / D_t; previous research has shown that this is an appropriate means to more accurately predict the ultimate moment capacity of a composite steel girder in positive bending (Roberts, 2004). Figures 6.2 and 6.3 illustrate the accuracy of Eq. 6.3 in predicting the capacity of the proposed system.

$$M_n = \begin{cases} M_p & D_p \le 0.1D_t \\ M_p\left(1.0228 - 0.228\frac{D_p}{D_t}\right) & 0.1D_t < D_p \le 0.42D_t \end{cases} \qquad \text{Eq. 6.3}$$

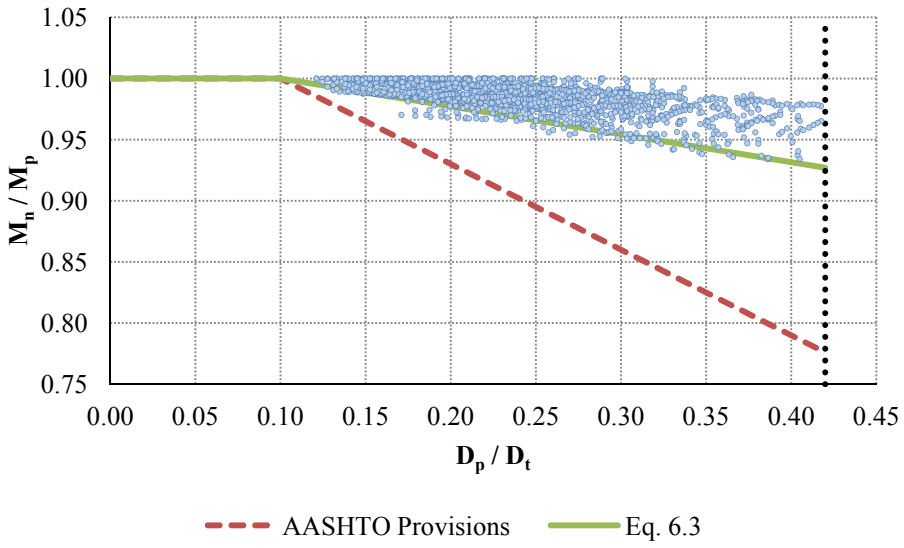

Figure 6.2: Evaluation of AASHTO Specifications and Eq. 6.3

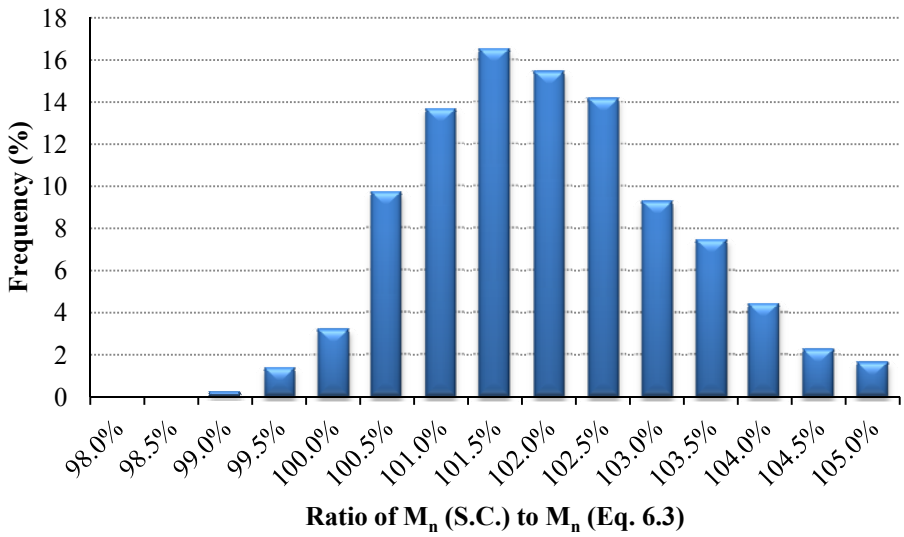

Figure 6.3: Histogram of M_n (Strain-Compatibility) versus M_n (Eq. 6.3)

Recall that the previously described suite of girders incorporates concrete decks sizes dependent on the dimensions of the steel girder. Upon observation, many of the composite girders in the parametric suite resulted in deck widths longer than 7.5 feet. Since this width is deemed the largest width that is feasible for shipping of the composite modular unit, the suite of

girders was reduced by eliminating composite girders with deck widths larger than 7.5 feet. This resulted in a reduced suite of 614 girders.

Using the same approach, Figure 6.3 was developed, which illustrates the accuracy of the Eq. 6.2 for the reduced suite of girders. For this reduced suite, Eq. 6.4 (derived by curve fitting a straight line to the 95th percentile of the strain-compatibility results with respect to D_p / D_t) is proposed to provide a more accurate estimate of girder capacity. Figures 6.4 and 6.5 illustrate the accuracy of Eq. 6.4 in predicting the capacity of the reduced suite of girders.

$$M_n = \begin{cases} M_p & D_p \le 0.1D_t \\ M_p\left(1.0229 - 0.229\dfrac{D_p}{D_t}\right) & 0.1D_t < D_p \le 0.42D_t \end{cases} \qquad \text{Eq. 6.4}$$

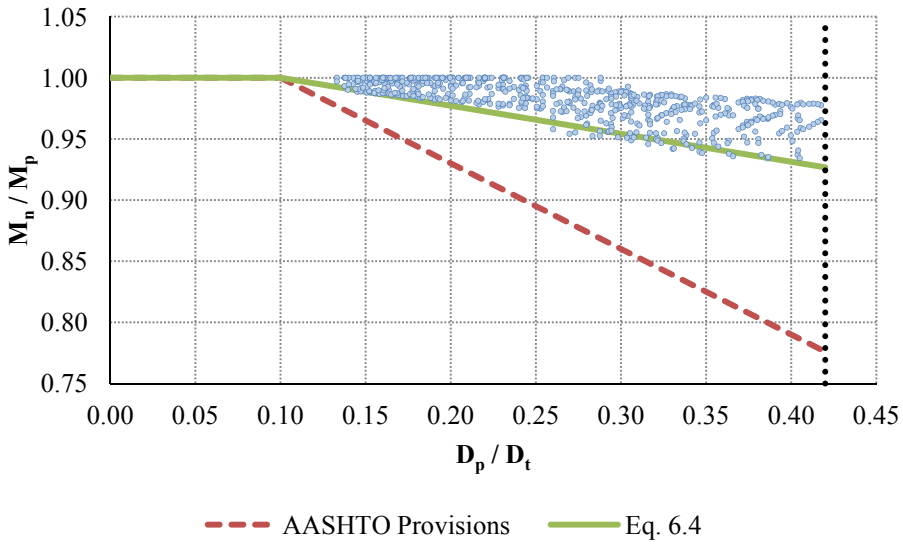

Figure 6.4: Evaluation of AASHTO Specifications and Eq. 6.4

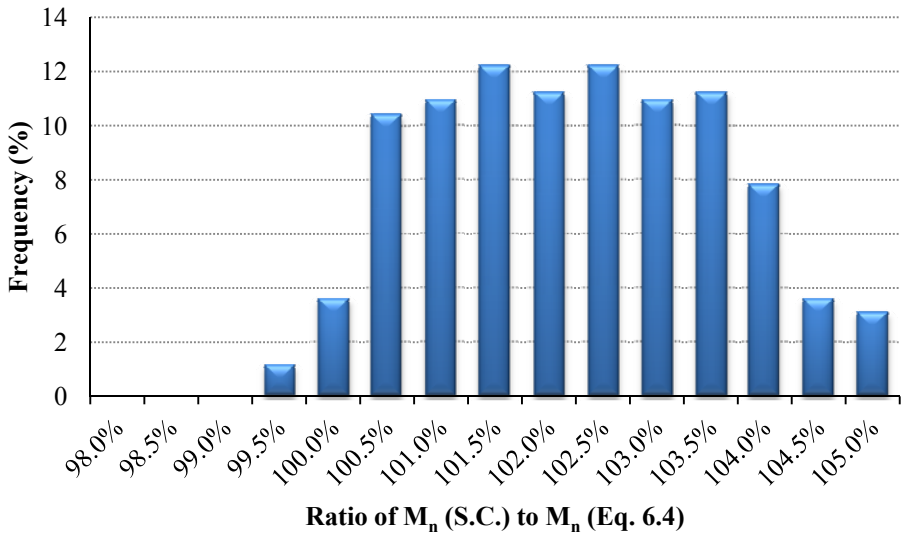

Figure 6.5: Histogram of M_n (Strain-Compatibility) versus M_n (Eq. 6.4)

6.2.3 AASHTO Definition of F_n for Noncompact Composite Girders

While the proposed dimensions of the girder coupled with reasonable deck dimensions have been shown to be classified as compact, variations in girder spacing or deck dimensions may classify a composite box girder as noncompact according to AASHTO Specifications. If this is the case, the capacity of the girder is essentially limited to the yield moment, M_y. Specifically, the compression flange capacity, F_{nc}, is taken as $R_b\ R_h\ F_{yc}$ and the tension flange capacity, F_{nt}, is taken as $R_h\ F_{yt}\ \Delta$. For the proposed system, the hybrid factor R_h would be taken as unity due to the single steel plate utilized and the web load-shedding factor R_b would be taken as unity since the section is composite and satisfies the D / t_w limit as previously discussed. The term Δ in the expression for tension flange capacity is intended to reduce the capacity of the tension flange under the presence of torsion; since the intended use of the proposed system is for short-span structures, it is unlikely that the girder will experience significant torsion and this term can be neglected.

6.2.4 Additional Assessment of Strain Compatibility Procedure

In order to further validate the accuracy of the strain-compatibility assessment procedure, 18 composite units (i.e. one for each of the girders presented in Chapter 3) were selected from the previously described suite of girders for comparison with the finite element analysis protocols discussed in Chapter 5. Specifically, the girders with assumed to have $2w$ wide × 8 inches thick concrete decks. Materials were modeled using the constitutive models discussed in Chapter 5. Strain-compatibility analysis were performed using the values of F_y and f_c' described in Chapter 5.

Figure 6.6 shows the comparison of maximum moments obtained from finite element analysis and from strain-compatibility assessments. As shown, the strain compatibility procedure captures the maximum flexural capacity of the proposed system quite well. In addition, the average M_n obtained from strain-compatibility is 95.7% of the average M_n obtained from finite element analysis, which indicated that the strain-compatibility procedure is slightly conservative. Also, in addition to Figure 6.6, the load-deflection curve for each of the 18 finite element models is documented in Appendix C (for each curve, the nominal moment capacity obtained from strain compatibility along with the yield moment and plastic moment are plotted).

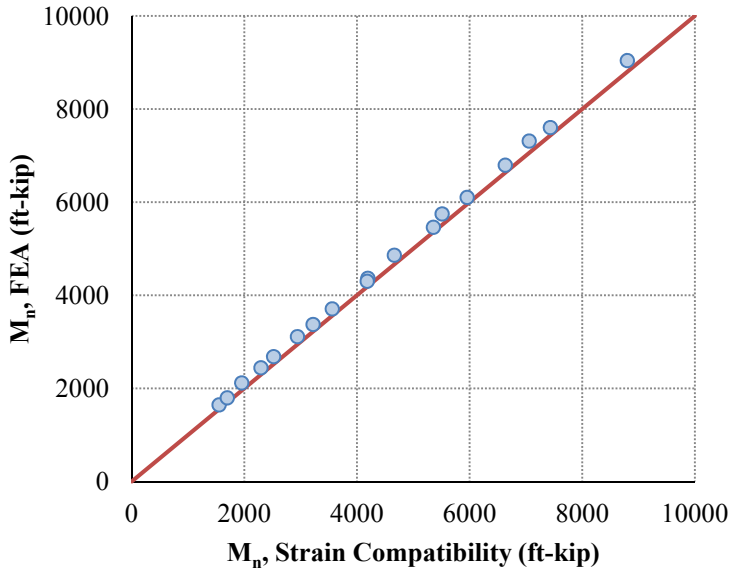

Figure 6.6: Comparison of Strain-Compatibility Procedure and Finite Element Analysis

6.2.5 Summary of Composite Girder Assessment

The goal of the previously described studies was to assess the applicability of AASHTO LRFD Specifications for the proposed composite units. Strain-compatibility procedures (verified by finite element analysis) demonstrate that AASHTO provisions are applicable and somewhat conservative when estimating the capacity of the proposed system. For simplicity, Eq. 6.5 (derived by rounding the constants of Eq. 6.4) is recommended for computing the capacity of the proposed system. Figures 6.7 and 6.8 illustrate the accuracy of Eq. 6.5 in predicting the capacity of the reduced suite of girders.

$$M_n = \begin{cases} M_p & D_p \le 0.1D_t \\ M_p\left(1.025 - 0.25\dfrac{D_p}{D_t}\right) & 0.1D_t < D_p \le 0.42D_t \end{cases} \qquad \text{Eq. 6.5}$$

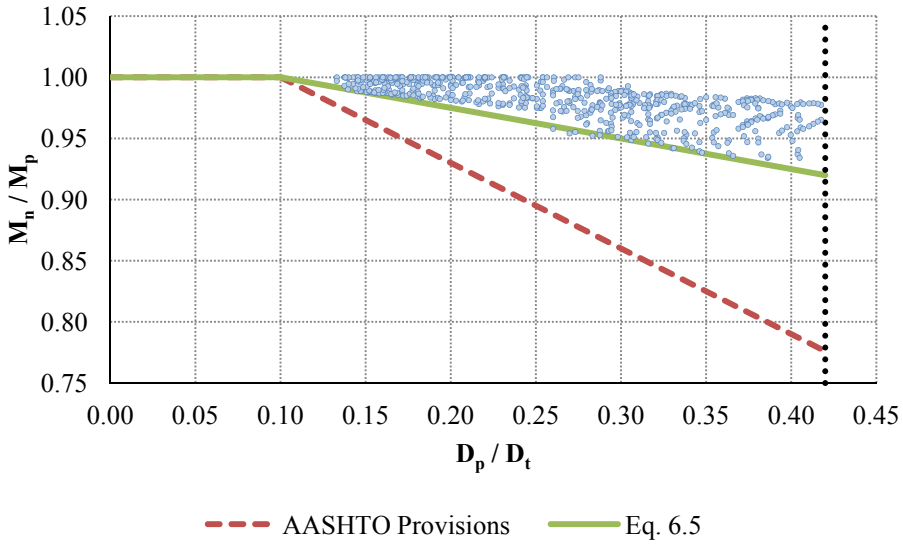

Figure 6.7: Evaluation of AASHTO Specifications and Eq. 6.5

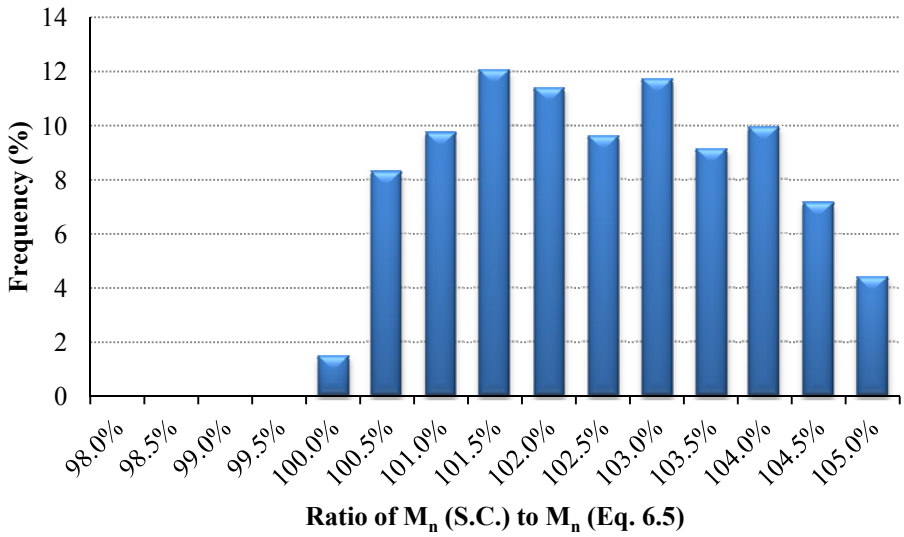

Figure 6.8: Histogram of M_n (Strain-Compatibility) versus M_n (Eq. 6.5)

6.3 Assessment of Noncomposite Girder Behavior

As stated, the goal of this research effort is the refinement of the proposed modular composite unit. However, while the assessment of the capacity of the composite unit is most critical to the intact, final state of the structure, an evaluation of the noncomposite stability of the steel tub girder would facilitate construction and handling of the girder and allow for other means of construction, such as utilizing cast-in-place decks.

Since the geometry of the proposed press-brake-formed tub girders differs significantly from the geometry of a typical box girder, a fundamental review of the stability of the noncomposite girder is warranted. Presented in this section is a review of the local and global buckling behavior of the proposed system. It should be noted that the following section demonstrates theoretical methods for computing buckling loads and torsional deformations; these demonstrations utilize the section properties of the girder described in Table 6.2 (note that the length of the girder is taken to be 38 feet, equal to the length of the experimental specimens discussed in Chapter 4).

Table 6.2: Example Girder Properties (PL 84" × 7/16")

Property	Value
E (ksi)	29000
G (ksi)	11154
L (in)	456
I_y (in^4)	8049.6
J_{open} (in^4)	2.3447
J_{closed} (in^4)	6900.0
C_w (in^6)	139952
β_x (in)	-19.704

6.3.1 Assessment of Governing Flexural Buckling Modes

To assess the stability of press-brake-formed tub girders, the governing flexural buckling modes were first assessed. Schaefer and Ádány (2006) developed CUFSM, a free open-source software program for assessing the buckling modes of cold-formed steel shapes. The program operates through use of the constrained finite strip method. The cross-section is divided into strip elements, and based on the strip length (also known as the half wavelength), various local, distortional, and global buckling modes can be assessed by computing the governing eigenvalue under a given stress state. Figure 6.9 shows an example finite strip analysis for a standard cold-formed lipped channel under axial loading. As shown, the section will experience local buckling under an axial load of 0.42 $F_y A$ and distortional buckling under an axial load of 0.75 $F_y A$.

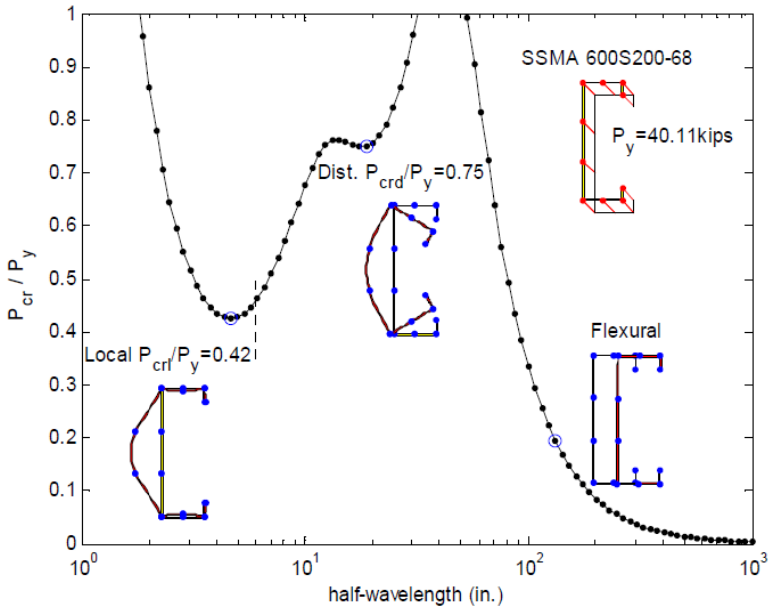

Figure 6.9: Example of Traditional Finite Strip Analysis (Schaefer & Ádány, 2006)

CUFSM was employed to assess the possible buckling modes of press-brake-formed tub girders under flexural loading. Figure 6.10 shows the results of the analysis of a representative girder from the matrix presented in Chapter 3. As shown, no local buckling modes govern the design of the representative girder. Distortional buckling modes for this girder will occur at a load approximately equal to 1.52 M_y. However, this will not govern the design as this load exceeds M_p for the section. Therefore, for this beam, only global lateral-torsional buckling modes need to be assessed.

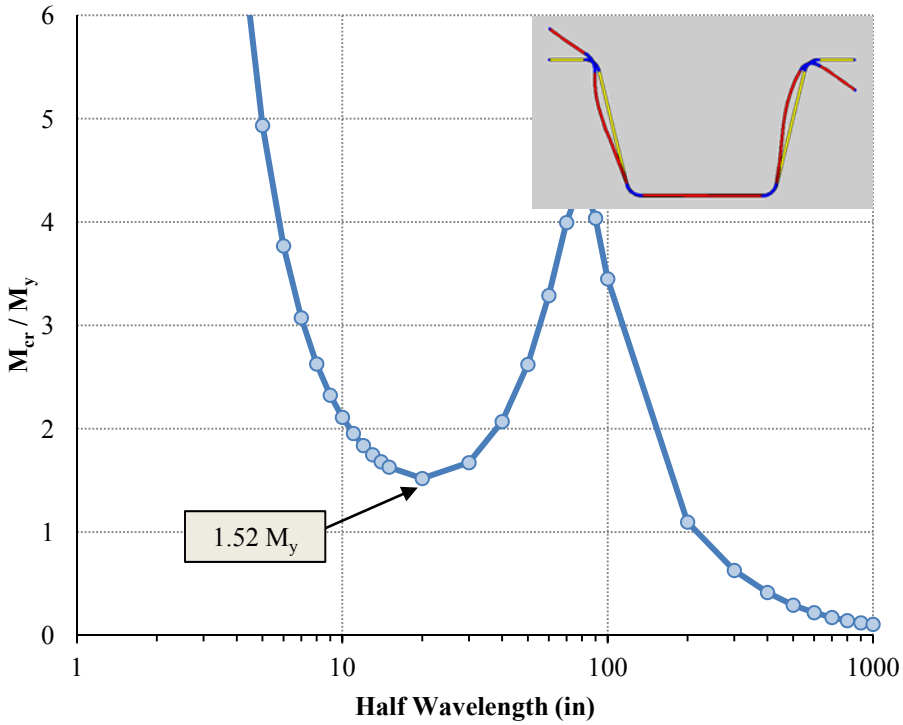

Figure 6.10: Example CUFSM Analysis (PL 84" × 7/16")

This observation was also found for the remaining girders in the parametric matrix. For all of the girders, no local buckling modes were found to occur. In addition, the average distortional buckling mode was found to be equal to 1.997 M_y. Therefore, it was deemed that local and distortional buckling modes need not be considered when assessing the stability of noncomposite press-brake-formed tub girders.

6.3.2 Consideration of Lateral Torsional Buckling

From the previous section, it was found that only global lateral-torsional buckling modes will govern the stability of the proposed system. Presented in this section is a summary of classical lateral-torsional buckling solutions for first-order and second-order lateral torsional buckling solutions for the proposed girder.

6.3.2.1 Derivation of Global Lateral Torsional Buckling Solution

The differential equations for lateral-torsional buckling of a singly-symmetric beam under uniform bending (Galambos, 1968) are as follows:

$$EI_y\left(u''\right) = -M_o\left(\phi\right) \qquad \text{Eq. 6.6}$$

$$EC_w\left(\phi'''\right) - \left(GJ + M_o\beta_x\right)\left(\phi'\right) = -M_o\left(u'\right) \qquad \text{Eq. 6.7}$$

For a simply-supported beam, the boundary conditions for these differential equations are as follows:

$$\phi\left(0\right) = \phi\left(L\right) = 0 \qquad \text{Eq. 6.8}$$

$$\phi''\left(0\right) = \phi''\left(L\right) = 0 \qquad \text{Eq. 6.9}$$

In order to simplify the solution process, the function for twist, which meets the criteria of the previously specified boundary conditions, is assumed to take the following form:

$$\phi = A_{\phi c}\sin\left(\frac{\pi z}{L}\right) \qquad \text{Eq. 6.10}$$

Using Eq. 6.10, the function for lateral deflection can be expressed as follows:

$$u = A_{\phi c}\left(\frac{M_o L^2}{\pi^2 EI_y}\right)\sin\left(\frac{\pi z}{L}\right) \qquad \text{Eq. 6.11}$$

Differentiating these trial functions and substituting into the second differential equation, the following equation is obtained. It should be noted that, while the actual magnitude of lateral deflection and twist at midspan, $A_{\phi c}$, is not obtainable, these terms factor out of the differential equation, and do not impact the solution.

$$EC_w\left(\phi'''\right)-\left(GJ+M_o\beta_x\right)\left(\phi'\right)=-M_o\left(u'\right)$$

$$EC_wA_{\phi c}\left(\frac{\pi^3}{L^3}\right)\cos\left(\frac{\pi z}{L}\right)-\left(GJ+M_o\beta_x\right)A_{\phi c}\left(\frac{\pi}{L}\right)\cos\left(\frac{\pi z}{L}\right)=-M_oA_{\phi c}\left(\frac{M_oL}{\pi EI_y}\right)\cos\left(\frac{\pi z}{L}\right)$$

$$\therefore {M_o}^2-\left(\frac{\pi^2EI_y\beta_x}{L^2}\right)M_o+\left(\frac{\pi^4E^2I_yC_w-\pi^2EI_yGJL^2}{L^4}\right)=0 \qquad \text{Eq. 6.12}$$

Solving this equation, the following expression for the critical buckling moment of a singly-symmetric beam is obtained. Note that the "±" sign results from the solution of the quadratic equation in M_o and refers to the direction of applied moment; if the larger flange of the cross-section is in compression, the sign is taken as positive:

$$M_o=\frac{\pi^2EI_y\beta_x}{2L^2}\left[1\pm\sqrt{1+\frac{4}{{\beta_x}^2}\left(\frac{GJL^2}{\pi^2EI_y}+\frac{C_w}{I_y}\right)}\right] \qquad \text{Eq. 6.13}$$

Using Eq. 6.13, the first-order lateral-torsional buckling capacity of the press-brake-formed tub girder is found as follows (assuming no lateral bracing throughout the span):

$$M_o=\frac{\pi^2EI_y\beta_x}{2L^2}\left[1-\sqrt{1+\frac{4}{{\beta_x}^2}\left(\frac{GJL^2}{\pi^2EI_y}+\frac{C_w}{I_y}\right)}\right]$$

$$=\frac{\pi^2\left(29000\text{ ksi}\right)\left(8049.6\text{ in}^4\right)\left(-19.704\text{ in}\right)}{2\left(456\text{ in}\right)^2}\left\{1-\sqrt{1+\frac{4}{\left(-19.704\text{ in}\right)^2}\left[\frac{\left(11154\text{ ksi}\right)\left(2.3447\text{ in}^4\right)\left(456\text{ in}\right)^2}{\pi^2\left(29000\text{ ksi}\right)\left(8049.6\text{ in}^4\right)}+\frac{\left(139952\text{ in}^6\right)}{\left(8049.6\text{ in}^4\right)}\right]}\right\}$$

$$=10590\text{ in-kip}$$

It should be noted that the moment gradient modifier C_b has not been included. However, according to AASHTO LRFD Specifications (2010), the C_b value for unbraced segments with mid-segment moments larger than brace-point moments is taken to be unity.

If this moment is caused by a concentrated load at midspan:

$$P_o = \frac{4M_o}{L} = \frac{4(10590 \text{ in-kip})}{456 \text{ in}} = 92.3 \text{ kip}$$

During flexural testing of Specimen #3 (a noncomposite weathering-steel girder), at a load level of approximately 95 kips, the girder failed in a sudden lateral-torsional buckling mode (it should be noted that this value of 95 kips closely agrees with the theoretically-derived critical load of 92.3 kips). Figure 6.10 shows the girder at the moment of failure. .

Figure 6.11: Specimen #3 Test (Load ≈ 95 kips)

6.3.2.2 Consideration of Second-Order Effects

In many practical applications, it is desirable to determine the effects of nonlinear, or second-order, deflections in flexural elements. Second-order effects arise primarily from the presence of eccentricity in applied load, either from a physical eccentricity of applied load, combined applications of load (i.e. moments, axial loads, torsions, and/or shears), or initial imperfections of the member. For the case of initial imperfections, an initial twist (and

corresponding initial lateral deflection) can be assumed to take the following form, where $A_{\phi o}$ is the initial twist at midspan:

$$\phi_o = A_{\phi o} \sin\left(\frac{\pi z}{L}\right) \qquad \text{Eq. 6.14}$$

The differential equations for lateral-torsional buckling considering second-order effects are then expressed as follows:

$$EI_y\left(u''\right) = -M_o\left(\phi + \phi_o\right) \qquad \text{Eq. 6.15}$$

$$EC_w\left(\phi'''\right) - \left(GJ + M_o\beta_x\right)\left(\phi'\right) = -M_o\left(u' + u_o'\right) \qquad \text{Eq. 6.16}$$

Using the same methods as shown in the previous section, the ratio of second-order effects to first-order effects, also known as an amplification factor, can be expressed as an amplification of the initial imperfection at midspan, where M_o is the first-order elastic lateral-torsional buckling moment. It should be noted that this measure of amplification agrees with results presented by Galambos (1968) and Kala (2013):

$$AF = \frac{M_o}{M_o - M} = \frac{1}{1 - M/M_o} \qquad \text{Eq. 6.17}$$

Therefore, the second-order lateral deflection that arises from an applied moment M on a singly-symmetric beam is as follows:

$$u\left(z\right) = A_{\phi o}\left(AF\right)\left(\frac{M_o L^2}{\pi^2 EI_y}\right)\sin\left(\frac{\pi z}{L}\right) = \left(\frac{A_{\phi o}}{1 - M/M_o}\right)\left(\frac{M_o L^2}{\pi^2 EI_y}\right)\sin\left(\frac{\pi z}{L}\right)$$

Eq. 6.18

If second-order effects are included in the analysis of press-brake-formed tub girders, critical load values can be significantly reduced based on limits of tolerable deformation. Figure 6.12 shows a plot of the second-order amplification of lateral that would result from an initial twist of 1° at midspan (note that one degree of initial twist at midspan is equivalent to an initial lateral deflection of 0.9730 inches).

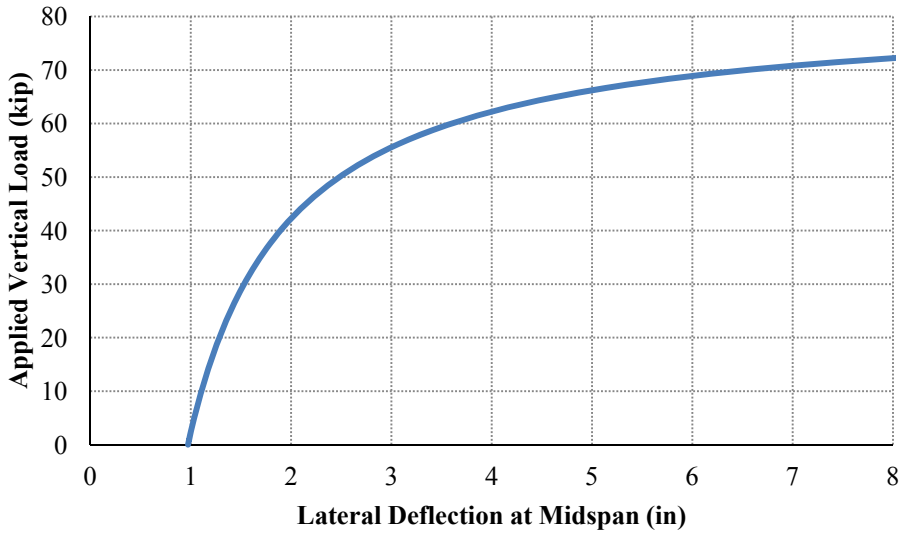

Figure 6.12: Second-Order Lateral Deflections

As stated, an additional physical test was performed (identical in configuration to the previous specimen) on a galvanized press-brake-formed tub girder (for more information, see Chapter 4). The girder exhibited an initial twist as shown in Figure 6.13.

Figure 6.13: Galvanized Girder Test (Initial Twist Present)

Flexural testing of this specimen was terminated at a load of approximately 33 kips due to excessive lateral deflection and twist. Figure 6.14 shows the girder at the point of test termination.

Figure 6.14: Specimen #4 Test (Load ≈ 33 kips)

6.3.2.3 Assessment of Flexural Capacity with SIP Forms

According to Helwig and Frank (1999), the lateral torsional buckling capacity of a girder may be improved by bracing the girder with stay-in-place (SIP) formwork. In their work, an expression for the augmented capacity of a girder braced by SIP forms (Ep. 6.19) was derived. In this expression, *G'* refers to the shear stiffness of the SIP deck forms, S_d refers to the lateral width of the deck forms (in the case of press-brake-formed tub girders, this is equal to the width between the top flanges), and *d* is the overall depth of the girders. The constant 3/8 value adjusted the moment capacity based on top flange loading conditions.

$$M_{cr} = C_b M_o + \frac{3}{8} G' S_d d \qquad \text{Eq. 6.19}$$

Egilmez et. al. (2007) reported shear stiffness values for various commonly-employed SIP formwork thicknesses. Table 6.3 lists the buckling capacity of the example press-brake-formed tub girder braced by SIP forms of varying thicknesses. For all values, unstiffened, seated connections were conservatively assumed for SIP forms. It should be noted that, by including SIP forms, all values of resulting critical buckling loads exceed the plastic moment capacity of the noncomposite shape.

Table 6.3: Assessment of Improved Stability with SIP Formwork

Property	18 gauge	20 gauge	22 gauge
C_b	1.0	1.0	1.0
M_o (in-kip)	10590	10590	10590
G' (kip/in)	36.408	29.133	13.504
M_{cr} (in-kip)	24565	21773	15774
M_p (in-kip)	14786	14786	14786

6.3.2 Assessment of Torsional Behavior

Under pure torsion (specifically, a concentrated torsional load at midspan) of a simply-supported member, the solution for torsional twist is as follows (note that, for simple supports, warping is not restrained).

$$\phi = \frac{\left(\frac{T}{2}\right)\left(\frac{L}{2}\right)}{GJ} = \frac{TL}{4GJ} \qquad \text{Eq. 6.20}$$

The computation of the St. Venant torsional constant, J, for noncircular cross-section can be inherently complex. Boresi and Schmidt (2003) present simplified formulas for J for open and closed cross-sections, and are expressed as shown below. For closed cross-secitons, A_o refers to the area enclosed by the closed shape and U refers to the median circumference of the enclosure. For more discussion of the computation of elastic section properties, the reader is referred to Appendix A.

$$J_{\text{open}} = \sum_{i=1}^{n}\left(\frac{b_i t_i^{\,3}}{3}\right) \qquad \text{Eq. 6.21}$$

$$J_{\text{closed}} = \frac{4A_o^{\,2}t}{U} \qquad \text{Eq. 6.22}$$

As demonstrated in Table 6.2, the torsional stiffness (represented by J) is substantially altered when SIP forms are included. This parameter has significant impact on the performance of press-brake-formed tub girders under torsional loading. Consider a simply-supported bridge girder undergoing torsional loading from a deck finishing machine. The NSBA Steel Bridge Design Handbook indicates a concentrated value of 3 kips is a reasonable estimate for finishing machine loads (NSBA, 2012). For an overhang of 3 feet (36 inches) from the exterior girder, this results in an applied torque of 108 in-kips. Therefore, the resulting rotations at midspan are as follows:

$$\phi_{\text{open}} = \frac{TL}{4GJ_{\text{open}}} = \frac{(108 \text{ in-kip})(456 \text{ in})}{4(11154 \text{ ksi})(2.3447 \text{ in}^4)} = 0.47077 \text{ radians} = 26.973°$$

$$\phi_{\text{closed}} = \frac{TL}{4GJ_{\text{closed}}} = \frac{(108 \text{ in-kip})(456 \text{ in})}{4(11154 \text{ ksi})(6900.0 \text{ in}^4)} = 0.00016 \text{ radians} = 0.00917°$$

Therefore, the resulting rotations from the application of the finishing machine are substantial for open press-brake-formed tub girders. It should be noted that the girder will be subjected to additional torsional loads during deck casting, such as loads from the construction walkway, eccentric concrete loads, etc. Closing the girder with stay-in-place formwork substantially improves the performance of the noncomposite girder under torsional loads.

6.4 CONCLUSION

The purpose of this chapter was to present several studies focused on assessing the behavior of the proposed system. The goal of these studies was to determine the applicability of AASHTO LRFD Specifications for the proposed system.

AASHTO LRFD Specifications were deemed to be somewhat conservative in computing the nominal capacity of composite modular units. An improved, simplified expression was derived to compute the nominal capacity of the proposed system, and is as follows:

$$M_n = \begin{cases} M_p & D_p \le 0.1D_t \\ M_p\left(1.025 - 0.25\dfrac{D_p}{D_t}\right) & 0.1D_t < D_p \le 0.42D_t \end{cases}$$

In addition, the noncomposite stability of the steel girder was assessed. It was found that the girder is susceptible to lateral-torsional buckling and torsional instability under relatively low load levels. However, this can be abated by simply installing SIP formwork prior to girder erection, which would serve to increase the torsional stiffness of the proposed girder and provide bracing to the girder against lateral torsional buckling.

CHAPTER 7: FEASIBILITY AND ECONOMIC ASSESSMENTS

7.1 INTRODUCTION

The following chapter details feasibility assessments and economic comparisons of the proposed system and traditional options for short-span bridges. The main goal of these studies was to assess the viability and competitiveness of the proposed system in the short-span market. Specifically, AASHTO LRFD Specifications were employed to determine the span ranges for which each of the girders discussed in Chapter 3 are applicable. Girder options were then reduced based on plate availability. Once girder options were reduced to a standardized set of modular solutions, the proposed system was then compared with traditional solutions for the short-span bridge market.

7.2 FEASIBILITY ASSESSMENTS

In order to assess the feasibility of the proposed system, design evaluations were performed in accordance with AASHTO Specifications (2010). Described in this section are the assumptions made for design evaluations along with the results for each of the girders in the parametric matrix described in Chapter 3.

7.2.1 Design Assumptions

Each of the girders in the parametric matrix were evaluated according to AASHTO Specifications (2010). For each girder, dead and live load force effects (i.e. moments, shears, and deflections) were computed for spans ranging from 20 feet to 140 feet in 5-foot increments. LEAP CONSYS (Bentley Systems, Inc., 2008), a comprehensive continuous beam analysis program, was used for the assessment of static and moving loads and was employed to perform influence-line analysis and generate live load envelopes for design evaluations.

DC loads (i.e. dead loads of structural components and nonstructural attachments) were assumed to consist of the self-weight of the girder and the concrete deck. For all of the girders assessed, the width of the girder was kept constant at 7.5 feet; this was selected as the maximum width that a modular unit could employ for feasible shipping. An integral wearing surface of 0.25 inches was assumed and applied in addition to the structural thickness of the concrete deck, which was assumed to be 8 inches. To account for the weight of shear studs, diaphragms, and other miscellaneous details, an additional 5% of the steel girder weight was applied as a distributed load. An additional load of 50 lb/ft was assumed to account for loads associated with steel guardrail systems. DW loads, or the loads of the future wearing surface, were assumed to consist of a 25 psf load applied over the 7.5 foot width of the concrete deck. LL loads (i.e. vehicular live loads) consisted of the AASHTO HL-93 live load model. Dynamic load allowance (i.e. IM factors) was taken as 1.33, in accordance with AASHTO Specifications.

Cross-sections that are assessed using live-load distribution factors must conform to deck proportion limits. According to AASHTO Specifications (Article 6.11.2.3), the distance center-to-center of flanges of adjacent boxes, *a*, taken at the midspan, shall neither be greater than 120 percent nor less than 80 percent of the distance center-to-center of the flanges of each adjacent box, *w*; this is illustrated in Figure 7.1.

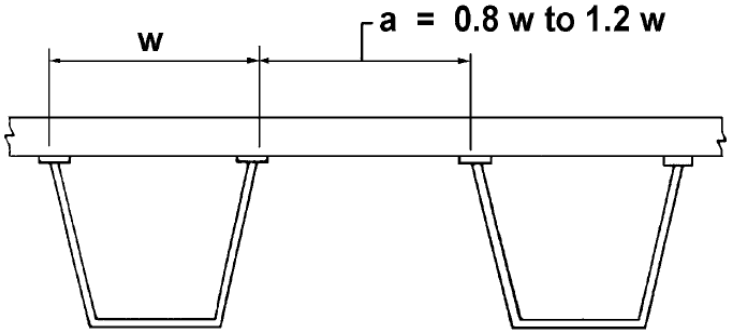

Figure 7.1: Limits on Deck Proportions (AASHTO, 2010)

By maintaining a constant deck width of 7.5 feet, this limit is violated for the majority of girders in the parametric matrix. Therefore, for feasibility assessments, the distribution factors for live load moments and shears are conservatively taken to be 1.0. For live load deflections, according to AASHTO Article 2.5.2.6.2, all girders in the bridge are assumed to deflect equally. Therefore, for feasibility assessments, the bridge is assumed to consist of two design lanes and

four girders. For two-lane-loaded scenarios, according to AASHTO Article 3.6.1.1.2, the multiple presence factor is equal to 1.0. Therefore, the live-load distribution factor for deflection is taken to be 1.0 (2/4) = 0.5.

Resistance for the girders in flexure was computed according to AASHTO Specifications as well as the proposed equations presented in Chapter 6. Resistance for the girders in shear was also computed according to AASHTO Specifications; the elements resisting shear were conservatively assumed to consist only of the flat portions of the inclined webs. All steel material for this assessment was assumed to have a yield stress, F_y = 50 ksi; all concrete was assumed to normal-weight with a compressive strength, f_c' = 4 ksi and a modular ration, n = 8.

7.2.2 Results of Feasibility Assessments

The feasibility assessment was conducted for each girder at the Strength I limit state (for moment and shear), the Service II limit state (for moment) and for live load deflection for each of the parametric girders. The results are comprehensively documented in Appendix C. Figure 7.2 shows a sample comparison at the Strength I limit state. Utilizing linear interpolation, this girder would be viable spans up to 61.44 feet according to AASHTO Specifications and 63.32 feet according to the equations proposed in Chapter 6.

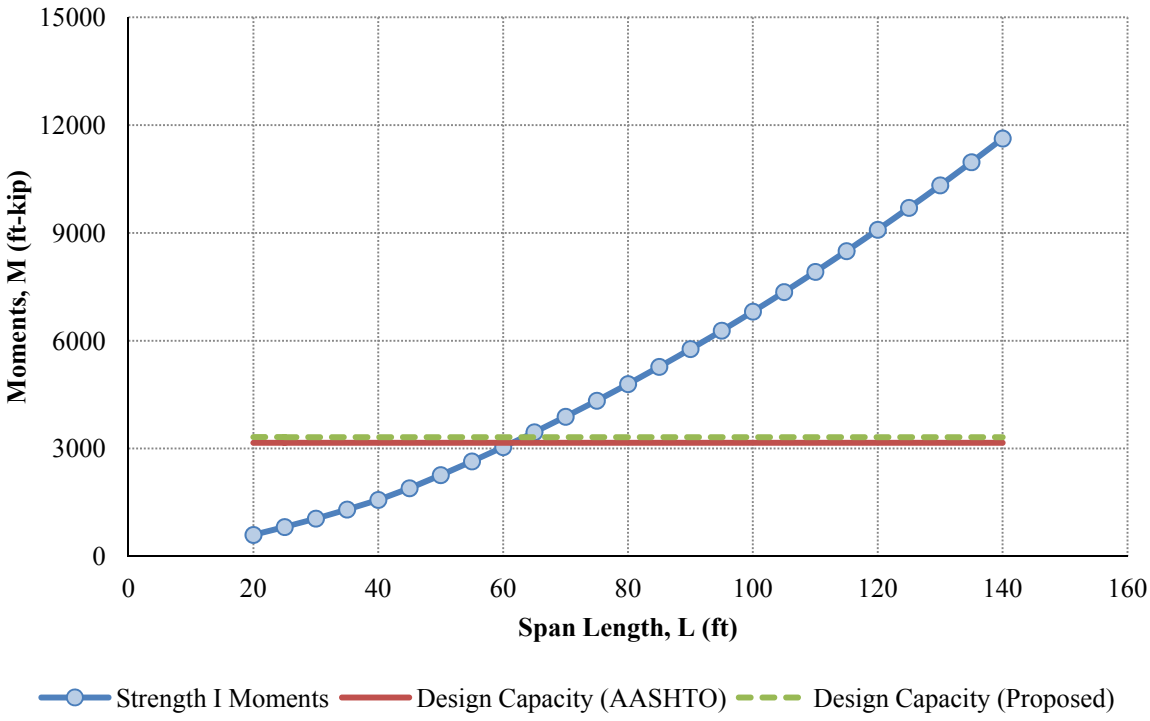

Figure 7.2: Strength I Moment Comparisons (PL 96" × 1/2")

Similar interpolations were conducted for remaining girders in the matrix. These maximum span length values are summarized in Table 7.1. In this table, "M" refers to moment limit states, "V" refers to shear limit states, and "Δ" refers to deflection limit states. Also, entries with "> 140" indicate that the girder has adequate capacity under all of the forces computed (i.e. up to 140 feet). Note that for all of the girders in the matrix (except for the PL 84" × 7/16"), the Strength I limit state governs the design. Figure 7.3 illustrates the maximum applicable span lengths for each of the girders in the parametric matrix.

Table 7.1: Interpolated Maximum Span Lengths

Girder	Maximum Span Length (ft) Listed by Limit State				
	Str. I (M)		Str. I (V)	Ser. II (M)	LL Def. (Δ)
	AASHTO	Proposed			
PL 60” × 7/16”	34.35	35.72	50.58	35.74	36.74
PL 60” × 1/2”	36.32	38.19	56.81	38.37	38.06
PL 60” × 5/8”	39.23	41.92	62.52	42.70	40.40
PL 72” × 7/16”	43.89	45.30	133.83	44.64	48.20
PL 72” × 1/2”	46.05	47.87	> 140	47.56	50.39
PL 72” × 5/8”	49.13	52.08	> 140	52.79	54.12
PL 84” × 7/16”	53.49	54.98	> 140	53.45	62.96
PL 84” × 1/2”	56.18	58.24	> 140	57.16	65.87
PL 84” × 5/8”	60.68	63.76	> 140	63.79	70.74
PL 96” × 7/16”	61.44	63.32	> 140	62.77	74.26
PL 96” × 1/2”	64.51	67.09	> 140	67.27	77.60
PL 96” × 5/8”	70.77	74.01	> 140	75.29	83.21
PL 108” × 7/16”	70.47	72.67	> 140	72.60	87.15
PL 108” × 1/2”	74.69	77.32	> 140	77.86	90.97
PL 108” × 5/8”	82.32	85.57	> 140	87.18	97.42
PL 120” × 7/16”	80.19	82.44	> 140	82.74	100.24
PL 120” × 1/2”	85.52	88.11	> 140	88.75	104.56
PL 120” × 5/8”	92.15	96.66	> 140	99.33	111.86

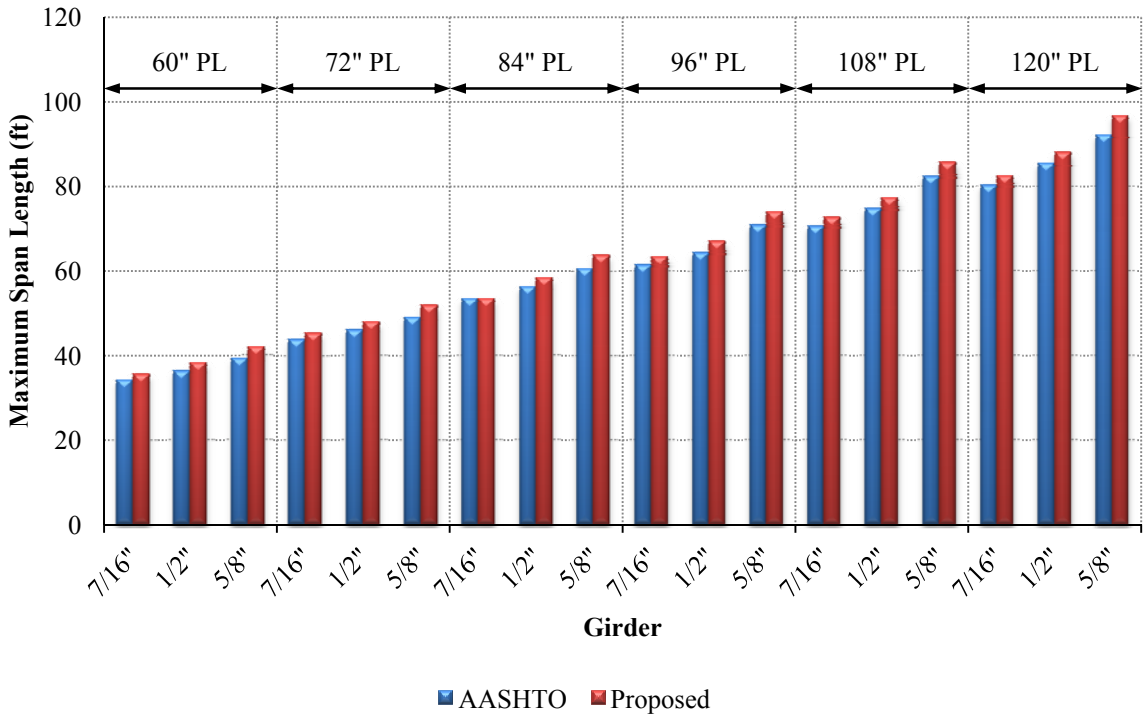

Figure 7.3: Maximum Applicable Span Lengths for Proposed System

7.3 Standardization of Proposed System

In order to simplify the implementation of the proposed system, the suite of parametric girders was reduced in the following section. Presented is the rationale for plate reduction and a summary of the standardized designs of the proposed system.

7.3.1 Plate Reduction Methodology

The goal of the proposed system dictates the use of standard mill plate in order to fabricate the steel girder component of the modular unit. Therefore, to reduce the matrix of girders, preference was given to plates that are produced on a regular basis. Mill widths of 72”, 96”, and 120” are considered industry standards; plates that fall outside these standard widths may not be as readily available (Garrell, 2011). Therefore, these plates should be given preference when developing standard solutions. The matrix was further reduced by restricting

the number of thicknesses employed in the matrix. Virtually all of the major plate producers in the United States produce steel plate with a 1/2" thickness (Garrell, 2011). However, consideration must be given to the maximum applicable span lengths, shown in Figure 7.3. As shown in Figure 7.4, 120" × 1/2" plates are typically only available in lengths up to 750 inches, or 62.5 feet. Therefore, the benefits of standardizing this plate would not be reached as the 96" × 1/2" solution is viable for this span range. Therefore, to capture the benefits of plate availability as well as maximum span-length application, the 120" × 5/8" plate should be employed (from Figure 7.4, this plate is available in lengths up to 972 inches, or 81 feet).

	Plate Width								
	72	**78**	**84**	**90**	**96**	**102**	**108**	**114**	**120**
3/8	972	972	972	972	972	972	972	972	750
1/2	972	972	972	972	972	972	972	972	750
9/16	972	972	972	972	972	972	972	972	972
5/8	972	972	972	972	972	972	972	972	972
3/4	1,030	1,030	1,030	1,030	1,030	1,030	1,030	1,030	1,030
7/8	1,030	1,030	1,030	1,030	1,030	1,030	1,007	954	907
1	1,030	1,030	1,030	1,030	992	933	882	835	793
1 1/4	1,030	1,030	907	846	793	747	705	668	635
1 1/2	1,030	1,030	756	705	661	622	588	557	529
1 3/4	1,030	1,030	648	604	567	533	504	477	453
2	937	937	567	529	496	467	441	418	397
2 1/4	833	833	504	470	441	415	392	371	353
2 1/2	749	749	453	423	397	373	353	334	317
2 3/4	681	681	412	385	361	339	321	304	288
3	624	624	378	353	331	311	294	278	264

Figure 7.4: Maximum Plate Length for Standard Mill Plates (Garrell, 2011)

7.3.2 Proposed Standardized Systems

Using the previously discussed rationale for the reduction of the parametric matrix of girders, the systems described in the following sections are proposed for mainstream use. Note that the dimensions of each steel girder match those listed in Chapter 3. In addition, it should be noted that applicable span ranges discussed in the following sections have been rounded in 20-

foot increments for simplicity. Also, in order to utilize single plates per girder (i.e. reducing the need for field splices and/or CJP welds), applicable spans have been limited to 80 feet.

7.3.2.1 Modular Single-Girder Systems

Three modular single-girder systems (employing normal-weight 7.5' × 8" concrete decks) are recommended:

- PL 72" × 1/2"
  - Applicable for spans up to 40 feet (see Figure 7.3)
- PL 96" × 1/2"
  - Applicable for spans up to 60 feet (see Figure 7.3)
- PL 120" × 5/8"
  - Applicable for spans up to 80 feet (see Figure 7.3)

7.3.2.2 Modular Double-Girder System

In cases where hydraulic opening or clearance requirements dictate the use of a shallow section, the use of a 60" × 1/2" standard mill plate may be advantageous as the resulting optimum girder design is only 12 inches deep. In addition, the optimum design of a 60" × 1/2" standard mill plate girder results in an out-to-out width less than half of the 7.5' modular concrete deck. Therefore, this girder may be employed in modular system such as the one shown in Figure 7.5.

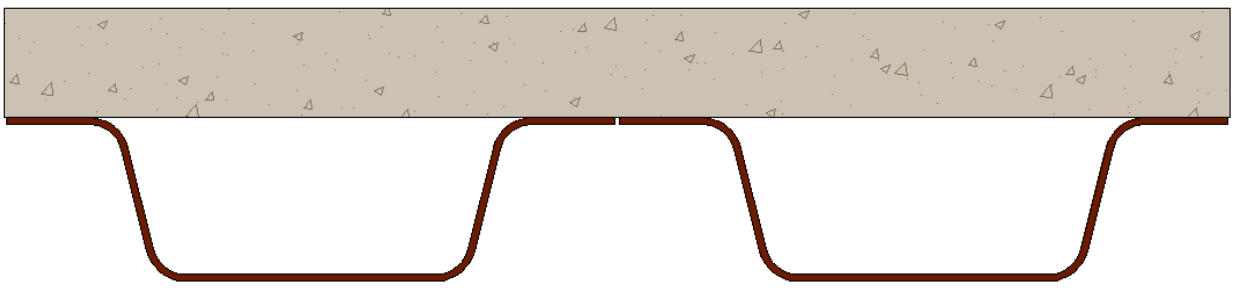

Figure 7.5: Conceptual View of Proposed Double-Girder Modular Layout

Using the same approach as discussed in Section 7.2, the feasibility of this proposed double-girder system was assessed. The plot of controlling limit state (Strength I) loads and resistances and is shown in Figure 7.6; it should be noted that the plots of the remaining limit states are also summarized in Appendix C. Utilizing linear interpolation, this girder would be viable spans up to 60.11 feet according to AASHTO Specifications and 66.26 feet according to the equations proposed in Chapter 6.

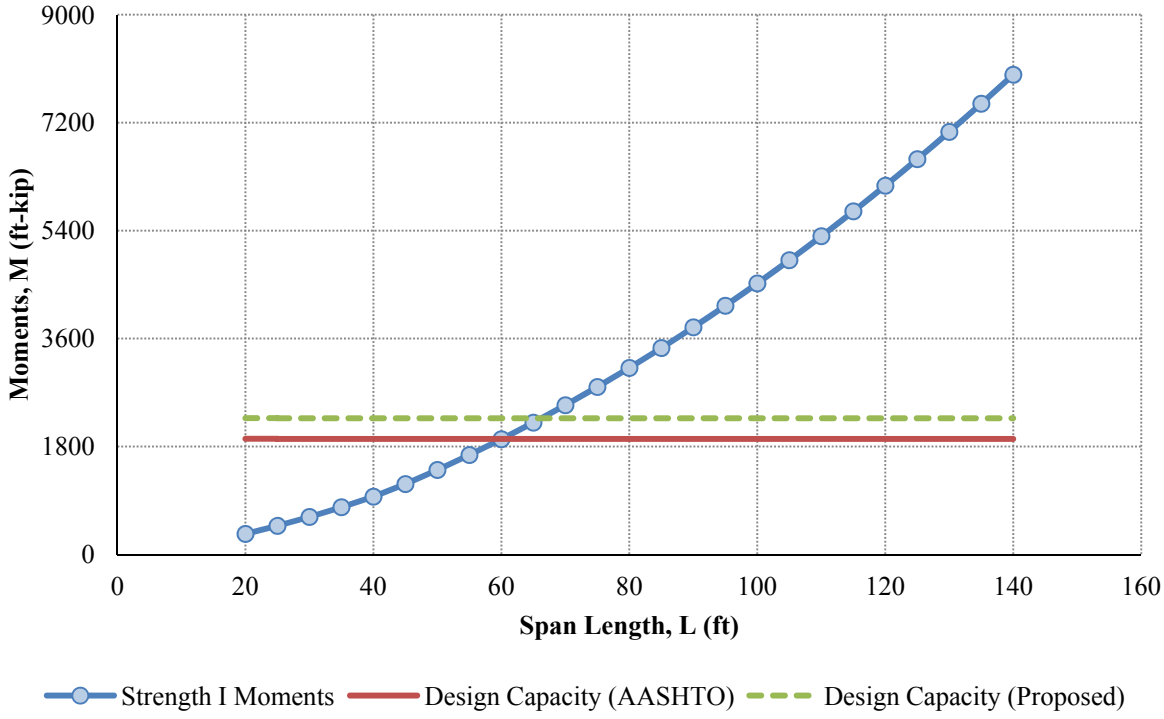

Figure 7.6: Strength I Moment Comparisons (Double-Girder System)

7.4 Comparisons to Standard Solutions

In order to assess the economic competitiveness of the proposed system, the selected standard girders were compared against traditional solutions for short-span highway bridges. Presented in this section is an overview of the systems used for comparison (along with their respective design assumptions) and weight comparisons, which assess the proposed system's viability in the short-span bridge market.

7.4.1 eSPAN140: Complimentary Solutions for Short-Span Steel Bridges

The Short Span Steel Bridge Alliance (SSSBA) is a group of bridge and culvert industry leaders (including steel manufacturers, fabricators, service centers, coaters, researchers, and representatives of related associations and government organizations) who have joined together to provide educational information on the design and construction of short span steel bridges in installations up to 140 feet in length. From within the SSSBA technical working group, standardized designs were developed based on optimized girder designs, which employ different bridge parameters and design approaches. The designs have been made available and complimentary to engineers through the use of a web-based design tool, and can be found at http://www.espan140.com/.

There are four major sets of bridge designs in this work: "limited depth" rolled beam sections, "lightest weight" rolled beam sections, homogeneous plate girder sections and hybrid plate girder sections. The girders designed to make up this wide range of bridge spans were designed for all spans between 40 and 140 feet in 5 foot increments. For each span length, girders arranged with four different girder spacings (6.0 ft, 7.5 ft, 9.0 ft, and 10.5 ft) were designed. From these optimized rolled girder designs, limited suites of rolled steel girder sections were selected to investigate the efficiency of using stockpiled girder sections for short span steel bridges. Also, the benefits of stockpiling common steel plate sizes are investigated in the design of steel plate girders.

7.4.1.1 Design Assumptions

The rolled beams and the homogeneous plate girders in these designs all employ 50-ksi steel. The hybrid steel plate girder sections employ 50-ksi steel in the compression flange and web plates and 70-ksi steel in the tension flange plate. For all girder sections, excluding the rolled beam sections of the "lightest weight" suite of girders, an L / D (Length/Depth) ratio of 25 was assumed. The depth in this ratio includes the entire depth of the bridge superstructure (i.e. bridge deck depth plus the concrete haunch thickness plus the girder depth). The concrete haunch is defined as the distance from the bottom of the compression flange to the bottom of the concrete deck.

The following parameters were assumed for each bridge girder design:

- Steel stay-in-place (SIP) formwork unit weight: 15 psf
- Future wearing surface: 25 psf
- Concrete barriers: 305 lbs/ft.
- Miscellaneous steel weight increase: 5%
- Compressive strength of concrete: 4,000 psi
- Concrete unit weight: 150 pcf
- Steel unit weight: 490 pcf
- Concrete haunch thickness: 2 in
- Constant flange width
- Constant web height

7.4.1.2 Design Results

Figure 7.7 shows a plot of the weight comparisons of the girders designed for eSPAN140 (Morgan, 2010) for a 7.5 foot girder spacing. This girder spacing was chosen as it is equivalent to the spacing between girders in the proposed system. For this plot, "S" refers to steel solutions, "LW" refers to lightest weight rolled beam designs, "LD" refers to limited depth rolled beam designs, "HO" refers to homogeneous plate girder designs, and "HY" refers to hybrid plate girder designs. These weights will be employed for economic comparisons with the proposed system.

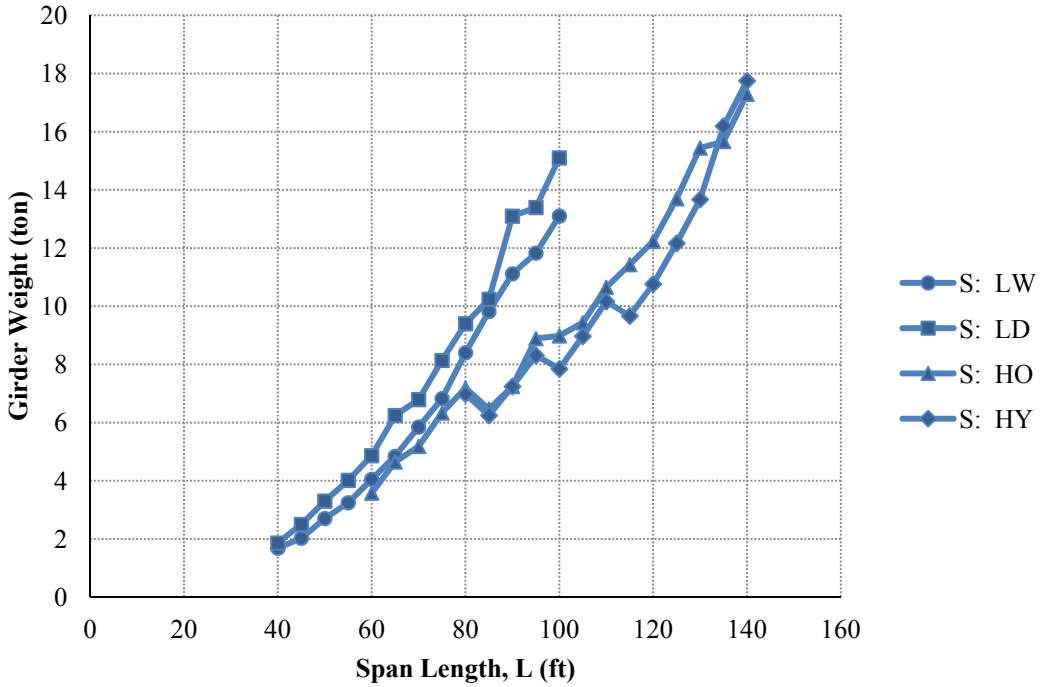

Figure 7.7: Weight Comparisons for Traditional Steel Solutions (Morgan, 2010)

7.4.2 Standardized Prestressed Concrete Solutions

Standardized prestressed concrete solutions, such as AASHTO standard girders (i.e. Type 3, Type 4, etc.), and Bulb Tees have been available to bridge engineers for decades. Many state DOTs have standard concrete solutions available (based on state-level design specifications). Standard girders from the Idaho Transportation Department's Bridge Design LRFD Manual (ITD, 2014) were employed in this section. Since these girders were designed according to assumptions quite similar to those made for the design of eSPAN140's girders as well as those made for the feasibility assessments of the proposed system, these girders proved ideal for economic comparison.

7.4.2.1 Design Assumptions

AASHTO LRFD Design Specifications (AASHTO, 2010) were employed for the design of prestressed girders. According to Article A5.4 (ITD, 2014), three different types of girders were evaluated: AASHTO, Bulb Tee, and Wide-Flange. Bulb Tee girders are available with either a 37-inch top flange width or a 48-inch top flange width. Designs are available utilizing 6-ksi and 10-ksi concrete; for the purposes of this evaluation, only designs utilizing 6-ksi concrete are employed.

The following parameters were assumed for each bridge girder design:

- 42 foot out-to-out bridge width
- Girder layouts:
  - 4 girders spaced at 12'-0"
  - 5 girders spaced at 9'-3"
  - 6 girders spaced at 7'-3"
  - 7 girders spaced at 6'-0"
- Future wearing surface: 28 psf
- Compressive strength of slab: 4,000 psi
- Concrete barriers are employed
- Tendon harp points at 0.4L and 0.6L, where L = span length
- Deck thickness is taken as (S + 10) / 30 where S is computed in accordance with Article 9.7.2.3
  - A minimum of 8 inches is employed

7.4.2.2 Design Results

As stated, girders were designed for 4 layouts with various girder spacing. Based on the previous assumptions (including girder spacing), the ITD Bridge Design Manual provides a series of plots indicating the maximum span range for each standard girder solution. Utilizing these plots, maximum span ranges for a girder spacing of 7.5 feet were determined by linear

interpolation. Figure 7.8 illustrates a representative interpolation for AASHTO girders; as shown:

- Type 2 girders are applicable for spans up to approximately 65 feet
- Type 3 girders are applicable for spans up to approximately 90 feet
- Type 4 girders are applicable for spans up to approximately 116 feet

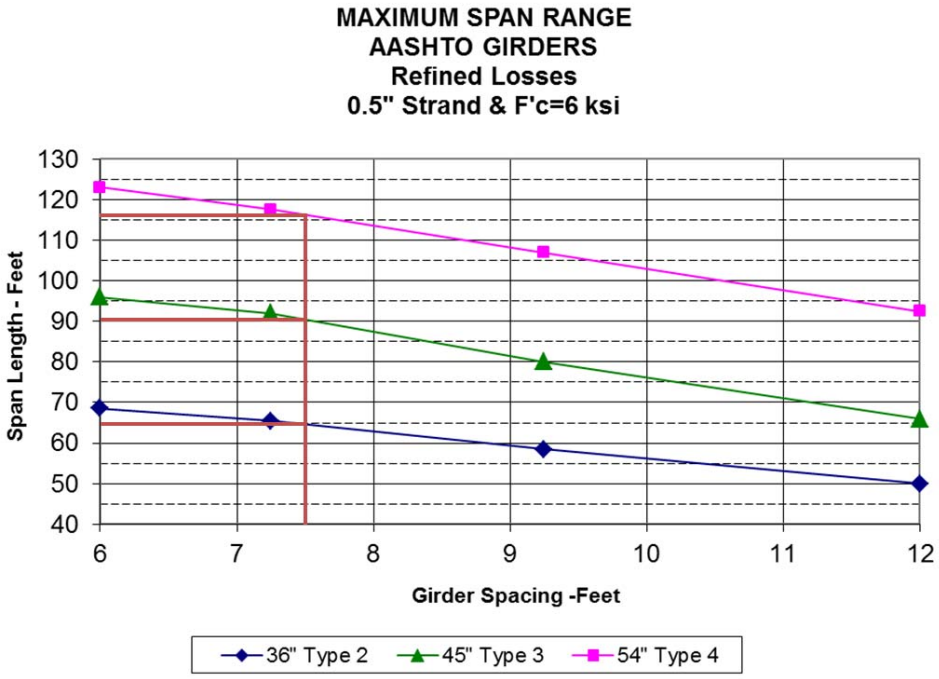

Figure 7.8: Sample Digitized Results for Determining Maximum Span Length (ITD, 2014)

Figure 7.9 shows a plot of the weight comparisons of the previously discussed prestressed concrete girders (ITD, 2014). For this plot, "C" refers to concrete solutions, "AG" refers to standard AASHTO girders, "BT1" refers to bulb-tee designs with 37-inch flanges, "BT2" refers to bulb-tee designs with 48-inch flanges, and "WF" refers to wide-flange designs. These weights will be employed for economic comparisons with the proposed system.

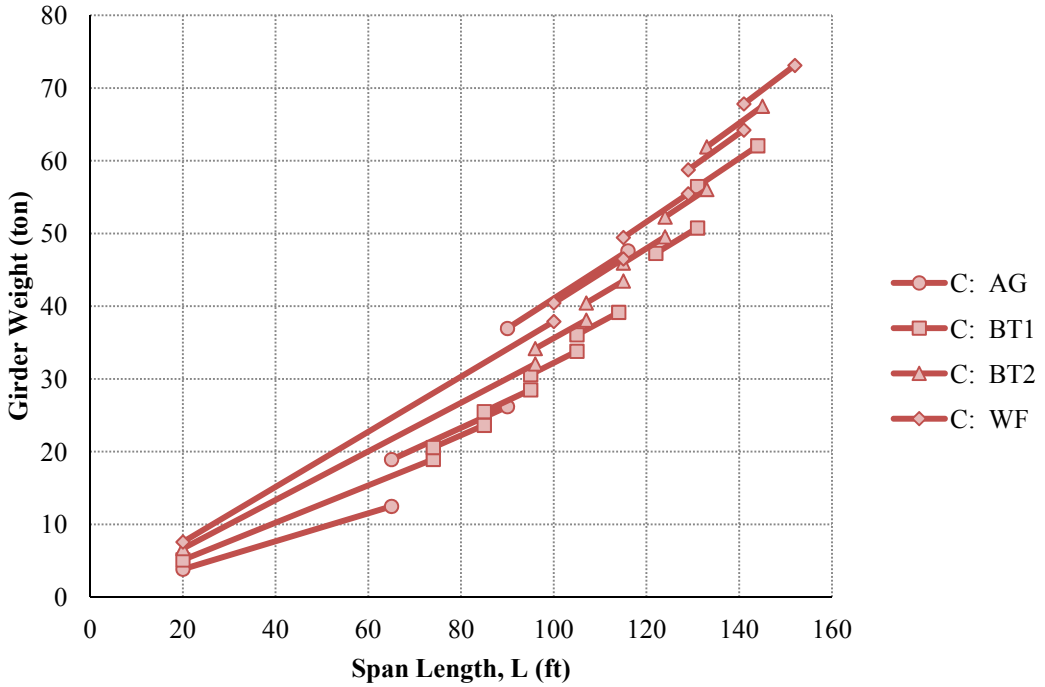

Figure 7.9: Weight Comparisons for Traditional Concrete Solutions

7.4.3 Comparisons with Proposed System

Using the weights of traditional girders from previous sections, economic comparisons were made with the proposed system, and are shown in Figure 7.10. For this plot, "PBF: 1" refers to the proposed modular single-girder systems, "PBF: 2" refers to the proposed modular double-girder system, and all other legend entries correspond to previous descriptions. As shown, the proposed system falls within the range expected for traditional steel and concrete girder solutions, thereby displaying its economic viability and competitiveness in the short-span bridge market.

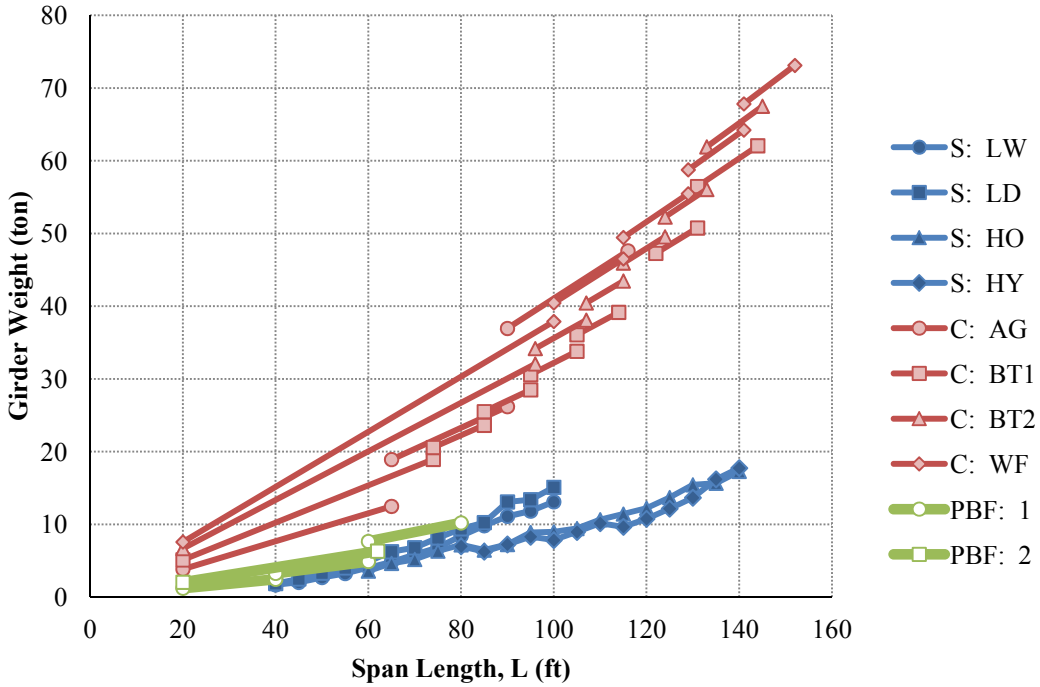

Figure 7.10: Economic Assessment of Proposed System

7.5 CONCLUSION

The preceding chapter details feasibility assessments and economic comparisons of the proposed system and traditional options for short-span bridges. Feasibility assessments, coupled with a reduction of the parametric matrix of girders (based on plate availability), resulted in the following systems:

- Modular single-girder systems employing 72" × 1/2" plate
  - Applicable for spans up to 40 feet (see Figure 7.3)
- Modular single-girder systems employing 96" × 1/2" plate
  - Applicable for spans up to 60 feet (see Figure 7.3)
- Modular single-girder systems employing 120" × 5/8" plate
  - Applicable for spans up to 80 feet (see Figure 7.3)
- Modular double-girder systems employing 60" × 1/2" plate
  - Applicable for spans up to 65 feet (see Figure 7.6)

In addition, the proposed systems were compared against traditional solutions for short-span bridges, such as steel rolled beams and AASHTO prestressed concrete girders. As shown, the proposed system is viable and economically competitive for the short-span bridge market. Also, it should be noted that feasibility assessments were conducted based on assuming that live load distribution factors for moment and shear was equal to 1.0; future research assessing live load distribution characteristics of the proposed system may result in increased span ranges for the proposed system, thereby increasing the economic competitiveness of shallow press-brake-formed steel tub girders.

CHAPTER 8: PROJECT SUMMARY AND CONCLUDING REMARKS

8.1 PROJECT SUMMARY

The scope of this project was to refine the development of modular press-brake-formed steel tub girder for short-span bridge applications. This was achieved by performing the following tasks:

- A rational methodology for the design of the proposed system was developed.
  - Associated dimensions and section properties from optimally-designed sections utilizing standard mill plates have been provided.
- Destructive flexural testing of representative specimens was performed.
  - All results from experimental testing have been provided.
- Analytical tools for assessing the behavior and capacity of the proposed system was developed.
  - Comparisons of experimental and analytical data have been provided.
- Behavioral studies were performed in order to assess the applicability of the current AASHTO LRFD Specifications in predicting the capacity the proposed system.
  - Improved expressions to compute the nominal capacity of the proposed system in its composite and noncomposite states were developed.
- Economic studies and feasibility assessments were performed to determine the system's competitiveness in the short-span bridge market.
  - These studies resulted in a reduced, standardized set of solutions.

8.2 PROPOSED STANDARDIZED SYSTEM

Feasibility assessments, coupled with a reduction of the parametric matrix of girders (based on plate availability) and conservative estimates of live load distribution, resulted in the following systems:

- Modular single-girder systems employing 72” × 1/2” plate
  - Applicable for spans up to 40 feet
- Modular single-girder systems employing 96” × 1/2” plate
  - Applicable for spans up to 60 feet
- Modular single-girder systems employing 120” × 5/8” plate
  - Applicable for spans up to 80 feet
- Modular double-girder systems employing 60” × 1/2” plate
  - Applicable for spans up to 65 feet

To longitudinally join the modular units, the author recommends the solutions presented by Graybeal (2010). This study investigated the structural performance of longitudinal UHPC connections for modular bridge deck components. The results demonstrated that the resulting connection facilitates construction of modular bridge components and results in deck systems whose behaviors meet or exceed those of a conventional cast-in-place bridge deck. Figure 8.1 illustrates a representative connection detail that would be applicable for the proposed system.

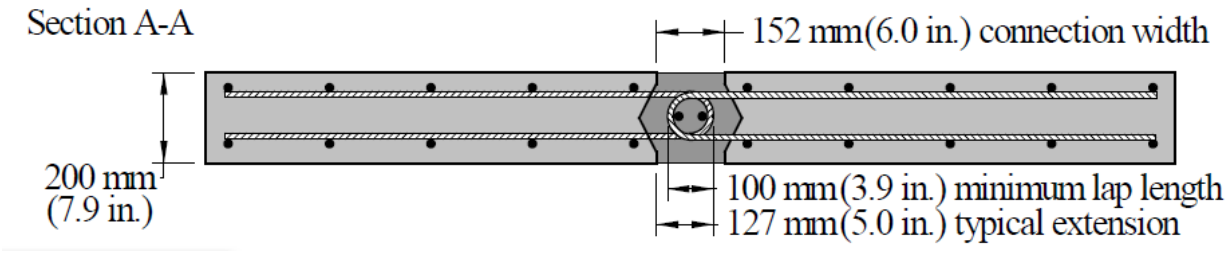

Figure 8.1: UHPC Longitudinal Joint (Graybeal, 2010)

8.3 RECOMMENDATIONS FOR CONTINUED RESEARCH

The author recommends the following tasks for future work and/or expansions to this project.

- To resist bearing forces, the thickness of the steel diaphragm at support locations was conservatively specified as 3/4 inches. While no bearing-related issues were observed during experimental testing or analytical studies, investigations should be conducted to assess the behavior of diaphragm bearing plates in steel tub girders.
- Utilizing a standard 7.5-foot-wide × 8-inch-thick concrete deck resulted in girder proportions that violate current requirements for employing AASHTO live load distribution factors for steel tub girders. While conservative estimates of live load distribution still guaranteed the economic competitiveness of the proposed, increased accuracy in determining live load distribution should be assessed; reduced live load distribution will result in increased span applicability for each of the proposed standard girder options.
    - For longer span ranges, it may also be a viable option to longitudinally splice units together. Therefore, best practices for bolted/welded splices should be assessed.
- The proposed steel girder was fabricated utilizing a large-capacity press brake. Bend radii of the proposed system were limited to 5 × the thickness of the standard mill plate, which is consistent with AASHTO Specifications. While no welding was used to fabricate the girder, the fatigue performance of the bend regions (and the modular unit, in general) should be assessed.
- Once the press-brake-formed steel tub girder has been implemented for mainstream use, long-term monitoring of candidate bridges may provide valuable information regarding inspection needs for the proposed system.

- The proposed modular unit was to be made composite with a concrete deck cast in the fabrication stage of construction. Other viable deck options, such as utilizing partial/full depth precast deck panels or sandwich plates, should be assessed as possible improvements to the system's economy. Figures 8.2 through 8.5 illustrate some of the various possible deck options available for the proposed system.

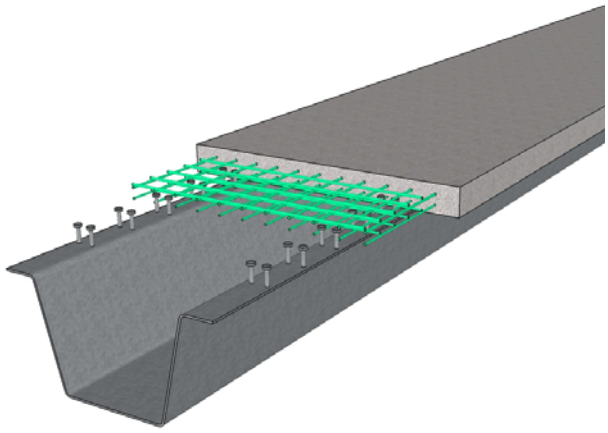

Figure 8.2: Precast Deck Option

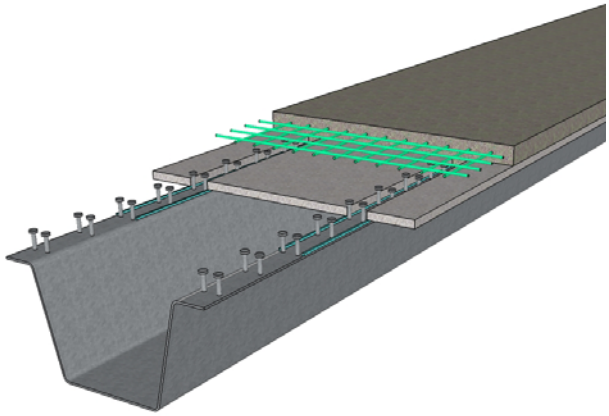

Figure 8.3: Partial-Depth Panel Deck Option

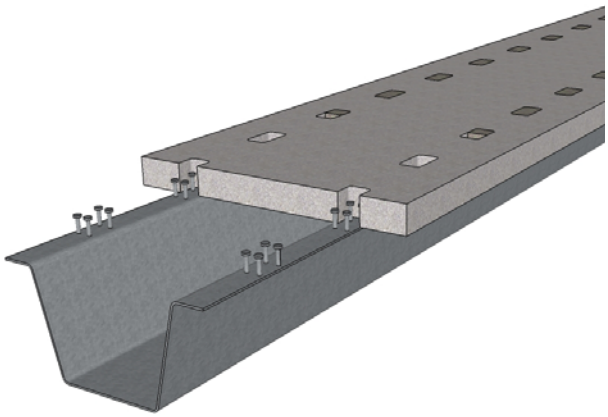

Figure 8.4: Full-Depth Panel Deck Option with Pocketed Shear Studs

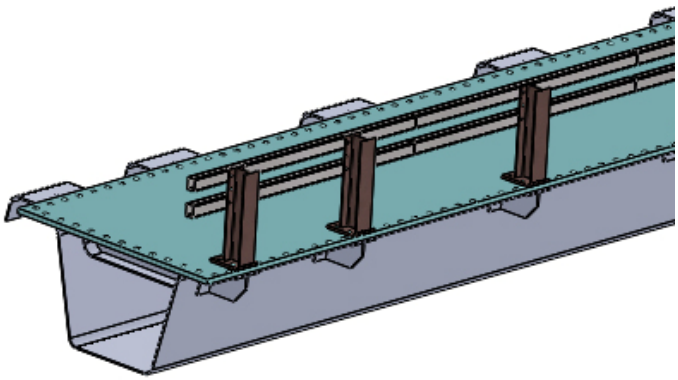

Figure 8.5: Sandwich Plate Deck Option

REFERENCES

AASHTO (2010). AASHTO LRFD Bridge Design Specifications. Washington, DC, American Association of State Highway and Transportation Officials.

Barth, K. E. (1996). Moment-Rotation Characteristics for Inelastic Design of Steel Bridge Beams and Girders. School of Civil Engineering. West Lafayette, IN, Purdue University. Doctor of Philosophy.

Barth, K. E. and H. Wu (2006). "Efficient Nonlinear Finite Element Modeling of Slab on Steel Stringer Bridges." Finite Elements in Analysis and Design 42(14): 10.

Beer, F., E. R. Johnston, et al. (2012). Mechanics of Materials. New York, NY, McGraw-Hill Higher Education.

Bentley Systems, Inc. (2008). LEAP CONSYS. Tampa, FL, Bentley Systems, Inc.

Boresi, A. P. and R. J. Schmidt (2003). Advanced Mechanics of Materials. Hoboken, NJ, John Wiley & Sons, Inc.

Burgueño, R. and B. S. Pavlich (2008). Evaluation of Prefabricated Composite Steel Box Girder Systems for Rapid Bridge Construction. East Lansing, MI, Michigan State University.

Burner, K. A. (2010). Experimental Investigation of Folded Plate Girders and Slab Joints Used in Modular Construction. Department of Civil Engineering. Lincoln, NE, University of Nebraska-Lincoln. Master of Science.

Chandar, G., M. D. Hyzak, et al. (2010). Rapid Economical Bridge Replacement. Modern Steel Construction. Chicago, IL, National Steel Bridge Alliance. 2010.

Chen, W. F. and D. J. Han (1988). Plasticity for Structural Engineers. New York, NY, Springer-Verlag.

Dassault-Systèmes (2010). Abaqus/CAE. Providence, RI, Dassault Systèmes Simulia Corp.

Egilmez, O. O., T. A. Helwig, et al. (2007). "Stiffness and Strength of Metal Bridge Deck Forms." ASCE Journal of Bridge Engineering 12(4): 8.

Galambos, T. V. (1968). Structural Members and Frames. Englewood Cliffs, NJ, Prentice-Hall, Inc.

Galindez, N. Y. (2009). Levels of Lateral Flange Bending in Straight, Skewed and Curved Steel I-Girder Bridges During Deck Placement. Department of Civil & Environmental Engineering. Morgantown, WV, West Virginia University. Doctor of Philosophy.

Garrell, C. (2011). Steel Plate Availability for Highway Bridges. Modern Steel Construction. Chicago, IL, National Steel Bridge Alliance. 2011.

Glaser, L. A. (2010). Constructability Testing of Folded Plate Girders. Department of Civil Engineering. Lincoln, NE, University of Nebraska-Lincoln. Master of Science.

Graybeal, B. A. (2010). Behavior of Field-Cast Ultra-High Performance Concrete Bridge Deck Connections Under Cyclic and Static Structural Loading. McLean, VA, Federal Highway Administration.

Helwig, T. A. and K. H. Frank (1999). "Bending Behavior of Composite Girders with Cold Formed Steel U Section." ASCE Journal of Structural Engineering 125(11):

ITD (2014). ITD Bridge Design LRFD Manual. Boise, ID, Idaho Transportation Department.

Kala, Z. (2013). Elastic Lateral-Torsional Buckling of Simply Supported Hot-Rolled Steel I-Beams with Random Imperfections. 11th International Conference on Modern Building Materials, Structures and Techniques. Vilnius, Lithuania.

Lay, M., Adams, P., and Galambos, T. "Experiments on High Strength Steel Members," Fritz Engineering Laboratory Report No. 297.8, Fritz Engineering Laboratory, Lehigh University, Bethlehem, PA. 1964.

Micro-Measurements, Inc. (2010). StrainSmart. Raliegh, NC, Micro-Measurements, Inc.

Morgan, S. A. (2010). Towards the Development of Efficient and Economical Short Span Modular Bridges. Department of Civil & Environmental Engineering. Morgantown, WV, West Virginia University. Master of Science.

Nakamura, S. (2002). "Bending Behavior of Composite Girders with Cold Formed Steel U Section." ASCE Journal of Structural Engineering 128(9): 8.

NSBA (2012). Design Example 2A: Two-Span Continuous Straight Steel I-Girder Bridge. Steel Bridge Design Handbook. Washington, DC, National Steel Bridge Alliance.

Righman, J. E. (2005). Rotation Compatibility Approach to Moment Redistribution for Design and Rating of Steel I-Girders. Department of Civil & Environmental Engineering. Morgantown, WV, West Virginia University. Doctor of Philosophy.

Roberts, N. R. (2004). Evaluation of the Ductility of Composite Steel I-Girders in Positive Bending. Department of Civil & Environmental Engineering. Morgantown, WV, West Virginia University. Master of Science.

Schafer, B. W. and S. Ádány (2006). Buckling analysis of cold-formed steel members using CUFSM: conventional and constrained finite strip methods 18th International Specialty Conference on Cold-Formed Steel Structures. Orlando, FL.

Schilling, C. and S. Morcos. Moment-Rotation Tests of Steel Girders with Ultra-Compact Flanges. Project 188 Autostress Design of Highway Bridges. American Iron and Steel Institute, 1988.

Taly, N. and H. Gangarao (1979). "Prefabricated Press-Formed Steel T-Box Girder Bridge System." AISC Engineering Journal 16(3): 9.

The Mathworks, Inc. (2010). MATLAB. Natick, MA, The Mathworks, Inc.

Tricon Precast, Con-Struct Prefabricated Bridge System. Standard plans. Tricon Engineering Group, Ltd. 2008.

Yang, L. (2004). Evaluation of Moment Redistribution for Hybrid HPS 70W Bridge Girders. Department of Civil & Environmental Engineering. Morgantown, WV, West Virginia University. Master of Science.

Ziemian, R. D. (2010). Guide to Stability Design Criteria for Metal Structures, John Wiley & Sons, Inc.

APPENDIX A: ELASTIC SECTION PROPERTIES

A.1 INTRODUCTION

The purpose of this appendix is to present the elastic section properties of the press-brake-formed steel tub girders proposed in this work. An in-depth derivation will be performed and will be accompanied by an illustrative example.

A.2 NOMENCLATURE

For the derivation, the following nomenclature is adopted (notation is also described in Figure A.1):

- w_{PL} = width of standard mill plate (in)
- t = plate thickness (in)
- r = bend radius measured at the center of the plate (in)
- b_{tf} = width of top flange (in)
- b_{bf} = width of bottom flange (in)
- d = total girder depth (in)
- D = length of the flat portion of the web (in)
- m = slope ratio of the inclined web (i.e.: 1 to m)

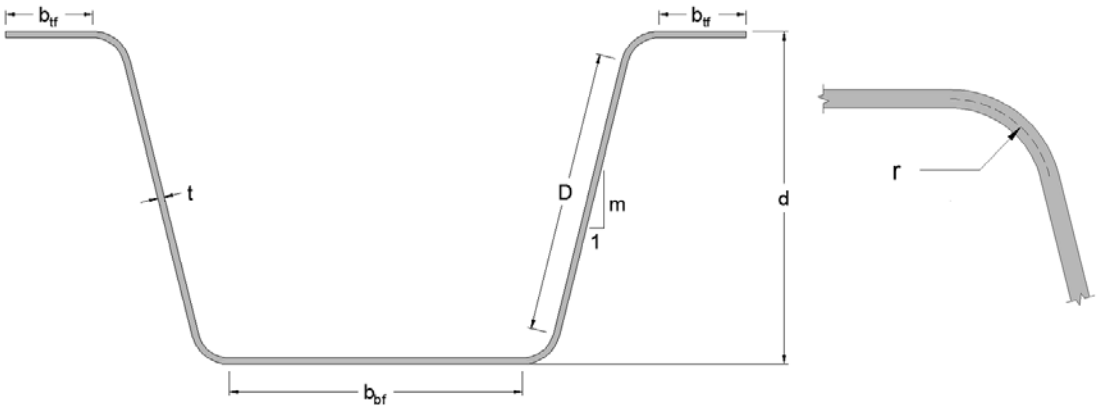

Figure A.1: Nomenclature for Elastic Section Property Derivations

A.3 DERIVATION OF FLEXURAL SECTION PROPERTIES

Moments of inertia of the proposed press-brake-formed steel tub girder are computed using the parallel-axis theorem (Beer et. al., 2012). The individual components of the steel girder consist of rectangular components (i.e. the flat portions of the flanges and webs) and the bend regions. The derivations of the required section properties for each individual component are discussed in this section.

A.3.1 Section Properties of Bend Regions (Sector of a Circular Ring)

The bend regions of the press-brake-formed tub girder are sectors of a circular ring. For clarity, the section properties of these regions are derived in the following section.

A.3.1.1 Geometry of Bend Regions

The geometry of the bend region and the notation used in the following derivation is shown in Figure A.2.

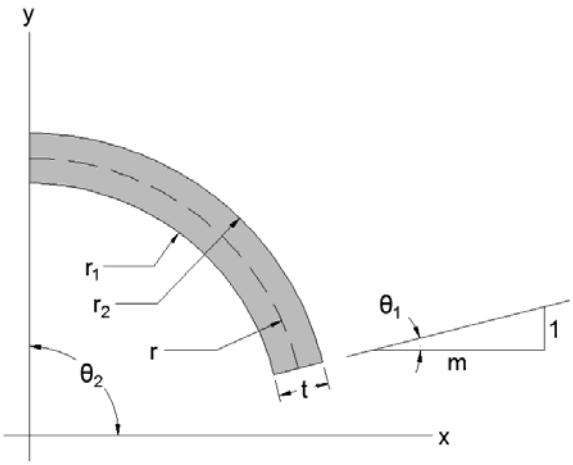

Figure A.2: Bend Region Geometry

From Figure A.2, $r_1 = r - t/2$ and $r_2 = r + t/2$. Using these definitions, the following polynomials can be evaluated and simplified as follows (these polynomials will be employed in Section A.3.1.2):

$$r_2^2 - r_1^2 = 2rt$$

$$r_2^3 - r_1^3 = 3r^2 t + \frac{t^3}{4}$$

$$r_2^4 - r_1^4 = 4r^3 t + rt^3$$

Also, from Figure A.2, $\theta_1 = \tan^{-1}(1/m)$ and $\theta_2 = \pi/2$. Using these definitions, the following trigonometric functions can be evaluated and simplified as follows (these functions will also be employed in Section A.3.1.2):

$$\sin(\theta_1) = \frac{1}{\sqrt{m^2+1}} \qquad \sin(\theta_2) = 1$$

$$\cos(\theta_1) = \frac{m}{\sqrt{m^2+1}} \qquad \cos(\theta_2) = 0$$

$$\sin(2\theta_1) = 2\sin(\theta_1)\cos(\theta_1) = \frac{2m}{m^2+1} \qquad \sin(2\theta_2) = \sin(\pi) = 0$$

$$\cos(2\theta_1) = \cos^2(\theta_1) - \sin^2(\theta_1) = \frac{m^2-1}{m^2+1} \qquad \cos(2\theta_2) = \cos(\pi) = -1$$

$$\alpha = \theta_2 - \theta_1 = \tan^{-1}(m)$$

A.3.1.2 Derivation of Bend-Region Section Properties

The area of a bend region (note that, in polar coordinates, $dA = r\,dr\,d\theta$) is derived as follows:

$$A_{bend} = \iint_A dA = \int_{\theta_1}^{\theta_2}\int_{r_1}^{r_2} r\,dr\,d\theta = \frac{\left(r_2^2 - r_1^2\right)\left(\theta_2 - \theta_1\right)}{2}$$

Substituting the previous definitions for r_1, r_2, θ_1, and θ_2 and simplifying:

$$\therefore A_{bend} = rt\left[\tan^{-1}(m)\right]$$

The center-of-gravity of the bend region (note that, in polar coordinates, $x = r\cos(\theta)$ and $y = r\sin(\theta)$) is derived as follows:

$$\overline{x}_{bend} = \frac{1}{A}\iint_A x\,dA = \frac{1}{A}\int_{\theta_1}^{\theta_2}\int_{r_1}^{r_2} r^2\cos(\theta)\,dr\,d\theta = \frac{\left(r_2^{\,3} - r_1^{\,3}\right)}{3A}\left[\sin(\theta_2) - \sin(\theta_1)\right]$$

$$\overline{y}_{bend} = \frac{1}{A}\iint_A y\,dA = \frac{1}{A}\int_{\theta_1}^{\theta_2}\int_{r_1}^{r_2} r^2\sin(\theta)\,dr\,d\theta = \frac{\left(r_2^{\,3} - r_1^{\,3}\right)}{3A}\left[\cos(\theta_1) - \cos(\theta_2)\right]$$

Substituting the previous expressions for r_1, r_2, θ_1, θ_2, and A and simplifying:

$$\therefore \overline{x}_{bend} = \frac{1}{\tan^{-1}(m)}\left(r + \frac{t^2}{12r}\right)\left(1 - \frac{1}{\sqrt{m^2+1}}\right)$$

$$\therefore \overline{y}_{bend} = \frac{1}{\tan^{-1}(m)}\left(r + \frac{t^2}{12r}\right)\left(\frac{m}{\sqrt{m^2+1}}\right)$$

The moments of inertia of the bend regions about the x- and y-axes (located at the center of the bend radii), respectively, are derived as follows:

$$I_x = \iint_A y^2\,dA = \int_{\theta_1}^{\theta_2}\int_{r_1}^{r_2} r^3\sin^2(\theta)\,dr\,d\theta = \frac{\left(r_2^{\,4} - r_1^{\,4}\right)}{16}\left[2(\theta_2 - \theta_1) + \sin(2\theta_1) - \sin(2\theta_2)\right]$$

$$I_y = \iint_A x^2\,dA = \int_{\theta_1}^{\theta_2}\int_{r_1}^{r_2} r^3\cos^2(\theta)\,dr\,d\theta = \frac{\left(r_2^{\,4} - r_1^{\,4}\right)}{16}\left[2(\theta_2 - \theta_1) - \sin(2\theta_1) + \sin(2\theta_2)\right]$$

Substituting the previous definitions for r_1, r_2, θ_1, and θ_2 and simplifying:

$$I_x = \frac{\left(4r^3t + rt^3\right)}{8}\left[\tan^{-1}\left(m\right) + \frac{m}{m^2+1}\right]$$

$$I_y = \frac{\left(4r^3t + rt^3\right)}{8}\left[\tan^{-1}\left(m\right) - \frac{m}{m^2+1}\right]$$

These expressions for I_x and I_y are expressed about the x- and y-axes located at the center of the bend radii (see Figure A.2). To shift these values to the center-of-gravity of the bend region, the parallel axis theorem is employed as follows:

$$\therefore I_{x_{bend}} = \frac{\left(4r^3t + rt^3\right)}{8}\left[\tan^{-1}\left(m\right) + \frac{m}{m^2+1}\right] - A_{bend}\left(\overline{y}_{bend}{}^2\right)$$

$$\therefore I_{y_{bend}} = \frac{\left(4r^3t + rt^3\right)}{8}\left[\tan^{-1}\left(m\right) - \frac{m}{m^2+1}\right] - A_{bend}\left(\overline{x}_{bend}{}^2\right)$$

Also, since the bend region is circular, the length of the plate in the bend region is simply equal to the radius at the mid-thickness of the bend (i.e. r) multiplied by the total angle the bend encompasses (i.e. $\theta_2 - \theta_1$):

$$L_{bend} = r\left[\tan^{-1}\left(m\right)\right]$$

It should be noted that, in the United States, it is typical that the web in a tub girder employed in bridge applications be inclined at a 1-to-4 slope. Therefore, for a value of $m = 4$:

$$A_{bend} = rt\left[\tan^{-1}(4)\right]$$

$$\bar{x}_{bend} = \frac{1}{\tan^{-1}(4)}\left(r + \frac{t^2}{12r}\right)\left(1 - \frac{1}{\sqrt{17}}\right)$$

$$\bar{y}_{bend} = \frac{1}{\tan^{-1}(4)}\left(r + \frac{t^2}{12r}\right)\left(\frac{4}{\sqrt{17}}\right)$$

$$I_{x_{bend}} = \frac{\left(4r^3t + rt^3\right)}{8}\left[\tan^{-1}(4) + \frac{4}{17}\right] - A_{bend}\left(\bar{y}_{bend}{}^2\right)$$

$$I_{y_{bend}} = \frac{\left(4r^3t + rt^3\right)}{8}\left[\tan^{-1}(4) - \frac{4}{17}\right] - A_{bend}\left(\bar{x}_{bend}{}^2\right)$$

$$L_{bend} = r\left[\tan^{-1}(4)\right]$$

A.3.2 Section Properties of Rectangular Regions

The section properties of a rectangle of width b and height h with respect to the center-of-gravity are easily derived (Beer et. al., 2012) and are as follows:

$$A = bh$$

$$\bar{x} = \frac{b}{2} \qquad \bar{y} = \frac{h}{2}$$

$$I_x = \frac{bh^3}{12} \qquad I_y = \frac{b^3h}{12}$$

For the web regions, the moments of inertia with respect to the center-of-gravity must be expressed about inclined axes as follows (Beer et. al., 2012):

$$I_{x'} = \frac{I_x + I_y}{2} + \frac{I_x - I_y}{2}\cos(2\phi) - I_{xy}\sin(2\phi)$$

$$I_{y'} = \frac{I_x + I_y}{2} - \frac{I_x - I_y}{2}\cos(2\phi) + I_{xy}\sin(2\phi)$$

Therefore, substituting the previous properties (note that, since rectangles are symmetric, $I_{xy} = 0$), the moments of inertia with respect to the center-of-gravity are:

$$I_{x'} = \frac{bh}{24}\left[b^2 + h^2 + \left(h^2 - b^2\right)\cos(2\phi)\right]$$

$$I_{y'} = \frac{bh}{24}\left[b^2 + h^2 - \left(h^2 - b^2\right)\cos(2\phi)\right]$$

The dimensions, b and h, of the inclined web are simply equal to the thickness of the plate, t, and the length of the flat portion of the web, D, respectively. Also, the angle of inclination for the web, $\phi = \theta_1 = \tan^{-1}(1/m)$. Therefore:

$$\therefore I_{x_{web}} = \frac{Dt}{24}\left[D^2 + t^2 + \left(D^2 - t^2\right)\left(\frac{m^2 - 1}{m^2 + 1}\right)\right]$$

$$\therefore I_{y_{web}} = \frac{Dt}{24}\left[D^2 + t^2 - \left(D^2 - t^2\right)\left(\frac{m^2 - 1}{m^2 + 1}\right)\right]$$

The length of the flat portion of the web, D, can be derived by determining the height of the flat portion of the web and employing the web slope ratio. This is shown in the Figure A.3.

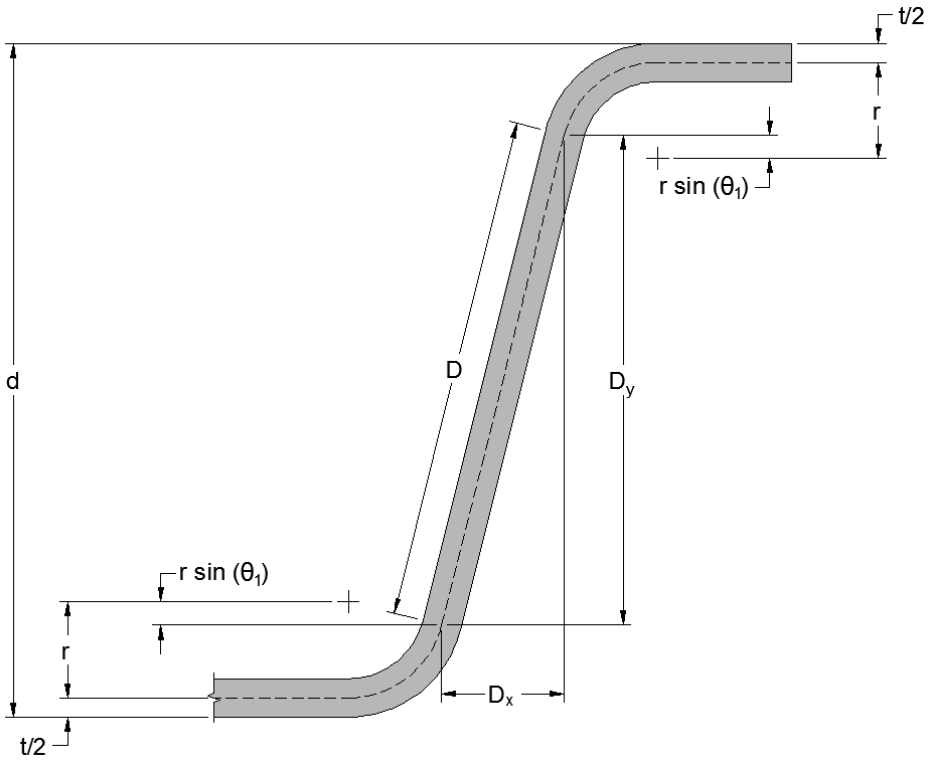

Figure A.3: Length of the Flat Portion of the Inclined Web

Therefore, the length of the flat portion of the web can be derived as follows:

$$D_y = d - 2\left[\frac{t}{2} + r - r\sin\left(\theta_1\right)\right] = d - t - 2r\left(1 - \frac{1}{\sqrt{m^2+1}}\right)$$

$$\therefore D_x = \left[d - t - 2r\left(1 - \frac{1}{\sqrt{m^2+1}}\right)\right]\frac{1}{m} = \frac{2r}{m\sqrt{m^2+1}} + \frac{d-t-2r}{m}$$

$$\therefore D = \left[d - t - 2r\left(1 - \frac{1}{\sqrt{m^2+1}}\right)\right]\frac{\sqrt{m^2+1}}{m} = \frac{2r + \left(d-t-2r\right)\sqrt{m^2+1}}{m}$$

For a 1-to-4 slope ratio of the web, these formulas can be simplified as follows:

$$D_x = \frac{r}{2\sqrt{17}} + \frac{d - t - 2r}{4}$$

$$D_y = d - t - 2r\left(1 - \frac{1}{\sqrt{17}}\right)$$

$$D = \frac{r}{2} + \frac{\sqrt{17}}{4}\left(d - t - 2r\right)$$

$$I_{x_{web}} = \frac{Dt}{24}\left[D^2 + t^2 + \frac{15}{17}\left(D^2 - t^2\right)\right]$$

$$I_{y_{web}} = \frac{Dt}{24}\left[D^2 + t^2 - \frac{15}{17}\left(D^2 - t^2\right)\right]$$

A.3.3 Parallel-Axis Theorem

The moments of inertia of the steel press-brake-formed tub girder are found using the parallel-axis theorem (Beer et. al., 2012):

$$I_{XX} = \sum_{i=1}^{n}\left(I_{x_i} + A_i {d_{y_i}}^2\right) \qquad I_{YY} = \sum_{i=1}^{n}\left(I_{y_i} + A_i {d_{x_i}}^2\right)$$

The d_i values are simply equal to the distance from the center-of-gravity of the individual regions to the center-of-gravity of the press-brake-formed steel tub girder as a whole:

$$d_{x_i} = \overline{x}_i - \overline{X} = \overline{x}_i - \frac{\sum_{i=1}^{n}\left(A_i \overline{x}_i\right)}{\sum_{i=1}^{n}\left(A_i\right)} \qquad d_y = \overline{y}_i - \overline{Y} = \overline{y}_i - \frac{\sum_{i=1}^{n}\left(A_i \overline{y}_i\right)}{\sum_{i=1}^{n}\left(A_i\right)}$$

Therefore, the $\overline{x}_i$ and $\overline{y}_i$ values need to be evaluated for each region in the press-brake-formed steel tub girder. Regions numbers are referenced from Figure A.4. Note that, in order to

determine the center-of-gravity, all $\bar{x}_i$ and $\bar{y}_i$ values must be referenced from a common datum. The location of the datum used in the following derivations is shown in Figure A.5.

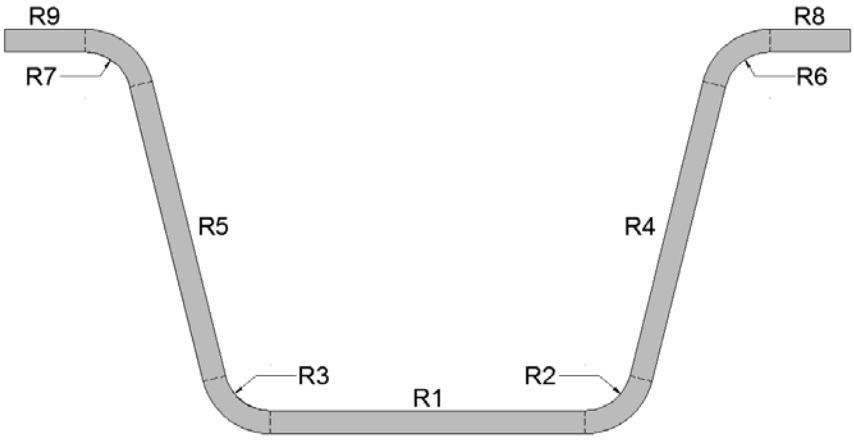

Figure A.4: Region Numbers

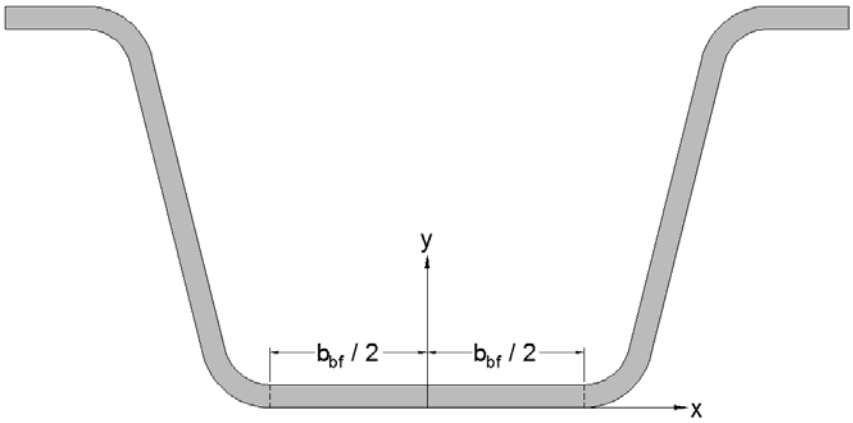

Figure A.5: Reference Datum Location

A.3.3.1 Region 1 (Bottom Flange)

The flat portion of the web is simply a rectangle of width b_{bf} and height t. Therefore, since the center-of-gravity of the bottom flange lies along the y-axis of the datum:

$$\bar{x}_1 = 0 \qquad \bar{y}_1 = \frac{t}{2}$$

A.3.3.2 Regions 2 and 3 (Bottom Bends)

The center-of-gravity of each of the bottom bend regions can be calculated as shown in Figure A.6.

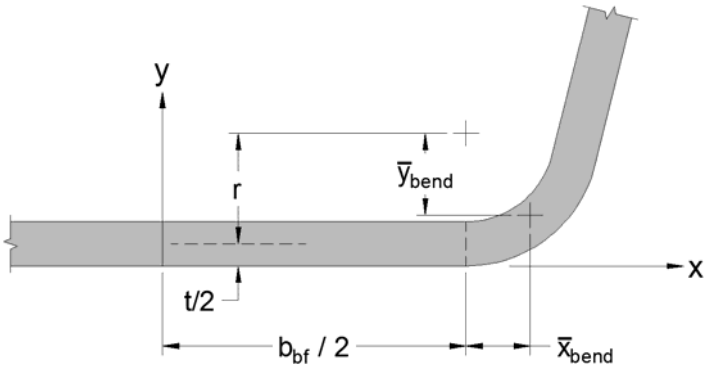

Figure A.6: Bottom Bend Region Center-of-Gravity

Therefore:

$$\bar{x}_2 = \frac{b_{bf}}{2} + \bar{x}_{bend} \qquad \bar{y}_2 = r + \frac{t}{2} - \bar{y}_{bend}$$

Note that, by symmetry:

$$\bar{x}_3 = -\bar{x}_2 \qquad \bar{y}_3 = \bar{y}_2$$

A.3.3.3 Regions 4 and 5 (Inclined Webs)

The *x*-axis center-of-gravity of each of the inclined web regions can be calculated as shown in Figure A.7. Also, since the top and bottom bend regions are both bent at the same angle and radius, the *y*-axis centers-of-gravity for the inclined web from the datum are simply equal to half of the total girder depth.

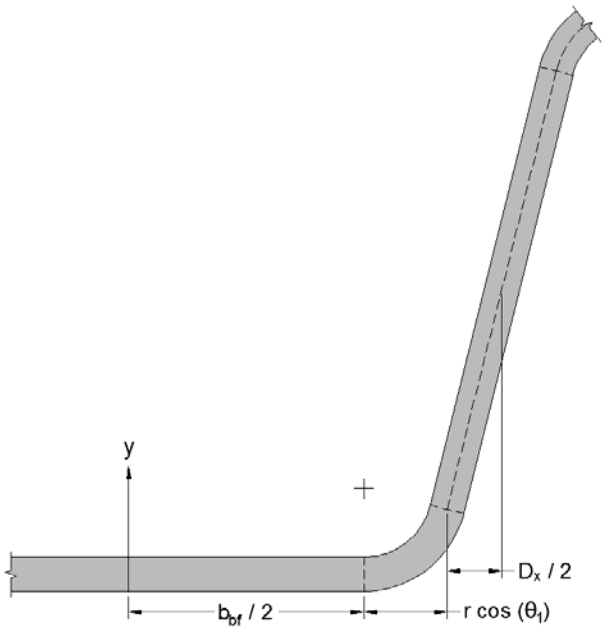

Figure A.7: Inclined Web Center-of-Gravity

Therefore:

$$\bar{x}_4 = \frac{b_{bf}}{2} + r\cos(\theta_1) + \frac{D_x}{2} \qquad \bar{y}_4 = \frac{d}{2}$$

Substituting previous expressions for $\cos(\theta_1)$ and D_x and expressing the formula for a 1-to-4 web slope ratio:

$$\therefore \bar{x}_4 = \frac{b_{bf}}{2} + \frac{d-t}{8} + r\left(\frac{17-\sqrt{17}}{4\sqrt{17}}\right) \qquad \bar{y}_4 = \frac{d}{2}$$

Note that, by symmetry:

$$\overline{x}_5 = -\overline{x}_4 \qquad\qquad \overline{y}_4 = \overline{y}_5$$

A.3.3.4 Regions 6 and 7 (Top Bends)

The centers-of-gravity of each of the top bend regions can be calculated as shown in Figure A.8.

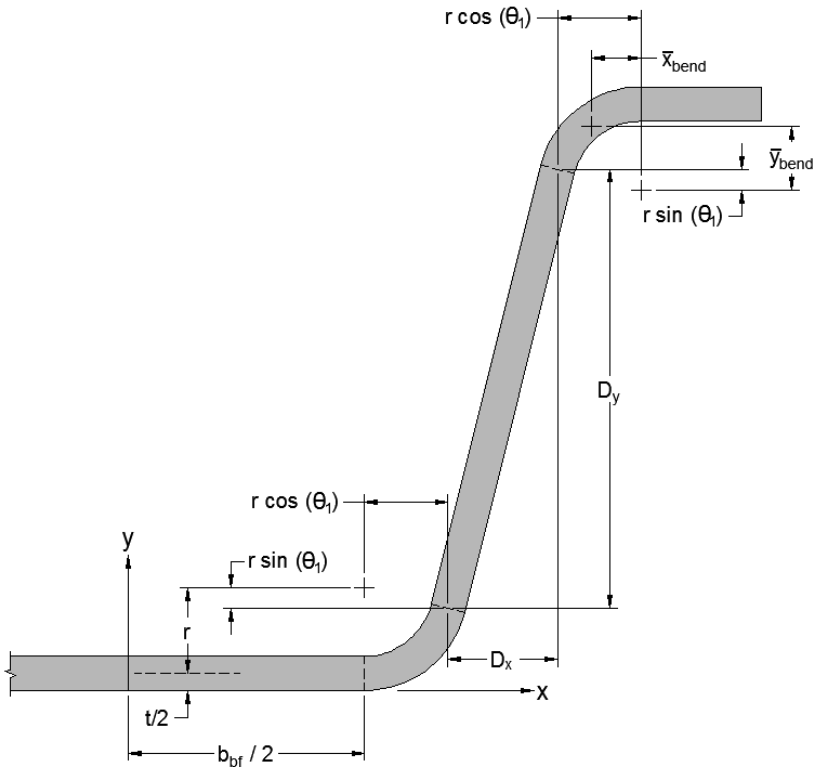

Figure A.8: Top Bend Center-of-Gravity

Therefore:

$$\overline{x}_6 = \frac{b_{bf}}{2} + 2r\cos\left(\theta_1\right) + D_x - \overline{x}_{bend} \qquad\qquad \overline{y}_6 = r + \frac{t}{2} - 2r\sin\left(\theta_1\right) + D_y + \overline{y}_{bend}$$

Substituting previous expressions for $\cos(\theta_1)$, D_x, D_y and expressing the formula for a 1-to-4 web slope ratio:

$$\therefore \bar{x}_6 = \frac{b_{bf}}{2} + \frac{d-t}{4} + r\left(\frac{17-\sqrt{17}}{2\sqrt{17}}\right) - \bar{x}_{bend} \qquad \therefore \bar{y}_6 = d - \left(r + \frac{t}{2} - \bar{y}_{bend}\right)$$

Note that, by symmetry:

$$\bar{x}_7 = -\bar{x}_6 \qquad \bar{y}_7 = \bar{y}_6$$

A.3.3.5 Regions 8 and 9 (Top Flanges)

The *x*-axis center-of-gravity of each of the top flanges can be calculated as shown in Figure A.9.

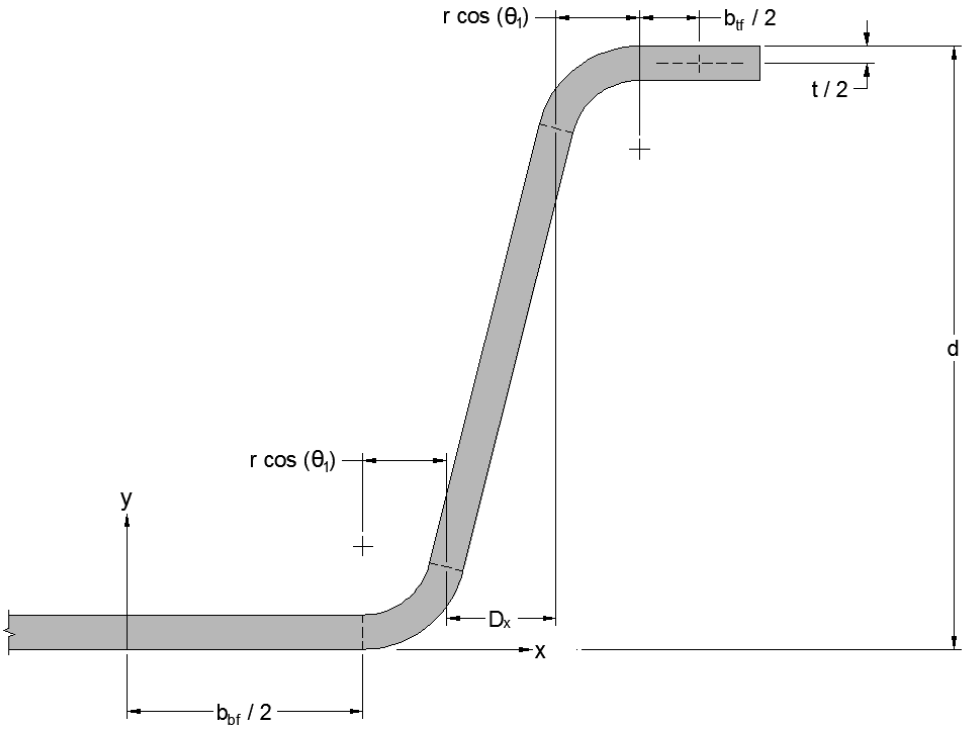

Figure A.9: Top Flange Center-of-Gravity

Therefore:

$$\bar{x}_8 = \frac{b_{bf}}{2} + 2r\cos(\theta_1) + D_x + \frac{b_{tf}}{2} \qquad \bar{y}_8 = d - \frac{t}{2}$$

Substituting previous expressions for $\cos(\theta_1)$ and D_x and expressing the formulas for a 1-to-4 web slope ratio:

$$\bar{x}_8 = \frac{b_{bf}}{2} + \frac{d-t}{4} + r\left(\frac{17-\sqrt{17}}{2\sqrt{17}}\right) + \frac{b_{tf}}{2} \qquad \bar{y}_8 = d - \frac{t}{2}$$

Note that, by symmetry:

$$\bar{x}_9 = -\bar{x}_8 \qquad \bar{y}_8 = \bar{y}_9$$

A.3.4 Summary of Derivation

The following summary of formulas used in computing the section properties of press-brake-formed steel tub girders is listed here. Note that all of the formulas reference the regions shown in Figure A.4 and the $\bar{x}_i$ and $\bar{y}_i$ values are measured from the datum referenced in Figure A.5. In addition, all of the formulas have been simplified for a 1-to-4 slope ratio (i.e. $m = 4$).

A.3.4.1 Constant Values

The following constants are referenced in the formulas in Section A.3.4.2:

$$A_{bend} = rt\left[\tan^{-1}(4)\right]$$

$$\bar{x}_{bend} = \frac{1}{\tan^{-1}(4)}\left(r + \frac{t^2}{12r}\right)\left(1 - \frac{1}{\sqrt{17}}\right)$$

$$\bar{y}_{bend} = \frac{1}{\tan^{-1}(4)}\left(r + \frac{t^2}{12r}\right)\left(\frac{4}{\sqrt{17}}\right)$$

$$I_{x_{bend}} = \frac{\left(4r^3t + rt^3\right)}{8}\left[\tan^{-1}(4) + \frac{4}{17}\right] - A_{bend}\left(\bar{y}_{bend}{}^2\right)$$

$$I_{y_{bend}} = \frac{\left(4r^3t + rt^3\right)}{8}\left[\tan^{-1}(4) - \frac{4}{17}\right] - A_{bend}\left(\bar{x}_{bend}{}^2\right)$$

$$L_{bend} = r\left[\tan^{-1}(4)\right]$$

$$D = \frac{r}{2} + \frac{\sqrt{17}}{4}(d - t - 2r)$$

$$I_{x_{web}} = \frac{Dt}{24}\left[D^2 + t^2 + \frac{15}{17}\left(D^2 - t^2\right)\right]$$

$$I_{y_{web}} = \frac{Dt}{24}\left[D^2 + t^2 - \frac{15}{17}\left(D^2 - t^2\right)\right]$$

A.3.4.2 Cross-Sectional Areas

The areas of the individual regions are computed as follows:

$$A_1 = b_{bf}\,t$$

$$A_2 = A_3 = A_{bend}$$

$$A_4 = A_5 = Dt$$

$$A_6 = A_7 = A_{bend}$$

$$A_8 = A_9 = b_{tf}\,t$$

A.3.4.3 Centers-of-Gravity

The centers-of-gravity of the individual regions are computed as follows:

$$\overline{x}_1 = 0 \qquad \overline{y}_1 = \frac{t}{2}$$

$$\overline{x}_2 = -\overline{x}_3 = \frac{b_{bf}}{2} + \overline{x}_{bend} \qquad \overline{y}_2 = \overline{y}_3 = r + \frac{t}{2} - \overline{y}_{bend}$$

$$\overline{x}_4 = -\overline{x}_5 = \frac{b_{bf}}{2} + \frac{d-t}{8} + r\left(\frac{17-\sqrt{17}}{4\sqrt{17}}\right) \qquad \overline{y}_4 = \overline{y}_5 = \frac{d}{2}$$

$$\overline{x}_6 = -\overline{x}_7 = \frac{b_{bf}}{2} + \frac{d-t}{4} + r\left(\frac{17-\sqrt{17}}{2\sqrt{17}}\right) - \overline{x}_{bend} \qquad \overline{y}_6 = \overline{y}_7 = d - \left(r + \frac{t}{2} - \overline{y}_{bend}\right)$$

$$\overline{x}_8 = -\overline{x}_9 = \frac{b_{bf}}{2} + \frac{d-t}{4} + r\left(\frac{17-\sqrt{17}}{2\sqrt{17}}\right) + \frac{b_{tf}}{2} \qquad \overline{y}_8 = \overline{y}_9 = d - \frac{t}{2}$$

A.3.4.4 Moments of Inertia

The moments of inertia of the individual regions are computed as follows:

$$I_{x_1} = \frac{b_{bf} t^3}{12} \qquad I_{y_1} = \frac{b_{bf}{}^3 t}{12}$$

$$I_{x_2} = I_{x_3} = I_{x_{bend}} \qquad I_{y_2} = I_{y_3} = I_{y_{bend}}$$

$$I_{x_4} = I_{x_5} = I_{x_{web}} \qquad I_{y_4} = I_{y_5} = I_{y_{web}}$$

$$I_{x_6} = I_{x_7} = I_{x_{bend}} \qquad I_{y_6} = I_{y_7} = I_{y_{bend}}$$

$$I_{x_8} = I_{x_9} = \frac{b_{tf} t^3}{12} \qquad I_{y_8} = I_{y_9} = \frac{b_{tf}{}^3 t}{12}$$

A.4 Derivation of Torsional Section Properties

St. Venant torsional constants, warping constants, and constants of monosymmetry of the proposed press-brake-formed steel tub girder are derived using provisions specified by Galambos (1968) and the Guide to Stability Design Criteria for Metal Structures (Ziemian, 2010). For the derivation of torsional properties, the girder is idealized as a series of straight-line segments of plates.

A.4.1 Relevant Functions and Integrals

Consider a plate element as illustrated in Figure A.10. For each plate element, spanning from point i to point $i + 1$, the x and y coordinates at any point along the plate width can be expressed as follows, where L_i is the length of the plate element in question, and s is the distance along the plate element mid-thickness from the i^{th} point:

$$x(s) = x_i N_1 + x_{i+1} N_2 = x_i \left(1 - \frac{s}{L_i}\right) + x_{i+1} \left(\frac{s}{L_i}\right)$$

$$y(s) = y_i N_1 + y_{i+1} N_2 = y_i \left(1 - \frac{s}{L_i}\right) + y_{i+1} \left(\frac{s}{L_i}\right)$$

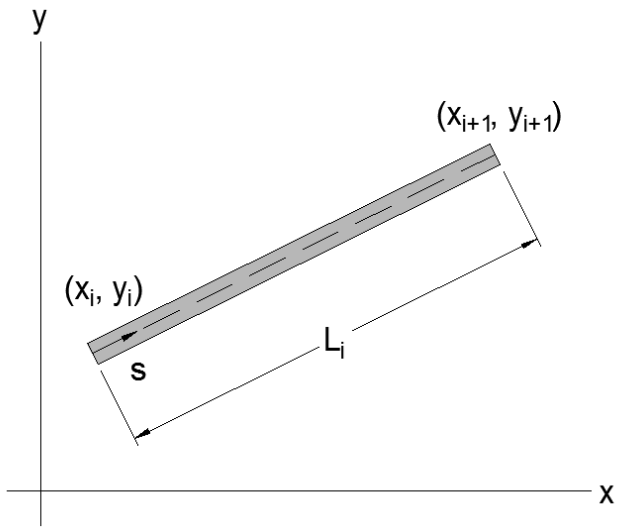

Figure A.10: Plate Element Notation

The following derivations contain repeated integration of the shape functions, N_1 and N_2, over the length of plate elements. These integrals take the following form:

$$\int_0^{L_i} N_1{}^A N_2{}^B \, ds = \int_0^{L_i} \left(1 - \frac{s}{L_i}\right)^A \left(\frac{s}{L_i}\right)^B ds = \frac{L_i}{C}$$

Depending on the values of the constants A and B, the integral will result in L_i divided by a constant value C. The resulting constants for varying values of A and B are summarized in Table A.1:

Table A.1: Integration Constants ("C" Values)

	A = 0	A = 1	A = 2	A = 3
B = 0	1	2	3	4
B = 1	2	6	12	20
B = 2	3	12	30	60
B = 3	4	20	60	140

To demonstrate the use of these shape functions and resulting integration constants, the definition of the moment of inertia about the x-axis, I_x, of a shape made up of k straight-line plate elements can be simplified as follows (assuming constant plate thickness throughout the cross-section), where $A_i = t\,L_i$:

$$
\begin{aligned}
I_x &= \iint_A y^2\,dA = t\left(\int_S y^2\,dS\right) \\
&= t\sum_{i=1}^{n}\int_0^{L_i} y^2\,ds = t\sum_{i=1}^{n}\int_0^{L_i}\left(y_i N_1 + y_{i+1}N_2\right)^2\,ds \\
&= t\sum_{i=1}^{n}\int_0^{L_i}\left[\left(y_i N_1\right)^2 + 2\left(y_i y_{i+1} N_1 N_2\right) + \left(y_{i+1}N_2\right)^2\right]ds \\
&= t\sum_{i=1}^{n}\left[\left(y_i^{\,2}\right)\left(\int_0^{L_i} N_1^{\,2}\,ds\right) + \left(2y_i y_{i+1}\right)\left(\int_0^{L_i} N_1 N_2\,ds\right) + \left(y_{i+1}^{\,2}\right)\left(\int_0^{L_i} N_2^{\,2}\,ds\right)\right] \\
&= t\sum_{i=1}^{n}\left[\left(y_i^{\,2}\right)\left(\frac{L_i}{3}\right) + \left(2y_i y_{i+1}\right)\left(\frac{L_i}{6}\right) + \left(y_{i+1}^{\,2}\right)\left(\frac{L_i}{3}\right)\right] \\
&= \sum_{i=1}^{n}\frac{A_i}{3}\left(y_i^{\,2} + y_i y_{i+1} + y_{i+1}^{\,2}\right)
\end{aligned}
$$

In addition, the following derivations require that all coordinates defining the endpoints of plate elements are referenced with respect to the center-of-gravity of the cross section. Using summation notation, the center-of-gravity can be determined as follows:

$$A = \sum_{i=1}^{n} A_i$$

$$
\begin{aligned}
Q_x &= \iint_A x\,dA = t\left(\int_S x\,dS\right) \\
&= t\sum_{i=1}^{n}\int_0^{L_i} x\,ds = t\sum_{i=1}^{n}\int_0^{L_i}\left(x_i N_1 + x_{i+1}N_2\right)ds \\
&= t\sum_{i=1}^{n}\left[\left(x_i\right)\left(\int_0^{L_i} N_1\,ds\right)+\left(x_{i+1}\right)\left(\int_0^{L_i} N_2\,ds\right)\right] \\
&= t\sum_{i=1}^{n}\left[\left(x_i\right)\left(\frac{L_i}{2}\right)+\left(x_{i+1}\right)\left(\frac{L_i}{2}\right)\right] \\
&= \sum_{i=1}^{n}\frac{A_i}{2}\left(x_i + x_{i+1}\right)
\end{aligned}
$$

$$
\begin{aligned}
Q_y &= \iint_A y\,dA = t\left(\int_S y\,dS\right) \\
&= t\sum_{i=1}^{n}\int_0^{L_i} y\,ds = t\sum_{i=1}^{n}\int_0^{L_i}\left(y_i N_1 + y_{i+1}N_2\right)ds \\
&= t\sum_{i=1}^{n}\left[\left(y_i\right)\left(\int_0^{L_i} N_1\,ds\right)+\left(y_{i+1}\right)\left(\int_0^{L_i} N_2\,ds\right)\right] \\
&= t\sum_{i=1}^{n}\left[\left(y_i\right)\left(\frac{L_i}{2}\right)+\left(y_{i+1}\right)\left(\frac{L_i}{2}\right)\right] \\
&= \sum_{i=1}^{n}\frac{A_i}{2}\left(y_i + y_{i+1}\right)
\end{aligned}
$$

$$\therefore \bar{X} = \frac{Q_x}{A}$$

$$\therefore \bar{Y} = \frac{Q_y}{A}$$

In addition the lengths of each element, L_i, are found using simple geometry as follows:

$$L_i = \sqrt{\left(x_{i+1} - x_i\right)^2 + \left(y_{i+1} - y_i\right)^2}$$

A.4.2 Location of Shear Center

For an open thin-walled cross-section, the coordinates of the shear center (X_o, Y_o) are determined as follows, where I_{wx} and I_{wy} are the warping products of inertia about the x- and y-axes, respectively, taken at the center of gravity (note that, if the shape exhibits symmetry about either axis, $I_{xy} = 0$):

$$X_o = \frac{I_{wx}I_{xy} - I_{wy}I_y}{I_{xy}^2 - I_xI_y} = \frac{I_{wy}}{I_x} \qquad Y_o = \frac{I_{wx}I_x - I_{wy}I_{xy}}{I_{xy}^2 - I_xI_y} = -\frac{I_{wx}}{I_y}$$

The warping products of inertia, I_{wx} and I_{wy}, are defined as follows, where ω is the unit warping across the section with respect to the center-of-gravity and s is the distance along the mid-thickness of the open cross-section (note that, if thickness is constant, it can be factored out of the integrand):

$$I_{wx} = \int_S \omega x t\, ds = t\left(\int_S \omega x\, ds\right) \qquad I_{wy} = \int_S \omega y t\, ds = t\left(\int_S \omega y\, ds\right)$$

The computation of I_{wx} and I_{wy} can be greatly simplified by recognizing that, for an open cross-section made up of straight-line elements of uniform thickness, the unit warping varies linearly along each segment. Therefore, using the previously defined shape functions, for I_{wx}:

$$
\begin{aligned}
I_{wx} &= t\left(\int_S \omega x\, ds\right) \\
&= t\sum_{i=1}^{n}\int_0^{L_i} \omega x\, ds \\
&= t\sum_{i=1}^{n}\int_0^{L_i} \left(\omega_i N_1 + \omega_{i+1} N_2\right)\left(x_i N_1 + x_{i+1} N_2\right) ds \\
&= t\sum_{i=1}^{n}\left[\left(\omega_i x_i\right)\left(\int_0^{L_i} {N_1}^2\, ds\right) + \left(\omega_i x_{i+1} + \omega_{i+1} x_i\right)\left(\int_0^{L_i} N_1 N_2\, ds\right) + \left(\omega_{i+1} x_{i+1}\right)\left(\int_0^{L_i} {N_2}^2\, ds\right)\right] \\
&= t\sum_{i=1}^{n}\left[\left(\omega_i x_i\right)\left(\frac{L_i}{3}\right) + \left(\omega_i x_{i+1} + \omega_{i+1} x_i\right)\left(\frac{L_i}{6}\right) + \left(\omega_{i+1} x_{i+1}\right)\left(\frac{L_i}{3}\right)\right] \\
&= \sum_{i=1}^{n}\frac{A_i}{3}\left(\omega_i x_i + \omega_{i+1} x_{i+1}\right) + \sum_{i=1}^{n}\frac{A_i}{6}\left(\omega_i x_{i+1} + \omega_{i+1} x_i\right)
\end{aligned}
$$

Similarly, for I_{wy}:

$$
I_{wy} = \sum_{i=1}^{n}\frac{A_i}{3}\left(\omega_i y_i + \omega_{i+1} y_{i+1}\right) + \sum_{i=1}^{n}\frac{A_i}{6}\left(\omega_i y_{i+1} + \omega_{i+1} y_i\right)
$$

The unit warping across the section with respect to the center-of-gravity, ω, is found by simply integrating the moment arm of the cross-section, ρ, along the cross-section coordinate s as follows:

$$
\omega(s) = \int_0^s \rho\, ds
$$

As stated, for straight-line elements of uniform thickness, the unit warping varies linearly along each segment. Therefore, the values of the unit warping function are determined as follows (note that the first value of unit warping in a cross-section is set to zero as the shear stress at this location is zero):

$$
\omega_{i+1} = \omega_i + \rho_i L_i
$$

The moment arm distances with respect to the center-of-gravity, ρ_i, are found using simple geometry as follows (note that, for straight-line elements, ρ_i is taken at the middle of each element at $s = L_i / 2$):

$$\frac{dx}{ds} = \frac{d}{ds}\left[x_i \left(1 - \frac{s}{L_i} \right) + x_{i+1} \left(\frac{s}{L_i} \right) \right] = \frac{x_{i+1} - x_i}{L_i}$$

$$\frac{dy}{ds} = \frac{d}{ds}\left[y_i \left(1 - \frac{s}{L_i} \right) + y_{i+1} \left(\frac{s}{L_i} \right) \right] = \frac{y_{i+1} - y_i}{L_i}$$

$$\rho(s) = x\frac{dy}{ds} - y\frac{dx}{ds} = \left[x_i \left(1 - \frac{s}{L_i} \right) + x_{i+1} \left(\frac{s}{L_i} \right) \right] \left[\frac{y_{i+1} - y_i}{L_i} \right] - \left[y_i \left(1 - \frac{s}{L_i} \right) + y_{i+1} \left(\frac{s}{L_i} \right) \right] \left[\frac{x_{i+1} - x_i}{L_i} \right]$$

$$\rho_i = \rho\left(\frac{L_i}{2} \right) = \left(\frac{x_i + x_{i+1}}{2} \right) \left(\frac{y_{i+1} - y_i}{L_i} \right) - \left(\frac{y_i + y_{i+1}}{2} \right) \left(\frac{x_{i+1} - x_i}{L_i} \right)$$

$$\therefore \rho_i = \frac{x_i y_{i+1} - x_{i+1} y_i}{L_i}$$

A.4.3 St. Venant Torsional Constant and Warping Constant

The St. Venant torsional constant, J, is computed as follows (assuming constant thickness throughout the cross-section):

$$J = \frac{t^3}{3} \sum_{i=1}^{n} L_i$$

The warping constant, C_w, is determined as follows, where ω_n is the normalized unit warping, W_o is the normalizing function, and ω_o is the unit warping across the section with respect to the shear center (note that, if thickness is constant, it can be factored out of the integrand):

$$C_w = \int_S \omega_n{}^2 t\, dS = t\left(\int_S \omega_n{}^2\, dS \right)$$

$$\omega_n = W_o - \omega_o$$

$$W_o = \frac{1}{A}\left(\int_S \omega_o t\, dS \right) = \frac{t}{A}\left(\int_S \omega_o\, dS \right)$$

Using the previously defined shape functions, these values may be computed as follows (note that A_i refers to the cross-sectional area of a given element whereas A refers to the total cross-sectional area):

$$\begin{aligned} W_o &= \frac{t}{A}\left(\int_S \omega_o\, dS \right) = \left(\frac{t}{A} \right)\left(\sum_{i=1}^{n} \int_0^{L_i} \omega_o\, ds \right) \\ &= \left(\frac{t}{A} \right)\left[\sum_{i=1}^{n} \int_0^{L_i} \left(\omega_{oi} N_1 + \omega_{o(i+1)} N_2 \right) \right] \\ &= \left(\frac{t}{A} \right)\left\{ \sum_{i=1}^{n} \left[\left(\omega_{oi} \right)\left(\int_0^{L_i} N_1\, ds \right) + \left(\omega_{o(i+1)} \right)\left(\int_0^{L_i} N_2\, ds \right) \right] \right\} \\ &= \left(\frac{t}{A} \right)\left\{ \sum_{i=1}^{n} \left[\left(\omega_{oi} \right)\left(\frac{L_i}{2} \right) + \left(\omega_{o(i+1)} \right)\left(\frac{L_i}{2} \right) \right] \right\} \\ &= \sum_{i=1}^{n} \frac{A_i}{2A}\left(\omega_{oi} + \omega_{o(i+1)} \right) \end{aligned}$$

$$\therefore \omega_{ni} = W_o - \omega_{oi}$$

$$\therefore \omega_{n(i+1)} = W_o - \omega_{o(i+1)}$$

$$
\begin{aligned}
C_w &= t\left(\int_S \omega_n{}^2\, ds\right) \\
&= t\sum_{i=1}^{n}\int_0^{L_i} \omega_n{}^2\, ds = t\sum_{i=1}^{n}\int_0^{L_i}\left(\omega_{ni}N_1 + \omega_{n(i+1)}N_2\right)^2 ds \\
&= t\sum_{i=1}^{n}\int_0^{L_i}\left[\left(\omega_{ni}N_1\right)^2 + 2\left(\omega_{ni}\omega_{n(i+1)}N_1N_2\right) + \left(\omega_{n(i+1)}N_2\right)^2\right] ds \\
&= t\sum_{i=1}^{n}\left[\left(\omega_{ni}{}^2\right)\left(\int_0^{L_i} N_1{}^2\, ds\right) + \left(2\omega_{ni}\omega_{n(i+1)}\right)\left(\int_0^{L_i} N_1N_2\, ds\right) + \left(\omega_{n(i+1)}{}^2\right)\left(\int_0^{L_i} N_2{}^2\, ds\right)\right] \\
&= t\sum_{i=1}^{n}\left[\left(\omega_{ni}{}^2\right)\left(\frac{L_i}{3}\right) + \left(2\omega_{ni}\omega_{n(i+1)}\right)\left(\frac{L_i}{6}\right) + \left(\omega_{n(i+1)}{}^2\right)\left(\frac{L_i}{3}\right)\right] \\
&= \sum_{i=1}^{n}\frac{A_i}{3}\left(\omega_{ni}{}^2 + \omega_{ni}\omega_{n(i+1)} + \omega_{n(i+1)}{}^2\right)
\end{aligned}
$$

As stated, for straight-line elements of uniform thickness, the unit warping varies linearly along each segment. Therefore, the values of ω_o are computed in the same manner as the method for ω:

$$\omega_{o(i+1)} = \omega_{oi} + \rho_{oi}L_i$$

The moment arm distances with respect to the shear center, ρ_{oi}, are computed in the same manner as the method for ρ (note that the original coordinates of the end points of each segment must be adjusted by the shear center coordinates):

$$\rho_i = \frac{x_i y_{i+1} - x_{i+1}y_i}{L_i}$$

$$\therefore \rho_{oi} = \frac{\left(x_i - X_o\right)\left(y_{i+1} - Y_o\right) - \left(x_{i+1} - X_o\right)\left(y_i - Y_o\right)}{L_i} = \rho_i - \frac{\left(y_{i+1} - y_i\right)X_o - \left(x_{i+1} - x_i\right)Y_o}{L_i}$$

A.4.4 Coefficient of Monosymmetry

According to the Guide to Stability Design Criteria for Metal Structures (Ziemian, 2010), the coefficient of monosymmetry, β_x, for a cross-section is expressed as follows (β_x is positive if

the larger flange is in tension), where x and y are the coordinates with respect to the center-of-gravity, I_x is the moment of inertia about the x-axis, and Y_o is the distance from the shear center to the center-of-gravity (taken positive if the larger flange is in tension):

$$\beta_x = \frac{B_1 + B_2}{I_x} - 2Y_o$$

$$B_1 = \iint_A y^3 \, dA$$

$$B_2 = \iint_A x^2 y \, dA$$

The first integral, B_1, is evaluated using summation notation as follows:

$$\begin{aligned} y^3 &= \left(y_i N_1 + y_{i+1} N_2\right)^3 \\ &= y_i^{\,3}\left(N_1^{\,3}\right) + 3y_i^{\,2} y_{i+1}\left(N_1^{\,2} N_2\right) + 3y_i y_{i+1}^{\,2}\left(N_1 N_2^{\,2}\right) + y_{i+1}^{\,3}\left(N_2^{\,3}\right) \end{aligned}$$

$$\begin{aligned} \int_0^{L_i} y^3 \, ds &= y_i^{\,3}\left(\int_0^{L_i} N_1^{\,3} \, ds\right) + 3y_i^{\,2} y_{i+1}\left(\int_0^{L_i} N_1^{\,2} N_2 \, ds\right) + 3y_i y_{i+1}^{\,2}\left(\int_0^{L_i} N_1 N_2^{\,2} \, ds\right) + y_{i+1}^{\,3}\left(\int_0^{L_i} N_2^{\,3} \, ds\right) \\ &= y_i^{\,3}\left(\frac{L_i}{4}\right) + 3y_i^{\,2} y_{i+1}\left(\frac{L_i}{12}\right) + 3y_i y_{i+1}^{\,2}\left(\frac{L_i}{12}\right) + y_{i+1}^{\,3}\left(\frac{L_i}{4}\right) \\ &= \frac{L_i}{4}\left(y_i^{\,3} + y_i^{\,2} y_{i+1} + y_i y_{i+1}^{\,2} + y_{i+1}^{\,3}\right) \\ &= \frac{L_i}{4}\left(y_i + y_{i+1}\right)\left(y_i^{\,2} + y_{i+1}^{\,2}\right) \end{aligned}$$

$$B_1 = \iint_A y^3 \, dA = t\left(\int_S y^3 \, dS\right) = t\left(\sum_{i=1}^{n} \int_0^{L_i} y^3 \, ds\right)$$

$$\therefore B_1 = \sum_{i=1}^{n} \frac{A_i}{4}\left(y_i + y_{i+1}\right)\left(y_i^{\,2} + y_{i+1}^{\,2}\right)$$

The second, B_2, is evaluated using summation notation as follows:

$$\begin{aligned} x^2 y &= \left(x_i N_1 + x_{i+1} N_2\right)^2 \left(y_i N_1 + y_{i+1} N_2\right) \\ &= \left(x_i{}^2 y_i\right)\left(N_1{}^3\right) + \left(x_i{}^2 y_{i+1} + 2x_i x_{i+1} y_i\right)\left(N_1{}^2 N_2\right) + \left(x_{i+1}{}^2 y_i + 2x_i x_{i+1} y_{i+1}\right)\left(N_1 N_2{}^2\right) \\ &\quad + \left(x_{i+1}{}^2 y_{i+1}\right)\left(N_2{}^3\right) \end{aligned}$$

$$\begin{aligned} \int_0^{L_i} x^2 y\, ds &= \left(x_i{}^2 y_i\right)\left(\int_0^{L_i} N_1{}^3\, ds\right) + \left(x_i{}^2 y_{i+1} + 2x_i x_{i+1} y_i\right)\left(\int_0^{L_i} N_1{}^2 N_2\, ds\right) \\ &\quad + \left(x_{i+1}{}^2 y_i + 2x_i x_{i+1} y_{i+1}\right)\left(\int_0^{L_i} N_1 N_2{}^2\, ds\right) + \left(x_{i+1}{}^2 y_{i+1}\right)\left(\int_0^{L_i} N_2{}^3\, ds\right) \\ &= \left(x_i{}^2 y_i\right)\left(\frac{L_i}{4}\right) + \left(x_i{}^2 y_{i+1} + 2x_i x_{i+1} y_i\right)\left(\frac{L_i}{12}\right) + \left(x_{i+1}{}^2 y_i + 2x_i x_{i+1} y_{i+1}\right)\left(\frac{L_i}{12}\right) + \left(x_{i+1}{}^2 y_{i+1}\right)\left(\frac{L_i}{4}\right) \\ &= \frac{L_i}{12}\left\{y_i\left[2x_i{}^2 + \left(x_i + x_{i+1}\right)^2\right] + y_{i+1}\left[2x_{i+1}{}^2 + \left(x_i + x_{i+1}\right)^2\right]\right\} \end{aligned}$$

$$B_2 = \iint_A x^2 y\, dA = t\left(\int_S x^2 y\, dS\right) = t\left(\sum_{i=1}^{n} \int_0^{L_i} x^2 y\, ds\right)$$

$$\therefore B_2 = \sum_{i=1}^{n} \frac{A_i}{12}\left\{y_i\left[2x_i{}^2 + \left(x_i + x_{i+1}\right)^2\right] + y_{i+1}\left[2x_{i+1}{}^2 + \left(x_i + x_{i+1}\right)^2\right]\right\}$$

A.5 ILLUSTRATIVE EXAMPLE

To demonstrate the use of these formulas, a numerical example on a typical press-brake formed tub girder is presented in the following section.

A.5.1 Parameters of Example Girder

The press-brake-formed steel tub girder shown in Figure A.10 will be employed to demonstrate the computation of elastic section properties derived in this appendix. For this girder:

- w_{PL} = width of standard mill plate = 84 in
- t = plate thickness = 7/16 in (0.4375 in)
- b_{tf} = width of top flange = 6 in
- d = total girder depth = 23 in
- m = slope ratio of the inclined web (i.e.: 1 to m) = 4

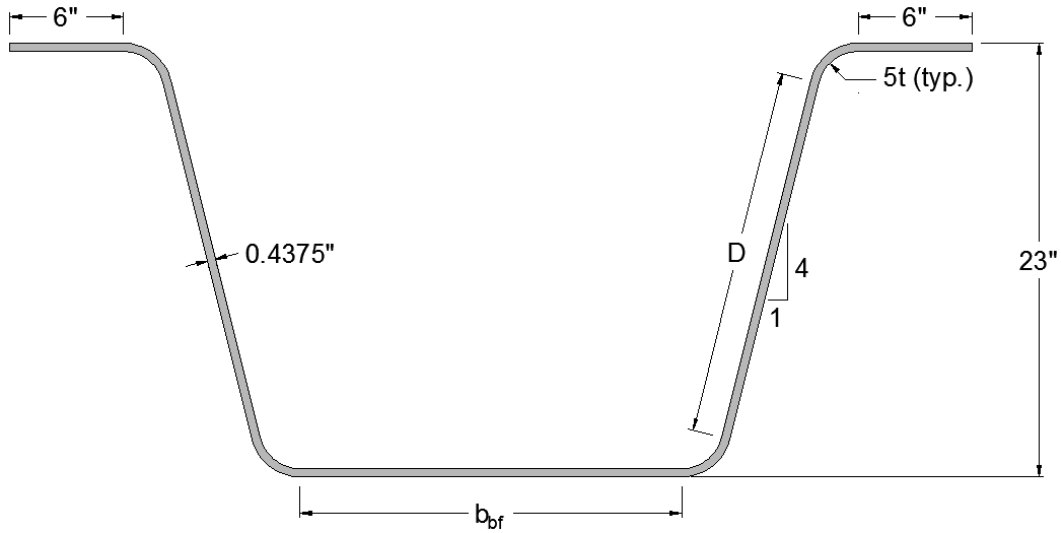

Figure A.11: Example Girder for Flexural Property Calculations

A.5.2 Related Flexural Expressions

For this example, the plate is to be bent such that the inside bend radius shall be equal to five times the thickness (i.e. $r_1 = 5t$). Therefore:

$$r = r_1 + \frac{t}{2} = 5t + \frac{t}{2} = \frac{11}{2}t$$

Employing this expression for r, the constants in Section A.3.4.1 can be simplified as follows:

$$A_{bend} = t^2\left[\frac{11}{2}\tan^{-1}(4)\right]$$

$$\overline{x}_{bend} = t\left(\frac{182}{33\tan^{-1}(4)}\right)\left(1-\frac{1}{\sqrt{17}}\right)$$

$$\overline{y}_{bend} = t\left(\frac{182}{33\tan^{-1}(4)}\right)\left(\frac{4}{\sqrt{17}}\right)$$

$$I_{x_{bend}} = t^4\left(\frac{671}{8}\right)\left[\tan^{-1}(4)+\frac{4}{17}\right]-A_{bend}\left(\overline{y}_{bend}{}^2\right)$$

$$I_{y_{bend}} = t^4\left(\frac{671}{8}\right)\left[\tan^{-1}(4)-\frac{4}{17}\right]-A_{bend}\left(\overline{x}_{bend}{}^2\right)$$

$$L_{bend} = t\left[\frac{11}{2}\tan^{-1}(4)\right]$$

$$D = d\left(\frac{\sqrt{17}}{4}\right)+t\left(\frac{11}{4}-3\sqrt{17}\right)$$

$$I_{x_{web}} = \frac{Dt}{24}\left[D^2+t^2+\frac{15}{17}\left(D^2-t^2\right)\right]$$

$$I_{y_{web}} = \frac{Dt}{24}\left[D^2+t^2-\frac{15}{17}\left(D^2-t^2\right)\right]$$

Since the sum of the lengths of all of the individual regions must equal the width of the standard mill plate, w, the resulting width of the bottom flange, b_{bf}, can be determined as follows:

$$b_{bf} = w_{PL}-\sum_{i=2}^{9}\left(L_i\right) = w_{PL}-\left(4L_{bend}+2D+2b_{tf}\right)$$

Substituting the previous expressions for L_{bend} and D:

$$\therefore b_{bf} = w_{PL} - d\left(\frac{\sqrt{17}}{2}\right) - t\left[\frac{11}{2} - 6\sqrt{17} + 22\tan^{-1}(4)\right] - 2b_{tf}$$

In addition, some of the centers-of-gravity of the individual regions listed in Section A.3.4.3 can be simplified as follows:

$$\bar{x}_1 = 0 \qquad \bar{y}_1 = \frac{t}{2}$$

$$\bar{x}_2 = -\bar{x}_3 = \frac{b_{bf}}{2} + \bar{x}_{bend} \qquad \bar{y}_2 = \bar{y}_3 = 6t - \bar{y}_{bend}$$

$$\bar{x}_4 = -\bar{x}_5 = \frac{b_{bf}}{2} + \frac{d}{8} + t\left(\frac{187 - 12\sqrt{17}}{8\sqrt{17}}\right) \qquad \bar{y}_4 = \bar{y}_5 = \frac{d}{2}$$

$$\bar{x}_6 = -\bar{x}_7 = \frac{b_{bf}}{2} + \frac{d}{4} + t\left(\frac{187 - 12\sqrt{17}}{4\sqrt{17}}\right) - \bar{x}_{bend} \qquad \bar{y}_6 = \bar{y}_7 = d - \left(6t - \bar{y}_{bend}\right)$$

$$\bar{x}_8 = -\bar{x}_9 = \frac{b_{bf}}{2} + \frac{d}{4} + t\left(\frac{187 - 12\sqrt{17}}{4\sqrt{17}}\right) + \frac{b_{tf}}{2} \qquad \bar{y}_8 = \bar{y}_9 = d - \frac{t}{2}$$

A.5.3 Calculation of Flexural Section Properties

Using the formulas in Section A.3.4.4 and Section A.4.1, the moments of inertia of the noncomposite press-brake-formed steel tub girder are computed. A summary of these computations are listed in Table A.2. From this calculation, the moments of inertia of the press-brake-formed tub girder are as follows:

$$I_{XX} = 2893.1\ \text{in}^4 \qquad I_{YY} = 8049.6\ \text{in}^4$$

Table A.2: Computation of Moments of Inertia

Region	L (in)	A (in^2)	$\bar{x}$ (in)	$\bar{y}$ (in)	$A\bar{x}$ (in^3)	$A\bar{y}$ (in^3)	I_x (in^4)	I_y (in^4)	d_x (in)	d_y (in)	I_{XX} (in^4)	I_{YY} (in^4)
1	20.240	8.8551	0	0.2188	0	1.9370	0.1412	302.30	0	-10.175	916.84	302.30
2	3.1902	1.3957	11.499	0.8594	16.049	1.1995	0.4462	0.6987	11.499	-9.5339	127.31	185.24
3	3.1902	1.3957	-11.499	0.8594	-16.049	1.1995	0.4462	0.6987	-11.499	-9.5339	127.31	185.24
4	19.499	8.5310	14.819	11.5	126.42	98.106	254.42	16.029	14.819	1.1067	264.86	1889.5
5	19.499	8.5310	-14.819	11.5	-126.42	98.106	254.42	16.029	-14.819	1.1067	264.86	1889.5
6	3.1902	1.3957	18.140	22.141	25.318	30.902	0.4462	0.6987	18.140	11.747	193.05	459.96
7	3.1902	1.3957	-18.140	22.141	-25.318	30.902	0.4462	0.6987	-18.140	11.747	193.05	459.96
8	6	2.6250	22.518	22.781	59.110	59.801	0.0419	7.8750	22.518	12.388	402.88	1338.9
9	6	2.6250	-22.518	22.781	-59.110	59.801	0.0419	7.8750	-22.518	12.388	402.88	1338.9
Σ =	84	36.75			0	381.96					2893.1	8049.6

A.5.4 Related Torsional Expressions

As shown in Section A.4, to compute torsional properties, the cross-section is idealized as a collection of straight-line elements. For the illustrative purposes of this example, the girder shown in Figure A.11 is simplified as a collection of straight-line elements as shown in Figure A.12.

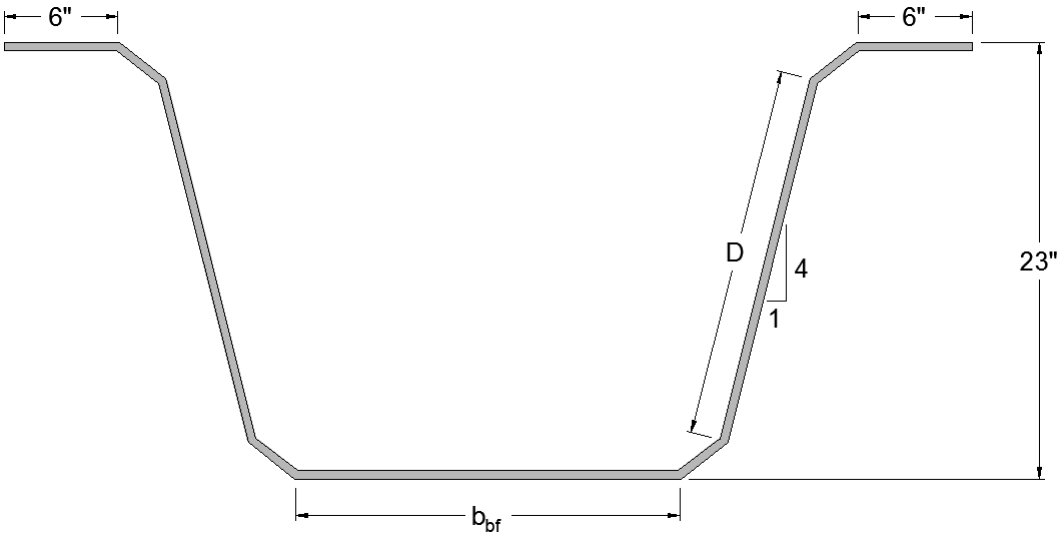

Figure A.12: Example Girder for Torsional Property Calculations

The coordinates of the endpoints of the elements in Figure A.12 were computed using the provisions derived in Sections A2 and A3. However, since the derived formulas reference the chosen datum shown in Figure A.5, these coordinates must be adjusted to be referenced from the center-of-gravity of the cross-section. This adjustment is completed in Table A.3. Recall, using summation notation:

$$L_i = \sqrt{\left(x_{i+1} - x_i\right)^2 + \left(y_{i+1} - y_i\right)^2} \qquad A_i = tL_i$$

$$Q_{xi} = \frac{A_i}{2}\left(x_i + x_{i+1}\right) \qquad Q_{yi} = \frac{A_i}{2}\left(y_i + y_{i+1}\right)$$

Table A.3: Adjustment of Coordinates

Element	Original Coordinates (in)				L_i (in)	A_i (in^2)	Qx_i (in^3)	Qy_i (in^3)	Adjusted Coordinates (in)			
	x_i	x_{i+1}	y_i	y_{i+1}					x_i	x_{i+1}	y_i	y_{i+1}
1	-25.518	-19.518	22.781	22.781	6.0000	2.6250	-59.110	59.801	-25.518	-19.518	12.400	12.400
2	-19.518	-17.184	22.781	20.959	2.9617	1.2957	-23.778	28.338	-19.518	-17.184	12.400	10.577
3	-17.184	-12.455	20.959	2.041	19.499	8.5310	-126.42	98.106	-17.184	-12.455	10.577	-8.3398
4	-12.455	-10.120	2.041	0.219	2.9617	1.2957	-14.625	1.4643	-12.455	-10.120	-8.3398	-10.162
5	-10.120	10.120	0.219	0.219	20.240	8.8551	0.0000	1.9370	-10.120	10.120	-10.162	-10.162
6	10.120	12.455	0.219	2.041	2.9617	1.2957	14.625	1.4643	10.120	12.455	-10.162	-8.3398
7	12.455	17.184	2.041	20.959	19.499	8.5310	126.42	98.106	12.455	17.184	-8.3398	10.577
8	17.184	19.518	20.959	22.781	2.9617	1.2957	23.778	28.338	17.184	19.518	10.577	12.400
9	19.518	25.518	22.781	22.781	6.0000	2.6250	59.110	59.801	19.518	25.518	12.400	12.400
Σ =						36.350	0.0000	377.36				

Therefore:

$$\bar{X} = \frac{Q_x}{A} = \frac{0.0000\ \text{in}^3}{36.350\ \text{in}^2} = 0.0000\ \text{in}$$

$$\bar{Y} = \frac{Q_y}{A} = \frac{399.36\ \text{in}^3}{36.350\ \text{in}^2} = 10.381\ \text{in}$$

Once adjusted, the endpoint coordinates, coupled with unit warping with respect to the center-of-gravity, can be employed to determine the location of the shear center. This calculation is completed in Table A.4. Note that the first value of unit warping, ω_1, is set to zero as the shear stress at this location is zero. Also, since by observation, the shape is symmetric about the y-axis, $I_{xy} = 0$ and is not computed. Recall, using summation notation:

$$L_i = \sqrt{\left(x_{i+1} - x_i\right)^2 + \left(y_{i+1} - y_i\right)^2}$$

$$\rho_i = \frac{x_i y_{i+1} - x_{i+1} y_i}{L_i}$$

$$\omega_{i+1} = \omega_i + \rho_i L_i$$

$$I_{xi} = \frac{A_i}{3}\left(y_i^{\,2} + y_i y_{i+1} + y_{i+1}^{\,2}\right)$$

$$I_y = \frac{A_i}{3}\left(x_i^{\,2} + x_i x_{i+1} + x_{i+1}^{\,2}\right)$$

$$I_{wxi} = \frac{A_i}{3}\left(\omega_i x_i + \omega_{i+1} x_{i+1}\right) + \frac{A_i}{6}\left(\omega_i x_{i+1} + \omega_{i+1} x_i\right)$$

$$I_{wy} = \frac{A_i}{3}\left(\omega_i y_i + \omega_{i+1} y_{i+1}\right) + \frac{A_i}{6}\left(\omega_i y_{i+1} + \omega_{i+1} y_i\right)$$

$$\therefore X_o = \frac{I_{wx} I_{xy} - I_{wy} I_y}{I_{xy}^{\,2} - I_x I_y} = \frac{I_{wy}}{I_x}$$

$$\therefore Y_o = \frac{I_{wx} I_x - I_{wy} I_{xy}}{I_{xy}^{\,2} - I_x I_y} = -\frac{I_{wx}}{I_y}$$

Table A.4: Computation of Shear Center Location

Element	Adjusted Coordinates (in)				L_i (in)	ρ_i (in)	Unit Warp. (in^2)		I_{xi} (in^4)	I_{yi} (in^4)	I_{wxi} (in^5)	I_{wyi} (in^5)
	x_i	x_{i+1}	y_i	y_{i+1}			ω_i	ω_{i+1}				
1	-25.518	-19.518	12.400	12.400	6.0000	-12.400	0	-74.401	403.63	1338.9	2101.3	-1210.9
2	-19.518	-17.184	12.400	10.577	2.9617	2.2379	-74.401	-67.773	171.38	436.94	1692.0	-1059.5
3	-17.184	-12.455	10.577	-8.3398	19.499	14.105	-67.773	207.27	265.09	1889.4	-7893.2	-3033.2
4	-12.455	-10.120	-8.3398	-10.162	2.9617	14.238	207.27	249.44	111.25	165.67	-3329.2	-2745.6
5	-10.120	10.120	-10.162	-10.162	20.240	10.162	249.44	455.13	914.50	302.30	3072.1	-31702
6	10.120	12.455	-10.162	-8.3398	2.9617	14.238	455.13	497.30	111.25	165.67	6975.4	-5700.1
7	12.455	17.184	-8.3398	10.577	19.499	14.105	497.30	772.34	265.09	1889.4	81180	9758.2
8	17.184	19.518	10.577	12.400	2.9617	2.2379	772.34	778.97	171.38	436.94	18445	11548
9	19.518	25.518	12.400	12.400	6.0000	-12.400	778.97	704.57	403.63	1338.9	43749	24145
Σ =									2817.2	7964.1	145993	0.0000

Therefore:

$$X_o = \frac{I_{wy}}{I_x} = \frac{0.0000\ \text{in}^5}{2817.2\ \text{in}^4} = 0.0000\ \text{in} \qquad Y_o = -\frac{I_{wx}}{I_y} = -\frac{145993\ \text{in}^5}{7964.1\ \text{in}^4} = -18.331\ \text{in}$$

Once the location of the shear center has been determined, utilizing a normalized unit warping with respect to the shear center, the warping constant can be computed. This calculation is completed in Table A.5 (in addition, the St. Venant torsional constant is computed here also). Note that the first value of unit warping with respect to the shear center, ω_{o1}, is set to zero as the shear stress at this location is zero. Recall, using summation notation (note that A_i refers to the cross-sectional area of a given element whereas A refers to the total cross-sectional area):

$$L_i = \sqrt{\left(x_{i+1} - x_i\right)^2 + \left(y_{i+1} - y_i\right)^2}$$

$$\rho_{oi} = \rho_i - \frac{\left(y_{i+1} - y_i\right)X_o - \left(x_{i+1} - x_i\right)Y_o}{L_i}$$

$$\omega_{o(i+1)} = \omega_{oi} + \rho_{oi} L_i$$

$$W_{oi} = \frac{A_i}{2A}\left(\omega_{oi} + \omega_{o(i+1)}\right)$$

$$\omega_{ni} = W_o - \omega_{oi}$$

$$\omega_{n(i+1)} = W_o - \omega_{o(i+1)}$$

$$\therefore J = \frac{t^3}{3}\sum_{i=1}^{n} L_i$$

$$\therefore C_{wi} = \frac{A_i}{3}\left(\omega_{ni}{}^2 + \omega_{ni}\omega_{n(i+1)} + \omega_{n(i+1)}{}^2\right)$$

Table A.5: Computation of St. Venant Torsional Constant and Warping Constant

Element	Adjusted Coordinates (in)				L_i (in)	ρ_{oi} (in)	Unit Warp. (in^2)		W_{oi} (in^2)	Norm Warp. (in^2)		C_{wi} (in^6)
	x_i	x_{i+1}	y_i	y_{i+1}			ω_{oi}	$\omega_{o(i+1)}$		ω_{ni}	$\omega_{n(i+1)}$	
1	-25.518	-19.518	12.400	12.400	6.0000	-30.731	0	-184.39	-6.6578	-115.50	68.893	8862.6
2	-19.518	-17.184	12.400	10.577	2.9617	-12.211	-184.39	-220.55	-7.2173	68.893	105.06	9943.0
3	-17.184	-12.455	10.577	-8.3398	19.499	9.6593	-220.55	-32.202	-29.660	105.06	-83.294	26231
4	-12.455	-10.120	-8.3398	-10.162	2.9617	-0.2107	-32.202	-32.826	-1.1590	-83.294	-82.670	8922.5
5	-10.120	10.120	-10.162	-10.162	20.240	-8.1689	-32.826	-198.17	-28.135	-82.670	82.670	20173
6	10.120	12.455	-10.162	-8.3398	2.9617	-0.2107	-198.17	-198.79	-7.0749	82.670	83.294	8922.5
7	12.455	17.184	-8.3398	10.577	19.499	9.6593	-198.79	-10.439	-24.552	83.294	-105.06	26231
8	17.184	19.518	10.577	12.400	2.9617	-12.211	-10.439	-46.603	-1.0167	-105.06	-68.893	9943.0
9	19.518	25.518	12.400	12.400	6.0000	-30.731	-46.603	-230.99	-10.023	-68.893	115.50	8862.6
Σ =					83.086				-115.50			128090

Therefore:

$$J = \frac{t^3}{3}\sum_{i=1}^{n} L_i = \frac{(0.4375\,\text{in})^3}{3}(83.086\,\text{in}) = 2.3192\,\text{in}^4 \qquad C_w = 128090\,\text{in}^6$$

In addition, once the endpoint coordinates have been adjusted to be referenced with respect to the center-of-gravity, the coefficient of monosymmetry can be computed (β_x is positive if the larger flange is in tension). This calculation is completed in Table A.6. Recall, using summation notation:

$$L_i = \sqrt{\left(x_{i+1} - x_i\right)^2 + \left(y_{i+1} - y_i\right)^2}$$

$$I_{xi} = \frac{A_i}{3}\left(y_i^{\,2} + y_i y_{i+1} + y_{i+1}^{\,2}\right)$$

$$I_y = \frac{A_i}{3}\left(x_i^{\,2} + x_i x_{i+1} + x_{i+1}^{\,2}\right)$$

$$B_1 = \frac{A_i}{4}\left(y_i + y_{i+1}\right)\left(y_i^{\,2} + y_{i+1}^{\,2}\right)$$

$$B_2 = \frac{A_i}{12}\left\{y_i\left[2x_i^{\,2} + \left(x_i + x_{i+1}\right)^2\right] + y_{i+1}\left[2x_{i+1}^{\,2} + \left(x_i + x_{i+1}\right)^2\right]\right\}$$

$$\therefore \beta_x = \frac{B_1 + B_2}{I_x} - 2Y_o$$

According to the Guide to Stability Design Criteria for Metal Structures (Ziemian, 2010), Y_o is the distance from the shear center to the center-of-gravity (taken positive if the larger flange is in tension). Therefore, in the following computations:

$$Y_o = 18.331\,\text{in}$$

Table A.6: Computation of Coefficient of Monosymmetry

Element	Adjusted Coordinates (in)				L_i (in)	I_{xi} (in^4)	Integrals (in^5)	
	x_i	x_{i+1}	y_i	y_{i+1}			B_{1i}	B_{2i}
1	-25.518	-19.518	12.400	12.400	6.0000	403.63	5005.0	16603
2	-19.518	-17.184	12.400	10.577	2.9617	171.38	1977.2	5036.7
3	-17.184	-12.455	10.577	-8.3398	19.499	265.09	865.88	3999.0
4	-12.455	-10.120	-8.3398	-10.162	2.9617	111.25	-1035.8	-1522.2
5	-10.120	10.120	-10.162	-10.162	20.240	914.50	-9293.6	-3072.1
6	10.120	12.455	-10.162	-8.3398	2.9617	111.25	-1035.8	-1522.2
7	12.455	17.184	-8.3398	10.577	19.499	265.09	865.88	3999.0
8	17.184	19.518	10.577	12.400	2.9617	171.38	1977.2	5036.7
9	19.518	25.518	12.400	12.400	6.0000	403.63	5005.0	16603
Σ =						2817.2	4331.0	45161

Therefore:

$$\therefore \beta_x = \frac{B_1 + B_2}{I_x} - 2Y_o = \frac{4331.0\,\text{in}^5 + 45161\,\text{in}^5}{2817.2\,\text{in}^4} - 2\left(18.331\,\text{in}\right) = -19.095\,\text{in}$$

Recall that the preceding computations are based on an "approximate" representation of the girder shown in Figure A.12 (i.e. only using one straight-line element per bend region). This was done in order to demonstrate the numerical methods for computing torsional constants. Using MATLAB (see Appendix D), this computation can be refined by incorporating more elements in bend regions. A comparison of results obtained using more elements in bend regions is shown in Table A.7. In addition, exact results from Table A.2 are shown, which illustrate the accuracy of each representation of the girder. As shown, using 10000 straight-line elements in bend regions is adequate to achieve accurate section properties.

Table A.7: Accuracy of Torsional Section Properties

Property	Number of Straight-Line Bend Segments in Bend Regions						Exact
	1	10	100	1000	10000	20000	
A (in^2)	36.350	36.746	36.750	36.750	36.750	36.750	36.750
$\bar{y}$ (in)	10.381	10.393	10.393	10.393	10.393	10.393	10.393
I_x (in^4)	2817.2	2891.4	2892.2	2892.2	2892.2	2892.2	2893.1
I_y (in^4)	7964.1	8048.5	8049.4	8049.4	8049.4	8049.4	8049.6
Y_o (in)	-18.331	-18.471	-18.472	-18.472	-18.472	-18.472	--
J (in^4)	2.3192	2.3445	2.3447	2.3447	2.3447	2.3447	2.3447
C_w (in^6)	128090	139824	139950	139951	139952	139952	--
β_x (in)	-19.095	-19.698	-19.704	-19.704	-19.704	-19.704	--

APPENDIX B: MATLAB PROGRAMS & ILLUSTRATIVE EXAMPLES

B.1 INTRODUCTION

The purpose of this appendix is to document the MATLAB (The Mathworks, Inc., 2010) functions and programs written for this research. Each program is documented, and selected examples are presented which illustrate the methodology the functions/programs implement.

B.2 MATLAB FUNCTIONS AND PROGRAMS

B.2.1 Function File: flexprop_NC.m

Function file "flexprop_NC.m" is employed to determine the noncomposite section properties of the press-brake-formed tub girder (see Appendix A). Given the standard mill plate width and thickness, the girder depth, the bend radii, the web slope ratio, and the width of the top flange, the function reports the cross-sectional area, center-of-gravity, and the X-axis moment of inertia of the noncomposite section. The MATLAB file is as follows:

```
function [A_NC,y_NC,Ix_NC] = flexprop_NC(w,t,d,r,m,btf)

% Constant Values
% ----------------------------------------
% A_bend = area of the bend region (in^2)
% y_bend = center-of-gravity of the bend region (in)
% Ix_bend = moment of inertia of the bend region (in^4)
% L_bend = length of the bend region (in)
% D = length of the inclined web (in)
% Ix_web = moment of inertia of the inclined web (in^4)
% bbf = bottom flange width (in)

A_bend=r*t*atan(m);
y_bend=(1/atan(m))*(r+t^2/(12*r))*(m/sqrt(m^2+1));
Ix_bend=((4*r^3*t+r*t^3)/8)*(atan(m)+m/(m^2+1))-A_bend*(y_bend^2);
L_bend=r*atan(m);
D=(2*r+(d-t-2*r)*sqrt(m^2+1))/m;
Ix_web=(D*t/24)*(D^2+t^2+(D^2-t^2)*((m^2-1)/(m^2+1)));
bbf=w-(4*L_bend+2*D+2*btf);
```

```
% Noncomposite Section Properties
% ----------------------------------------
% A_i = area (in^2)
% y_i = centers-of-gravity (in)
% Ay_i = first moment (in^3)
% I_i = moment of inertia (in^4)
% d_i = parallel axis (in)
% Ix_i = parallel axis theorem (in^4)

A_1=bbf*t;      y_1=t/2;                Ay_1=A_1*y_1;
A_2=A_bend;     y_2=r+t/2-y_bend;       Ay_2=A_2*y_2;
A_3=A_bend;     y_3=r+t/2-y_bend;       Ay_3=A_3*y_3;
A_4=D*t;        y_4=d/2;                Ay_4=A_4*y_4;
A_5=D*t;        y_5=d/2;                Ay_5=A_5*y_5;
A_6=A_bend;     y_6=d-(r+t/2-y_bend);   Ay_6=A_6*y_6;
A_7=A_bend;     y_7=d-(r+t/2-y_bend);   Ay_7=A_7*y_7;
A_8=btf*t;      y_8=d-t/2;              Ay_8=A_8*y_8;
A_9=btf*t;      y_9=d-t/2;              Ay_9=A_9*y_9;

A_NC=A_1+A_2+A_3+A_4+A_5+A_6+A_7+A_8+A_9;
Ay_NC=Ay_1+Ay_2+Ay_3+Ay_4+Ay_5+Ay_6+Ay_7+Ay_8+Ay_9;
y_NC=Ay_NC/A_NC;

I_1=(bbf*(t^3))/12;     d_1=y_1-y_NC;       Ix_1=I_1+A_1*(d_1^2);
I_2=Ix_bend;            d_2=y_2-y_NC;       Ix_2=I_2+A_2*(d_2^2);
I_3=Ix_bend;            d_3=y_3-y_NC;       Ix_3=I_3+A_3*(d_3^2);
I_4=Ix_web;             d_4=y_4-y_NC;       Ix_4=I_4+A_4*(d_4^2);
I_5=Ix_web;             d_5=y_5-y_NC;       Ix_5=I_5+A_5*(d_5^2);
I_6=Ix_bend;            d_6=y_6-y_NC;       Ix_6=I_6+A_6*(d_6^2);
I_7=Ix_bend;            d_7=y_7-y_NC;       Ix_7=I_7+A_7*(d_7^2);
I_8=(btf*(t^3))/12;     d_8=y_8-y_NC;       Ix_8=I_8+A_8*(d_8^2);
I_9=(btf*(t^3))/12;     d_9=y_9-y_NC;       Ix_9=I_9+A_9*(d_9^2);

Ix_NC=Ix_1+Ix_2+Ix_3+Ix_4+Ix_5+Ix_6+Ix_7+Ix_8+Ix_9;

end
```

B.2.2 Function File: flexprop_C.m

Function file "flexprop_C.m" is employed to determine the composite section properties of the press-brake-formed tub girder (see Appendix A). Given the results from "flexprop_NC.m" along with the slab properties, such as the width, the thickness, and the modular ratio, the function reports the X-axis moment of inertia of the composite section. The MATLAB file is as follows:

```
function Ix_C = flexprop_C(A_NC,y_NC,Ix_NC,bs,n,ts,d)

% Composite Section Properties
% ----------------------------------------
% A_i = area (in^2)
% y_i = centers-of-gravity (in)
% Ay_i = first moment (in^3)
% I_i = moment of inertia (in^4)
% d_i = parallel axis (in)
% Ix_i = parallel axis theorem (in^4)

A_1=A_NC;           y_1=y_NC;       Ay_1=A_1*y_1;
A_2=(bs/n)*(ts);    y_2=d+ts/2;     Ay_2=A_2*y_2;

A_C=A_1+A_2;
Ay_C=Ay_1+Ay_2;
y_C=Ay_C/A_C;

I_1=Ix_NC;              d_1=y_1-y_C;        Ix_1=I_1+A_1*(d_1^2);
I_2=(bs/n)*(ts^3)/12;   d_2=y_2-y_C;        Ix_2=I_2+A_2*(d_2^2);

Ix_C=Ix_1+Ix_2;

end
```

B.2.3 Program File: torsprop_C.m

Program file "torsprop_C.m" is employed to determine the torsional properties of the press-brake-formed tub girder (see Appendix A). Given the parameters defining the geometry of the girder along with the desired precision (defined by the number of elements in each region of the cross-cection), the function reports the St. Venant torsional constant, the location of the shear center, the warping constant, and the coefficient of monosymmetry. Using the desired precision, the program first calculates the location of nodes required to define the cross-section. Then, the program uses the algorithm described in Appendix A to compute relevant section properties. The MATLAB file is as follows (input for the girder used in the demonstrated example in Appendix A is shown):

```
clc
clear all

% ========================================================================
% PART 1:  FUNDAMENTAL PARAMETERS & CONSTANT VALUES
% ========================================================================

% Fundamental Parameters
% ----------------------------------------
w=84;        % standard mill plate width (in)
t=7/16;      % plate thickness (in)
r=5*t+t/2;   % bend radius at mid-thickness (in)
m=4;         % slope radio of the web (i.e 1:4)
d=23;        % total girder depth (in)
btf=6;       % top flange width (in)

ne_tf=1;     % number of elements along the top flange
ne_b=10000;  % number of elements along the bend
ne_w=1;      % number of elements along the web
ne_bf=1;     % number of elements along the bottom flange

% Constant Values
% ----------------------------------------
% theta = bend angle (rad)
% A_bend = area of the bend region (in^2)
% x_bend = x-axis center-of-gravity of the bend region (in)
% y_bend = y-axis center-of-gravity of the bend region (in)
% L_bend = length of the bend region (in)
% Dx = length of the x-portion inclined web (in)
% Dy = length of the y-portion inclined web (in)
% D = length of the inclined web (in)
% bbf = bottom flange width (in)

theta=pi/2-atan(1/m);
```

```
L_bend=r*atan(m);
Dx=2*r/(m*sqrt(m^2+1))+(d-t-2*r)/m;
Dy=d-t-2*r*(1-1/sqrt(m^2+1));
D=(2*r+(d-t-2*r)*sqrt(m^2+1))/m;
bbf=w-(4*L_bend+2*D+2*btf);

% ========================================================================
% PART 2:  NODE LAYOUT
% ========================================================================

% Node Layout - Top Flange
% ----------------------------------------
n_tf_x=((0):(btf/ne_tf):(btf))'+2*r*sin(theta)+Dx+bbf/2;
n_tf_y=zeros(ne_tf+1,1)+d-t;

n_tf_x1=-n_tf_x;    n_tf_y1=n_tf_y;
n_tf_x2=+n_tf_x;    n_tf_y2=n_tf_y;
clear n_tf_x n_tf_y

% Node Layout - Top Bend Regions
% ----------------------------------------
n_theta=(pi/2-theta):(theta/ne_b):(pi/2);
n_tb_x=-r*cos(n_theta)+2*r*sin(theta)+Dx+bbf/2;
n_tb_y=r*sin(n_theta)-2*r*cos(theta)+Dy+r;

n_tb_x1=-n_tb_x';   n_tb_y1=n_tb_y';
n_tb_x2=+n_tb_x';   n_tb_y2=n_tb_y';
clear n_theta n_tb_x n_tb_y

% Node Layout - Flat Web Regions
% ----------------------------------------
n_w_x=((0):(Dx/ne_w):(Dx))'+r*sin(theta)+bbf/2;
n_w_y=((0):(Dy/ne_w):(Dy))'+2*r*(sin(theta/2))^2;

n_w_x1=-n_w_x;      n_w_y1=n_w_y;
n_w_x2=+n_w_x;      n_w_y2=n_w_y;
clear n_w_x n_w_y

% Node Layout - Bottom Bend Regions
% ----------------------------------------
n_theta=(3*pi/2):(theta/ne_b):(3*pi/2+theta);
n_bb_x=r*cos(n_theta)+bbf/2;
n_bb_y=r*sin(n_theta)+r;

n_bb_x1=-n_bb_x';   n_bb_x2=n_bb_x';
n_bb_y1=+n_bb_y';   n_bb_y2=n_bb_y';
clear n_theta n_bb_x n_bb_y

% Node Layout - Bottom Flange
% ----------------------------------------
n_bf_x=((-bbf/2):(bbf/ne_bf):(bbf/2))';
n_bf_y=zeros(ne_bf+1,1);

% Node Layout - Concatenation
% ----------------------------------------
```

```
nx1=vertcat(n_tf_x1,n_tb_x1,n_w_x1); ny1=vertcat(n_tf_y1,n_tb_y1,n_w_y1);
nx2=vertcat(n_bb_x1,n_bf_x,n_bb_x2); ny2=vertcat(n_bb_y1,n_bf_y,n_bb_y2);
nx3=vertcat(n_w_x2,n_tb_x2,n_tf_x2); ny3=vertcat(n_w_y2,n_tb_y2,n_tf_y2);

nx=vertcat(nx1,nx2,nx3);    ny=vertcat(ny1,ny2,ny3);
nx=round(nx*1e6)/1e6;       ny=round(ny*1e6)/1e6;
clear nx1 nx2 nx3 ny1 ny2 ny3

node=horzcat(nx,ny);
node=unique(node,'rows');
node(:,2)=node(:,2)+t/2;
node=round(node*1e6)/1e6;
clear nx ny

% Node Layout - Clear Statements
% ------------------------------------------
clear n_tf_x1 n_tb_x1 n_w_x1    n_tf_y1 n_tb_y1 n_w_y1
clear n_bb_x1 n_bf_x n_bb_x2    n_bb_y1 n_bf_y n_bb_y2
clear n_w_x2 n_tb_x2 n_tf_x2    n_w_y2 n_tb_y2 n_tf_y2
clear theta L_bend Dx Dy D bbf
clear ne_tf ne_b ne_w ne_bf

% ========================================================================
% PART 3:  TORSIONAL PROPERTIES
% ========================================================================

% Fundamental Terms
% ------------------------------------------
nnode=length(node(:,1)); % nnode = number of nodes
nele=nnode-1;            % nele = number of elements

% Torsional Properties - Lengths & Area
% ------------------------------------------
Lij=zeros(nele,1); % Lij = length of each element (in)
Aij=zeros(nele,1); % Aij = area of each element (in^2)
for i=1:nele
    xi=node(i,1);
    xj=node(i+1,1);
    yi=node(i,2);
    yj=node(i+1,2);
    Lij(i)=sqrt((xj-xi)^2+(yj-yi)^2);
    Aij(i)=t*Lij(i);
    clear xi xj yi yj
end
clear ans i
A=sum(Aij);        % A = area of cross-section (in^2)

% Torsional Properties - Center-of-Gravity
% ------------------------------------------
Qxij=zeros(nele,1); % Qxij = first moment of area about X-axis (in^3)
Qyij=zeros(nele,1); % Qyij = first moment of area about X-axis (in^3)
for i=1:nele
    xi=node(i,1);
    xj=node(i+1,1);
    yi=node(i,2);
```

```
    yj=node(i+1,2);
    Qxij(i)=(Aij(i)/2)*(xi+xj);
    Qyij(i)=(Aij(i)/2)*(yi+yj);
    clear xi xj yi yj
end
clear ans i
x_bar=sum(Qxij)/A;  % x_bar = X-axis centroid (in)
y_bar=sum(Qyij)/A;  % y_bar = Y-axis centroid (in)

% Torsional Properties - Moments of Inertia
% ------------------------------------------
pij=zeros(nele,1);   % pij = distances from elements to the C.G. (in)
Ixxij=zeros(nele,1); % Ixxij = X-axis element moment of inertia (in^4)
Iyyij=zeros(nele,1); % Iyyij = Y-axis element moment of inertia (in^4)
for i=1:nele
    xi=node(i,1)-x_bar;
    xj=node(i+1,1)-x_bar;
    yi=node(i,2)-y_bar;
    yj=node(i+1,2)-y_bar;
    pij(i)=(xi*yj-xj*yi)/Lij(i);
    Ixxij(i,1)=(Aij(i)/3)*(yi^2+yi*yj+yj^2);
    Iyyij(i,1)=(Aij(i)/3)*(xi^2+xi*xj+xj^2);
    clear xi xj yi yj
end
clear ans i
Ixx=sum(Ixxij);      % Ixx = X-axis moment of inertia (in^4)
Iyy=sum(Iyyij);      % Iyy = Y-axis moment of inertia (in^4)

% Torsional Properties - Unit Warping (C.G.)
% ------------------------------------------
wij=zeros(nele,2); % wij = unit warp. with respect to the C.G. (in^2)
for i=1:nele
    if i==1
        wij(i,1)=0;
        wij(i,2)=pij(i)*Lij(i);
    else
        wij(i,1)=wij(i-1,2);
        wij(i,2)=wij(i,1)+pij(i)*Lij(i);
    end
end
clear ans i

% Torsional Properties - Warping Products
% ---------------------------------------
Iwxij=zeros(nele,1); % Iwxij = X-axis element warp. prod. (in^5)
Iwyij=zeros(nele,1); % Iwyij = Y-axis element warp. prod. (in^5)
for i=1:nele
    xi=node(i,1)-x_bar;
    xj=node(i+1,1)-x_bar;
    yi=node(i,2)-y_bar;
    yj=node(i+1,2)-y_bar;
    wi=wij(i,1);
    wj=wij(i,2);
    Iwxij(i,1)=(Aij(i)/3)*(wi*xi+wj*xj)+(Aij(i)/6)*(wi*xj+wj*xi);
    Iwyij(i,1)=(Aij(i)/3)*(wi*yi+wj*yj)+(Aij(i)/6)*(wi*yj+wj*yi);
    clear xi xj yi yj wi wj
```

```
end
clear ans i
Iwx=sum(Iwxij);      % Iwx = X-axis warping product of inertia (in^5)
Iwy=sum(Iwyij);      % Iwy = Y-axis warping product of inertia (in^5)
Xo=+Iwy/Ixx;         % Xo = X-axis shear center (in)
Yo=-Iwx/Iyy;         % Yo = Y-axis shear center (in)

% Torsional Properties - Distances to S.C.
% ----------------------------------------
poij=zeros(nele,1); % poij = distances from elements to the S.C. (in)
for i=1:nele
    xi=node(i,1)-x_bar;
    xj=node(i+1,1)-x_bar;
    yi=node(i,2)-y_bar;
    yj=node(i+1,2)-y_bar;
    poij(i)=pij(i)-((yj-yi)*Xo-(xj-xi)*Yo)/Lij(i);
    clear xi xj yi yj
end
clear ans i

% Torsional Properties - Unit Warping (S.C.)
% ------------------------------------------
woij=zeros(nele,2); % woij = unit warp. with respect to the S.C. (in^2)
for i=1:nele
    if i==1
        woij(i,1)=0;
        woij(i,2)=poij(i)*Lij(i);
    else
        woij(i,1)=woij(i-1,2);
        woij(i,2)=woij(i,1)+poij(i)*Lij(i);
    end
end
clear ans i

% Torsional Properties - Normalizing Function
% -------------------------------------------
Woij=zeros(nele,1); % Woij = normalizing function for unit warp. (in^2)
for i=1:nele
    woi=woij(i,1);
    woj=woij(i,2);
    Woij(i)=(Aij(i)/(2*A))*(woi+woj);
    clear woi woj
end
clear ans i

% Torsional Properties - Warping Constant
% ---------------------------------------
Cwij=zeros(nele,1); % Cwij = element warping constants (in^6)
for i=1:nele
    Wni=sum(Woij)-woij(i,1);
    Wnj=sum(Woij)-woij(i,2);
    Cwij(i)=(Aij(i)/3)*(Wni^2+Wni*Wnj+Wnj^2);
    clear Wni Wnj
end
clear ans i
Cw=sum(Cwij);       % Cw = warping constant (in^6)
```

```
% Torsional Properties - St. Venant Constant
% ------------------------------------------
J=w*(t^3)/3; % J = St. Venant torsional constant (in^4)

% Torsional Properties - Integrals
% --------------------------------------------
B1ij=zeros(nele,1); % B1ij = 1st monosymmetry constant integral (in^5)
B2ij=zeros(nele,1); % B2ij = 2nd monosymmetry constant integral (in^5)
for i=1:nele
    xi=node(i,1)-x_bar;
    xj=node(i+1,1)-x_bar;
    yi=node(i,2)-y_bar;
    yj=node(i+1,2)-y_bar;
    B1ij(i)=(Aij(i)/4)*(yi+yj)*(yi^2+yj^2);
    B2ij(i)=(Aij(i)/12)*(yi*(2*xi^2+(xi+xj)^2)+yj*(2*xj^2+(xi+xj)^2));
    clear xi xj yi yj
end
clear ans i

% Torsional Properties - Monosym. Constant
% ----------------------------------------
B1=sum(B1ij);          % B1 = 1st monosymmetry constant integral (in^5)
B2=sum(B2ij);          % B2 = 2nd monosymmetry constant integral (in^5)
bx=((B1+B2)/Ixx)+2*Yo; % bx = coefficient of monosymmetry (in)

% Torsional Properties - Clear Statements
% ---------------------------------------
clear nnode nele node
clear Lij Aij Qxij Qyij Ixxij Iyyij wij pij
clear Iwxij Iwyij Iwx Iwy
clear poij woij Woij Cwij B1ij B2ij B1 B2
clear A Ixx Iyy x_bar y_bar
clear w t r m d btf
```

B.2.4 Program File: tubFEA.m

Program file "tubFEA.m" is employed to preprocess Abaqus .inp files. Given data defining the geometry of a given flexural specimen, "tubFEA.m" automatically generates the required nodes and elements to simulate the girder in question (see Chapter 5). The program specifically operates in the following order:

- Part 1 reads the data necessary to generate the finite element mesh
- Part 2 calculates the location of nodes required to define the cross-section (note that this methodology is identical to the methodology described in Section B.2.3)
- Part 3 extends the results of Part 2 to generate the three-dimensional mesh of the steel press-brake-formed tub girder utilizing shell elements.
- Part 4 determines the nodes and elements required to simulate a generic stiffener/diaphragm (i.e. a stiffener/diaphragm at any location along the span of the girder).
- Part 5 deposits the mesh generated in Part 4 to each location that a stiffener/diaphragm is present (i.e. placing a stiffener/diaphragm at each desired location).
- Part 6 generates the mesh of the concrete deck. Based on the longitudinal discretization of the steel girder and a desired element width, node and element locations are calculated in order to generate the desired mesh.
- Part 7 determines the sets of nodes that will be assigned multi-point constraints (i.e. the rows of nodes between the top flanges and the deck).
- Part 8 determines the sets of nodes that will be assigned appropriate boundary conditions.
- Part 9 determines the sets of nodes that will be assigned loads as well as those nodes that will be monitored during analysis (i.e. deflections at midspan).
- Part 10 uses the results generated in Parts 1 through 9 to write the required information to an Abaqus .inp file. In addition, material models (see Chapter 5) are also computed here and exported to the input file.

The MATLAB file is as follows (input for the composite girder tests discussed in Chapter 4 is presented):

```
clc
clear all


% ========================================================================
% PART 1:  INPUT PARAMETERS
% ========================================================================

% Specimen Dimensions
% ------------------------------------------------------------------------
w=84;           % standard mill plate width [in]
t=7/16;         % plate thickness [in]
d=23;           % total girder depth [in]
dw=90;          % deck width [in]

L=39.5;         % span length [ft]
r=11/2*t;       % bend radius at mid-thickness [in]
slope=04;       % slope ratio of web
btf=06;         % top flange width [in]
dt=8;           % deck thickness [in]

% Stiffener/Diaphragm Locations [ft]
% ------------------------------------------------------------------------
Loc_St=[0.00*L;1.00*L];

% Transverse Node Layout Parameters
% ------------------------------------------------------------------------
ne_bf=02;     % Number of elements along the bottom flange (MUST BE EVEN)
ne_w=02;      % Number of elements along the web
ne_b=03;      % Number of elements along the bend
ne_tf=02;     % Number of elements along the top flange (MUST BE EVEN)
ea_deck=12;   % Approximate width of deck elements [in]

% Longitudinal Node Layout [in]
% ------------------------------------------------------------------------
ny1=-3;
ny2=((0):((L*12)/(L+0.5)):(L*12))';
ny3=L*12+3;
node_y=vertcat(ny1,ny2,ny3);
clear ny1 ny2 ny3

% Boundary Conditions
% ------------------------------------------------------------------------
bc_vert=[0.00*L;1.00*L]; % vertical boundary conditions
bc_lat=[0.00*L;1.00*L];  % lateral boundary conditions

% Load
% ------------------------------------------------------------------------
load=330;   % Applied load [kip]
```

```
% ========================================================================
% PART 2:  TRANSVERSE NODE LAYOUT (GIRDER)
% ========================================================================

% Constants Used in FEA
% ------------------------------------------------------------------------
theta=pi/2-atan(1/slope);              % bend angle [rad]
L_R=theta*r;                           % arc length of bend [in]
Web_z=d-t+2*r*(1/(sqrt(slope^2+1))-1); % Z-portion of straight web [in]
Web_x=Web_z/slope;                     % X-portion of straight web [in]
L_W=sqrt(Web_x^2+Web_z^2);             % length of straight web [in]
bbf=w-(4*L_R+2*L_W+2*btf);             % width of bottom flange [in]

% Nodes - Top Flange
% ------------------------------------------------------------------------
n_tf_x=((0):(btf/ne_tf):(btf))'+2*r*sin(theta)+Web_x+bbf/2;
n_tf_z=zeros(ne_tf+1,1)+d-t;

n_tf_x1=-n_tf_x;
n_tf_z1=n_tf_z;
n_tf_x2=n_tf_x;
n_tf_z2=n_tf_z;

clear n_tf_x n_tf_z

% Node Coordinates (Top Flange Bends)
% ------------------------------------------------------------------------
n_theta=(pi/2-theta):(theta/ne_b):(pi/2);

n_tb_x=-r*cos(n_theta)+2*r*sin(theta)+Web_x+bbf/2;
n_tb_z=r*sin(n_theta)-2*r*cos(theta)+Web_z+r;

n_tb_x1=-n_tb_x';
n_tb_z1=n_tb_z';
n_tb_x2=n_tb_x';
n_tb_z2=n_tb_z';

clear n_theta n_tb_x n_tb_z

% Node Coordinates (Webs)
% ------------------------------------------------------------------------
n_w_x=((0):(Web_x/ne_w):(Web_x))'+r*sin(theta)+bbf/2;
n_w_z=((0):(Web_z/ne_w):(Web_z))'+2*r*(sin(theta/2))^2;

n_w_x1=-n_w_x;
n_w_z1=n_w_z;
n_w_x2=n_w_x;
n_w_z2=n_w_z;

clear n_w_x n_w_z

% Node Coordinates (Bottom Flange Bends)
```

```
% ------------------------------------------------------------------------
n_theta=(3*pi/2):(theta/ne_b):(3*pi/2+theta);
n_bb_x=r*cos(n_theta)+bbf/2;
n_bb_z=r*sin(n_theta)+r;

n_bb_x1=-n_bb_x';
n_bb_z1=n_bb_z';
n_bb_x2=n_bb_x';
n_bb_z2=n_bb_z';

clear n_theta n_bb_x n_bb_z

% Node Coordinates (Bottom Flange)
% ------------------------------------------------------------------------
n_bf_x=((-bbf/2):(bbf/ne_bf):(bbf/2))';
n_bf_z=zeros(ne_bf+1,1);

% Concatenation
% ------------------------------------------------------------------------
nx1=vertcat(n_tf_x1,n_tb_x1,n_w_x1);
nx2=vertcat(n_bb_x1,n_bf_x,n_bb_x2);
nx3=vertcat(n_w_x2,n_tb_x2,n_tf_x2);
nx=vertcat(nx1,nx2,nx3);
nx=round(nx*1e6)/1e6;
clear nx1 nx2 nx3

nz1=vertcat(n_tf_z1,n_tb_z1,n_w_z1);
nz2=vertcat(n_bb_z1,n_bf_z,n_bb_z2);
nz3=vertcat(n_w_z2,n_tb_z2,n_tf_z2);
nz=vertcat(nz1,nz2,nz3);
nz=round(nz*1e6)/1e6;
clear nz1 nz2 nz3

node_cs=horzcat(nx,nz);
clear nx nz
node_cs=unique(node_cs,'rows');
node_x=node_cs(:,1);
node_z=node_cs(:,2);

% Additional Clear Statements
% ------------------------------------------------------------------------
clear L_R L_W Web_x Web_z theta
clear n_tf_x1 n_tb_x1 n_w_x1 n_tf_z1 n_tb_z1 n_w_z1
clear n_bb_x1 n_bf_x n_bb_x2 n_bb_z1 n_bf_z n_bb_z2
clear n_w_x2 n_tb_x2 n_tf_x2 n_w_z2 n_tb_z2 n_tf_z2


% ========================================================================
% PART 3:  NODE & ELEMENT LAYOUT (GIRDER)
% ========================================================================

% Node Matrix
% ------------------------------------------------------------------------
nn=((1):(1):(length(node_x)*length(node_y)))';
nx=repmat(node_x,length(node_y),1);
```

```
ny=repmat(node_y,1,length(node_x))';
ny=ny(:);
nz=repmat(node_z,length(node_y),1);
node_girder=horzcat(nn,nx,ny,nz);
clear nn nx ny nz

% Element Matrix
% -------------------------------------------------------------------------
nn_x_girder=length(node_x);
nn_y_girder=length(node_y);
ne_x_girder=nn_x_girder-1;
ne_y_girder=nn_y_girder-1;
ne_girder=ne_x_girder*ne_y_girder;
element_girder=zeros(ne_girder,5);

% Element numbering
for i=1:ne_girder;
    element_girder(i,1)=i;
end
clear ans i

% First row of elements
ne_1_1=1:1:ne_x_girder;
ne_2_1=2:1:ne_x_girder+1;
ne_3_1=nn_x_girder+2:1:2*nn_x_girder;
ne_4_1=nn_x_girder+1:1:2*nn_x_girder-1;
for i=1:ne_x_girder;
    element_girder(i,2)=ne_1_1(i);
    element_girder(i,3)=ne_2_1(i);
    element_girder(i,4)=ne_3_1(i);
    element_girder(i,5)=ne_4_1(i);
end
clear ans i ne_1_1 ne_2_1 ne_3_1 ne_4_1

% Remaining rows of elements
for i=ne_x_girder+1:ne_girder;
    element_girder(i,2)=element_girder(i-ne_x_girder,2)+nn_x_girder;
    element_girder(i,3)=element_girder(i-ne_x_girder,3)+nn_x_girder;
    element_girder(i,4)=element_girder(i-ne_x_girder,4)+nn_x_girder;
    element_girder(i,5)=element_girder(i-ne_x_girder,5)+nn_x_girder;
end
clear ans i

% Additional Clear Statements
% -------------------------------------------------------------------------
clear nn_x_girder nn_y_girder ne_x_girder ne_y_girder ne_girder


% =========================================================================
% PART 4:  TRANSVERSE NODE LAYOUT (STIFFENER)
% =========================================================================

% Common Calculations
% -------------------------------------------------------------------------
theta=pi/2-atan(1/slope);              % bend angle [rad]
```

```
L_R=theta*r;                              % arc length of bend [in]
Web_z=d-t+2*r*(1/(sqrt(slope^2+1))-1); % Z-portion of straight web [in]
Web_x=Web_z/slope;                        % X-portion of straight web [in]
L_W=sqrt(Web_x^2+Web_z^2);                % length of straight web [in]
bbf=w-(4*L_R+2*L_W+2*btf);                % width of bottom flange [in]
n_w_x=((0):(Web_x/ne_w):(Web_x))'+r*sin(theta)+bbf/2;
n_w_z=((0):(Web_z/ne_w):(Web_z))'+2*r*(sin(theta/2))^2;


% Node Layouts Along the Top/Bottom of the Diaphragm (X-direction)
% -------------------------------------------------------------------------
st_px=Web_x+bbf/2;
n_top_x=((-st_px):(2*st_px/ne_bf):(st_px))';
n_bot_x=((-bbf/2):(bbf/ne_bf):(bbf/2))';
clear st_px

ns_x=length(n_top_x); % Number of unique stiffener nodes in the X-direction
ns_z=length(n_w_z)+1; % Number of unique stiffener nodes in the Z-direction
n_stiff=zeros(ns_x*ns_z,2);

% Node Layout for Generic Stiffener
% -------------------------------------------------------------------------
for i=1:ns_x
    x1=round(n_top_x(i)*1e6)/1e6;
    z1=round((d-t)*1e6)/1e6;
    x2=round(n_bot_x(i)*1e6)/1e6;
    z2=0;
    if x1~=x2
        % z = m*x + b
        m=(z2-z1)/(x2-x1);
        b=z1-m*x1;
        for j=1:ns_z
            if j<ns_z
                z_index=n_w_z(j);
            else
                z_index=d-t/2;
            end
            x_index=(z_index-b)/m;
            n_stiff((i-1)*ns_z+j,1)=x_index;
            n_stiff((i-1)*ns_z+j,2)=z_index;
            clear x_index z_index
        end
        clear m
    else
        % x = 0
        clear m b
        range=median(1:1:ns_x);
        for j=1:ns_z
            if j<ns_z
                z_index=n_w_z(j);
            else
                z_index=d-t/2;
            end
            n_stiff((range-1)*ns_z+j,1)=0;
            n_stiff((range-1)*ns_z+j,2)=z_index;
            clear z_index
```

```
        end
        clear j range
    end
    clear m b
end
clear ans i
clear x1 x2 z1 z2 z_index
n_stiff=round(n_stiff*1e6)/1e6;

% Additional Clear Statements
% -------------------------------------------------------------------------
clear L_R L_W Web_x Web_z theta

% =========================================================================
% PART 5:  NODE & ELEMENT LAYOUT (STIFFENER)
% =========================================================================

% General Parameters
% -------------------------------------------------------------------------
nn_girder=length(node_girder(:,1));
ne_stiff=(ns_z)*(length(n_bot_x)-1)+2*(length(n_w_z)-1);
rect_stiff=zeros(ne_stiff*length(Loc_St),5);
rect_stiff(:,1)=(1:1:length(rect_stiff(:,1)))';
rect_stiff(:,1)=rect_stiff(:,1)+length(element_girder(:,1));
tri_stiff=zeros(4*length(Loc_St),4);
tri_stiff(:,1)=(1:1:length(tri_stiff(:,1)))';
tri_stiff(:,1)=tri_stiff(:,1)+length(element_girder(:,1));
tri_stiff(:,1)=tri_stiff(:,1)+length(rect_stiff(:,1));


% Node Matrix
% -------------------------------------------------------------------------
node_stiff=zeros(length(n_stiff(:,1))*length(Loc_St),4);
for i=1:length(Loc_St)
    ind_stiff=((i-1)*length(n_stiff(:,1))+1):1:(i*length(n_stiff(:,1)));
    node_stiff(ind_stiff,2)=n_stiff(:,1);
    node_stiff(ind_stiff,3)=Loc_St(i)*12;
    node_stiff(ind_stiff,4)=n_stiff(:,2);
    clear ind_stiff
end
clear ans i
node_stiff(:,1)=(1:1:length(node_stiff(:,1)))'+nn_girder;
node_stiff=round(node_stiff*1e6)/1e6;

% Element Matrix
% -------------------------------------------------------------------------
for i=1:length(Loc_St)
    y_index=Loc_St(i)*12;          % Y-coordinate of individual stiff.
    cs_line=find(node_y==y_index); % Search for node loc. along girder

    ind_LW1=ne_tf+ne_b+1;  % ind_LW1 = stiff. node on the LW (start)
    ind_LW2=ind_LW1+ne_w;  % ind_LW2 = stiff. node on the LW (end)
    ind_BF1=ind_LW2+ne_b;  % ind_BF1 = stiff. node on the BF (start)
    ind_BF2=ind_BF1+ne_bf; % ind_BF2 = stiff. node on the BF (end)
    ind_RW1=ind_BF2+ne_b;  % ind_RW1 = stiff. node on the RW (start)
```

```
ind_RW2=ind_RW1+ne_w;  % ind_RW2 = stiff. node on the RW (end)

ind_LW1=ind_LW1+(cs_line-1)*length(node_cs); % Shift for ith stiff.
ind_LW2=ind_LW2+(cs_line-1)*length(node_cs); % Shift for ith stiff.
ind_BF1=ind_BF1+(cs_line-1)*length(node_cs); % Shift for ith stiff.
ind_BF2=ind_BF2+(cs_line-1)*length(node_cs); % Shift for ith stiff.
ind_RW1=ind_RW1+(cs_line-1)*length(node_cs); % Shift for ith stiff.
ind_RW2=ind_RW2+(cs_line-1)*length(node_cs); % Shift for ith stiff.

nn_LW=(ind_LW1:1:ind_LW2)'; % nn_LW = left web nodes
nn_BF=(ind_BF1:1:ind_BF2)'; % nn_BF = bottom flange nodes
nn_RW=(ind_RW1:1:ind_RW2)'; % nn_RW = right web nodes

clear ind_LW1 ind_LW2 ind_BF1 ind_BF2 ind_RW1 ind_RW2

% First Vertical Row of Elements
% ------------------------------------------------------------------
n1=nn_LW(2:1:end);
n1=n1(end:-1:1);
n2=(1:1:length(n_w_z(:,1))-1)';
n2=n2+nn_girder+(i-1)*ns_x*ns_z;
n3=(2:1:length(n_w_z(:,1)))';
n3=n3+nn_girder+(i-1)*ns_x*ns_z;
n4=nn_LW(1:1:(end-1));
n4=n4(end:-1:1);
es1=horzcat(n1,n2,n3,n4);
clear n1 n2 n3 n4

% Main Body of Elements
% ------------------------------------------------------------------
es2=zeros((ne_w+2)*(length(nn_BF)-1),4);
for j=1:(length(nn_BF)-1)
    v1=(((j-1)*(ns_z)+1):1:(j*ns_z))';
    v1=v1+nn_girder+(i-1)*ns_x*ns_z;
    vn1=vertcat(nn_BF(j,1),v1);
    clear v1
    v2=((j*ns_z+1):1:((j+1)*(ns_z)))';
    v2=v2+nn_girder+(i-1)*ns_x*ns_z;
    vn2=vertcat(nn_BF(j+1,1),v2);
    clear v2
    n1=vn1(1:1:(end-1));
    n2=vn2(1:1:(end-1));
    n3=vn2(2:1:end);
    n4=vn1(2:1:end);
    es2((((j-1)*(ne_w+2)+1):1:(j*(ne_w+2))),:)=horzcat(n1,n2,n3,n4);
    clear vn1 vn2
end
clear ans j

% Last Vertical Row of Elements
% ------------------------------------------------------------------
n1=((ns_z*(ns_x-1)+1):1:(ns_x*ns_z-2))';
n1=n1+nn_girder+(i-1)*ns_x*ns_z;
n2=nn_RW(1:1:(end-1));
n3=nn_RW(2:1:end);
n4=((ns_z*(ns_x-1)+2):1:(ns_x*ns_z-1))';
```

```
    n4=n4+nn_girder+(i-1)*ns_x*ns_z;
    es3=horzcat(n1,n2,n3,n4);
    clear n1 n2 n3 n4

    % All Rectangular Elements
    % -------------------------------------------------------------------
    es=vertcat(es1,es2,es3);
    rect_stiff(((i-1)*ne_stiff+1):1:(i*ne_stiff),(2:1:5))=es;
    clear es es1 es2 es3

    % All Triangular Elements
    % -------------------------------------------------------------------
    t11=nn_BF(1);
    t12=length(node_girder(:,1))+(i-1)*ns_x*ns_z+1;
    t13=nn_LW(end);
    t21=nn_LW(1);
    t22=length(node_girder(:,1))+(i-1)*ns_x*ns_z+ns_z-1;
    t23=length(node_girder(:,1))+(i-1)*ns_x*ns_z+ns_z;
    t31=nn_BF(end);
    t32=nn_RW(1);
    t33=length(node_girder(:,1))+(i-1)*ns_x*ns_z+(ns_x-1)*ns_z+1;
    t41=length(node_girder(:,1))+(i-1)*ns_x*ns_z+(ns_x-1)*ns_z++ns_z-1;
    t42=nn_RW(end);
    t43=length(node_girder(:,1))+(i-1)*ns_x*ns_z+(ns_x-1)*ns_z++ns_z;

    t1=[t11,t12,t13];
    t2=[t21,t22,t23];
    t3=[t31,t32,t33];
    t4=[t41,t42,t43];

    ele_t=[t1;t2;t3;t4];

    i1=(i-1)*4+1;
    i2=4*i;
    tri_stiff(i1:i2,2:4)=ele_t;

    clear t11 t12 t13 t21 t22 t23 t31 t32 t33 t41 t42 t43
    clear t1 t2 t3 t4
    clear i1 i2 ele_t
    clear nn_LW nn_BF nn_RW

end
clear ans i y_index

% ========================================================================
% PART 6:  NODE & ELEMENT LAYOUT (DECK)
% ========================================================================

% Transverse Node Layout
% -------------------------------------------------------------------------
d_n1=ne_tf/2+1;
d_n2=2*ne_tf+4*ne_b+2*ne_w+ne_bf+1-(ne_tf/2);

d_node1=round(-dw/2*1e6)/1e6;
d_node2=round(node_x(d_n1,1)*1e6)/1e6;
```

```
d_node3=round(node_x(d_n2,1)*1e6)/1e6;
d_node4=round(dw/2*1e6)/1e6;

di_int=round((d_node2-d_node1)/ea_deck);
di_ext=round((d_node3-d_node2)/ea_deck);

nx_d1=((d_node1):((d_node2-d_node1)/di_int):(d_node2))';
nx_d2=((d_node2):((d_node3-d_node2)/di_ext):(d_node3))';
nx_d3=((d_node3):((d_node4-d_node3)/di_int):(d_node4))';

d_node_x=vertcat(nx_d1,nx_d2,nx_d3);
d_node_x=unique(d_node_x,'rows');

clear d_n1 d_n2
clear d_node1 d_node2 d_node3 d_node4
clear di_int di_ext
clear nx_d1 nx_d2 nx_d3

% Node Matrix
% -------------------------------------------------------------------------
nn=((1):(1):(length(d_node_x)*length(node_y)))';
nn=nn+length(node_girder(:,1))+length(node_stiff(:,1));
nx=repmat(d_node_x,length(node_y),1);
ny=repmat(node_y,1,length(d_node_x))';
ny=ny(:);
nz=zeros(length(nn(:,1)),1);
nz=nz+d+dt/2-t/2;
node_deck=horzcat(nn,nx,ny,nz);
clear nn nx ny nz

% Element Matrix
% -------------------------------------------------------------------------
nn_girder=length(node_girder(:,1));
nn_stiff=length(node_stiff(:,1));
ne_girder=length(element_girder(:,1));
ne_rect=length(rect_stiff(:,1));
ne_tri=length(tri_stiff(:,1));

nn_x_deck=length(d_node_x);
nn_y_deck=length(node_y);
ne_x_deck=nn_x_deck-1;
ne_y_deck=nn_y_deck-1;
ne_deck=ne_x_deck*ne_y_deck;
element_deck=zeros(ne_deck,5);

% Element numbering
for i=1:ne_deck;
    element_deck(i,1)=i+ne_girder+ne_rect+ne_tri;
end
clear ans i

% First row of elements
ne_1_1=1:1:ne_x_deck;
ne_2_1=2:1:ne_x_deck+1;
ne_3_1=nn_x_deck+2:1:2*nn_x_deck;
```

```
ne_4_1=nn_x_deck+1:1:2*nn_x_deck-1;
for i=1:ne_x_deck;
    element_deck(i,2)=ne_1_1(i);
    element_deck(i,3)=ne_2_1(i);
    element_deck(i,4)=ne_3_1(i);
    element_deck(i,5)=ne_4_1(i);
end
clear ans i ne_1_1 ne_2_1 ne_3_1 ne_4_1

% Remaining rows of elements
for i=ne_x_deck+1:ne_deck;
    element_deck(i,2)=element_deck(i-ne_x_deck,2)+nn_x_deck;
    element_deck(i,3)=element_deck(i-ne_x_deck,3)+nn_x_deck;
    element_deck(i,4)=element_deck(i-ne_x_deck,4)+nn_x_deck;
    element_deck(i,5)=element_deck(i-ne_x_deck,5)+nn_x_deck;
end
clear ans i

element_deck(:,2:5)=element_deck(:,2:5)+nn_girder+nn_stiff;

clear nn_x_deck nn_y_deck ne_x_deck ne_y_deck ne_deck
clear d_node_x node_z

clear Web_x Web_z delta

% ========================================================================
% PART 7:  MULTI-POINT CONSTRAINTS
% ========================================================================

% Girder Nodes
% ------------------------------------------------------------------------
inc_y=2*ne_tf+4*ne_b+2*ne_w+ne_bf+1;

m_g1=ne_tf/2+1;
mpc_g1=((m_g1):(inc_y):(inc_y*(length(node_y(:,1))-1)+m_g1))';
clear m_g1

m_g2=2*ne_tf+4*ne_b+2*ne_w+ne_bf+1-(ne_tf/2);
mpc_g2=((m_g2):(inc_y):(inc_y*(length(node_y(:,1))-1)+m_g2))';
clear m_g2

clear inc_y

% Deck Nodes
% ------------------------------------------------------------------------
d_n1=ne_tf/2+1;
d_n2=2*ne_tf+4*ne_b+2*ne_w+ne_bf+1-(ne_tf/2);

d_node1=round(-dw/2*1e6)/1e6;
d_node2=round(node_x(d_n1,1)*1e6)/1e6;
d_node3=round(node_x(d_n2,1)*1e6)/1e6;
d_node4=round(dw/2*1e6)/1e6;

di_int=round((d_node2-d_node1)/ea_deck);
```

```
di_ext=round((d_node3-d_node2)/ea_deck);

nx_d1=((d_node1):((d_node2-d_node1)/di_int):(d_node2))';
nx_d2=((d_node2):((d_node3-d_node2)/di_ext):(d_node3))';
nx_d3=((d_node3):((d_node4-d_node3)/di_int):(d_node4))';

d_node_x=vertcat(nx_d1,nx_d2,nx_d3);
d_node_x=unique(d_node_x,'rows');

m_d1=di_int+1;
m_d2=length(d_node_x(:,1));
m_d3=length(d_node_x(:,1))*(length(node_y(:,1))-1)+m_d1;

mpc_d1=(m_d1:m_d2:m_d3)';
mpc_d1=mpc_d1+length(node_girder(:,1))+length(node_stiff(:,1));
clear m_d1 m_d2 m_d3

m_d1=di_int+di_ext+1;
m_d2=length(d_node_x(:,1));
m_d3=length(d_node_x(:,1))*(length(node_y(:,1))-1)+m_d1;

mpc_d2=(m_d1:m_d2:m_d3)';
mpc_d2=mpc_d2+length(node_girder(:,1))+length(node_stiff(:,1));
clear m_d1 m_d2 m_d3

% Combination
% -------------------------------------------------------------------------
mpc1=horzcat(mpc_g1,mpc_d1);
mpc2=horzcat(mpc_g2,mpc_d2);
mpc=vertcat(mpc1,mpc2);
clear mpc1 mpc2

% Additional Clear Statements
% -------------------------------------------------------------------------
clear d_n1 d_n2
clear d_node1 d_node2 d_node3 d_node4
clear di_int di_ext
clear nx_d1 nx_d2 nx_d3 d_node_x
clear mpc_d1 mpc_d2 mpc_g1 mpc_g2 m_d1 m_d2

% =========================================================================
% PART 8:  BOUNDARY CONDITIONS
% =========================================================================

% Z-Direction Boundary Conditions
% -------------------------------------------------------------------------
bc_z=zeros(length(bc_vert(:,1))*(ne_bf+1),1);
for i=1:length(bc_vert(:,1))
    y_index=bc_vert(i)*12;         % Y-coordinate of B.C.
    cs_line=find(node_y==y_index); % Search for node loc. along girder

    ind_v1=ne_tf+ne_b+ne_w+ne_b+1;        % ind_v1 = B.C node (start)
    ind_v2=ne_tf+ne_b+ne_w+ne_b+ne_bf+1;  % ind_v2 = B.C node (end)
```

```
    ind_v1=ind_v1+(cs_line-1)*length(node_cs); % Shift for ith B.C.
    ind_v2=ind_v2+(cs_line-1)*length(node_cs); % Shift for ith B.C.

    ind_v=((ind_v1):1:(ind_v2))';
    clear ind_v1 ind_v2

    i1=(i-1)*(ne_bf+1)+1;
    i2=i*(ne_bf+1);

    bc_z(i1:i2,1)=ind_v;
    clear ind_v
end
clear ans i y_index cs_line

% Y-Direction Boundary Conditions
% -------------------------------------------------------------------------
bc_y=bc_z(1:(ne_bf+1),1);

% X-Direction Boundary Conditions
% -------------------------------------------------------------------------
bc_x=zeros(length(bc_lat(:,1))*(ne_w+1)*2,1);
for i=1:length(bc_lat(:,1))
    y_index=bc_lat(i)*12;         % Y-coordinate of B.C.
    cs_line=find(node_y==y_index); % Search for node location along girder

    ind_lw1=ne_tf+ne_b+1;                              % B.C node (start)
    ind_lw2=ne_tf+ne_b+ne_w+1;                         % B.C node (end)
    ind_rw1=ne_tf+ne_b+ne_w+ne_b+ne_bf+ne_b+1;         % B.C node (start)
    ind_rw2=ne_tf+ne_b+ne_w+ne_b+ne_bf+ne_b+ne_w+1; % B.C node (end)

    ind_lw1=ind_lw1+(cs_line-1)*length(node_cs); % Shift for ith B.C.
    ind_lw2=ind_lw2+(cs_line-1)*length(node_cs); % Shift for ith B.C.
    ind_rw1=ind_rw1+(cs_line-1)*length(node_cs); % Shift for ith B.C.
    ind_rw2=ind_rw2+(cs_line-1)*length(node_cs); % Shift for ith B.C.

    ind_lw=((ind_lw1):1:(ind_lw2))';
    ind_rw=((ind_rw1):1:(ind_rw2))';
    ind_w=vertcat(ind_lw,ind_rw);
    clear ind_lw1 ind_lw2 ind_rw1 ind_rw2 ind_lw ind_rw

    i1=(i-1)*(ne_w+1)*2+1;
    i2=i*(ne_w+1)*2;

    bc_x(i1:i2,1)=ind_w;
    clear ind_v i1 i2 y_index
end
clear ans i

% =========================================================================
% PART 9:  EXPERIMENTAL PARAMETERS
% =========================================================================

% Deflection Measurements
% -------------------------------------------------------------------------
```

```
defl_cl=(L*12)/2;
defl_cl=round(defl_cl*1e6)/1e6;
cs_line=find(node_y==defl_cl);
ind_cl=ne_tf+ne_b+ne_w+ne_b+ne_bf/2+1;
ind_cl=ind_cl+(cs_line-1)*length(node_cs);
clear cs_line find_cl defl_cl

defl_qp=(L*12)/4;
defl_qp=round(defl_qp*1e6)/1e6;
cs_line=find(node_y==defl_qp);
ind_qp=ne_tf+ne_b+ne_w+ne_b+ne_bf/2+1;
ind_qp=ind_qp+(cs_line-1)*length(node_cs);
clear cs_line find_qp defl_qp

% Transverse Deck Nodes
% ---------------------------------------------------------------------
d_n1=ne_tf/2+1;
d_n2=2*ne_tf+4*ne_b+2*ne_w+ne_bf+1-(ne_tf/2);

d_node1=round(-dw/2*1e6)/1e6;
d_node2=round(node_x(d_n1,1)*1e6)/1e6;
d_node3=round(node_x(d_n2,1)*1e6)/1e6;
d_node4=round(dw/2*1e6)/1e6;

di_int=round((d_node2-d_node1)/ea_deck);
di_ext=round((d_node3-d_node2)/ea_deck);

nx_d1=((d_node1):((d_node2-d_node1)/di_int):(d_node2))';
nx_d2=((d_node2):((d_node3-d_node2)/di_ext):(d_node3))';
nx_d3=((d_node3):((d_node4-d_node3)/di_int):(d_node4))';

d_node_x=vertcat(nx_d1,nx_d2,nx_d3);
d_node_x=unique(d_node_x,'rows');

clear d_n1 d_n2
clear d_node1 d_node2 d_node3 d_node4
clear di_int di_ext
clear nx_d1 nx_d2 nx_d3

% Node Position at Center Span & Load Application
% ---------------------------------------------------------------------
load_pos=(L*12)/2;
load_pos=round(load_pos*1e6)/1e6;
cs_line=find(node_deck(:,3)==load_pos);
d_ele_x=d_node_x(2:end)-d_node_x(1:(end-1));
d_ele_x=d_ele_x/dw;

load_mag=zeros(length(cs_line(:,1)),1);
for i=1:length(load_mag(:,1))
    if i==1
        load_mag(i,1)=d_ele_x(1,1)/2;
    elseif i==length(load_mag(:,1))
        load_mag(i,1)=d_ele_x(end,1)/2;
    else
        load_mag(i,1)=d_ele_x(i-1,1)/2+d_ele_x(i,1)/2;
```

```
    end
end
clear ans i

load_num=node_deck(cs_line,1);

load_mag=load_mag*-load;
load_mag=round(load_mag*1e6)/1e6;
dof=zeros(length(load_mag(:,1)),1)+3;
cload=horzcat(load_num,dof,load_mag);
clear cs_line load_pos load_mag load_num dof d_node_x d_ele_x

% ========================================================================
% PART 10:  ABAQUS INPUT FILE
% ========================================================================

% Heading
% ------------------------------------------------------------------------
inputfile='tubFEA.inp';
fid=fopen(inputfile,'wt');
fprintf(fid,'** Gregory K. Michaelson \n');
fprintf(fid,'** West Virginia University \n');
fprintf(fid,'** Department of Civil & Environmental Engineering \n');
date = datestr(now, 0);
fprintf(fid,'** %s\n', date);
fprintf(fid,'**\n');
clear date

% Nodes & Elements
% ------------------------------------------------------------------------
fprintf(fid,'*NODE \n');
for i=1:length(node_girder(:,1))
    fprintf(fid,'%15.0f, %15.6f, %15.6f, %15.6f',node_girder(i,:)');
    fprintf(fid,'\n');
end
clear ans i node_girder
for i=1:length(node_stiff(:,1))
    fprintf(fid,'%15.0f, %15.6f, %15.6f, %15.6f',node_stiff(i,:)');
    fprintf(fid,'\n');
end
clear ans i node_stiff
for i=1:length(node_deck(:,1))
    fprintf(fid,'%15.0f, %15.6f, %15.6f, %15.6f',node_deck(i,:)');
    fprintf(fid,'\n');
end
clear ans i node_deck
fprintf(fid,'*ELEMENT, TYPE=S4R, ELSET=GIRDER \n');
for i=1:length(element_girder(:,1))
    fprintf(fid,'%15.0f, %15.0f, %15.0f, %15.0f,
%15.0f',element_girder(i,:)');
    fprintf(fid,'\n');
end
clear ans i element_girder
fprintf(fid,'*ELEMENT, TYPE=S4R, ELSET=STIFFENER \n');
for i=1:length(rect_stiff(:,1))
    fprintf(fid,'%15.0f, %15.0f, %15.0f, %15.0f, %15.0f',rect_stiff(i,:)');
```

```
    fprintf(fid,'\n');
end
clear ans i rect_stiff
fprintf(fid,'*ELEMENT, TYPE=S3R, ELSET=STIFFENER \n');
for i=1:length(tri_stiff(:,1))
    fprintf(fid,'%15.0f, %15.0f, %15.0f, %15.0f',tri_stiff(i,:)');
    fprintf(fid,'\n');
end
clear ans i tri_stiff
fprintf(fid,'*ELEMENT, TYPE=S4R, ELSET=DECK \n');
for i=1:length(element_deck(:,1))
    fprintf(fid,'%15.0f, %15.0f, %15.0f, %15.0f, %15.0f',element_deck(i,:)');
    fprintf(fid,'\n');
end
clear ans i element_deck
fprintf(fid,'*MPC \n');
for i=1:length(mpc(:,1))
    fprintf(fid,'           BEAM,');
    fprintf(fid,'%15.0f, %15.0f',mpc(i,:)');
    fprintf(fid,'\n');
end
clear ans i mpc
fprintf(fid,'*NSET, NSET=BC-X \n');
for i=1:length(bc_x(:,1))
    fprintf(fid,'%15.0f,',bc_x(i,:)');
    fprintf(fid,'\n');
end
clear ans i bc_x
fprintf(fid,'*NSET, NSET=BC-Y \n');
for i=1:length(bc_y(:,1))
    fprintf(fid,'%15.0f,',bc_y(i,:)');
    fprintf(fid,'\n');
end
clear ans i bc_y
fprintf(fid,'*NSET, NSET=BC-Z \n');
for i=1:length(bc_z(:,1))
    fprintf(fid,'%15.0f,',bc_z(i,:)');
    fprintf(fid,'\n');
end
clear ans i bc_z
fprintf(fid,'*BOUNDARY \n');
fprintf(fid,'           BC-X,              1 \n');
fprintf(fid,'           BC-Y,              2 \n');
fprintf(fid,'           BC-Z,              3 \n');
fprintf(fid,'*NSET, NSET=DEFL-CL \n');
fprintf(fid,'%15.0f,',ind_cl);
fprintf(fid,'\n');
clear ind_cl

% Steel Material Model
% ------------------------------------------------------------------------
E=29559.160900899;      % modulus of elasticity (ksi)
ssy=60.9620413788773;   % static yield strength (ksi)
s02=63.05;              % offset yield strength (ksi)
est=0.0178825333333333; % strain at the onset of strain hardening
Est=1033.46262739326;   % strain hardening modulus (ksi)
su=84.3821008182302;    % tensile strength (ksi)
```

```
eu=0.131645626079353;   % strain at the tensile strength

e1=ssy/E;   e2=est;     e3=(eu-est)/10+est;
s1=ssy;     s2=ssy;     s3=Est*(eu-est)/10+ssy;

e6=eu-(eu-est)/10;                      e7=eu;
s6=(ssy/s02)*su-(100*(eu-est))/Est;     s7=(ssy/s02)*su;

e4=2*(e6-e3)/7+e3;      e5=2*(e6-e3)/7+e4;
s4=4*(s6-s3)/7+s3;      s5=2*(s6-s3)/7+s4;

e_eng=[e1;e2;e3;e4;e5;e6;e7];
s_eng=[s1;s2;s3;s4;s5;s6;s7];

e_true=log(1+e_eng);
e_true=e_true-e_true(1);
s_true=s_eng.*(1+e_eng);

steel=horzcat(s_true,e_true);

clear e1 e2 e3 e4 e5 e6 e7
clear s1 s2 s3 s4 s5 s6 s7
clear s_eng e_eng
clear e_true s_true
clear ssy s02 est Est su eu

% Concrete Material Model
% ------------------------------------------------------------------------
fc=4.74975330652133;
a=6193.3*((0.85*fc+1.015)^(-0.953));
b=8074.1*((0.85*fc+1.450)^(-1.085))-850;
Ec=((0.85*fc*(a-206000*0.0003)*0.0003)/(1+b*0.0003))/0.0003;

e_conc=vertcat((0.0003:0.0002:0.0029)',0.003);
f_conc=0.85*fc*(a-206000.*e_conc).*e_conc./(1+b.*e_conc);
e_conc=e_conc-e_conc(1);

ft=0.4;
Et=1820*sqrt(4);
e_crack=ft/Et;

concrete=horzcat(f_conc,e_conc);
concrete_tension=[1,0;0,(0.003-e_crack)];

clear fc a b
clear f_conc e_conc
clear ft Et e_crack

% Reinforcement Material Model
% ------------------------------------------------------------------------
r1=[60.124,0.0000000];
r2=[60.372,0.0041060];
r3=[72.665,0.0172970];
r4=[84.365,0.0363116];
```

```
r5=[92.305,0.0550860];
r6=[97.666,0.0783780];

rebar=vertcat(r1,r2,r3,r4,r5,r6);
clear r1 r2 r3 r4 r5 r6

% Abaqus Material Models
% ------------------------------------------------------------------------
fprintf(fid,'*MATERIAL, NAME=STEEL \n');
fprintf(fid,'*DENSITY \n');
fprintf(fid,'%12.4E',0.49/(12^3*386.08858267716533));
fprintf(fid,'\n');
fprintf(fid,'*ELASTIC \n');
fprintf(fid,'%12.2f, %12.2f',[E,0.30]);
fprintf(fid,'\n');
clear E
fprintf(fid,'*PLASTIC \n');
for i=1:length(steel(:,1))
    fprintf(fid,'%12.3f, %12.7f',steel(i,:)');
    fprintf(fid,'\n');
end
clear ans i steel
fprintf(fid,'*MATERIAL, NAME=CONCRETE \n');
fprintf(fid,'*DENSITY \n');
fprintf(fid,'%12.4E',0.15/(12^3*386.08858267716533));
fprintf(fid,'\n');
fprintf(fid,'*ELASTIC \n');
fprintf(fid,'%12.2f, %12.2f',[Ec,0.20]);
fprintf(fid,'\n');
clear Ec
fprintf(fid,'*CONCRETE \n');
for i=1:length(concrete(:,1))
    fprintf(fid,'%12.3f, %12.7f',concrete(i,:)');
    fprintf(fid,'\n');
end
clear ans i concrete
fprintf(fid,'*TENSION STIFFENING, TYPE=STRAIN \n');
for i=1:length(concrete_tension(:,1))
    fprintf(fid,'%12.3f, %12.7f',concrete_tension(i,:)');
    fprintf(fid,'\n');
end
clear ans i concrete_tension
fprintf(fid,'*MATERIAL, NAME=REINF \n');
fprintf(fid,'*ELASTIC \n');
fprintf(fid,'%12.2f, %12.2f',[29000,0.30]);
fprintf(fid,'\n');
fprintf(fid,'*PLASTIC \n');
for i=1:length(rebar(:,1))
    fprintf(fid,'%12.3f, %12.7f',rebar(i,:)');
    fprintf(fid,'\n');
end
clear ans i rebar

% Concrete Cover Requirements
% ------------------------------------------------------------------------
t_stiff=3/4;
```

```
A_top=pi/4*(1/2)^2;     t_cov=2.5;
A_bot=pi/4*(5/8)^2;     b_cov=1;

% Abaqus Shell Definitions
% -----------------------------------------------------------------------
fprintf(fid,'*SECTION CONTROLS, NAME=CONT, HOURGLASS=ENHANCED \n');
fprintf(fid,'%12.0f, %12.0f, %12.0f, %12.0f, %12.0f',[1,1,1,1,]);
fprintf(fid,'\n');
fprintf(fid,'*SHELL SECTION, ELSET=GIRDER, MATERIAL=STEEL, ');
fprintf(fid,'CONTROLS=CONT');
fprintf(fid,'\n');
fprintf(fid,'%12.6f',t);
fprintf(fid,'\n');
fprintf(fid,'*SHELL SECTION, ELSET=STIFFENER, MATERIAL=STEEL, ');
fprintf(fid,'CONTROLS=CONT');
fprintf(fid,'\n');
fprintf(fid,'%12.6f',t_stiff);
fprintf(fid,'\n');
fprintf(fid,'*SHELL SECTION, ELSET=DECK, MATERIAL=CONCRETE, ');
fprintf(fid,'CONTROLS=CONT, SECTION INTEGRATION=GAUSS');
fprintf(fid,'\n');
fprintf(fid,'%12.6f, %12.0f',[dt,7]);
fprintf(fid,'\n');
fprintf(fid,'*REBAR LAYER, GEOMETRY=CONSTANT \n');
fprintf(fid,'    LONG-TOP,');
fprintf(fid,' %12.6f,',A_top);
fprintf(fid,' %12.0f,',12);
fprintf(fid,' %12.6f,',+dt/2-t_cov-1/2-0.5*(1/2));
fprintf(fid,'       REINF,');
fprintf(fid,' %12.0f',90);
fprintf(fid,'\n');
fprintf(fid,'    LONG-BOT,');
fprintf(fid,' %12.6f,',A_bot);
fprintf(fid,' %12.0f,',12);
fprintf(fid,' %12.6f,',-dt/2+b_cov+0.5*(5/8));
fprintf(fid,'       REINF,');
fprintf(fid,' %12.0f',90);
fprintf(fid,'\n');
fprintf(fid,'    TRAN-TOP,');
fprintf(fid,' %12.6f,',A_top);
fprintf(fid,' %12.0f,',12);
fprintf(fid,' %12.6f,',+dt/2-t_cov-0.5*(1/2));
fprintf(fid,'       REINF,');
fprintf(fid,' %12.0f',0);
fprintf(fid,'\n');
fprintf(fid,'    TRAN-BOT,');
fprintf(fid,' %12.6f,',A_bot);
fprintf(fid,' %12.0f,',12);
fprintf(fid,' %12.6f,',-dt/2+b_cov+5/8+0.5*(5/8));
fprintf(fid,'       REINF,');
fprintf(fid,' %12.0f',0);
fprintf(fid,'\n');
clear t_stiff A_top A_bot t_cov b_cov

% Abaqus Step Definitions
% -----------------------------------------------------------------------
```

```
fprintf(fid,'*STEP, NLGEOM=YES, INC=2000 \n');
fprintf(fid,'*STATIC, RIKS \n');
fprintf(fid,'%12.4f, %12.2f, %12.7f, %12.1f, %12.1f',[0.005,1,1e-7,2,2]);
fprintf(fid,'\n');
fprintf(fid,'*NODE PRINT, FREQUENCY=1, NSET=DEFL-CL \n');
fprintf(fid,'U3, \n');
fprintf(fid,'*CLOAD, OP=NEW \n');
for i=1:length(cload(:,1))
    fprintf(fid,'%15.0f, %15.0f, %15.6f,',cload(i,:)');
    fprintf(fid,'\n');
end
clear ans i cload
fprintf(fid,'*END STEP');

% Close Program
% ------------------------------------------------------------------------
fclose(fid);
clear all
```

B.2.5 Program File: tubPOST.m

Program file "tubPOST.m" is employed to postprocess Abaqus .dat files. Given the results of an Abaqus analysis (see Chapter 5 and Section B.2.4), the program extracts the desired information (in this case, deflections belonging to the node set "DEFL-CL") and reports the data in tabular form. This program can easily be modified to extract other desired data. The MATLAB file is as follows:

```
clc
clear all

name_file='tubFEA.dat';

C=textscan(fopen(name_file,'r'),'%s','Delimiter','\n');
data=C{1,1};
clear C

heading='PRINTED FOR NODES BELONGING TO NODE SET DEFL-CL';

index_c=strfind(data,heading);
index=find(not(cellfun('isempty',index_c)));
clear index_c title

results=zeros(length(index(:,1)),2);
for i=1:length(index)
    id=index(i,1);
    defl_line=data(id+5,1);
    defl_dat=defl_line{1,1};
    defl=sscanf(defl_dat,'%f');
    results(i,1)=defl(2,1);
    clear defl_line defl_dat defl
    lpf_line=data(id-11,1);
    lpf_dat=lpf_line{1,1};
    lpf=str2double(lpf_dat(36:length(lpf_dat)));
    results(i,2)=lpf;
    clear lpf_line lpf_dat lpf
end
clear ans i id index

results=vertcat([0,0],results);
results(:,1)=results(:,1)*-1;
results(:,2)=results(:,2)*330;
results=round(results*1e6)/1e6;

clear name_file
close all
```

B.2.6 Function File: slices.m

Function file "slices.m" is employed in both strain-compatibility analyses and plastic moment calculations. Given the required parameters defining the geometry of the cross-section, the routine uses the geometric definitions discussed in Appendix A to divide the cross-section into rectangular slices. For example, if the total depth of a cross-section is 30 inches and 1000 slices are desired, the cross-section is divided into slices that are assumed to be rectangles with a thickness of 0.03 inches. The program then, for each slice, computes the corresponding width and reports them into a column vector. The MATLAB file is as follows:

```
function wi = slices(w,t,d,r,m,btf,bs,ts,Ns,yi)

% Constant Values
% ----------------------------------------
% L_bend = length of the bend region (in)
% Dy = length of the inclined web in the Y-direction (in)
% D = length of the inclined web (in)
% bbf = bottom flange width (in)
% db = bend depth (in)

L_bend=r*atan(m);
Dy=d-t-2*r*(1-1/sqrt(m^2+1));
D=(2*r+(d-t-2*r)*sqrt(m^2+1))/m;
bbf=w-(4*L_bend+2*D+2*btf);
db=r*(1-1/sqrt(m^2+1))-t/2;

% Slice Widths, wi (in)
% ----------------------------------------
% hi = height of slice (in)
% yi = centers of slices, composite (in)
% wi = slice widths (in)

wi=zeros(Ns,1);
for i=1:Ns
    y=yi(i);
    if y<(ts)
        wi(i)=bs;
    elseif y<(ts+t)
        c2=(2*r+t)*sqrt(1-(1-(y-ts)/(r+t/2))^2);
        wi(i)=2*btf+c2;
        clear c2
    elseif y<(ts+t+db)
        c2=(2*r+t)*sqrt(1-(1-(y-ts)/(r+t/2))^2);
        c1=(2*r-t)*sqrt(1-(1-(y-t-ts)/(r-t/2))^2);
        wi(i)=c2-c1;
        clear c2 c1
    elseif y<(ts+t+db+Dy)
        wi(i)=2*t*sqrt(m^2+1)/m;
```

```
    elseif y<(ts+t+2*db+Dy)
        c2=(2*r+t)*sqrt(1-(1-(d+ts-y)/(r+t/2))^2);
        c1=(2*r-t)*sqrt(1-(1-(d+ts-t-y)/(r-t/2))^2);
        wi(i)=c2-c1;
        clear h2 h1 c2 c1
    else
        c2=(2*r+t)*sqrt(1-(1-(d+ts-y)/(r+t/2))^2);
        wi(i)=bbf+c2;
        clear h2 c2
    end
    clear y
end
clear ans i

end
```

B.2.7 Program File: tubMn.m

Function file "tubMn.m" is employed to perform strain compatibility iterations for computing the nominal capacity of composite press-brake-formed tub girders. The program begins by applying strains to the noncomposite section resulting from the chosen level of dead load moment. A neutral axis depth is chosen and a linear strain profile resulting in a compressive strain of 0.003 is superimposed onto the composite section. The program then iterates the depth of the neutral axis such that the net sum of compressive forces equal the net sum of tensile forces. Once a sufficient balance is achieved, the program sums the moments of each slice (equal to the force in each slice multiplied by the moment arm from the neutral axis) to obtain the nominal moment capacity of the section (see Chapter 5). The MATLAB file is as follows (input for the girder used in the demonstrated example in Appendix A with a 7.5' × 8" concrete deck is shown):

```
% Material Constants
% ------------------------------------------
E=29000;     % modulus of elasticity of steel (ksi)
Fy=50;       % steel yield stress (ksi)
fc=4;        % concrete compressive stress (ksi)

% Input Parameters
% ------------------------------------------
w=84;        % standard mill plate width (in)
t=7/16;      % plate thickness (in)
d=23;        % total girder depth (in)
r=(11/2)*t;  % bend radius at mid-thickness (in)
m=4;         % slope ratio of the inclined web
btf=6;       % top flange width (in)
bs=90;       % concrete deck width (in)
ts=8;        % concrete deck thickness (in)
DLratio=0.5; % dead load moment ratio

% Slice Widths, wi (in)
% ------------------------------------------
Ns=2000;
hi=(d+ts)/Ns;
yi=((hi/2):(hi):((d+ts)-hi/2))';
wi=slices(w,t,d,r,m,btf,bs,ts,Ns,yi);

% Noncomposite Strains
% ------------------------------------------
% c_NC = noncomposite centroid from the top (in)
% ei_NC = Noncomposite section strains
```

```
[~,y_NC,Ix_NC]=flexprop_NC(w,t,d,r,m,btf);
Sx=Ix_NC/y_NC;
My=Fy*Sx;
c_NC=(d-y_NC);

ei_NC=zeros(Ns,1);
for i=1:Ns
    y=yi(i);
    if y<ts
        ei_NC(i)=0;
    else
        ei_NC(i)=DLratio*My*((y-ts-c_NC)/(E*Ix_NC));
    end
    clear y
end
clear ans i
clear A_NC y_NC Ix_NC Sx My c_NC

% Nominal Moment Capacity (ft-kip)
% ----------------------------------------
c1=hi;           % lower bound guess for neutral axis location (in)
si1=zeros(Ns,1); % lower bound guess for section stresses (ksi)
bi1=1;           % lower bound balance "C=T" check (kip)
while bi1>0
    ei1=ei_NC+0.003*(yi-c1)/c1;
    for j=1:Ns
        y=yi(j);
        if y<ts
            if ei1(j)<0
                si1(j)=-0.85*fc;
            else
                si1(j)=0;
            end
        else
            if ei1(j)>0
                si1(j)=min(Fy,ei1(j)*E);
            else
                si1(j)=max(-Fy,ei1(j)*E);
            end
        end
        clear y
    end
    clear ans j
    bi1=sum(si1.*wi*hi);
    c1=c1+hi;
    clear ei1
end

c2=c1-2*hi;           % upper bound guess for neutral axis location (in)
si2=zeros(Ns,1);      % upper bound guess for section stresses (ksi)
ei2=ei_NC+0.003*(yi-c2)/c2;
for j=1:Ns
    y=yi(j);
    if y<ts
        if ei2(j)<0
            si2(j)=-0.85*fc;
```

```
        else
            si2(j)=0;
        end
    else
        if ei2(j)>0
            si2(j)=min(Fy,ei2(j)*E);
        else
            si2(j)=max(-Fy,ei2(j)*E);
        end
    end
    clear y
end
clear ans j
bi2=sum(si2.*wi*hi); % upper bound balance "C=T" check (kip)

if abs(bi1)<abs(bi2)
    si=si1;
    c=c1;
else
    si=si2;
    c=c2;
end
clear ei1 si1 bi1 c1
clear ei2 si2 bi2 c2

ei=ei_NC+0.003*(yi-c)/c;  % slice strains (in)
ri=yi-c;                  % slice moment arms (in)
fi=si.*wi*hi;             % slice forces (kip)
mi=fi.*ri;                % slice moments (in-kip)
Mn=sum(mi)/12;            % nominal moment capactiy (ft-kip)

clear w t d r m btf bs ts DLratio
clear Ns hi yi wi
clear ei_NC c ri fi mi
clear E Fy fc
```

B.2.8 Program File: tubMp.m

Function file "tubMp.m" is employed to compute the plastic moment capacity of composite press-brake-formed tub girders. The program begins by applying strains to the noncomposite section resulting from the chosen level of dead load moment. A neutral axis depth is chosen and a linear strain profile resulting in a compressive strain of 0.003 is superimposed onto the composite section. The program employs the same methods in "tubMn.m" to compute the nominal moment capacity. However, instead of applying strain profiles to slices, the program simply assumes that the stress in each slice is equal to 0.85 f_c' or F_y, as appropriate. In addition, if the total plastic force supplied by the concrete slab is greater than the total plastic force supplied by the steel girder, the program simply computes the plastic moment directly. The MATLAB file is as follows (input for the girder used in the demonstrated example in Appendix A with a 7.5' × 8" concrete deck is shown):

```
clc
clear all

% Material Constants
% ------------------------------------------
Fy=50;   % steel yield stress (ksi)
fc=4;    % concrete compressive stress (ksi)

% Input Parameters
% ------------------------------------------
w=84;        % standard mill plate width (in)
t=7/16;      % plate thickness (in)
d=23;        % total girder depth (in)
r=(11/2)*t;  % bend radius at mid-thickness (in)
m=4;         % slope ratio of the inclined web
btf=6;       % top flange width (in)
bs=90;       % concrete deck width (in)
ts=8;        % concrete deck thickness (in)

% Plastic Moment Capacity (PNA in slab)
% ------------------------------------------
if 0.85*fc*bs*ts>=Fy*w*t
    a=Fy*w*t/(0.85*fc*bs);                  % stress block depth (in)
    Dp_Dt=a/(d+ts);                         % Dp/Dt
    [~,y_NC,~]=flexprop_NC(w,t,d,r,m,btf);  % noncomposite N.A. (in)
    Mp=(Fy*w*t*(d-y_NC+ts-a/2))/12;         % plastic moment (ft-kip)
    clear Fy fc w t d r m btf bs ts a y_NC
    break
end
```

```
% Slice Widths, wi (in)
% ------------------------------------------
Ns=2000;
hi=(d+ts)/Ns;
yi=((hi/2):(hi):((d+ts)-hi/2))';
wi=slices(w,t,d,r,m,btf,bs,ts,Ns,yi);

% Plastic Moment Capacity (PNA in steel)
% ------------------------------------------
c1=hi;           % lower bound guess for neutral axis location (in)
si1=zeros(Ns,1); % lower bound guess for section stresses (ksi)
bi1=1;           % lower bound balance "C=T" check (kip)
while bi1>0
    for j=1:Ns
        y=yi(j);
        if c1<ts
            if y<c1
                si1(j)=-0.85*fc;
            elseif y<ts
                si1(j)=0;
            else
                si1(j)=Fy;
            end
        else
            if y<ts
                si1(j)=-0.85*fc;
            elseif y<c1
                si1(j)=-Fy;
            else
                si1(j)=Fy;
            end
        end
        clear y
    end
    clear ans j
    bi1=sum(si1.*wi*hi);
    c1=c1+hi;
end

c2=c1-2*hi;           % upper bound guess for neutral axis location (in)
si2=zeros(Ns,1);      % upper bound guess for section stresses (ksi)
for j=1:Ns
    y=yi(j);
    if c2<ts
        if y<c2
            si2(j)=-0.85*fc;
        elseif y<ts
            si2(j)=0;
        else
            si2(j)=Fy;
        end
    else
        if y<ts
            si2(j)=-0.85*fc;
        elseif y<c2
            si2(j)=-Fy;
```

```
        else
            si2(j)=Fy;
        end
    end
    clear y
end
clear ans j
bi2=sum(si2.*wi*hi); % upper bound balance "C=T" check (kip)

if abs(bi1)<abs(bi2)
    si=si1;     ri=yi-c1;       Dp=c1;
else
    si=si2;     ri=yi-c2;       Dp=c2;
end
clear si1 bi1 c1 si2 bi2 c2

fi=si.*wi*hi;           % slice forces (kip)
mi=fi.*ri;              % slice moments (in-kip)
Mp=sum(mi)/12;          % total moment capactiy (ft-kip)
Dp_Dt=Dp/(d+ts);        % Dp/Dt

clear Fy fc w t d r m btf bs ts Ns hi yi wi ri si fi mi Dp
```

B.3 ILLUSTRATIVE EXAMPLES

In order to demonstrate the capabilities of the documented MATLAB routines, two example girders will be assessed. Specifically, for each girder, a strain compatibility analysis is presented and the plastic moment is computed. For both girders, a yield stress of 50 ksi is assumed, and the concrete deck is assumed to be 7.5' wide × 8" thick and to have compressive stress equal to 4 ksi.

B.3.1 Example Girder 1

The first example girder incorporates the steel tub design corresponding to the PL 84" × 7/16" option listed in Chapter 3. For this example, it is assumed that the noncomposite section will see an initial stress profile equal to 0.50 M_y. Figure B.1 displays the geometry of the example girder; note that the point "C.G." refers to the center-of-gravity of the noncomposite section.

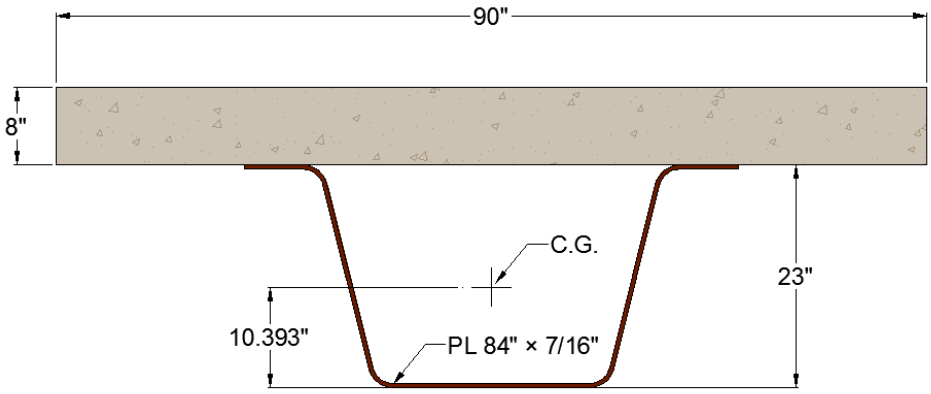

Figure B.1: Example Girder 1

B.3.1.1 Computation of Plastic Moment

To compute the plastic moment, the first step is to determine the location of the plastic neutral axis. This is determined based on the magnitude of the plastic forces for both the steel and concrete components of the composite girder. Therefore, these values are computed as follows:

$$P_{conc} = 0.85 f_c' b_s t_s = 0.85(4 \text{ ksi})(90 \text{ in})(8 \text{ in}) = 2448 \text{ kip}$$

$$P_{steel} = F_y A_g = (50 \text{ ksi})(84 \text{ in})\left(\frac{7}{16} \text{ in}\right) = 1837.5 \text{ kip}$$

Therefore, since the plastic force in the concrete exceeds the plastic force in the steel, the plastic neutral axis is located in the slab. The depth to the plastic neutral axis, D_p, can therefore be determined as follows:

$$D_p = \frac{F_y A_g}{0.85 f_c' b_s} = \frac{1837.5 \text{ kip}}{0.85(4 \text{ ksi})(90 \text{ in})} = 6.005 \text{ in}$$

The plastic moment, M_p, can therefore be determined as follows:

$$\begin{aligned} M_p &= F_y A_g \left(d + t_s - \bar{y} - \frac{D_p}{2} \right) \\ &= \frac{1837.5 \text{ kip}}{12 \text{ in/ft}} \left(23 \text{ in} + 8 \text{ in} - 10.393 \text{ in} - \frac{6.005 \text{ in}}{2} \right) \\ &= 2695.6 \text{ ft-kip} \end{aligned}$$

The resulting plastic force distribution for this girder is also shown in Figure B.2.

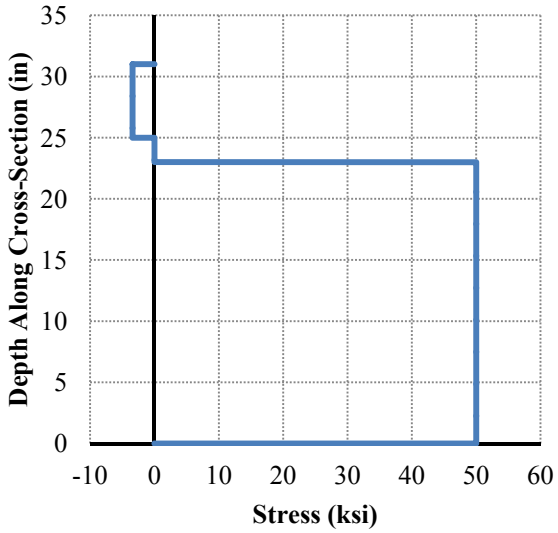

Figure B.2: Plastic Stress Distribution (Example Girder 1)

B.3.1.2 Computation of Nominal Moment (Strain Compatibility)

Utilizing the strain-compatibility approach discussed in Chapter 5, the nominal moment capacity of the example girder was computed. First, the strains corresponding to an applied stress profile of 0.50 M_y was applied to the noncomposite girder. Assuming a neutral axis depth, a strain profile corresponding to a maximum concrete compressive strain of 0.003 was superimposed onto the initial strain profile. The depth of the neutral axis was then iterated such that the sum of forces in the cross-section was equal to zero (the force in each slice was computed by multiplying the stress in the slice by the area, equal to the thickness of the slice multiplied by the width). Figure B.3 shows the resulting strain and stress profiles from strain-compatibility analysis; as shown, the neutral axis was found to be at a depth of approximately 5.29 inches.

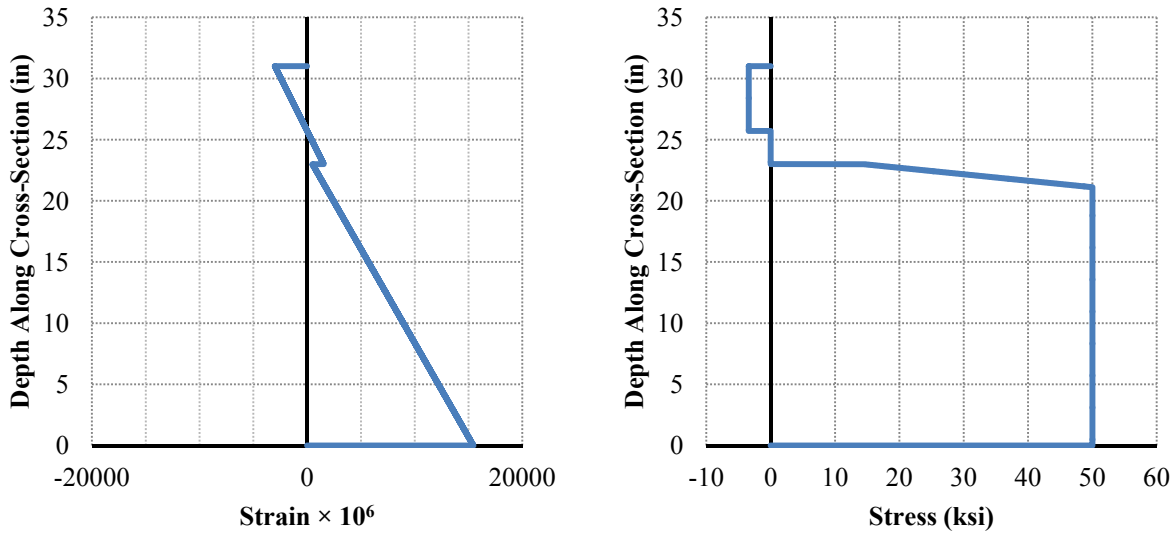

Figure B.3: Strain Compatibility Analysis (Example Girder 1)

Utilizing the resulting stress profile, the nominal moment capacity was found by summing the forces in each slice about the neutral axis. The resulting nominal moment capacity was found to be 2646.3 ft-kip.

B.3.2 Example Girder 2

The second example girder incorporates the steel tub design corresponding to the PL 120" × 1/2" option listed in Chapter 3. For this example, it is assumed that the noncomposite section will see no initial stress. Figure B.1 displays the geometry of the example girder; note that the point "C.G." refers to the center-of-gravity of the noncomposite section.

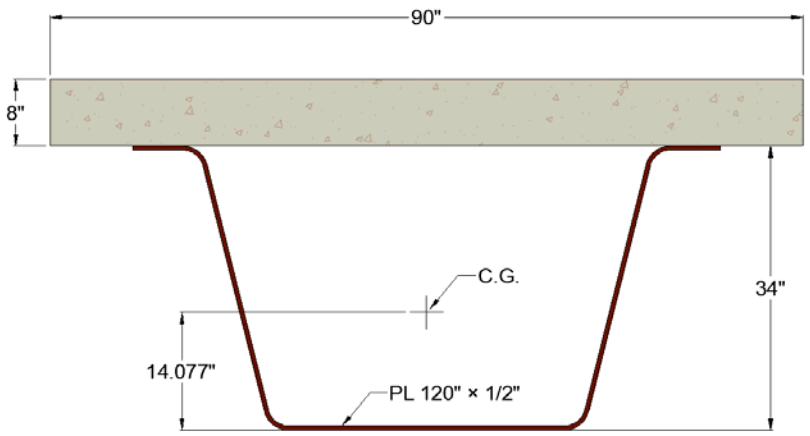

Figure B.4: Example Girder 2

B.3.2.1 Computation of Plastic Moment

Following the previous process, the first step is to determine the location of the plastic neutral axis. The magnitudes of the plastic forces for both the steel and concrete components of the composite girder are as follows:

$$P_{conc} = 0.85 f_c' b_s t_s = 0.85(4 \text{ ksi})(90 \text{ in})(8 \text{ in}) = 2448 \text{ kip}$$

$$P_{steel} = F_y A_g = (50 \text{ ksi})(120 \text{ in})\left(\frac{1}{2} \text{ in}\right) = 3000 \text{ kip}$$

Therefore, since the plastic force in the steel exceeds the plastic force in the concrete, the plastic neutral axis is located within the steel girder. Therefore, the depth to the plastic neutral axis and the corresponding plastic moment are computed using a similar iterative technique, as described in the previous section. However, instead of applying strain profiles, each slice is assumed to reach either 0.85 f_c' or F_y, as appropriate. Figure B.5 shows the plastic force distribution for this girder; as shown, a portion of the steel girder is in compression (as predicted).

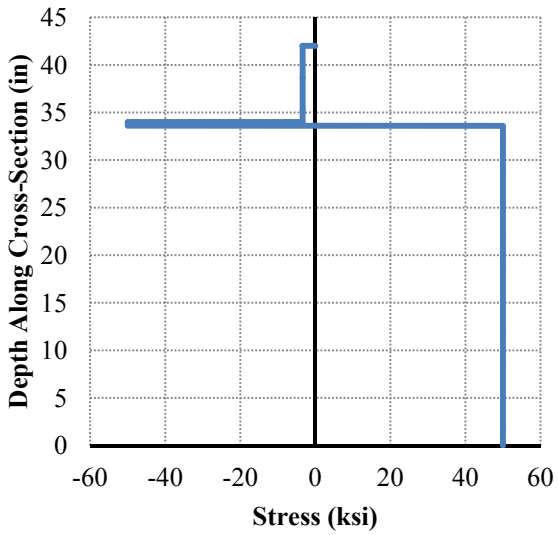

Figure B.5: Plastic Stress Distribution (Example Girder 2)

Utilizing the resulting stress profile, it was found that D_p = 8.408 inches and M_p = 5805.8 ft-kip.

B.3.2.2 Computation of Nominal Moment (Strain Compatibility)

Utilizing the previously discussed strain-compatibility approach, the nominal moment capacity of the example girder was computed. Figure B.6 shows the resulting strain and stress profiles from strain-compatibility analysis; as shown, the neutral axis was found to be at a depth of approximately 8.66 inches.

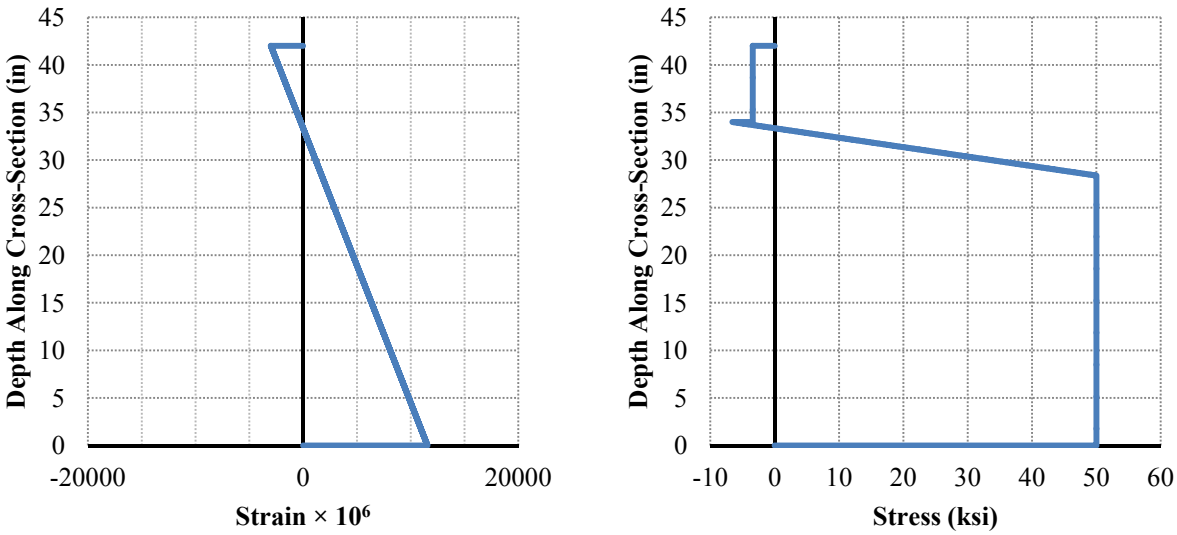

Figure B.6: Strain Compatibility Analysis (Example Girder 2)

Utilizing the resulting stress profile, the nominal moment capacity was found by summing the forces in each slice about the neutral axis. The resulting nominal moment capacity was found to be 5760.4 ft-kip.

APPENDIX C: EXPERIMENTAL AND ANALYTICAL DATA

C.1 INTRODUCTION

The purpose of this appendix is to document the experimental and analytical data employed in this research. Experimental data for each physical test discussed in Chapter 4 is presented, along with comparisons of finite element analysis results using methods discussed in Chapter 5. In addition, analytical plots from the behavioral studies in Chapter 6 and feasibility assessments from Chapter 7 are also presented.

C.2 EXPERIMENTAL DATA (CHAPTER 4)

The following section documents the instrument readings for the physical tests discussed in Chapter 4. Titles of figures plotting gage readings correspond to the legend shown in Figure C.1. Recall that the same gage pattern was employed for both composite and noncomposite physical tests. It should also be noted that, for clarity, data from rectangular rosettes (installed on the webs) have been reduced to shear strains. In addition, data from LVDTs at quarter-points and midspan have been averaged.

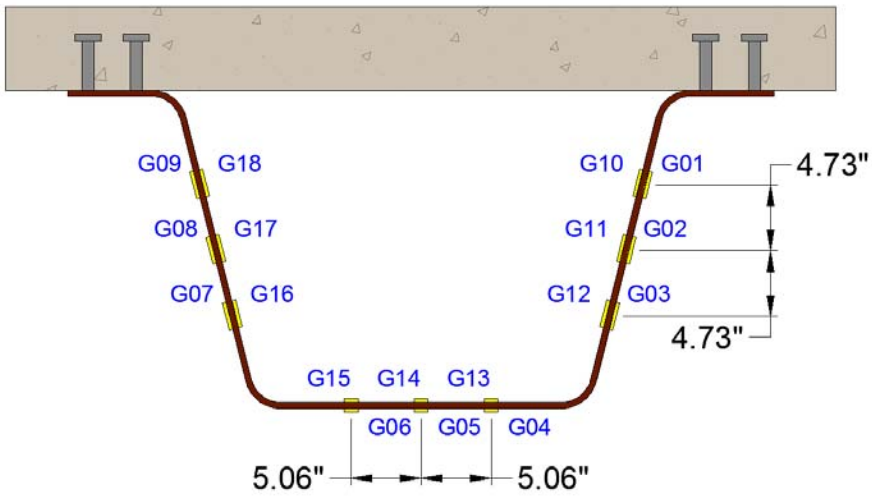

Figure C.1: Strain Gage Data Legend

C.2.1 Data from Experiments 1 and 2 (Composite Girder Tests)

The following plots document the results from Experiments 1 and 2 discussed in Chapter 4. In addition, finite element analysis results, using methods discussed in Chapter 5, have been included in each plot.

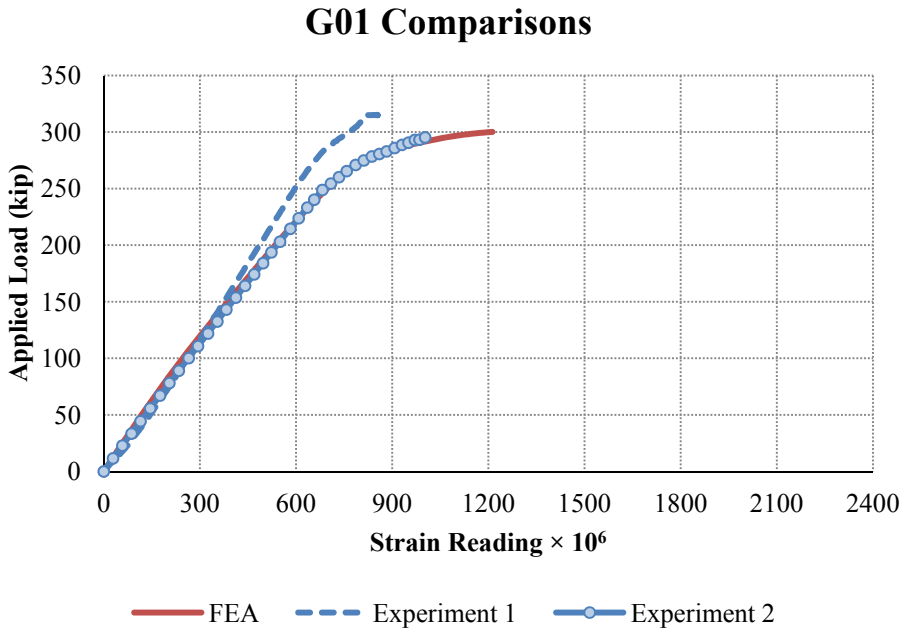

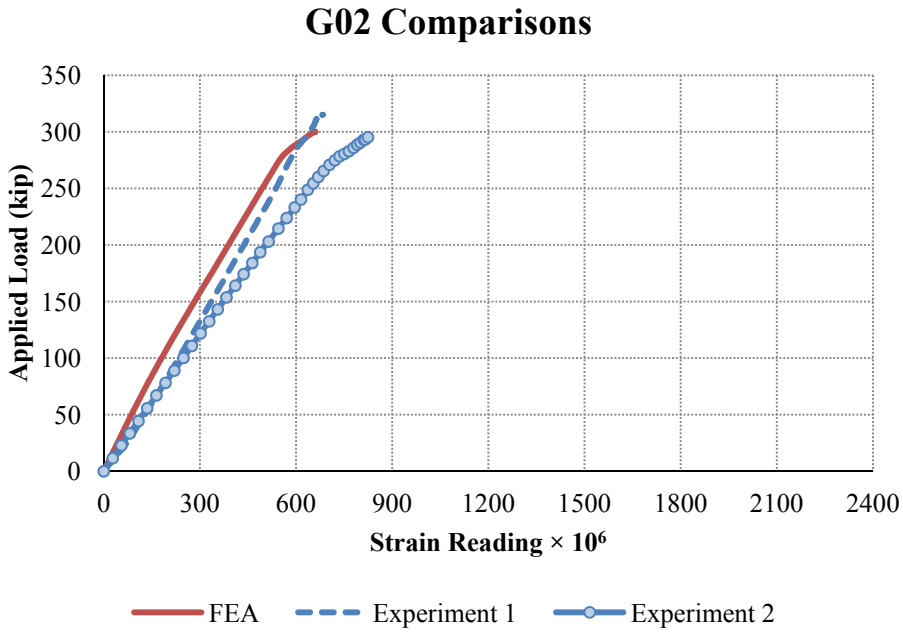
G02 Comparisons
Applied Load (kip)
350
300
250
200
150
100
50
0
0
300
600
900
1200
1500
1800
2100
2400
Strain Reading × 10⁶
FEA
Experiment 1
Experiment 2

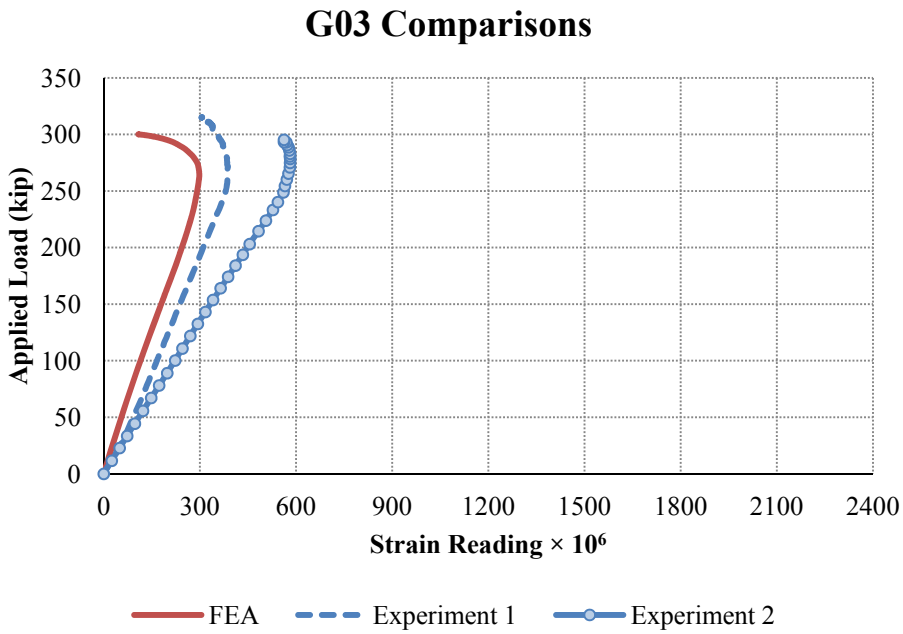
G03 Comparisons
Applied Load (kip)
350
300
250
200
150
100
50
0
0
300
600
900
1200
1500
1800
2100
2400
Strain Reading × 10⁶
FEA
Experiment 1
Experiment 2

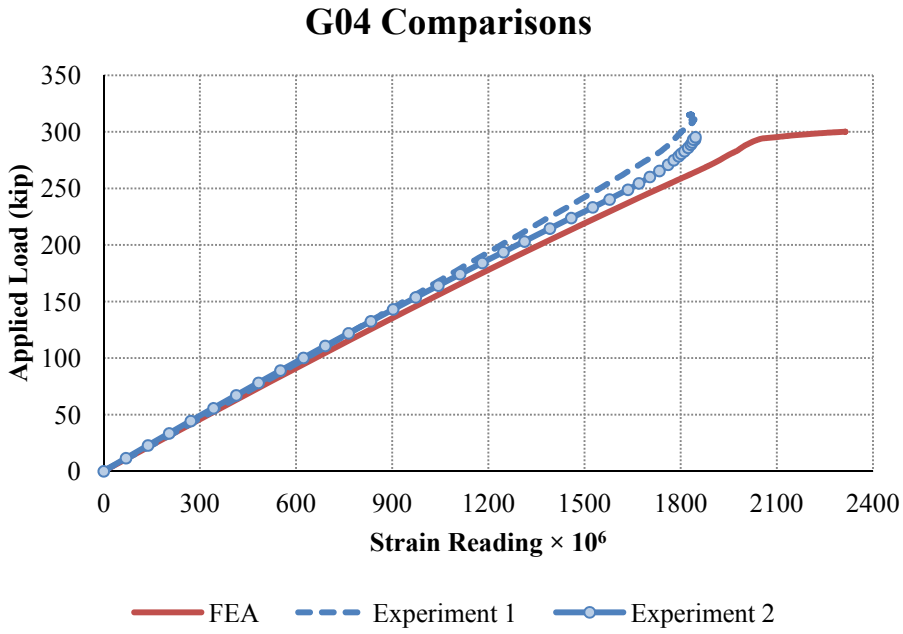
G04 Comparisons
Applied Load (kip)
350
300
250
200
150
100
50
0
0
300
600
900
1200
1500
1800
2100
2400
Strain Reading × 10⁶
FEA
Experiment 1
Experiment 2

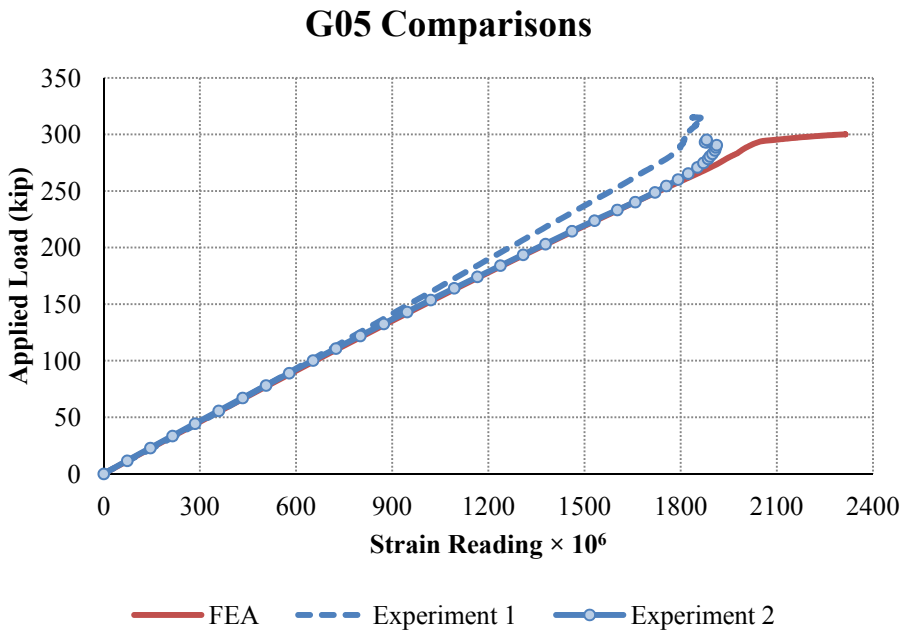
G05 Comparisons
Applied Load (kip)
350
300
250
200
150
100
50
0
0
300
600
900
1200
1500
1800
2100
2400
Strain Reading × 10⁶
FEA
Experiment 1
Experiment 2

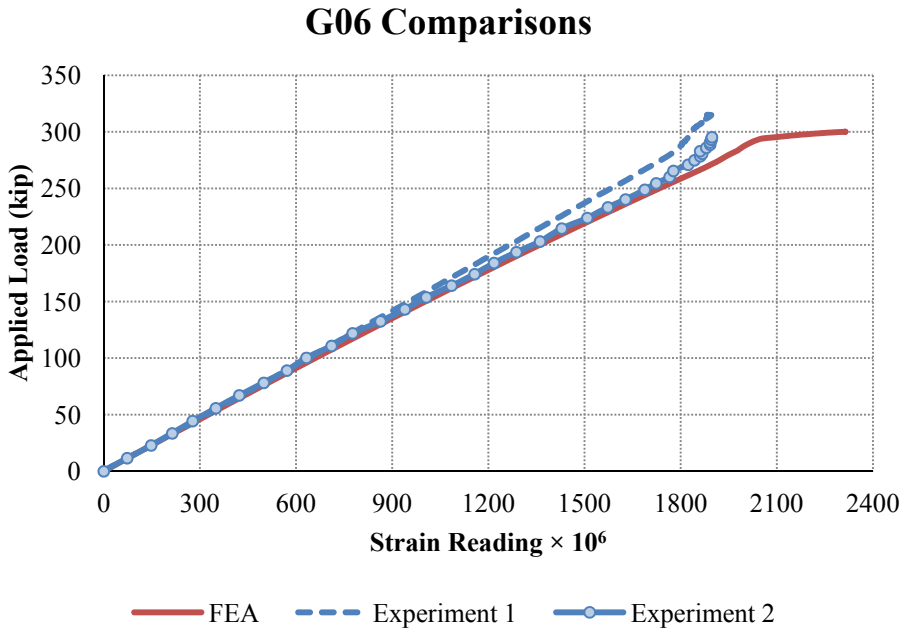
G06 Comparisons
Applied Load (kip)
350
300
250
200
150
100
50
0
0
300
600
900
1200
1500
1800
2100
2400
Strain Reading × 10⁶
FEA
Experiment 1
Experiment 2

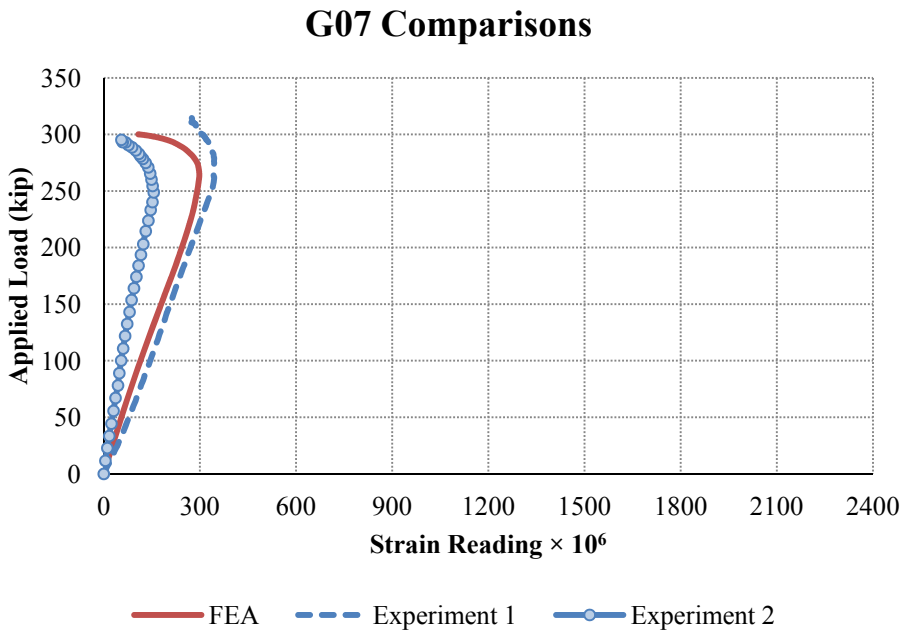
G07 Comparisons
Applied Load (kip)
350
300
250
200
150
100
50
0
0
300
600
900
1200
1500
1800
2100
2400
Strain Reading × 10⁶
FEA
Experiment 1
Experiment 2

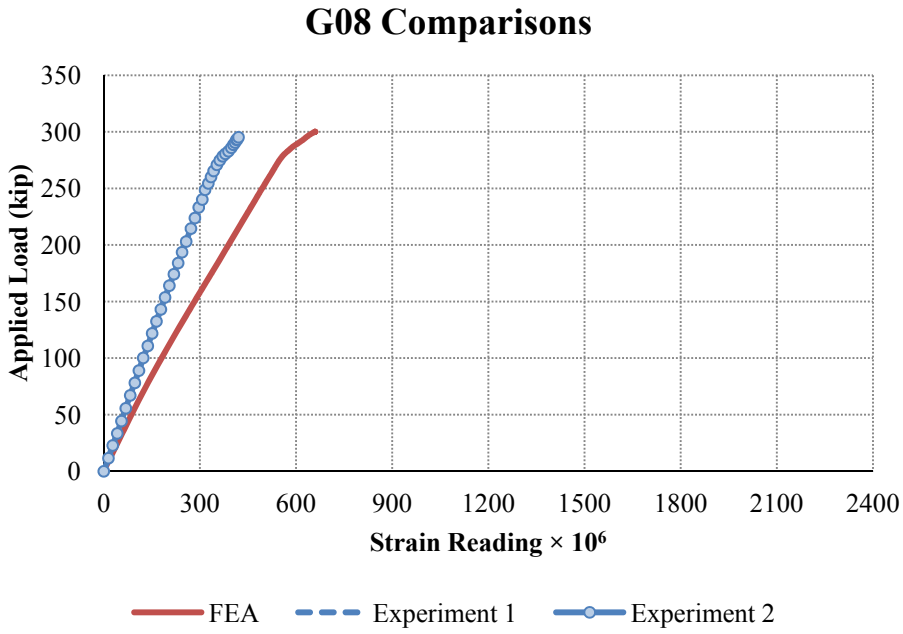
G08 Comparisons
Applied Load (kip)
350
300
250
200
150
100
50
0
0
300
600
900
1200
1500
1800
2100
2400
Strain Reading × 10⁶
FEA
Experiment 1
Experiment 2

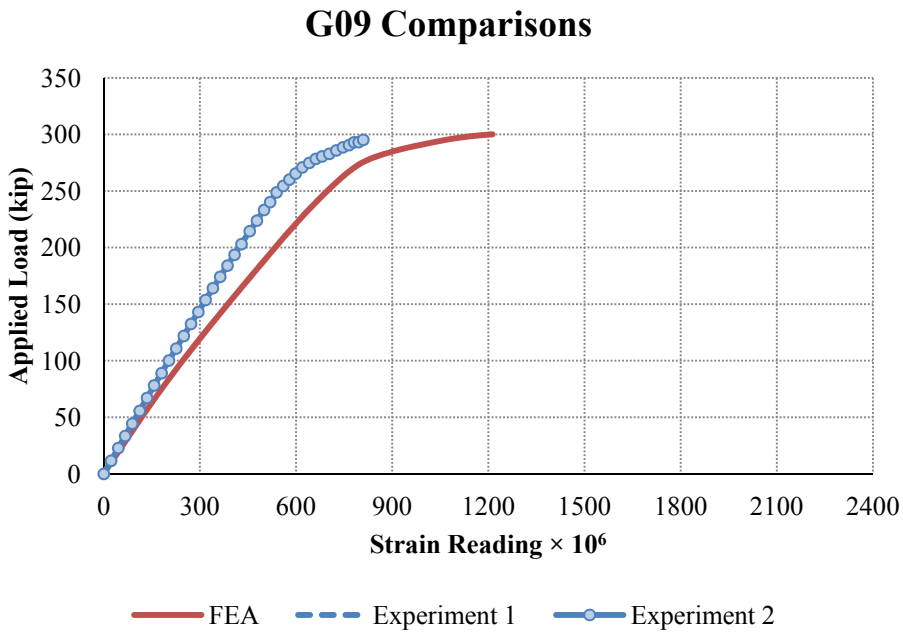
G09 Comparisons
Applied Load (kip)
350
300
250
200
150
100
50
0
0
300
600
900
1200
1500
1800
2100
2400
Strain Reading × 10⁶
FEA
Experiment 1
Experiment 2

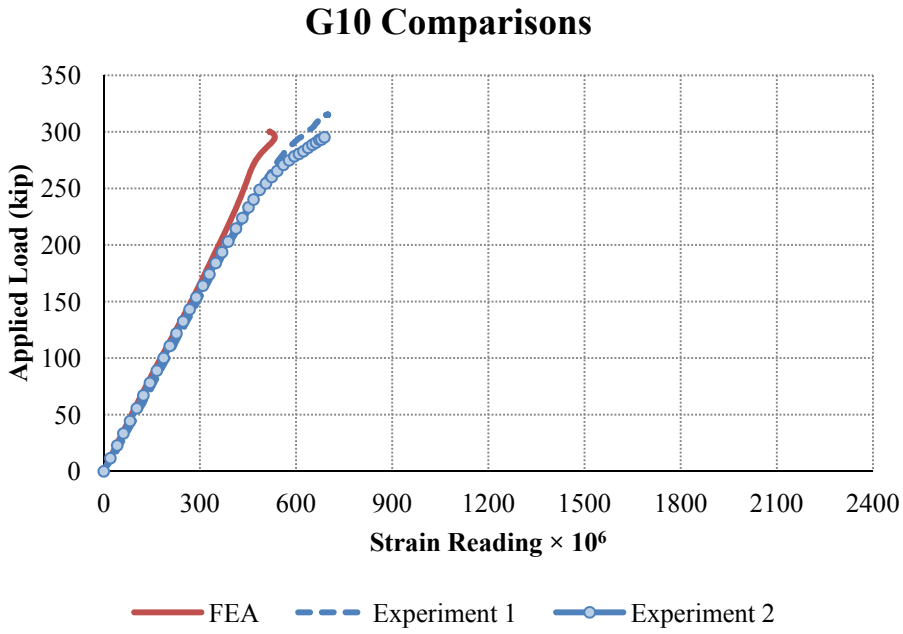
G10 Comparisons
Applied Load (kip)
350
300
250
200
150
100
50
0
0
300
600
900
1200
1500
1800
2100
2400
Strain Reading × 10⁶
FEA
Experiment 1
Experiment 2

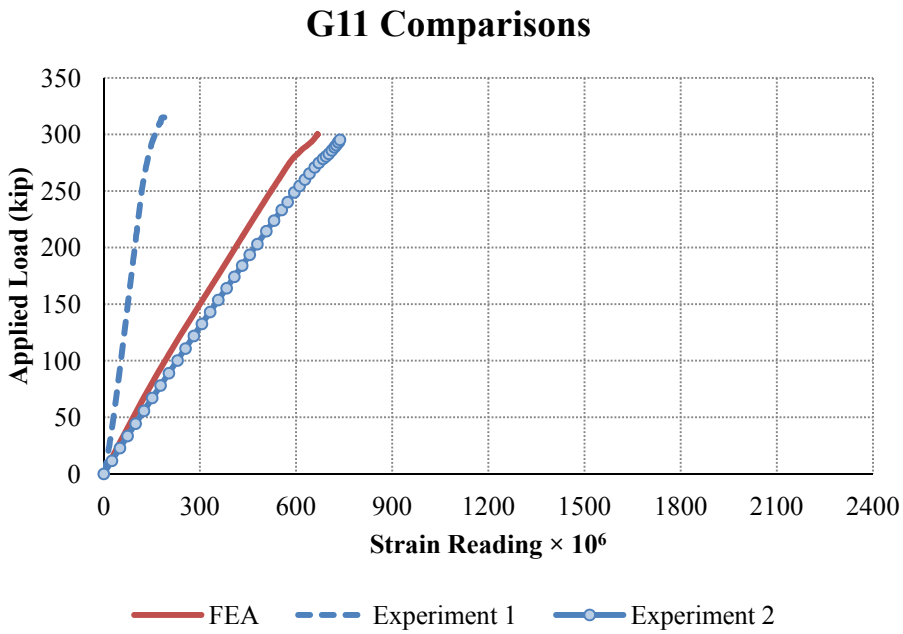
G11 Comparisons
Applied Load (kip)
350
300
250
200
150
100
50
0
0
300
600
900
1200
1500
1800
2100
2400
Strain Reading × 10⁶
FEA
Experiment 1
Experiment 2

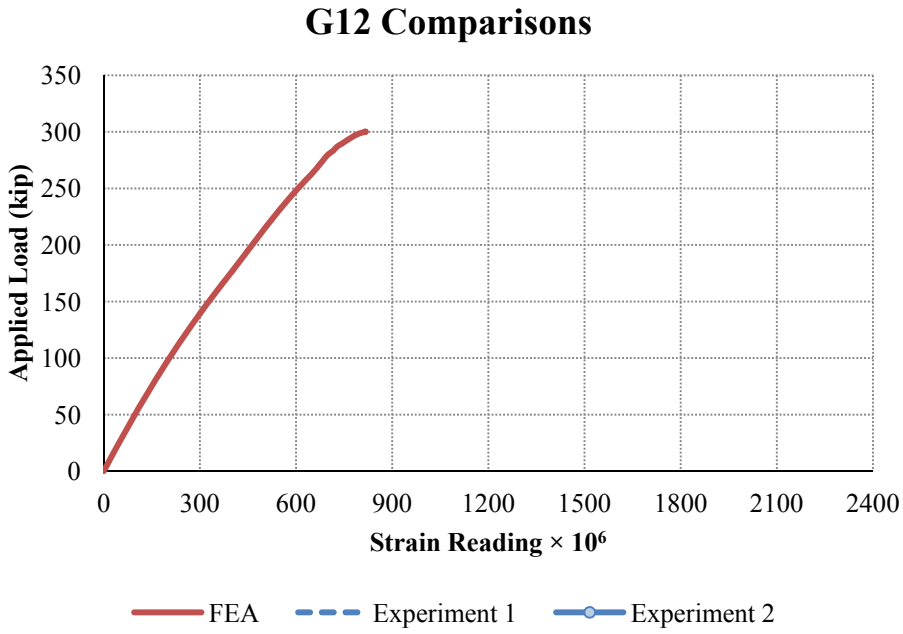
G12 Comparisons
Applied Load (kip)
350
300
250
200
150
100
50
0
0
300
600
900
1200
1500
1800
2100
2400
Strain Reading × 10⁶
FEA
Experiment 1
Experiment 2

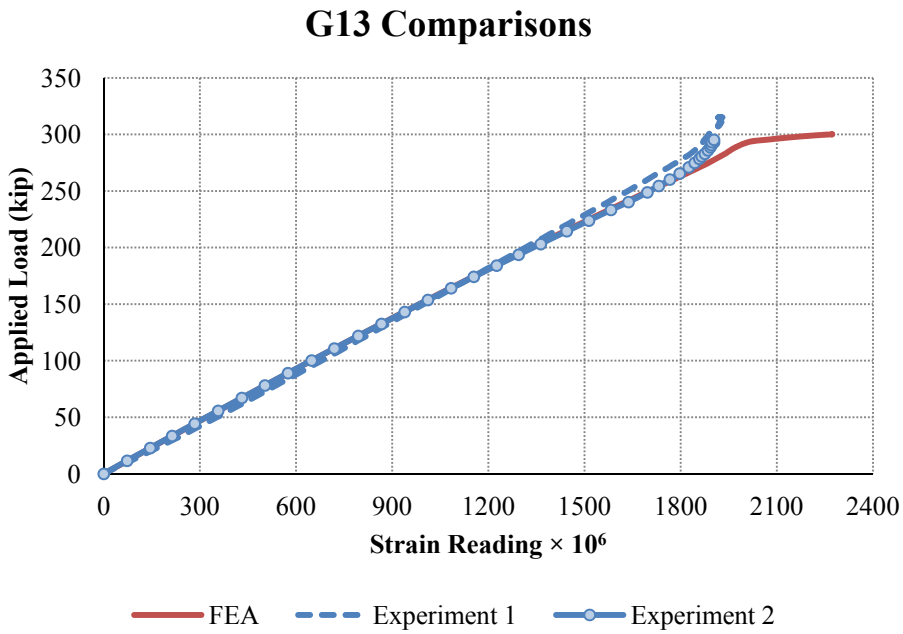
G13 Comparisons
Applied Load (kip)
350
300
250
200
150
100
50
0
0
300
600
900
1200
1500
1800
2100
2400
Strain Reading × 10⁶
FEA
Experiment 1
Experiment 2

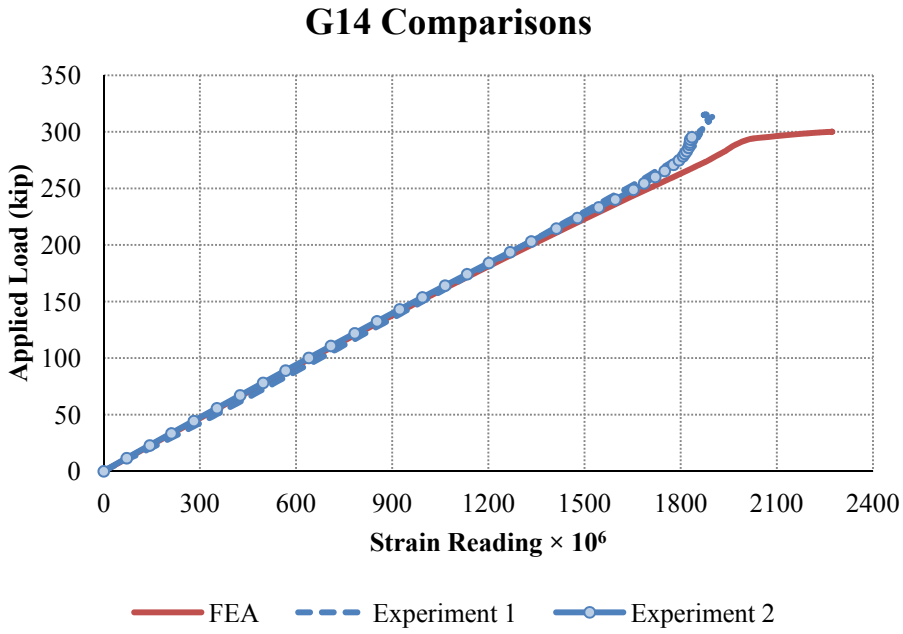
G14 Comparisons
Applied Load (kip)
350
300
250
200
150
100
50
0
0
300
600
900
1200
1500
1800
2100
2400
Strain Reading × 10⁶
FEA
Experiment 1
Experiment 2

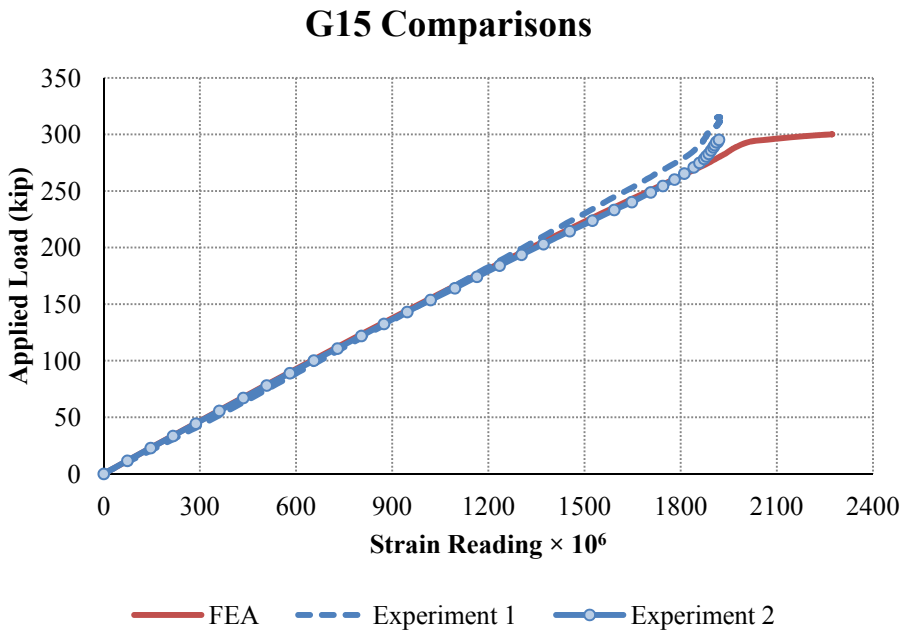
G15 Comparisons
Applied Load (kip)
350
300
250
200
150
100
50
0
0
300
600
900
1200
1500
1800
2100
2400
Strain Reading × 10⁶
FEA
Experiment 1
Experiment 2

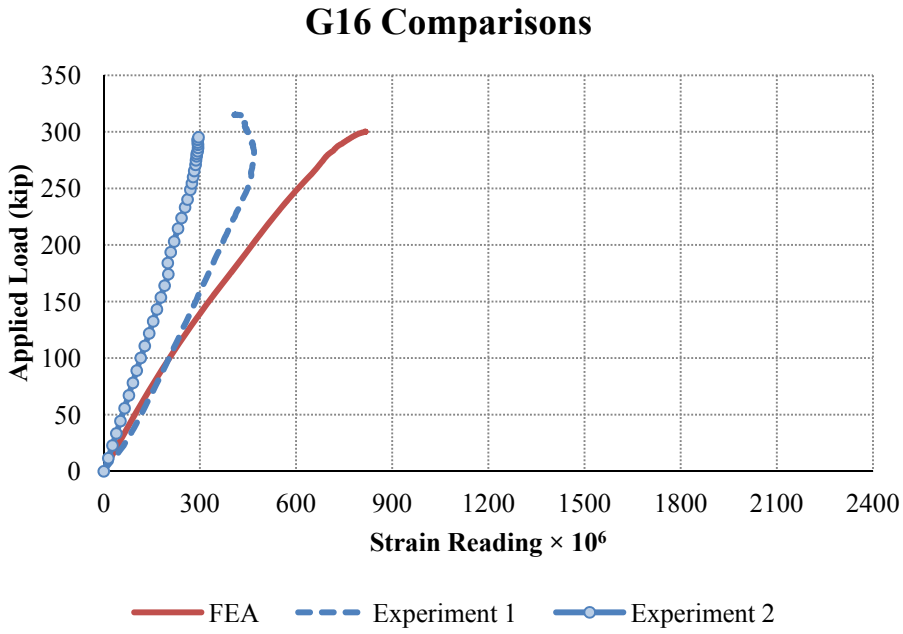
G16 Comparisons
Applied Load (kip)
350
300
250
200
150
100
50
0
0
300
600
900
1200
1500
1800
2100
2400
Strain Reading × 10⁶
FEA
Experiment 1
Experiment 2

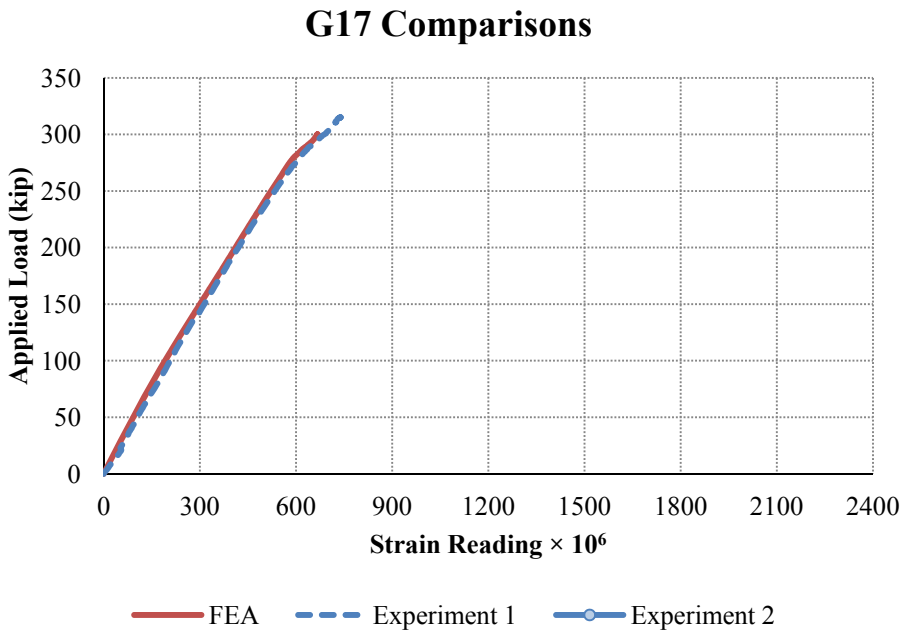
G17 Comparisons
Applied Load (kip)
350
300
250
200
150
100
50
0
0
300
600
900
1200
1500
1800
2100
2400
Strain Reading × 10⁶
FEA
Experiment 1
Experiment 2

G18 Comparisons

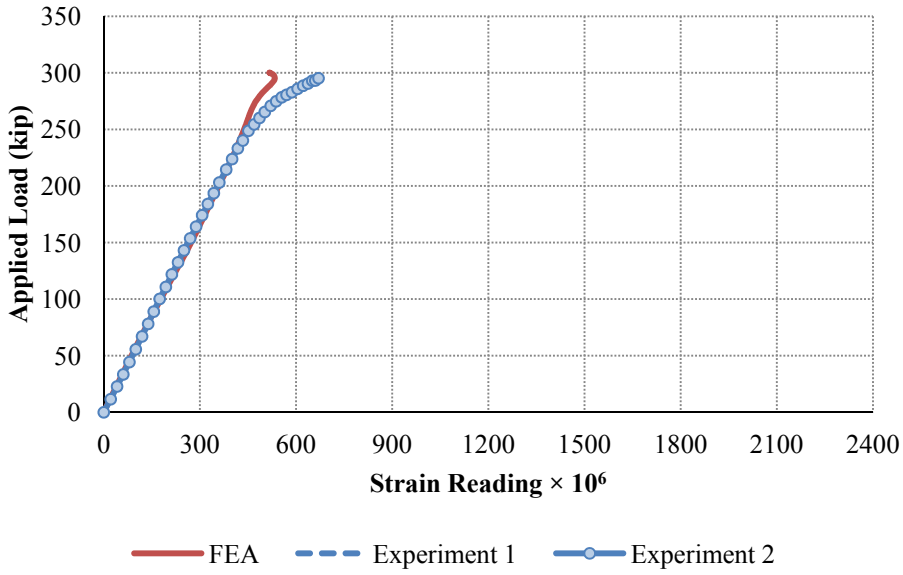

Deflection at 0.25 L

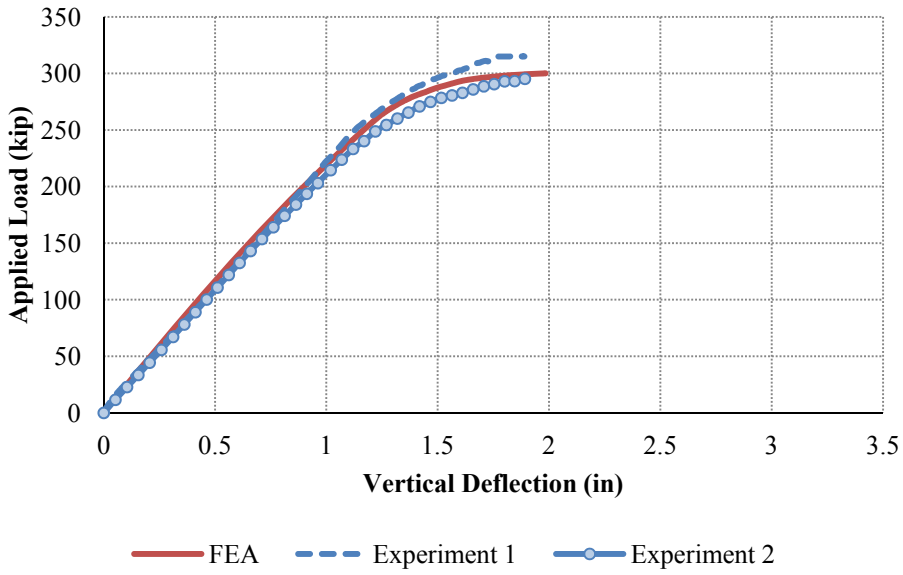

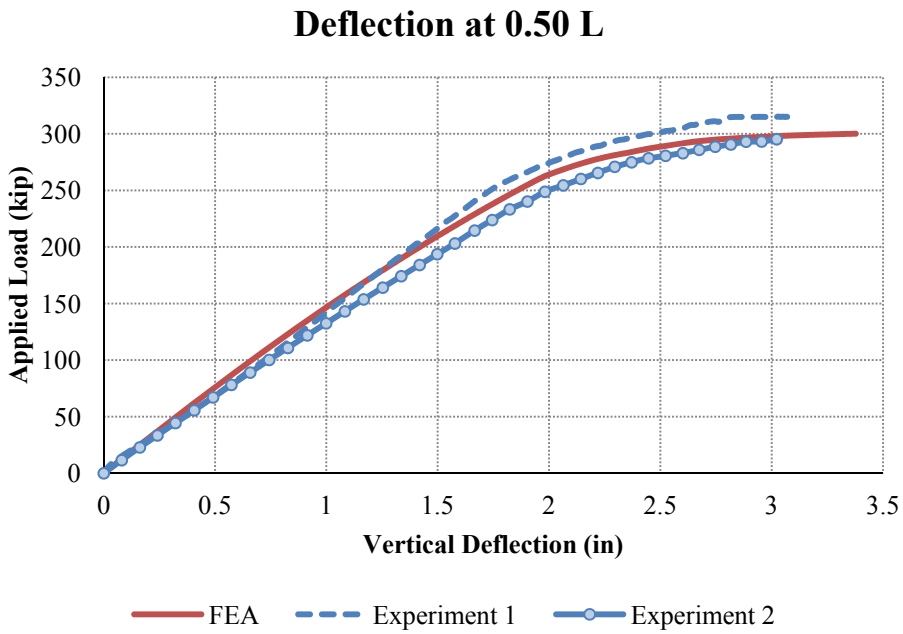

C.2.2 Data from Experiments 3 and 4 (Noncomposite Girder Tests)

The following plots document the results from Experiments 3 and 4 discussed in Chapter 4. In addition, finite element analysis results, using methods discussed in Chapter 5, have been included in each plot.

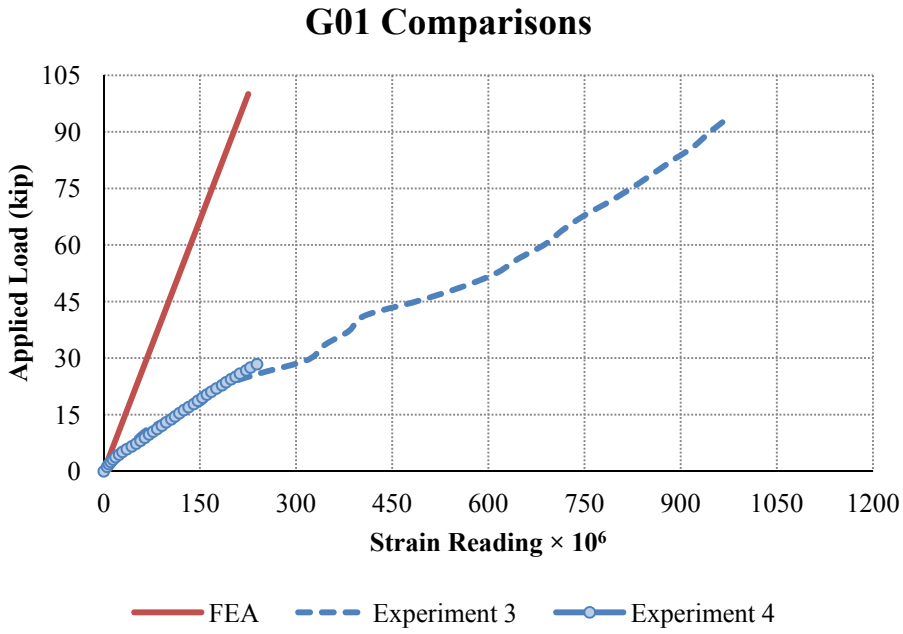
G01 Comparisons
Applied Load (kip)
105
90
75
60
45
30
15
0
0
150
300
450
600
750
900
1050
1200
Strain Reading × 10⁶
FEA
Experiment 3
Experiment 4

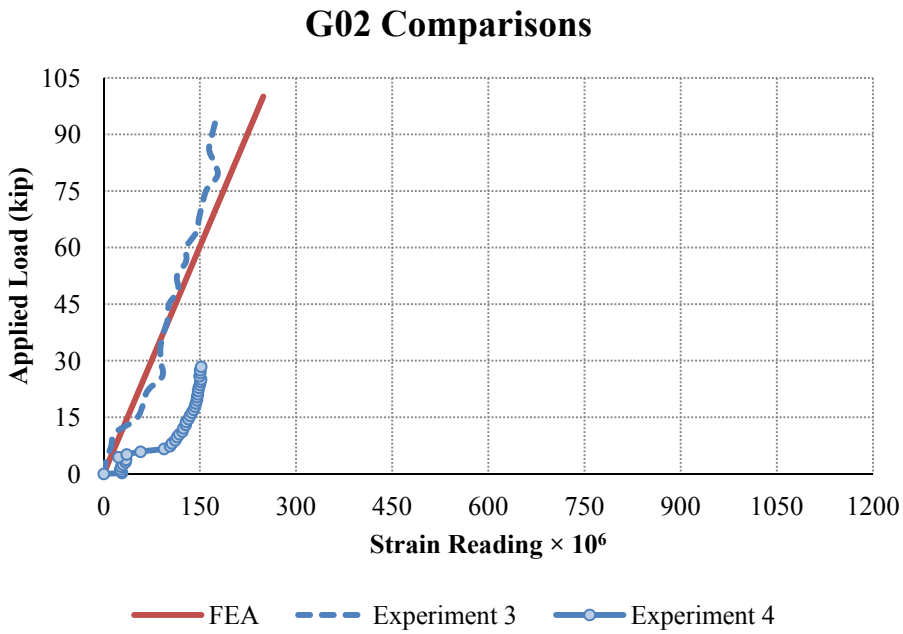
G02 Comparisons
Applied Load (kip)
105
90
75
60
45
30
15
0
0
150
300
450
600
750
900
1050
1200
Strain Reading × 10⁶
FEA
Experiment 3
Experiment 4

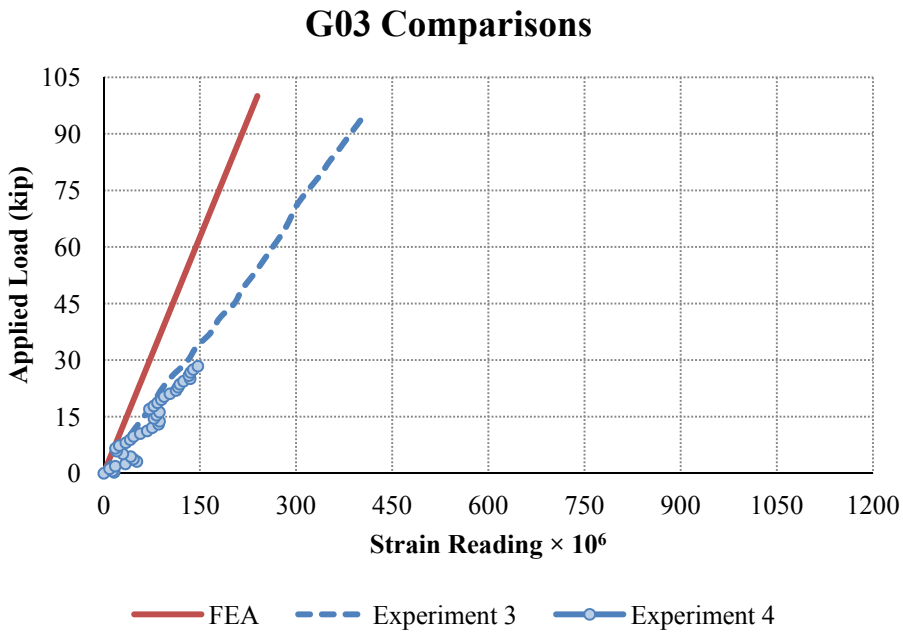
G03 Comparisons
Applied Load (kip)
105
90
75
60
45
30
15
0
0
150
300
450
600
750
900
1050
1200
Strain Reading × 10⁶
FEA
Experiment 3
Experiment 4

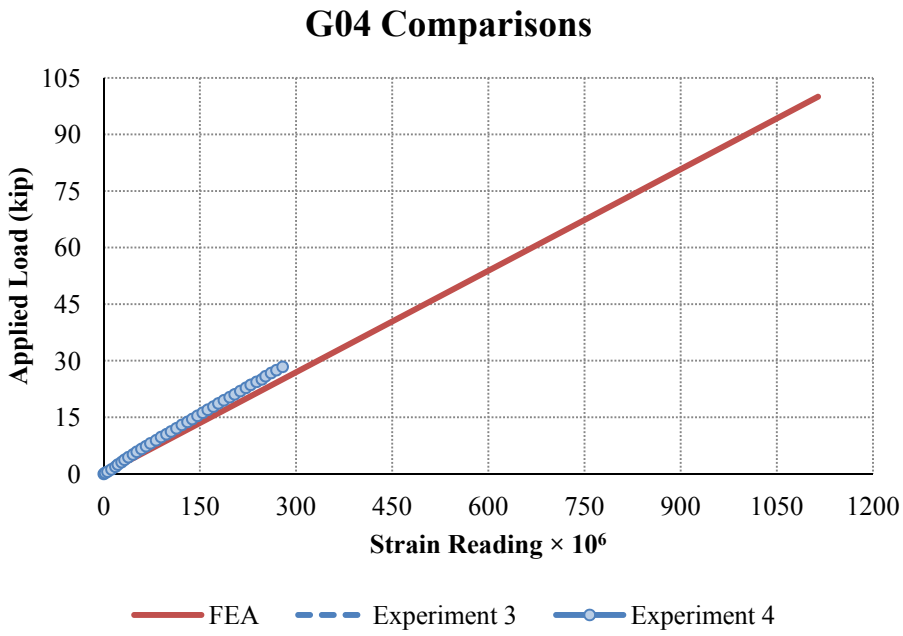
G04 Comparisons
Applied Load (kip)
105
90
75
60
45
30
15
0
0
150
300
450
600
750
900
1050
1200
Strain Reading × 10⁶
FEA
Experiment 3
Experiment 4

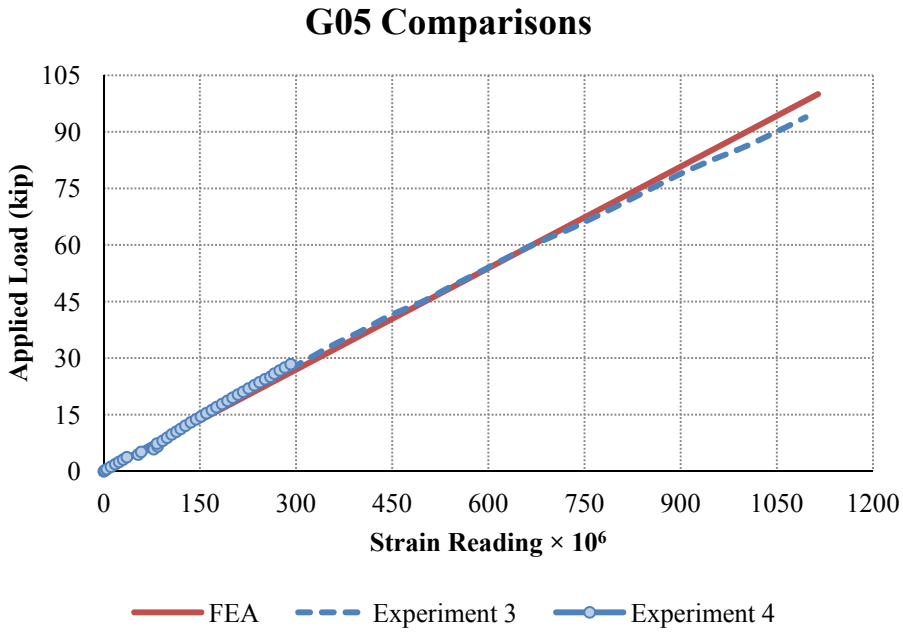
G05 Comparisons
Applied Load (kip)
105
90
75
60
45
30
15
0
0
150
300
450
600
750
900
1050
1200
Strain Reading × 10⁶
FEA
Experiment 3
Experiment 4

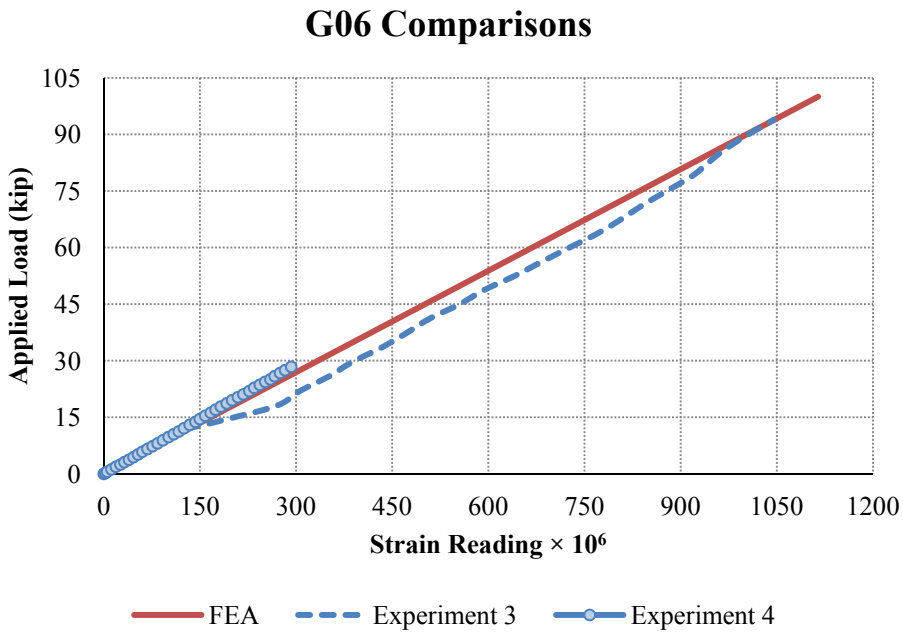
G06 Comparisons
Applied Load (kip)
105
90
75
60
45
30
15
0
0
150
300
450
600
750
900
1050
1200
Strain Reading × 10⁶
FEA
Experiment 3
Experiment 4

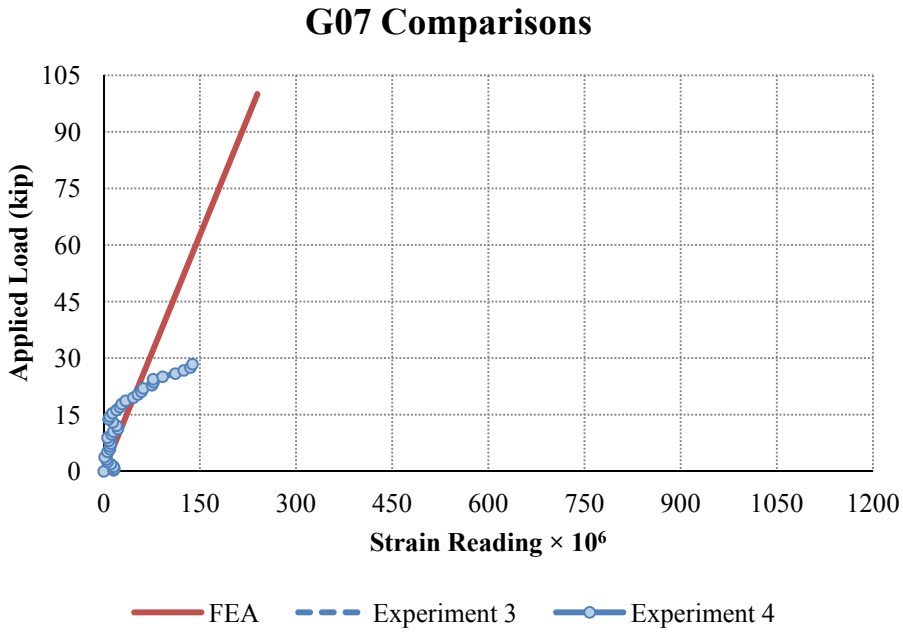
G07 Comparisons
Applied Load (kip)
105
90
75
60
45
30
15
0
0
150
300
450
600
750
900
1050
1200
Strain Reading × 10⁶
FEA
Experiment 3
Experiment 4

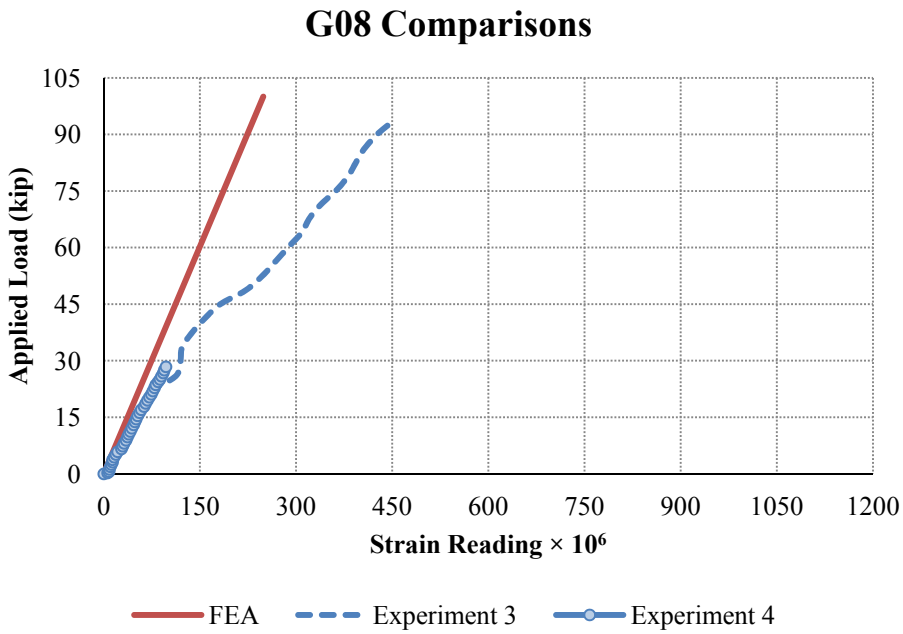
G08 Comparisons
Applied Load (kip)
105
90
75
60
45
30
15
0
0
150
300
450
600
750
900
1050
1200
Strain Reading × 10⁶
FEA
Experiment 3
Experiment 4

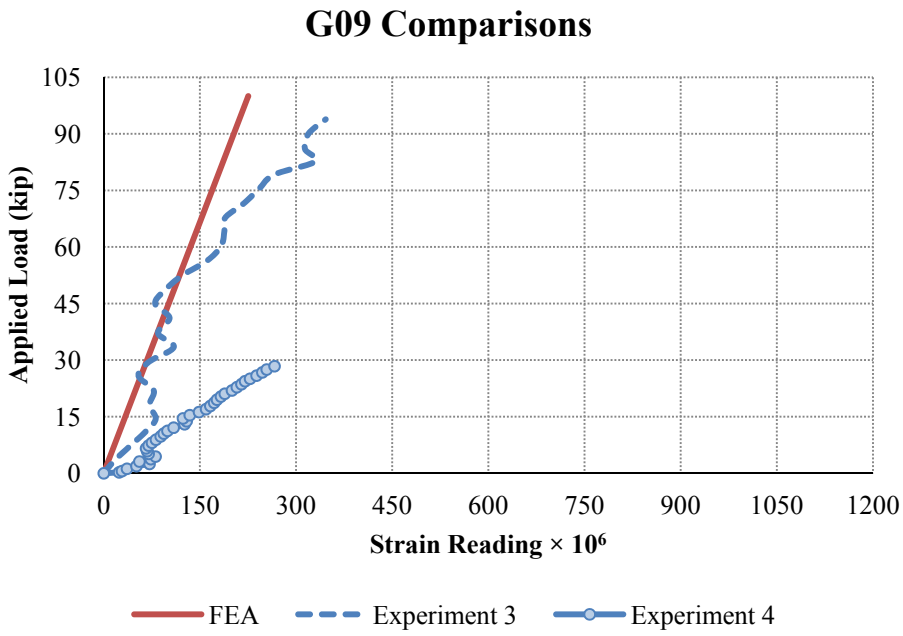
G09 Comparisons
Applied Load (kip)
105
90
75
60
45
30
15
0
0
150
300
450
600
750
900
1050
1200
Strain Reading × 10⁶
FEA
Experiment 3
Experiment 4

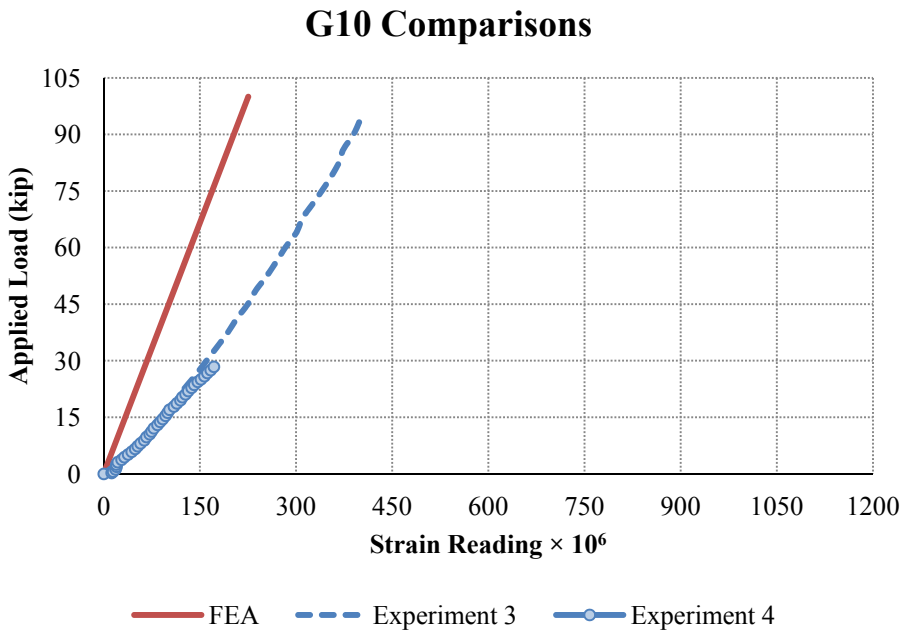
G10 Comparisons
Applied Load (kip)
105
90
75
60
45
30
15
0
0
150
300
450
600
750
900
1050
1200
Strain Reading × 10⁶
FEA
Experiment 3
Experiment 4

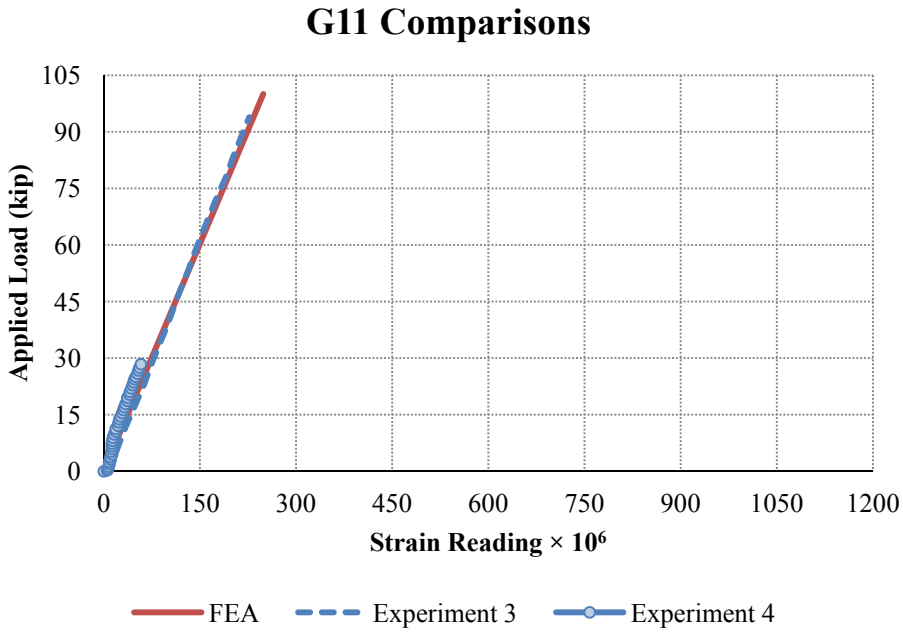
G11 Comparisons
Applied Load (kip)
105
90
75
60
45
30
15
0
0
150
300
450
600
750
900
1050
1200
Strain Reading × 10⁶
FEA
Experiment 3
Experiment 4

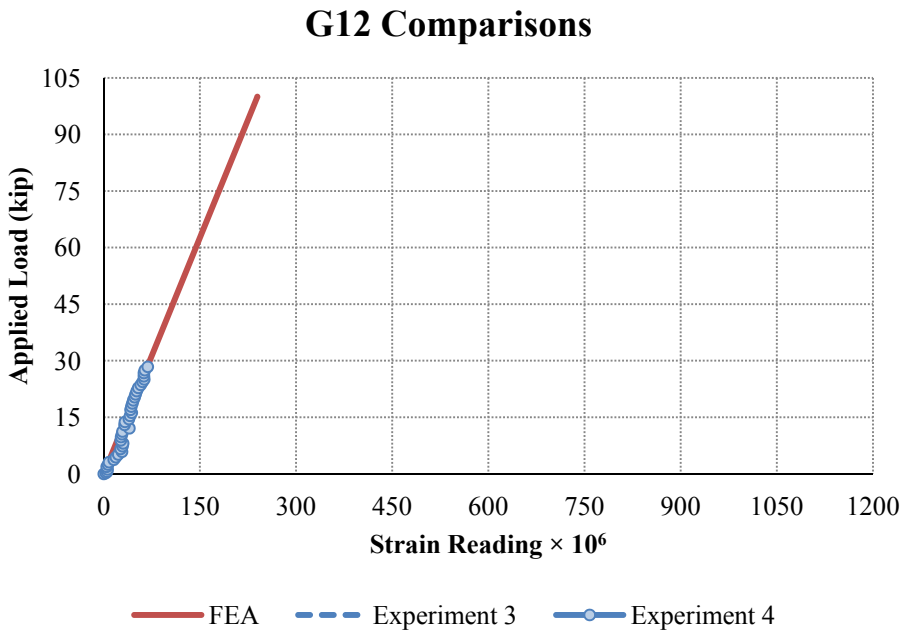
G12 Comparisons
Applied Load (kip)
105
90
75
60
45
30
15
0
0
150
300
450
600
750
900
1050
1200
Strain Reading × 10⁶
FEA
Experiment 3
Experiment 4

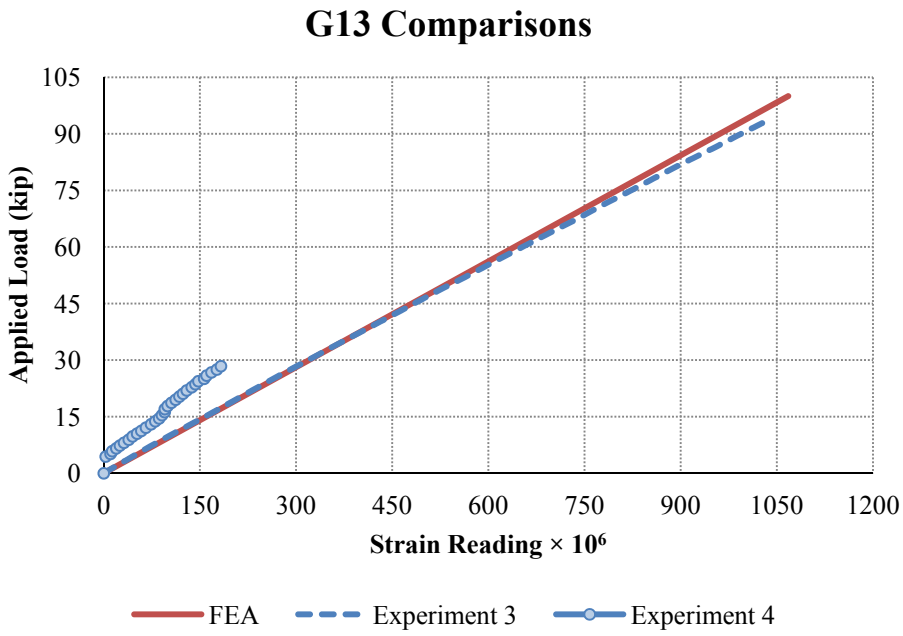
G13 Comparisons
Applied Load (kip)
105
90
75
60
45
30
15
0
0
150
300
450
600
750
900
1050
1200
Strain Reading × 10⁶
FEA
Experiment 3
Experiment 4

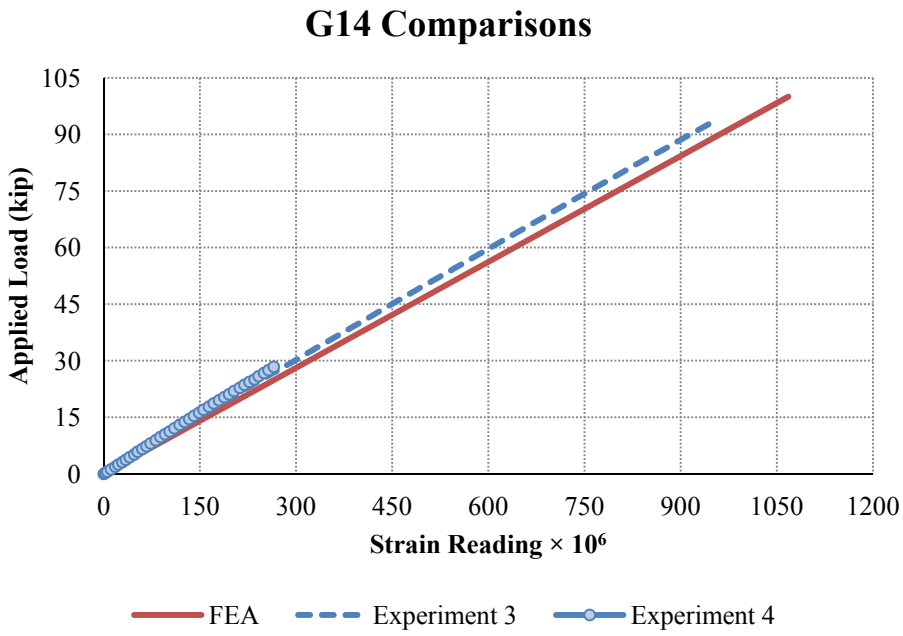
G14 Comparisons
Applied Load (kip)
105
90
75
60
45
30
15
0
0
150
300
450
600
750
900
1050
1200
Strain Reading × 10⁶
FEA
Experiment 3
Experiment 4

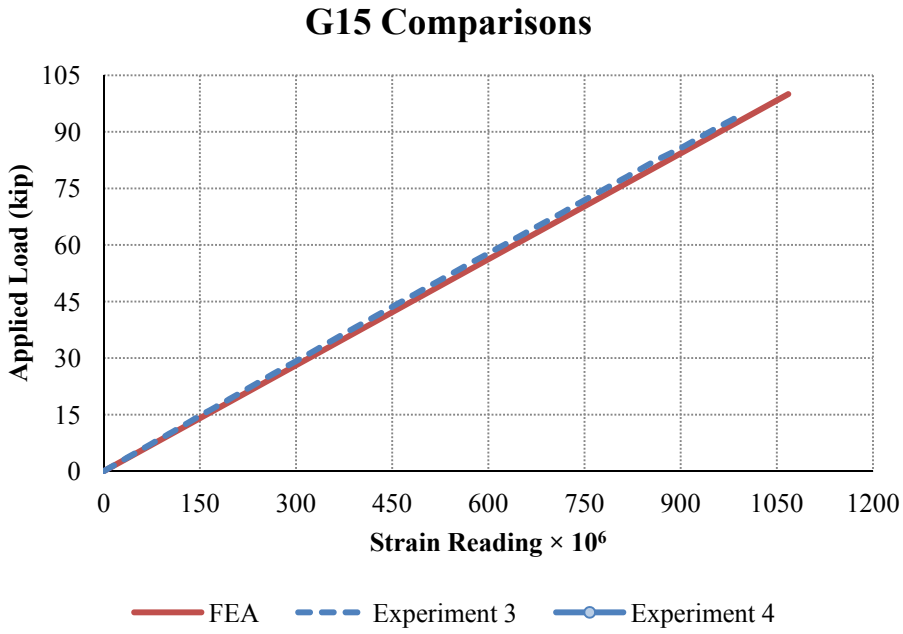
G15 Comparisons
Applied Load (kip)
105
90
75
60
45
30
15
0
0
150
300
450
600
750
900
1050
1200
Strain Reading × 10⁶
FEA
Experiment 3
Experiment 4

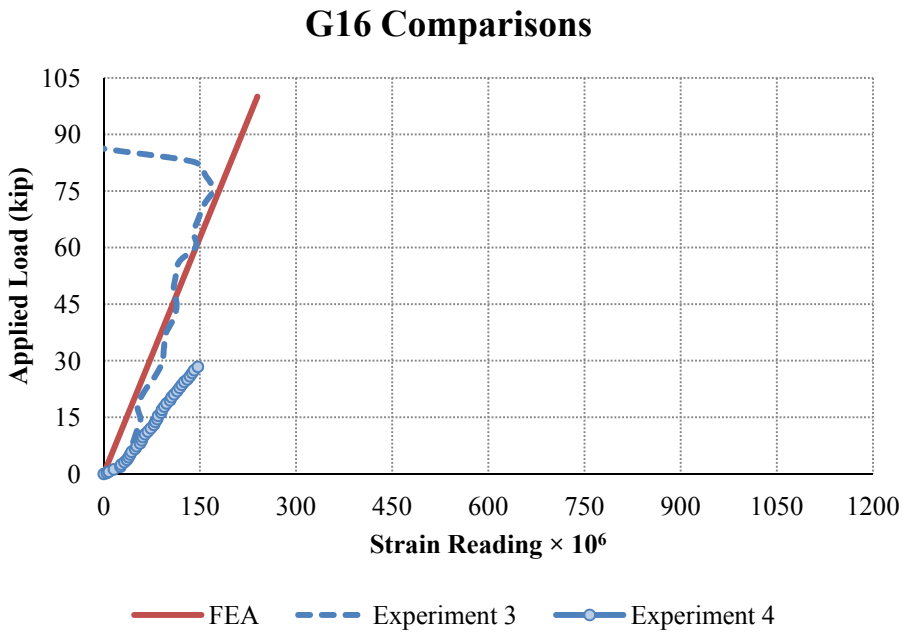
G16 Comparisons
Applied Load (kip)
105
90
75
60
45
30
15
0
0
150
300
450
600
750
900
1050
1200
Strain Reading × 10⁶
FEA
Experiment 3
Experiment 4

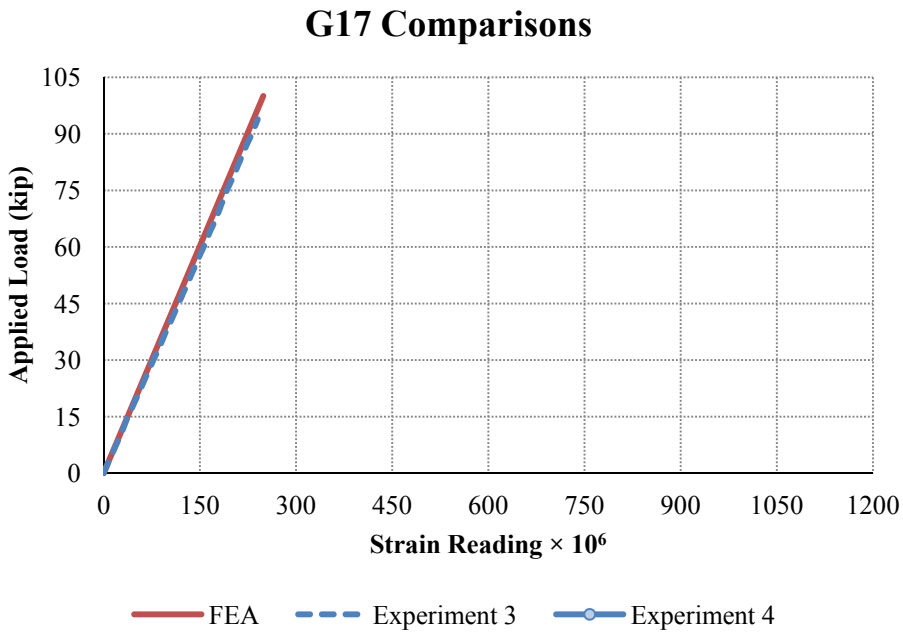
G17 Comparisons
Applied Load (kip)
105
90
75
60
45
30
15
0
0
150
300
450
600
750
900
1050
1200
Strain Reading × 10⁶
FEA
Experiment 3
Experiment 4

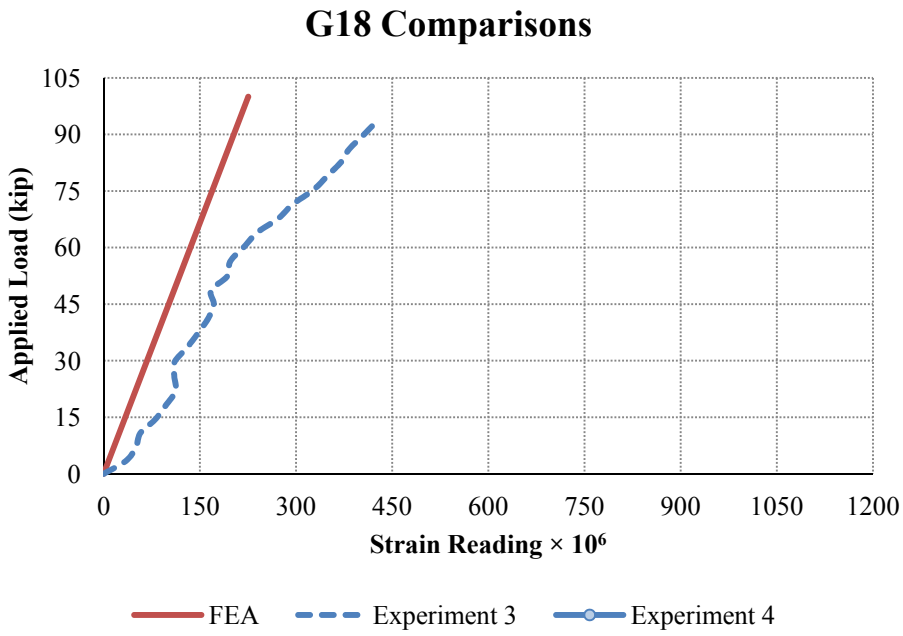
G18 Comparisons
Applied Load (kip)
105
90
75
60
45
30
15
0
0
150
300
450
600
750
900
1050
1200
Strain Reading × 10⁶
FEA
Experiment 3
Experiment 4

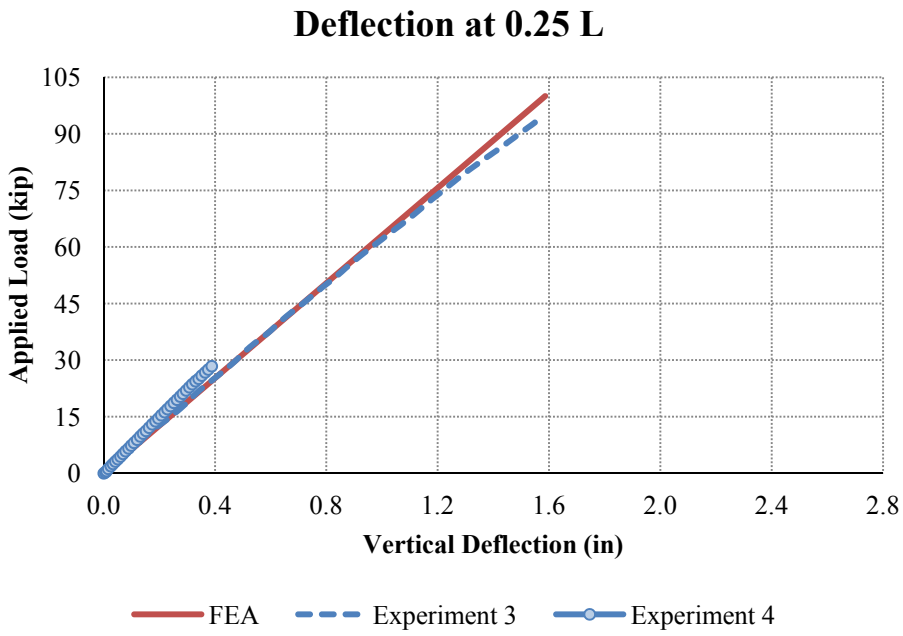
Deflection at 0.25 L
Applied Load (kip)
105
90
75
60
45
30
15
0
0.0
0.4
0.8
1.2
1.6
2.0
2.4
2.8
Vertical Deflection (in)
FEA
Experiment 3
Experiment 4

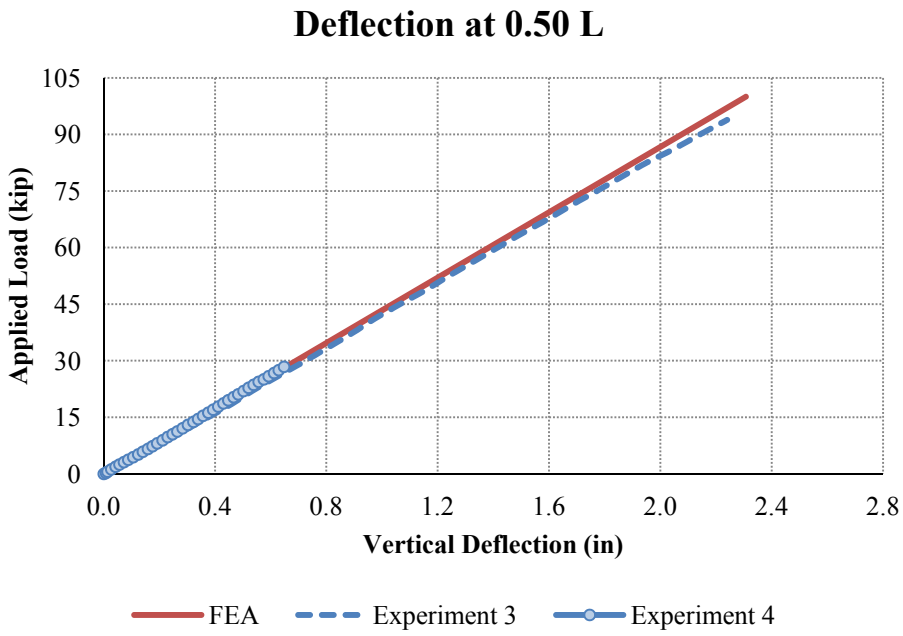
Deflection at 0.50 L
Applied Load (kip)
105
90
75
60
45
30
15
0
0.0
0.4
0.8
1.2
1.6
2.0
2.4
2.8
Vertical Deflection (in)
FEA
Experiment 3
Experiment 4

C.3 Analytical Data (Chapter 6)

The following section documents results from the analytical and behavioral studies discussed in Chapter 6. Plots are titled according to the suite of 18 girders discussed in Chapters 3 and 6.

C.3.1 Comparisons of Finite Element and Strain Compatibility Results

The following plots document the results obtained from the finite element analysis of the parametric matrix of girders studied in Chapter 6. In addition, for each plot, three points of interest, in the following order, are identified: the yield moment, the moment obtained from strain compatibility, and the plastic moment. It should be noted that, due to the nonlinear finite element method employed, the load at which the theoretical yield moment occurs does not necessarily coincide with the corresponding yield-moment deflection.

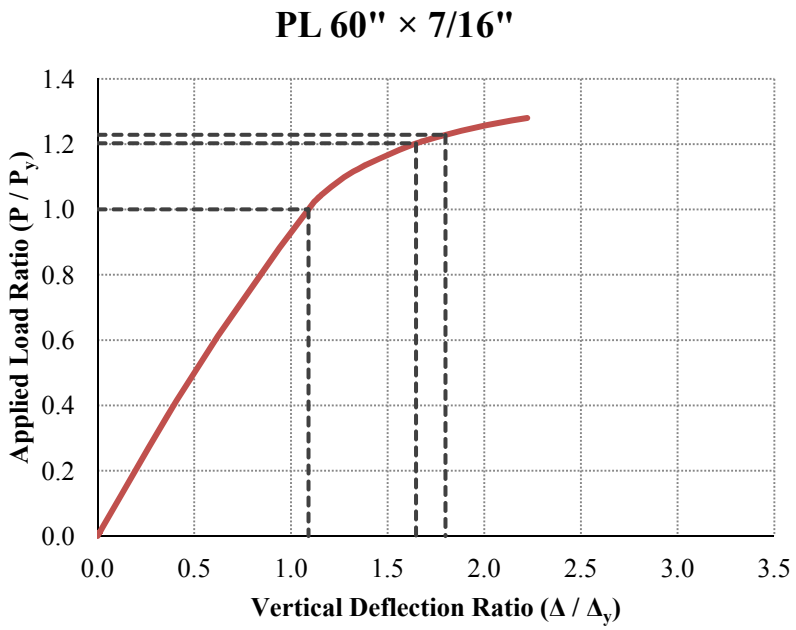

PL 60" × 1/2"

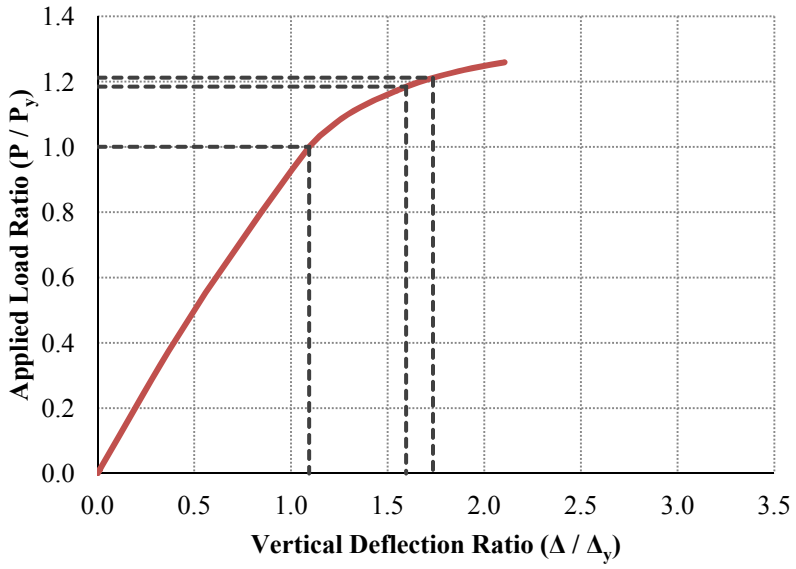

PL 60" × 5/8"

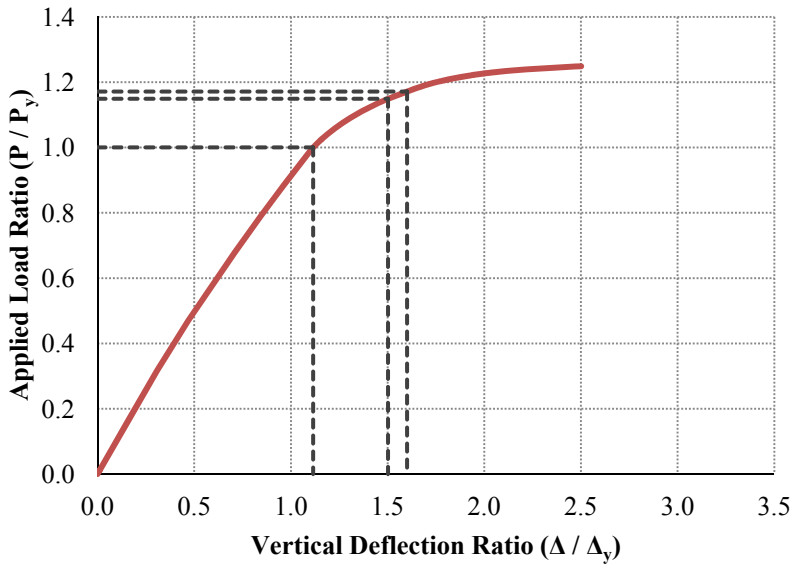

PL 72" × 7/16"

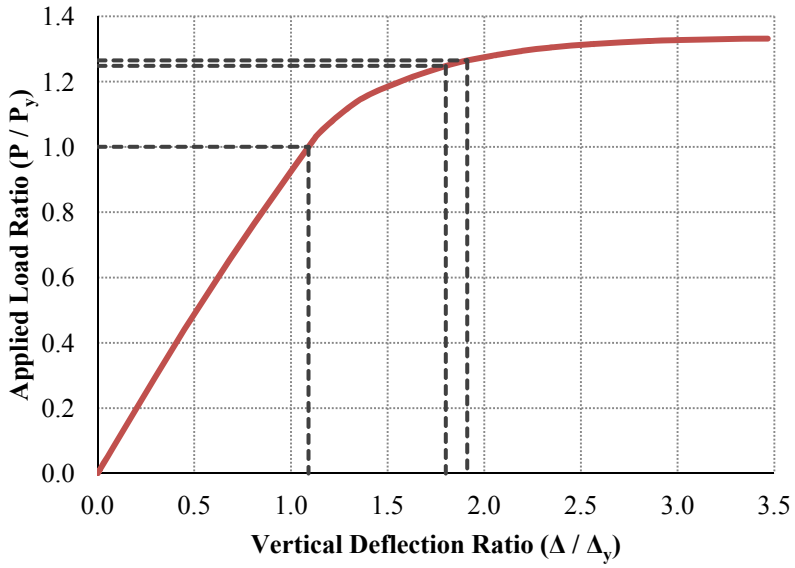

PL 72" × 1/2"

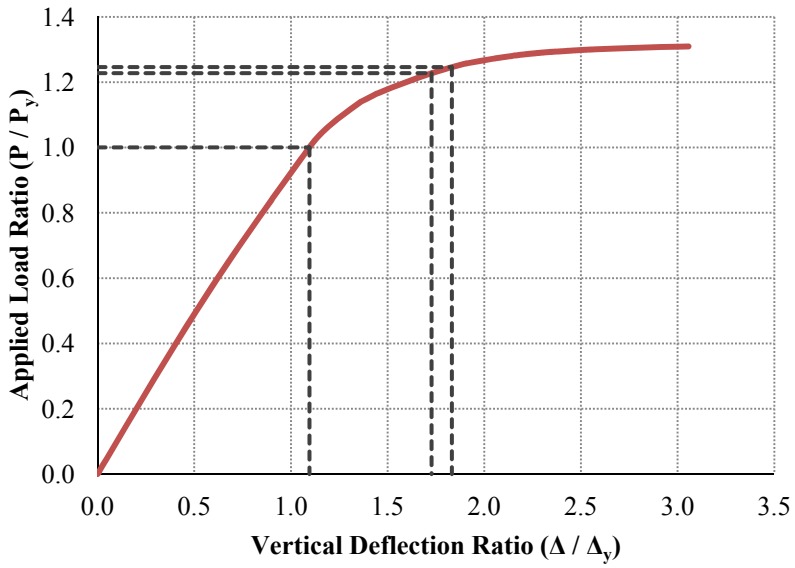

PL 72" × 5/8"

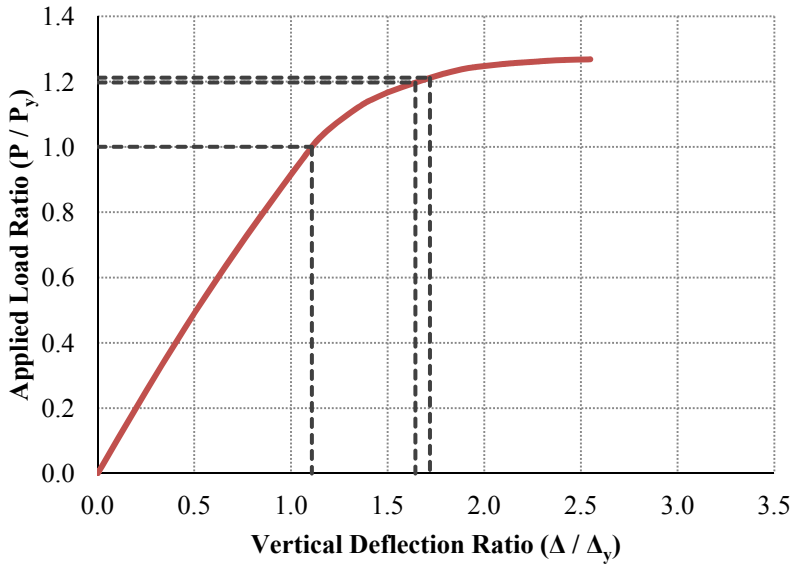

PL 84" × 7/16"

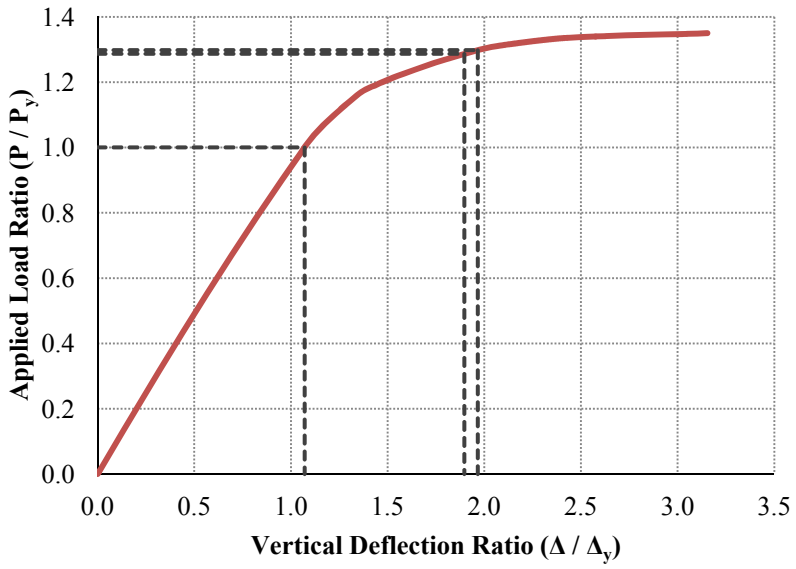

PL 84" × 1/2"

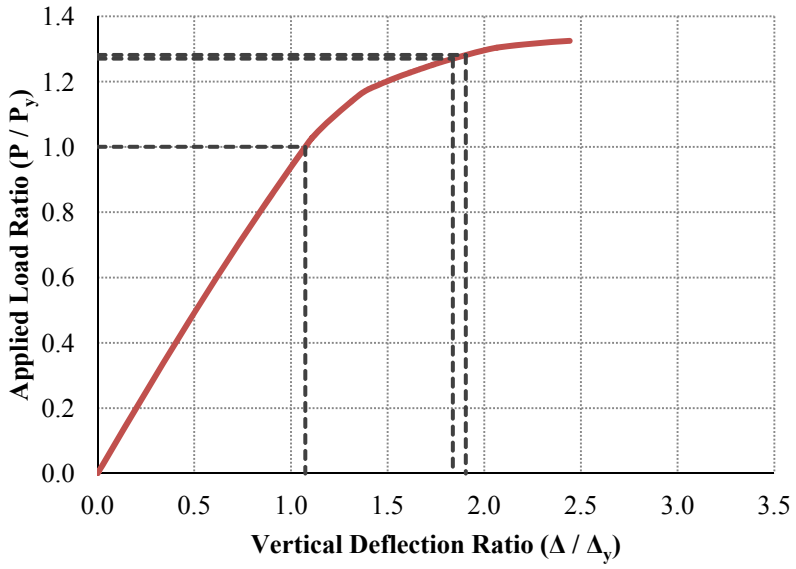

PL 84" × 5/8"

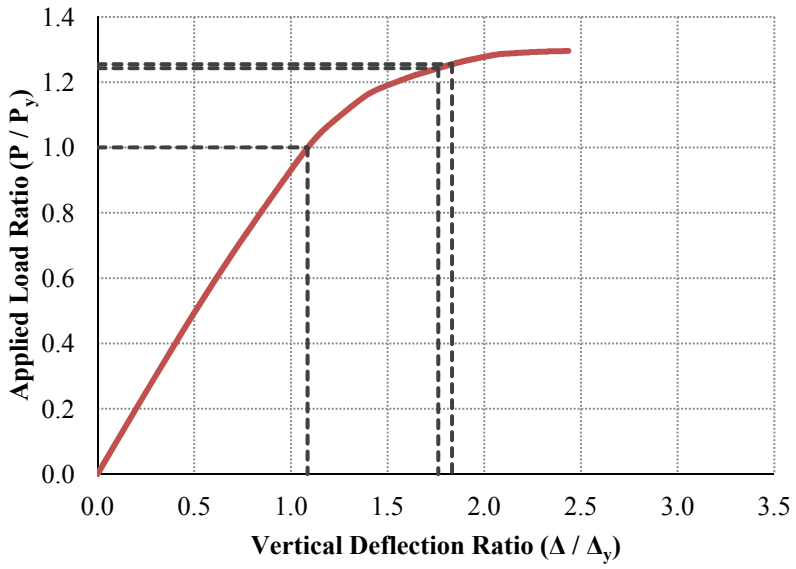

PL 96" × 7/16"

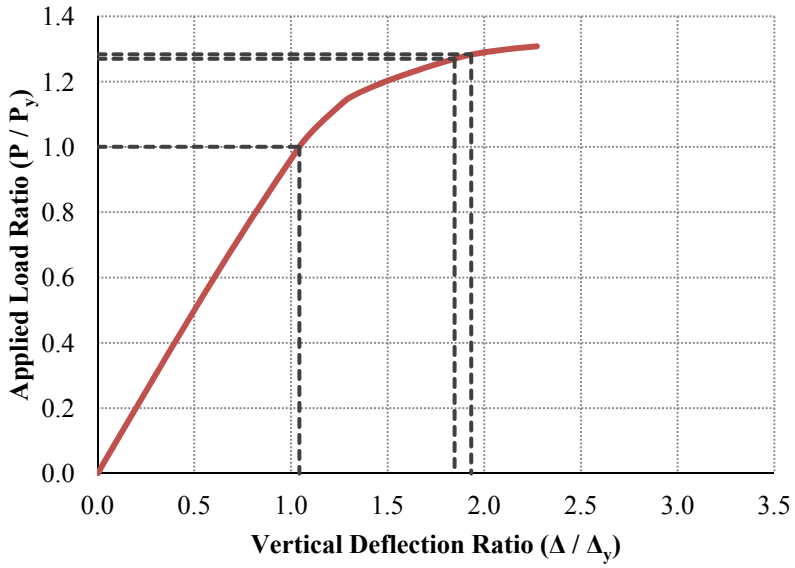

PL 96" × 1/2"

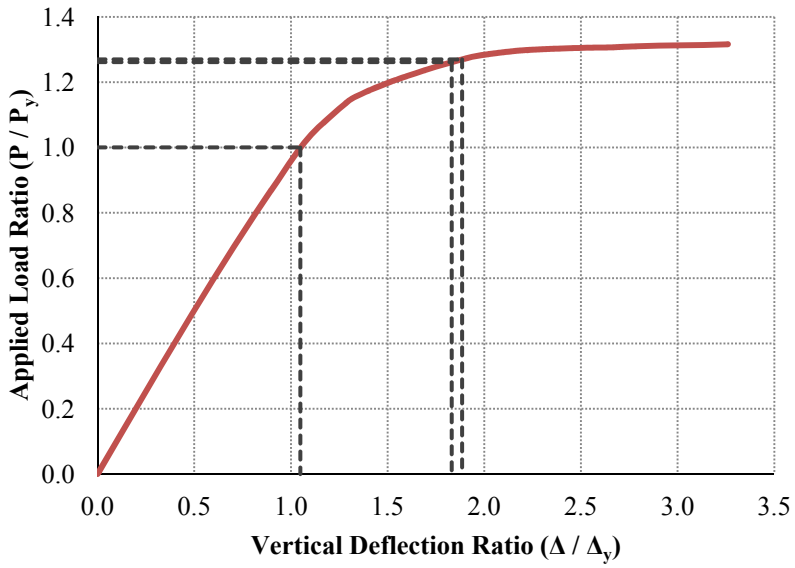

PL 96" × 5/8"

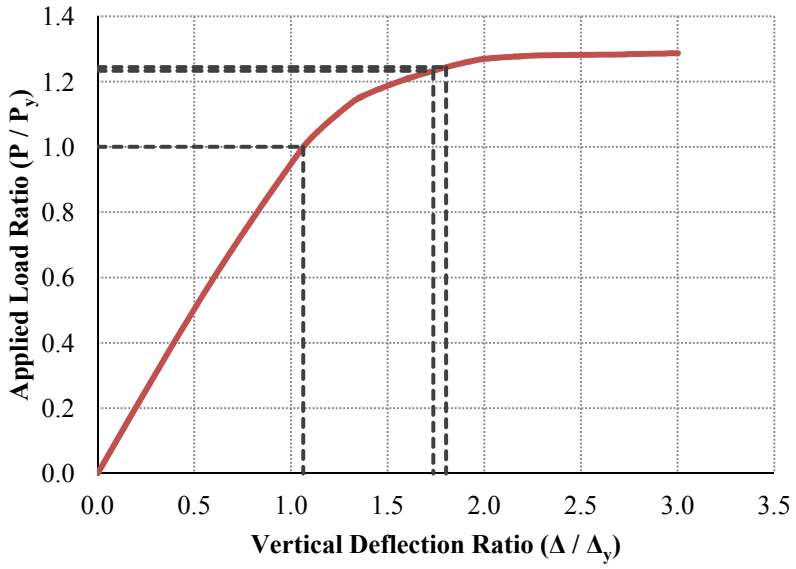

PL 108" × 7/16"

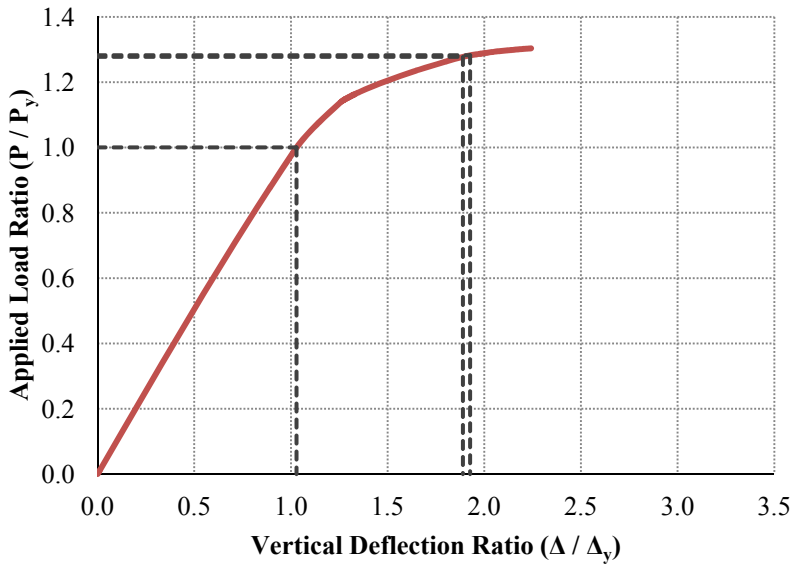

PL 108" × 1/2"

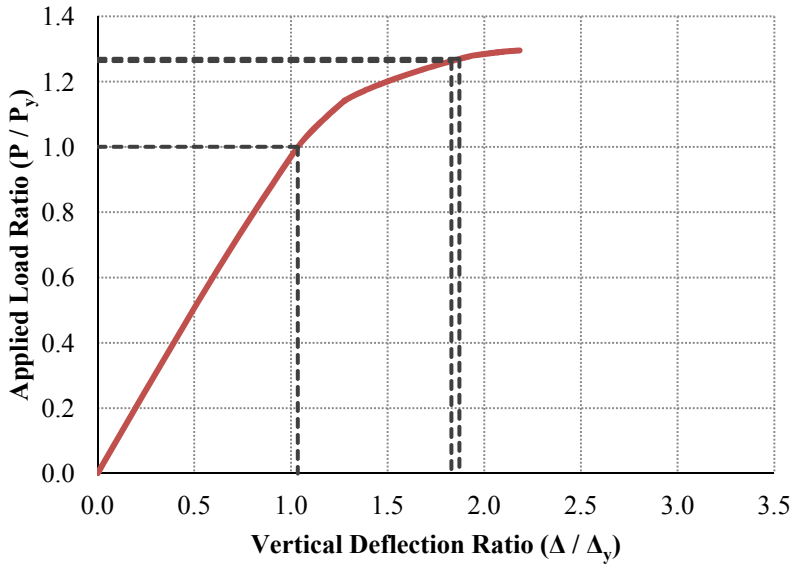

PL 108" × 5/8"

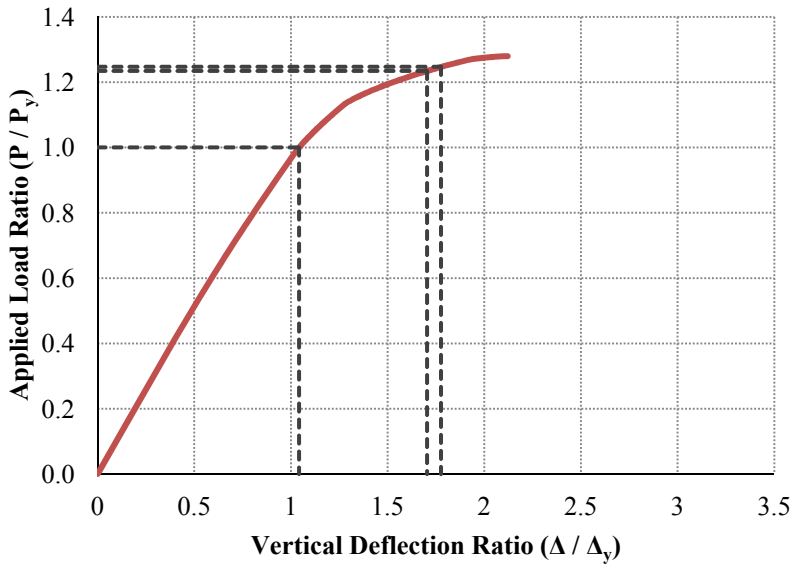

PL 120" × 7/16"

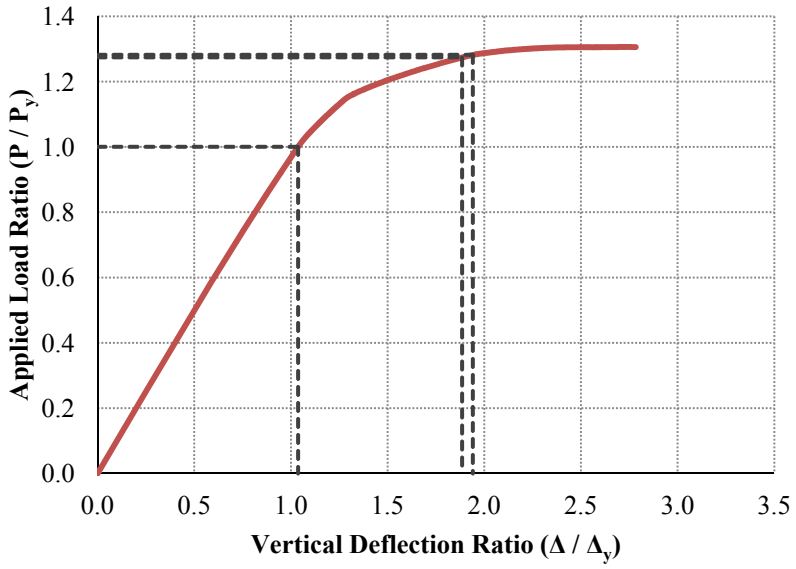

PL 120" × 1/2"

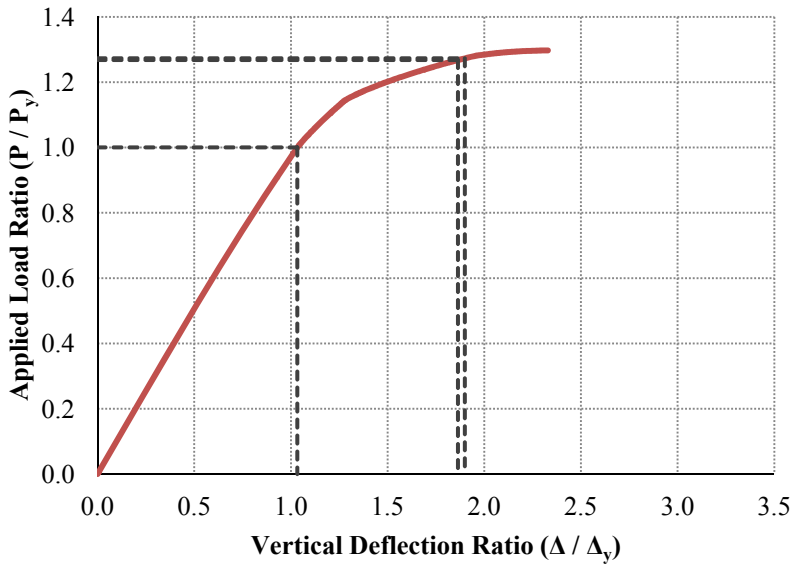

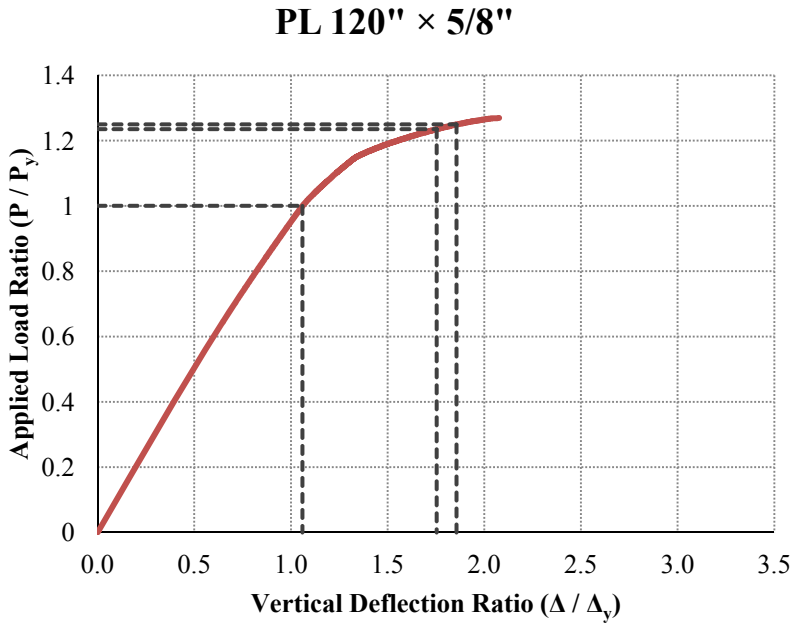

C.3.2 Constrained Finite Strip Analyses using CUFSM

The following plots document the results obtained from finite strip analysis (using CUFSM) of the parametric matrix of girders studied in Chapter 6. Each analysis was performed assuming a bending stress profile to attain a yield stress of 50 ksi. For each plot, the local minimum is identified. In addition, for each plot, a qualitative plot of the mode shape of the cross-section at the indicated minimum is shown.

PL 60" × 7/16"

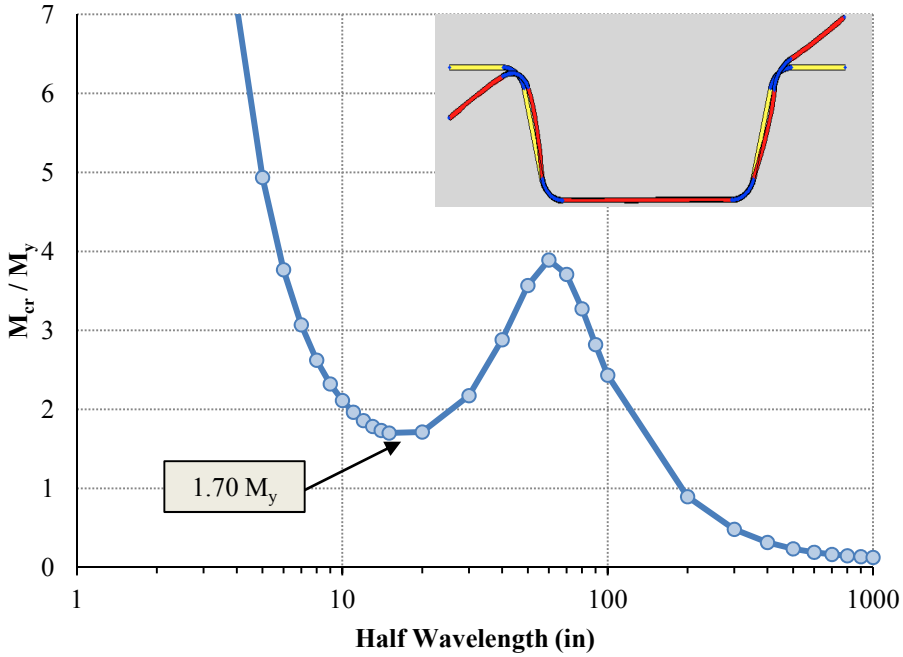

PL 60" × 1/2"

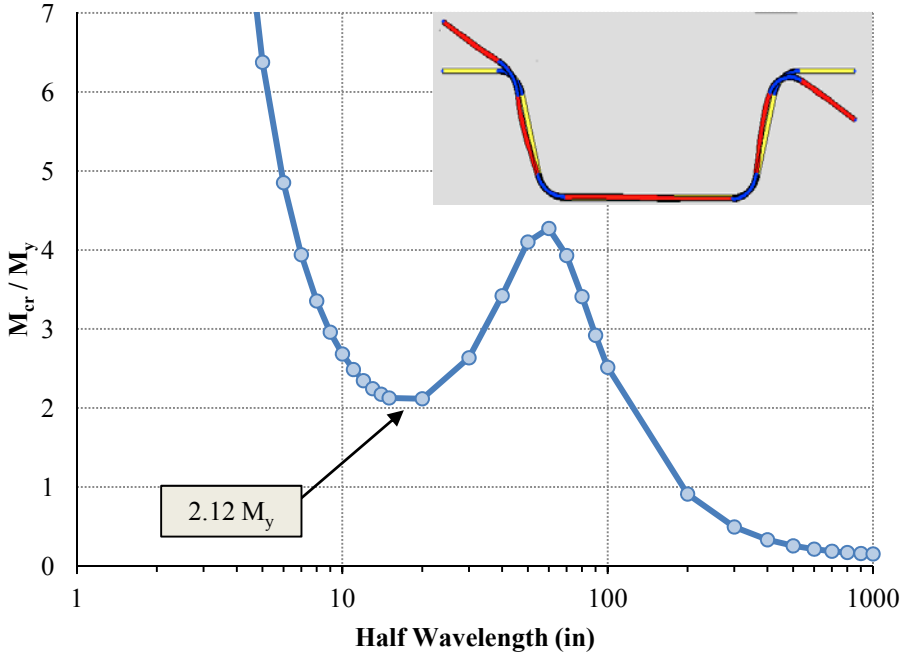

PL 60" × 5/8"

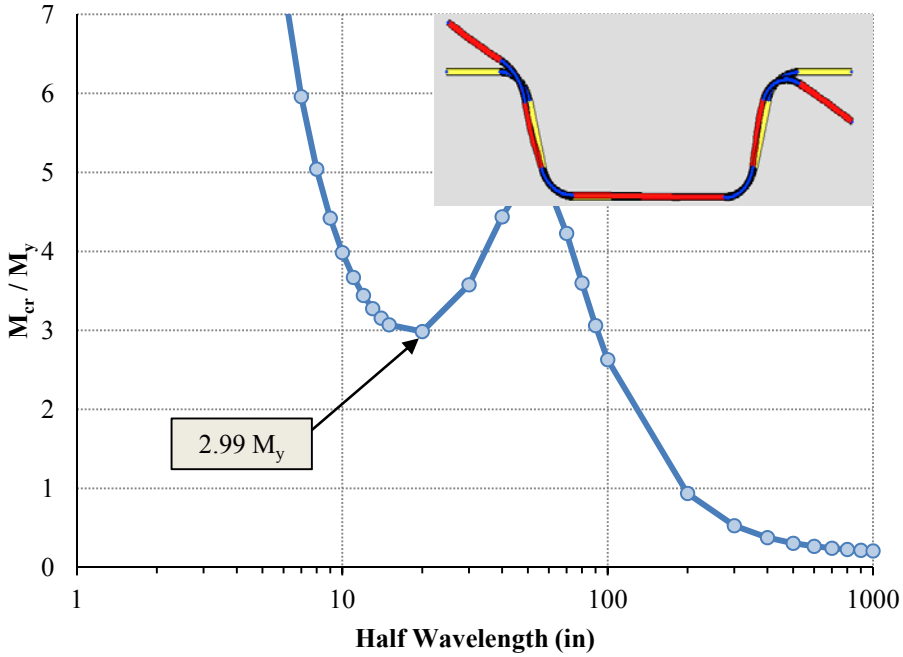

PL 72" × 7/16"

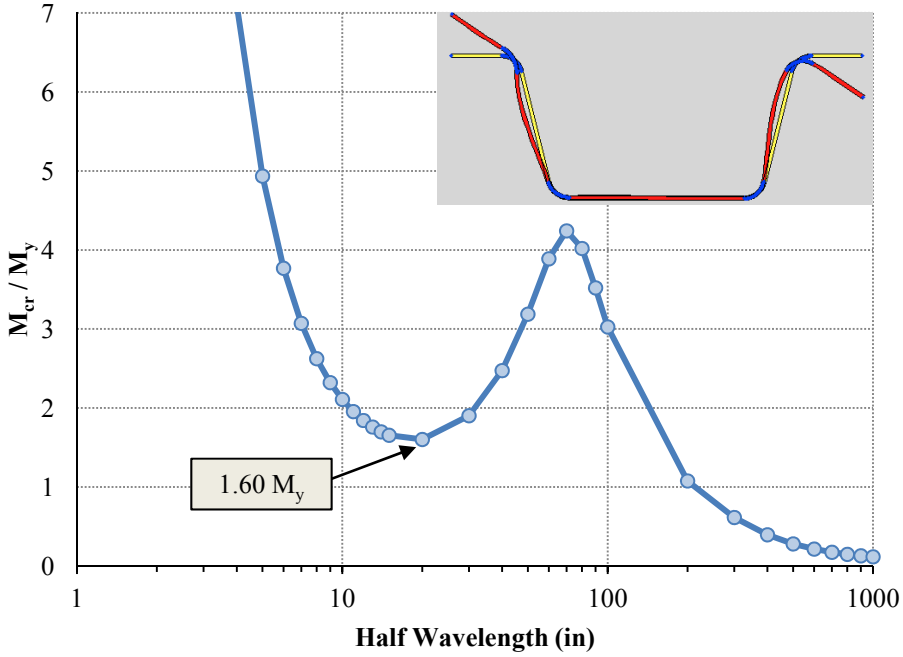

PL 72" × 1/2"

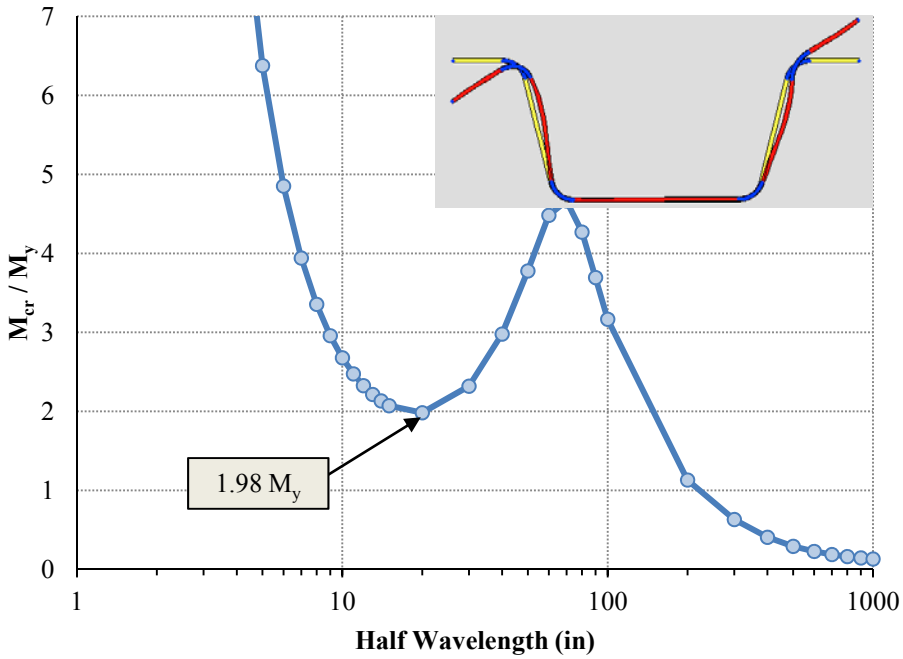

PL 72" × 5/8"

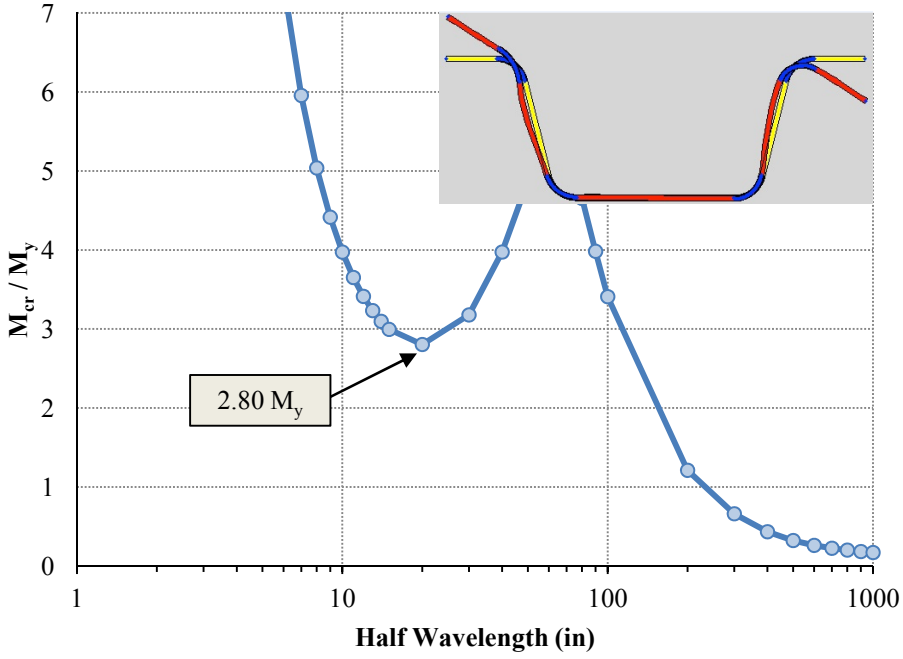

PL 84" × 7/16"

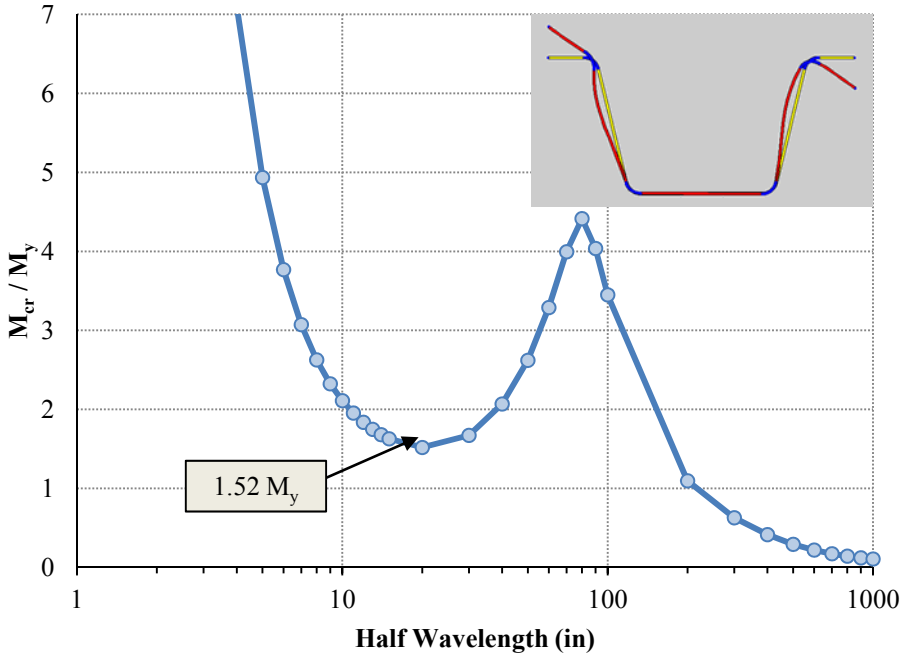

PL 84" × 1/2"

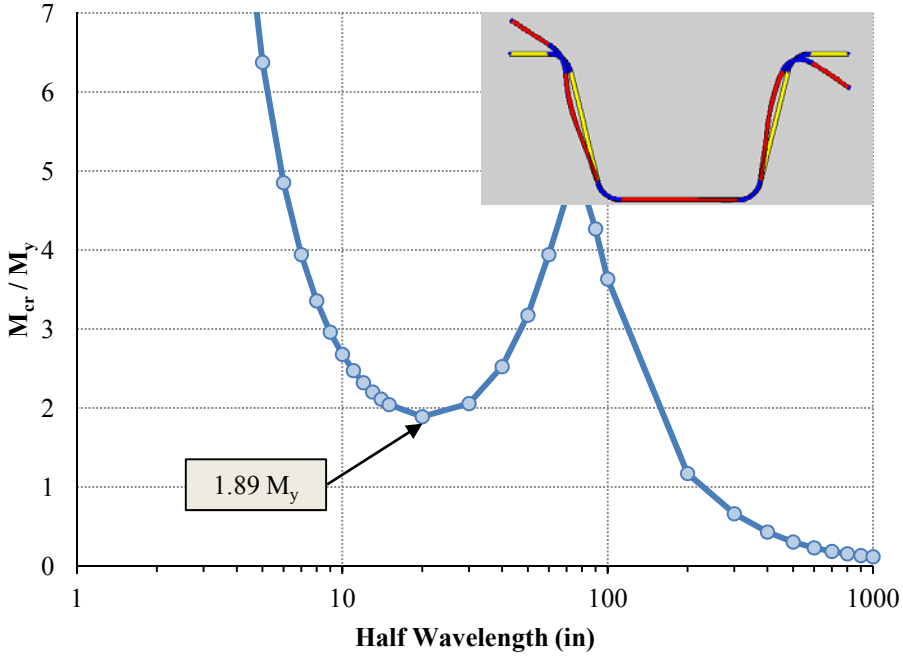

PL 84" × 5/8"

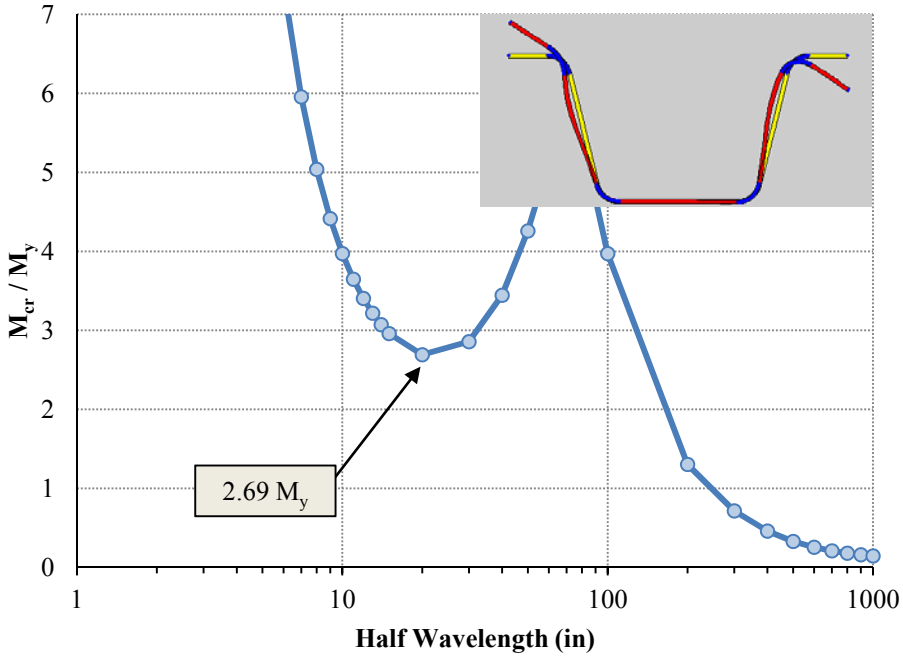

PL 96" × 7/16"

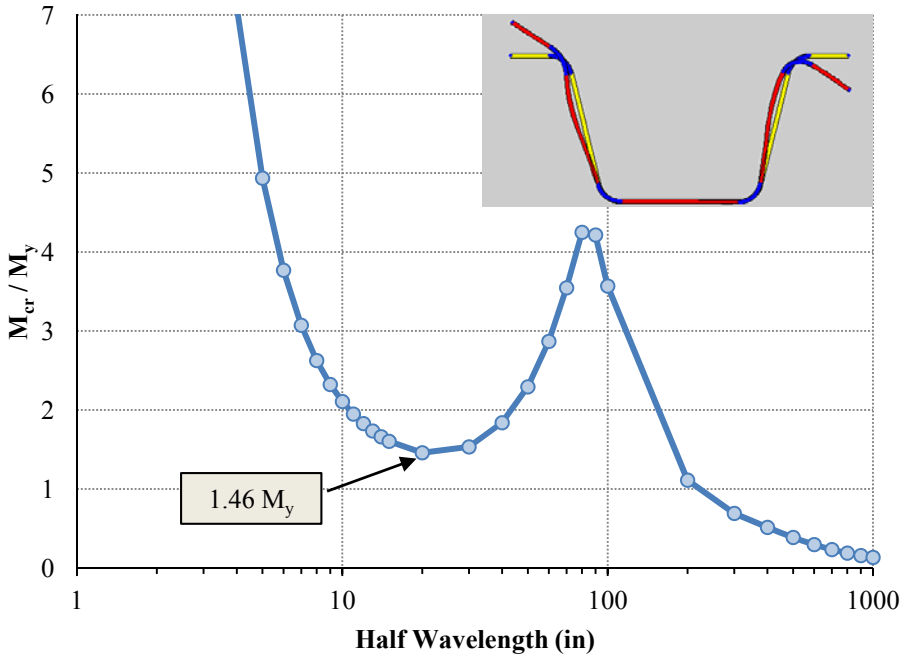

PL 96" × 1/2"

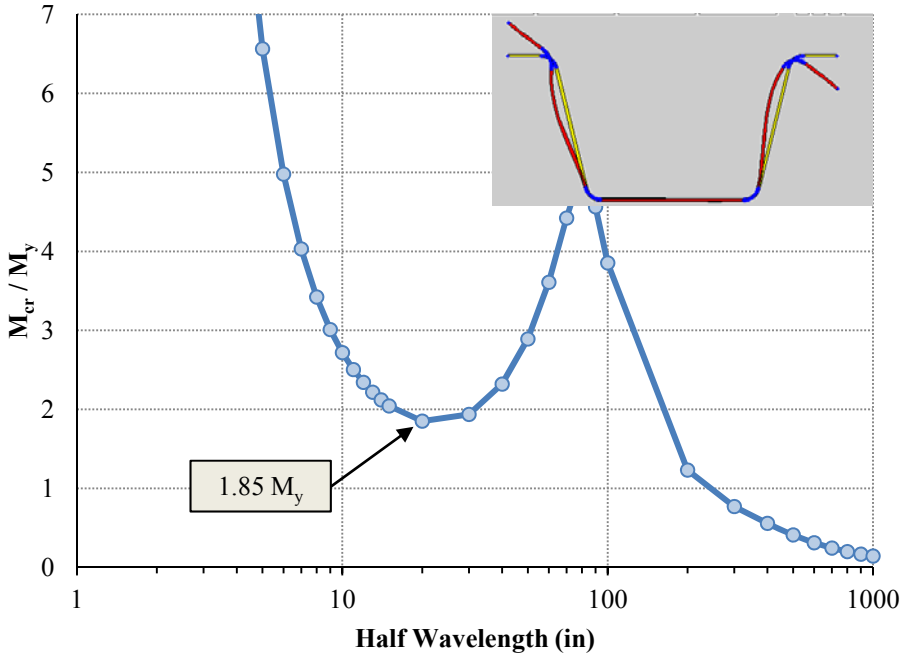

PL 96" × 5/8"

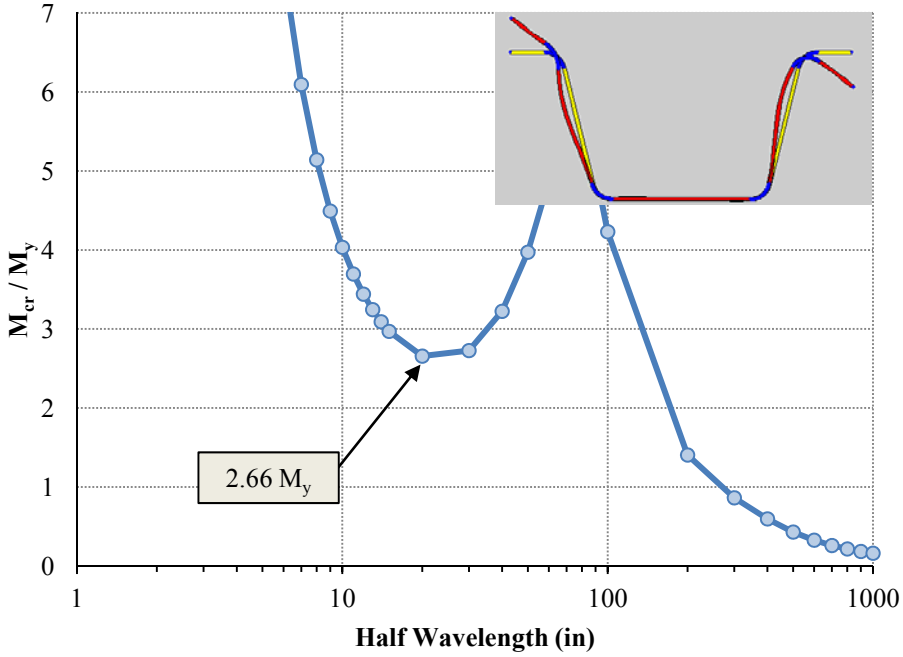

PL 108" × 7/16"

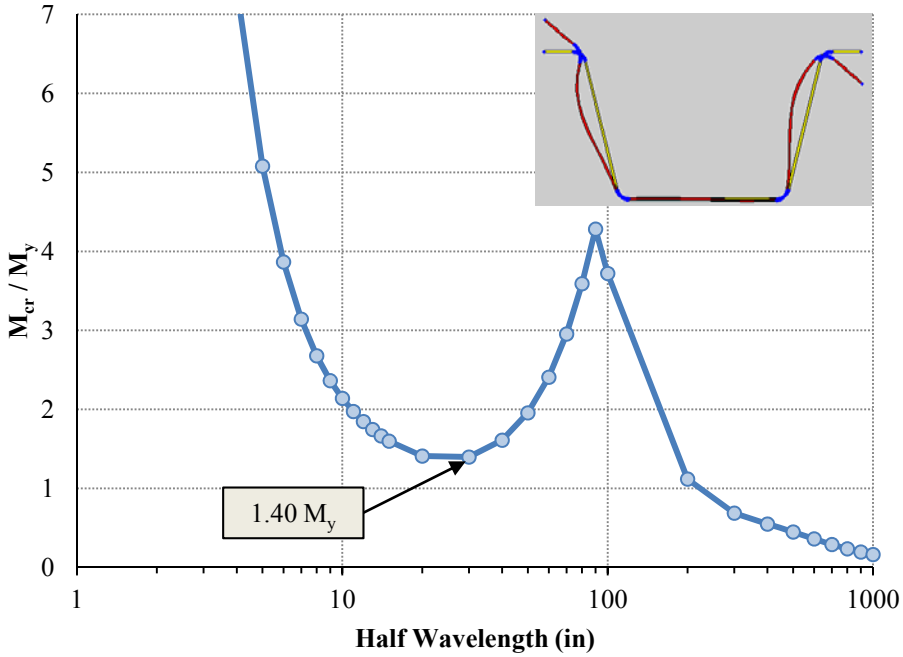

PL 108" × 1/2"

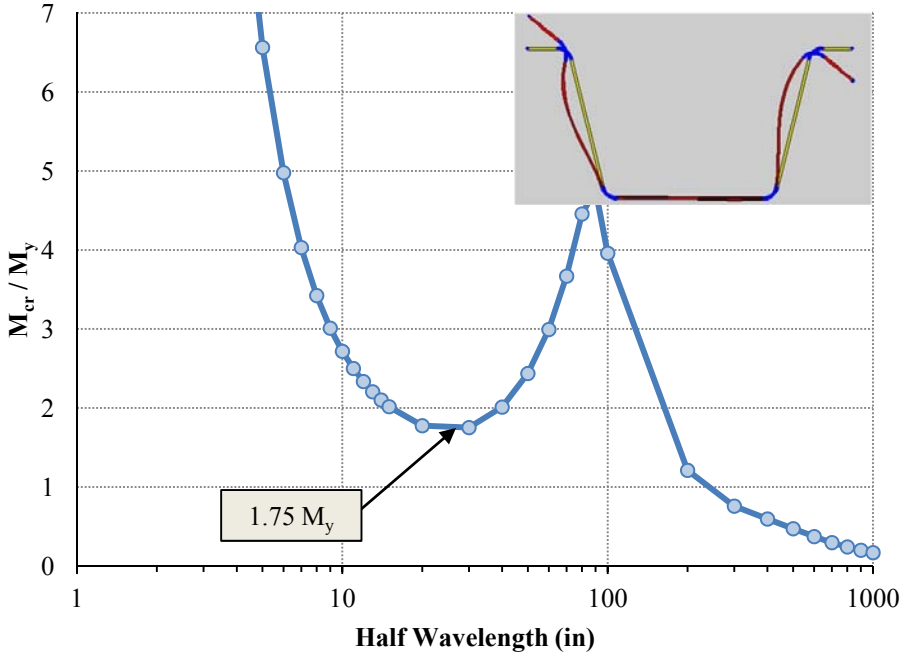

PL 108" × 5/8"

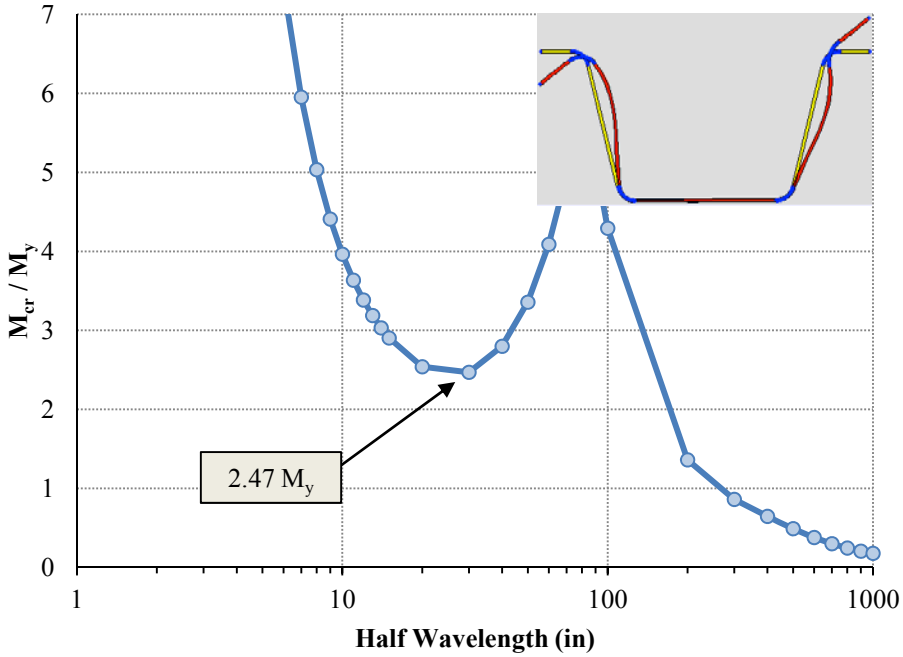

PL 120" × 7/16"

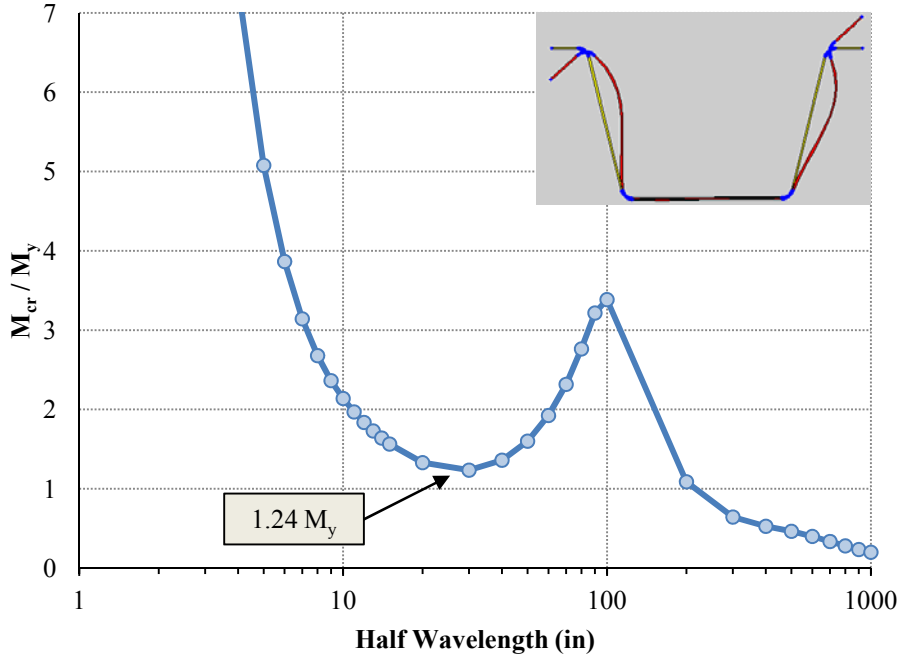

PL 120" × 1/2"

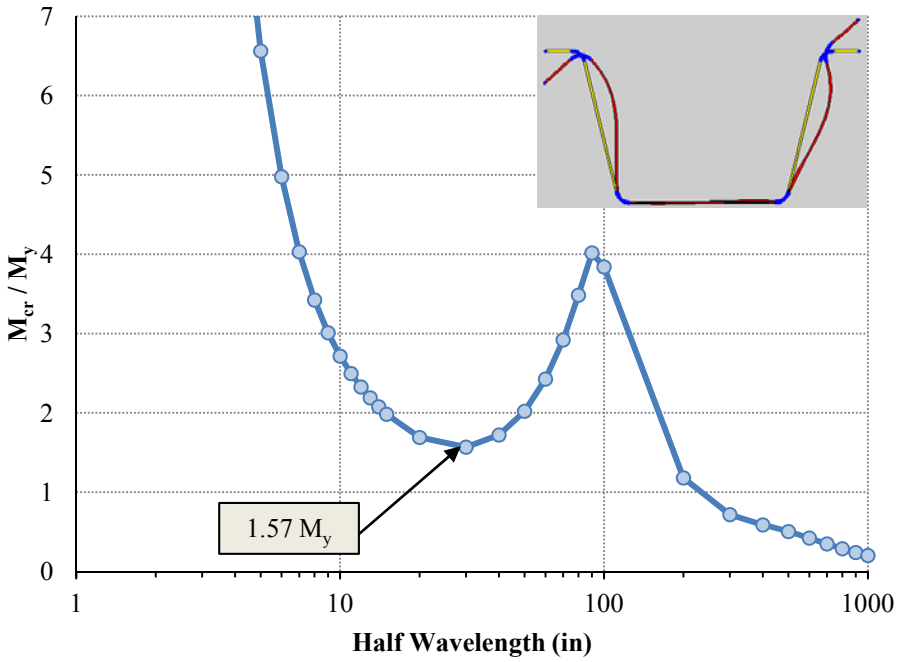

PL 120" × 5/8"

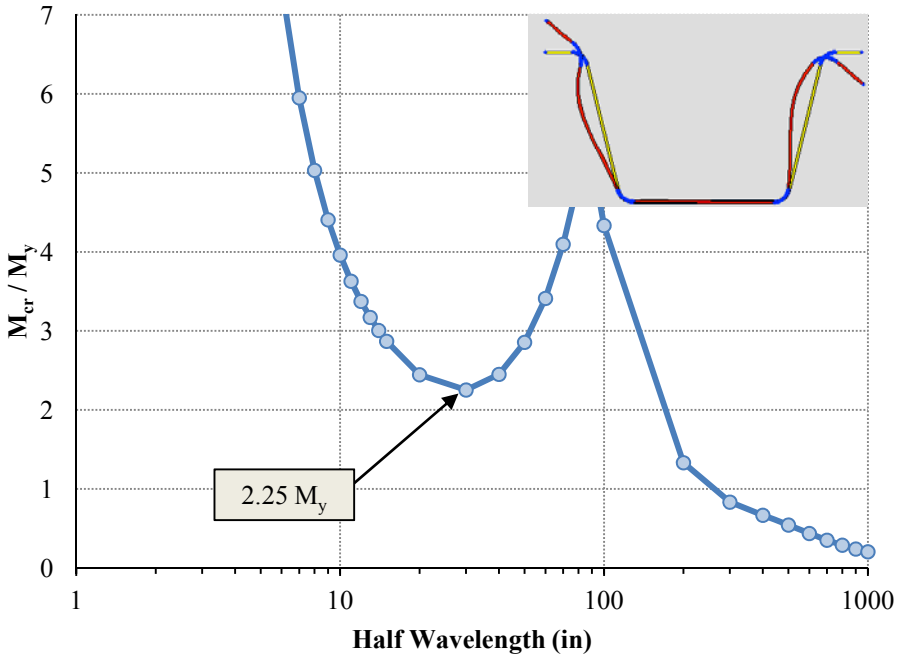

C.4 FEASIBILITY ASSESSMENTS (CHAPTER 7)

The following section documents results from the feasibility assessments and economic conparisons discussed in Chapter 7. Plots are titled according to the suite of 18 girders discussed in Chapters 3 and 6. Moments and shears from the Strength I and Service II limit states (AASHTO, 2010) along with live load deflections are plotted against design capacities and the live load deflection limit of L/800, respectively.

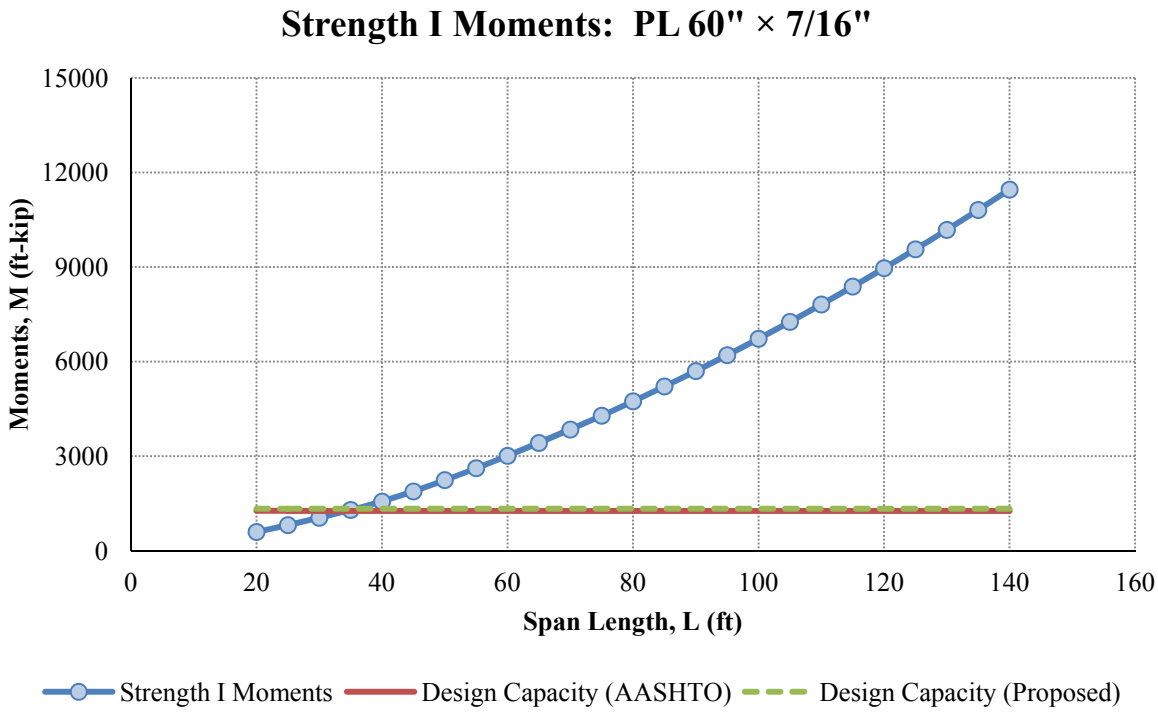

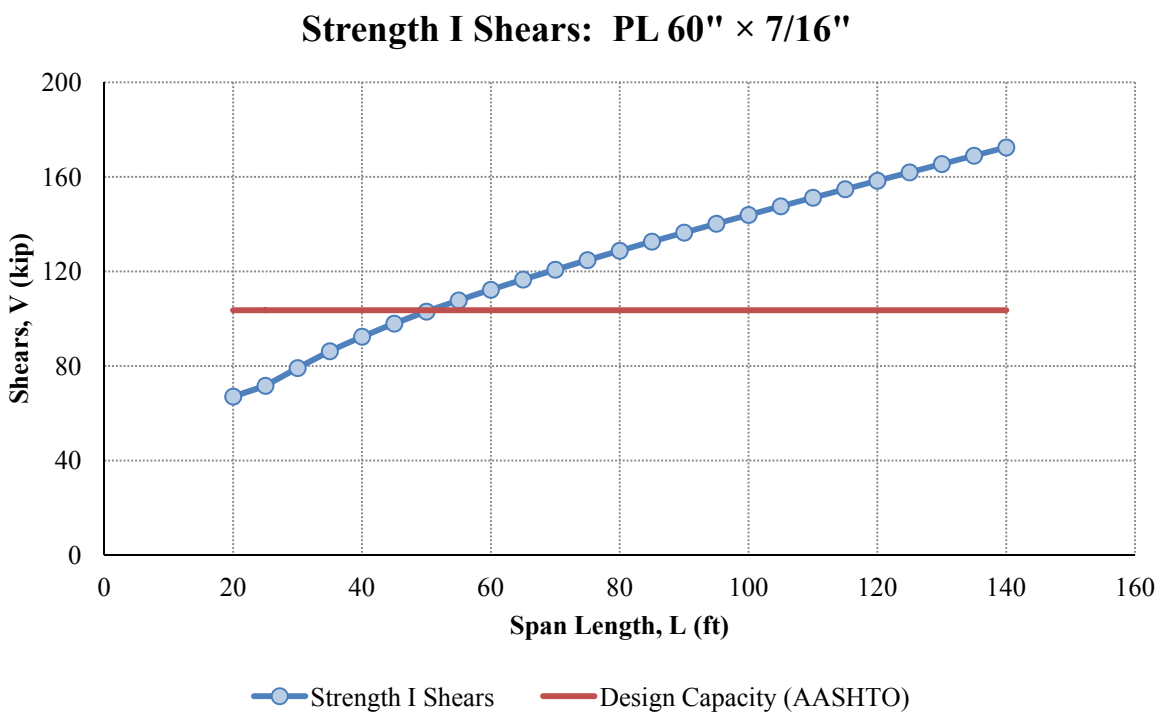
Strength I Shears: PL 60" × 7/16"
Shears, V (kip)
200
160
120
80
40
0
0
20
40
60
80
100
120
140
160
Span Length, L (ft)
Strength I Shears
Design Capacity (AASHTO)

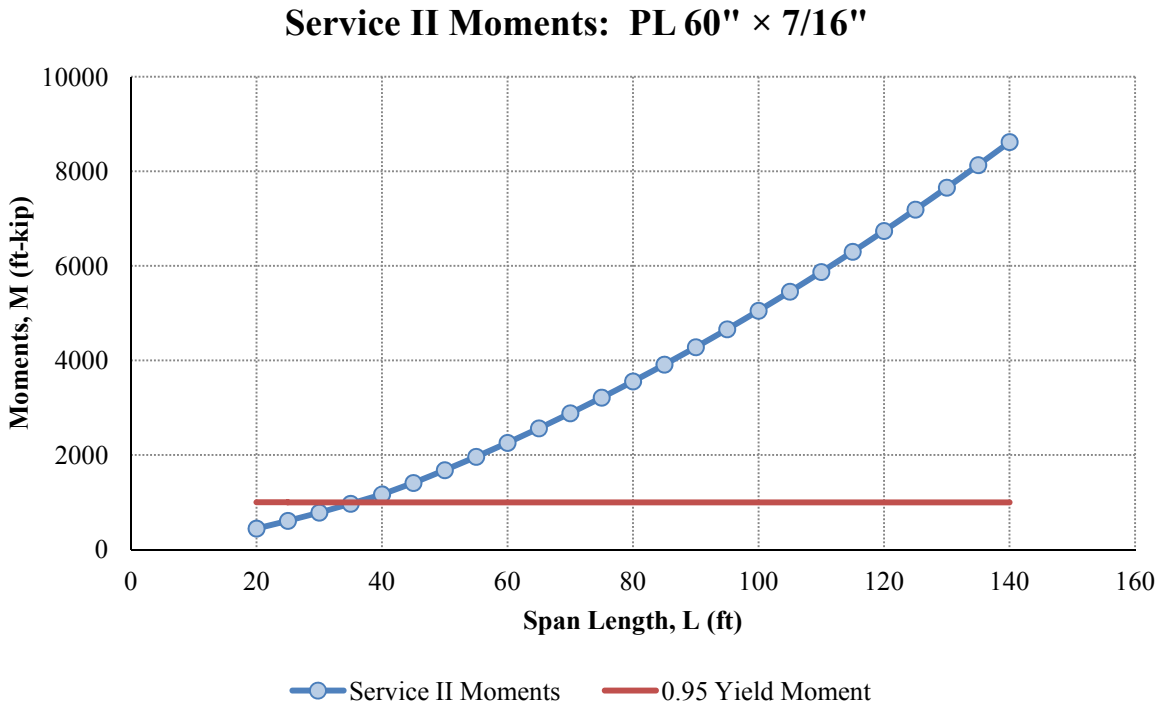
Service II Moments: PL 60" × 7/16"
Moments, M (ft-kip)
10000
8000
6000
4000
2000
0
0
20
40
60
80
100
120
140
160
Span Length, L (ft)
Service II Moments
0.95 Yield Moment

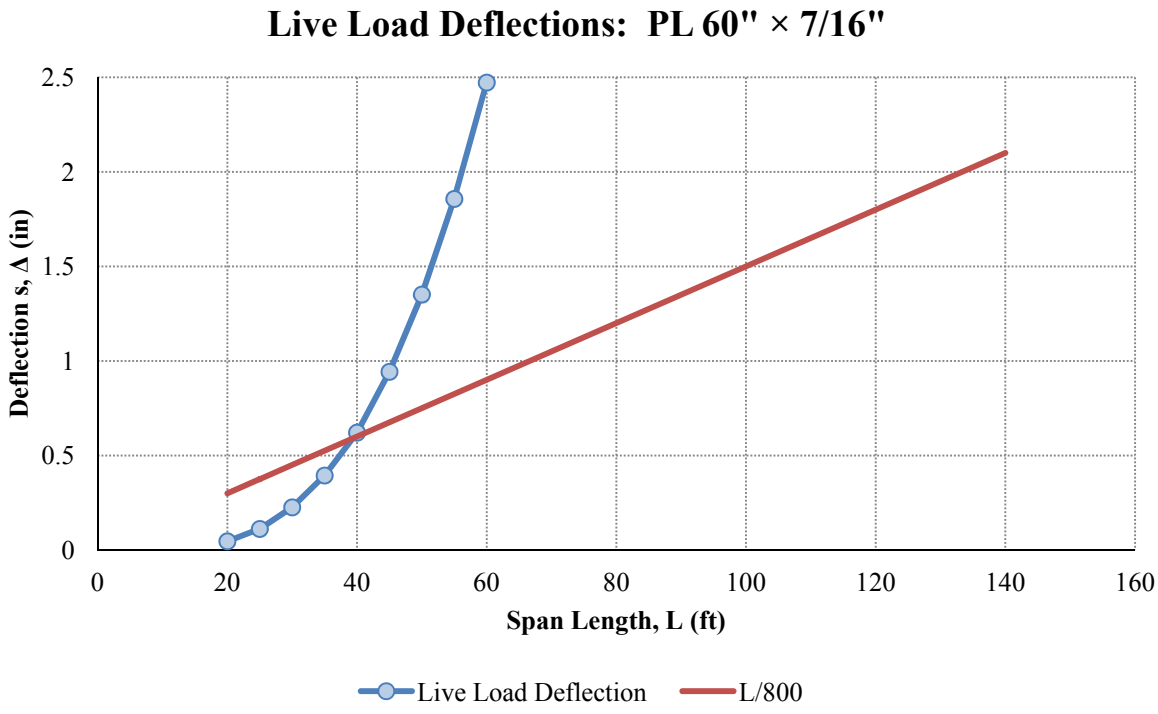
Live Load Deflections: PL 60" × 7/16"
Deflection s, Δ (in)
2.5
2
1.5
1
0.5
0
0
20
40
60
80
100
120
140
160
Span Length, L (ft)
Live Load Deflection
L/800

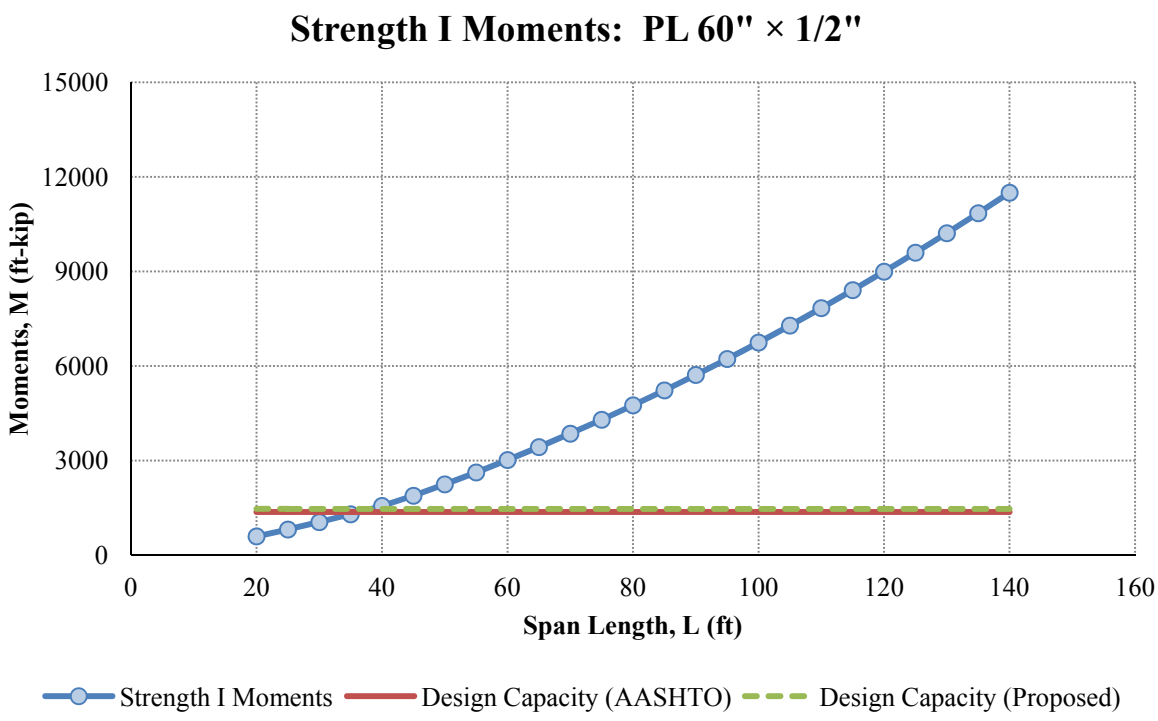
Strength I Moments: PL 60" × 1/2"
15000
12000
9000
6000
3000
0
Moments, M (ft-kip)
0
20
40
60
80
100
120
140
160
Span Length, L (ft)
Strength I Moments
Design Capacity (AASHTO)
Design Capacity (Proposed)

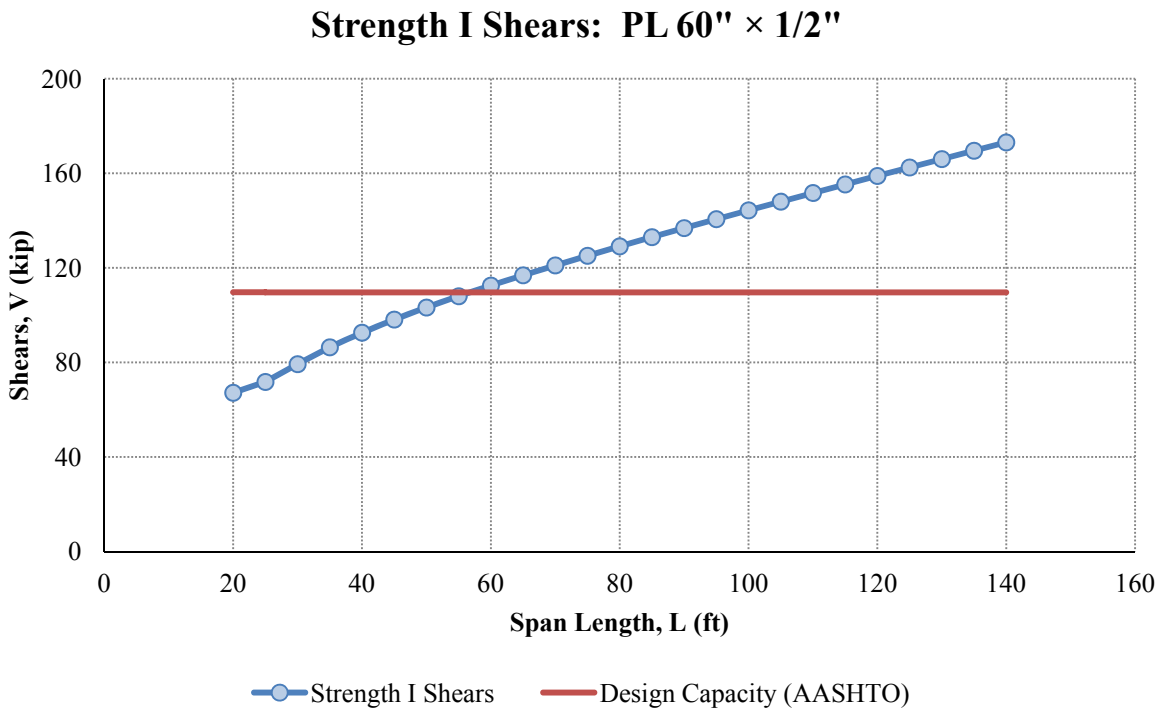
Strength I Shears: PL 60" × 1/2"
200
160
120
80
40
0
Shears, V (kip)
0
20
40
60
80
100
120
140
160
Span Length, L (ft)
Strength I Shears
Design Capacity (AASHTO)

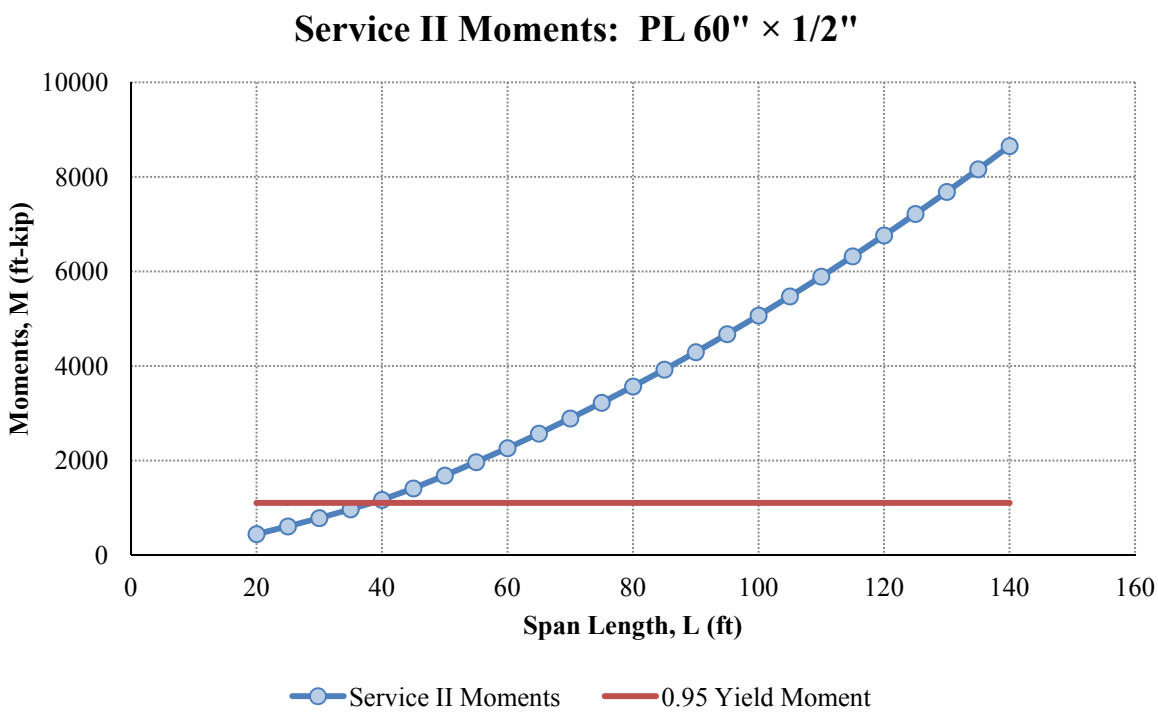
Service II Moments: PL 60" × 1/2"
Moments, M (ft-kip)
10000
8000
6000
4000
2000
0
0
20
40
60
80
100
120
140
160
Span Length, L (ft)
Service II Moments
0.95 Yield Moment

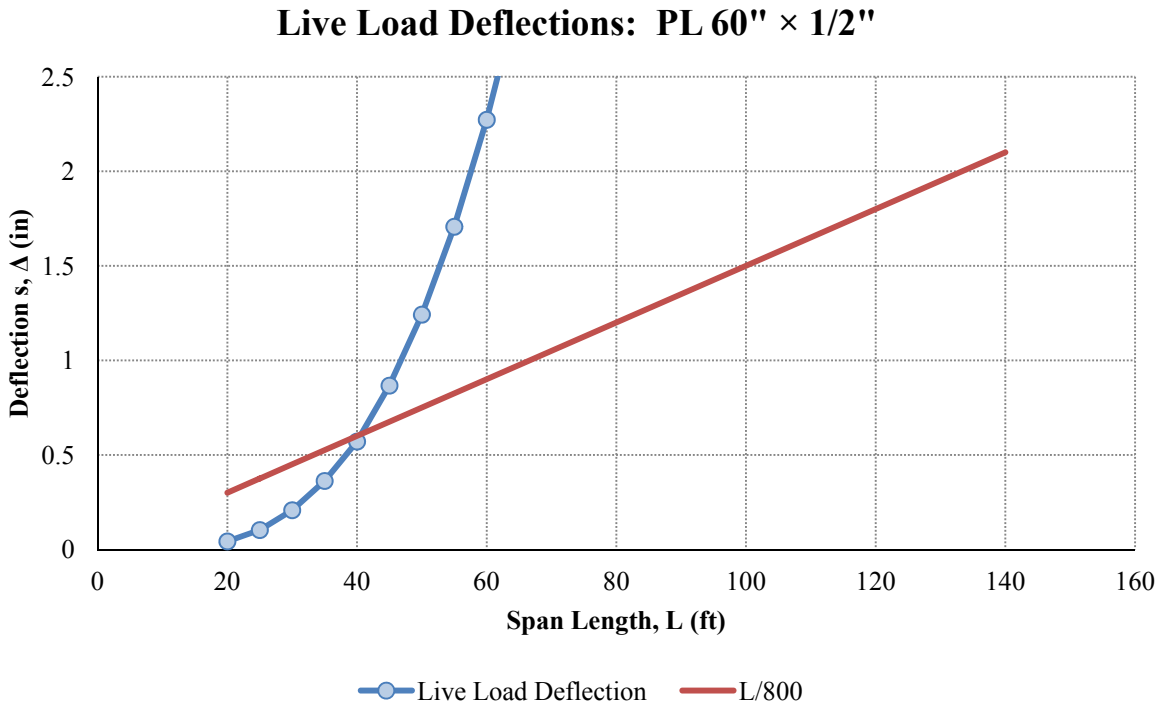
Live Load Deflections: PL 60" × 1/2"
Deflection s, Δ (in)
2.5
2
1.5
1
0.5
0
0
20
40
60
80
100
120
140
160
Span Length, L (ft)
Live Load Deflection
L/800

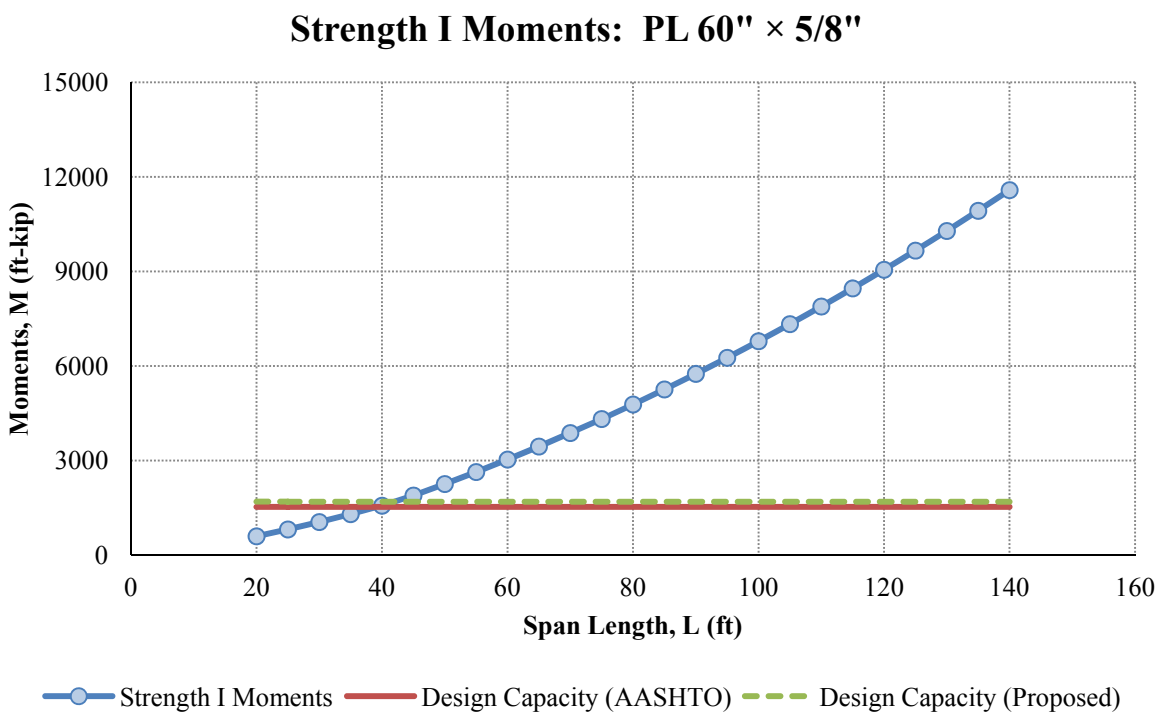
Strength I Moments: PL 60" × 5/8"
15000
12000
9000
6000
3000
0
Moments, M (ft-kip)
0
20
40
60
80
100
120
140
160
Span Length, L (ft)
Strength I Moments
Design Capacity (AASHTO)
Design Capacity (Proposed)

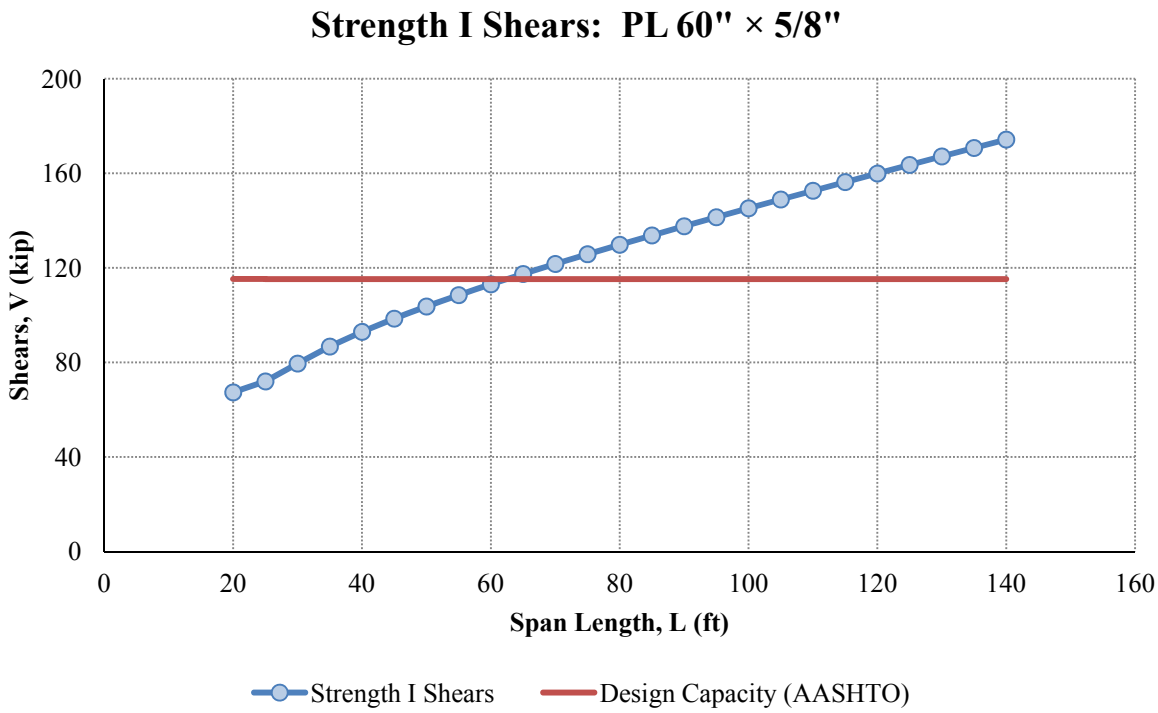
Strength I Shears: PL 60" × 5/8"
200
160
120
80
40
0
Shears, V (kip)
0
20
40
60
80
100
120
140
160
Span Length, L (ft)
Strength I Shears
Design Capacity (AASHTO)

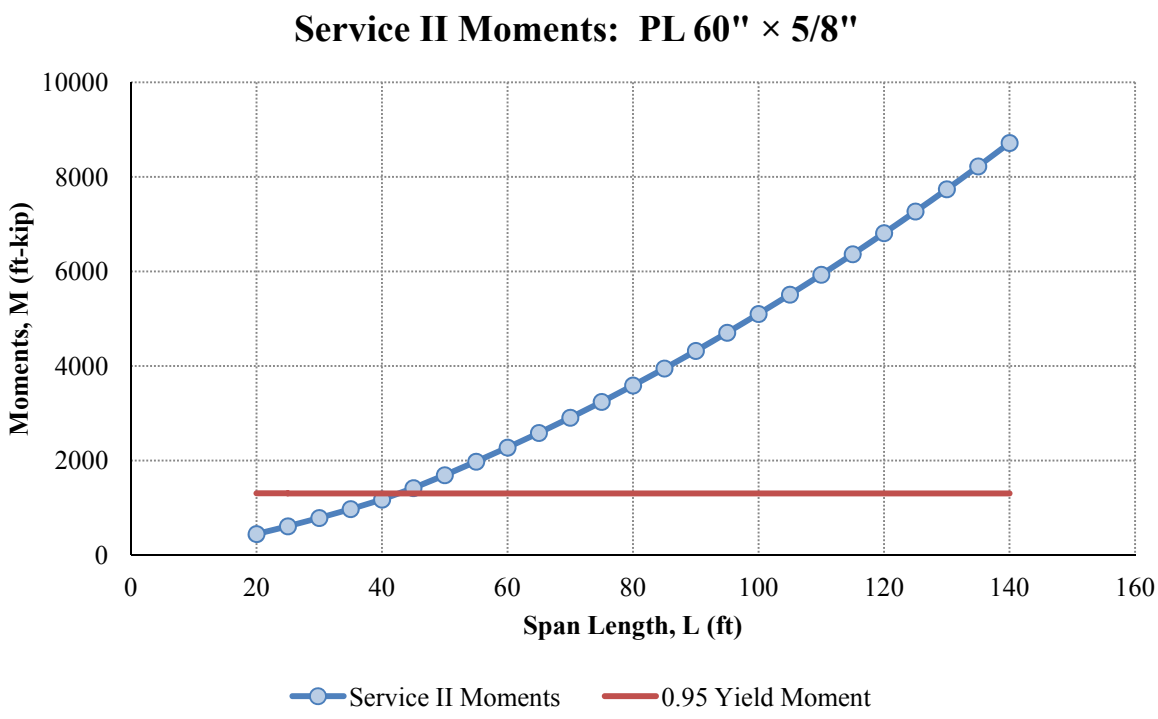
Service II Moments: PL 60" × 5/8"
Moments, M (ft-kip)
10000
8000
6000
4000
2000
0
0
20
40
60
80
100
120
140
160
Span Length, L (ft)
Service II Moments
0.95 Yield Moment

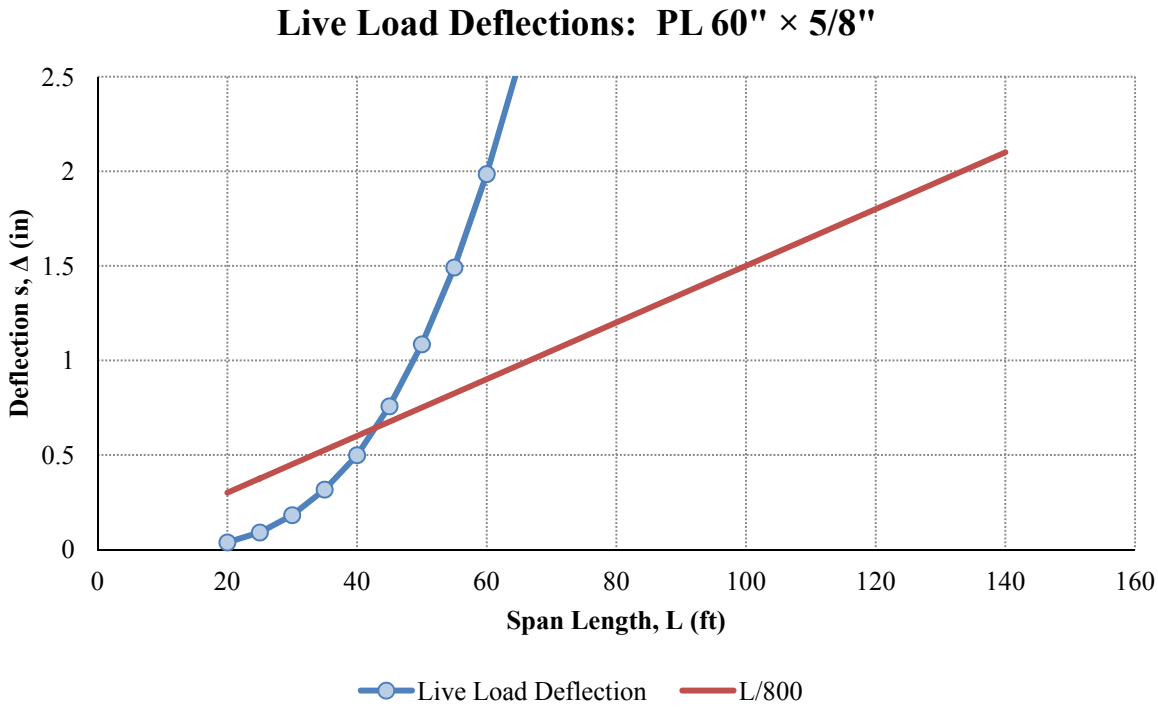
Live Load Deflections: PL 60" × 5/8"
Deflection s, Δ (in)
2.5
2
1.5
1
0.5
0
0
20
40
60
80
100
120
140
160
Span Length, L (ft)
Live Load Deflection
L/800

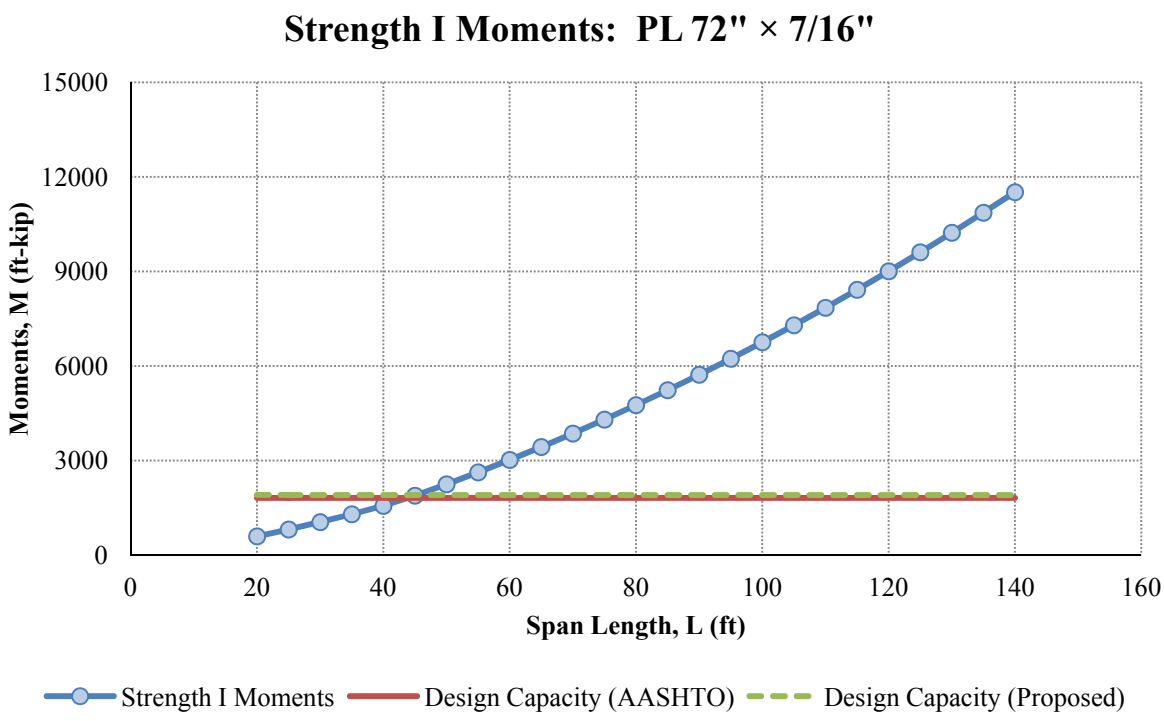
Strength I Moments: PL 72" × 7/16"
15000
12000
9000
6000
3000
0
Moments, M (ft-kip)
0
20
40
60
80
100
120
140
160
Span Length, L (ft)
Strength I Moments
Design Capacity (AASHTO)
Design Capacity (Proposed)

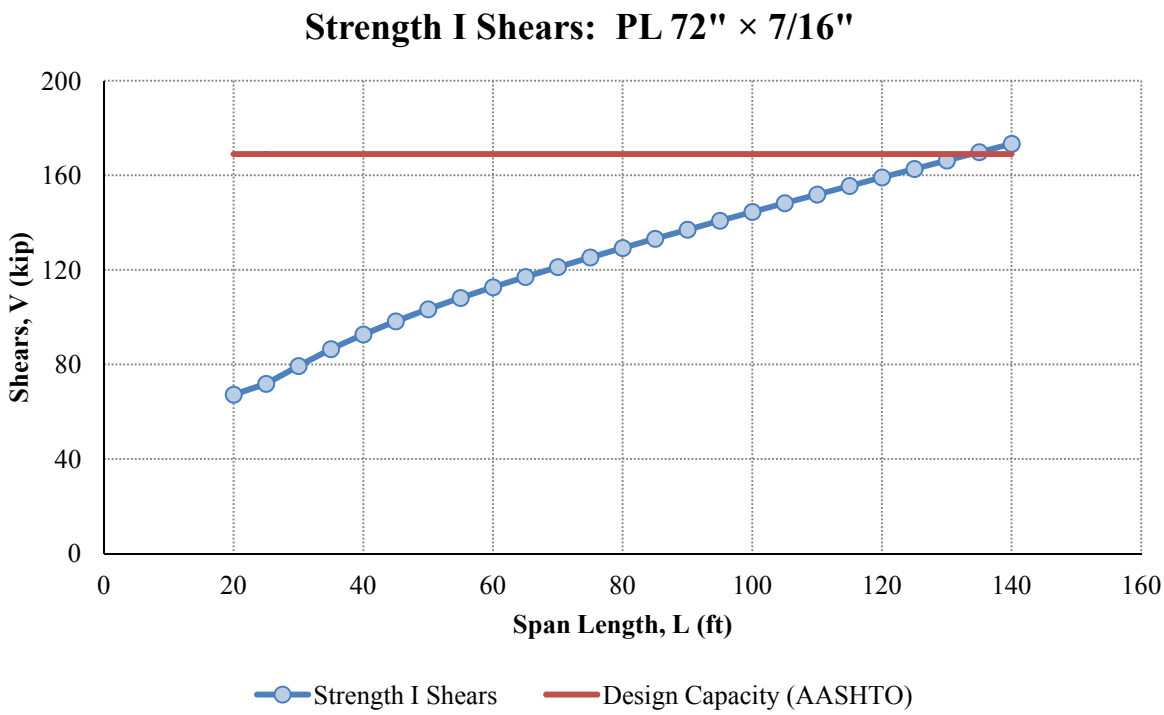
Strength I Shears: PL 72" × 7/16"
200
160
120
80
40
0
Shears, V (kip)
0
20
40
60
80
100
120
140
160
Span Length, L (ft)
Strength I Shears
Design Capacity (AASHTO)

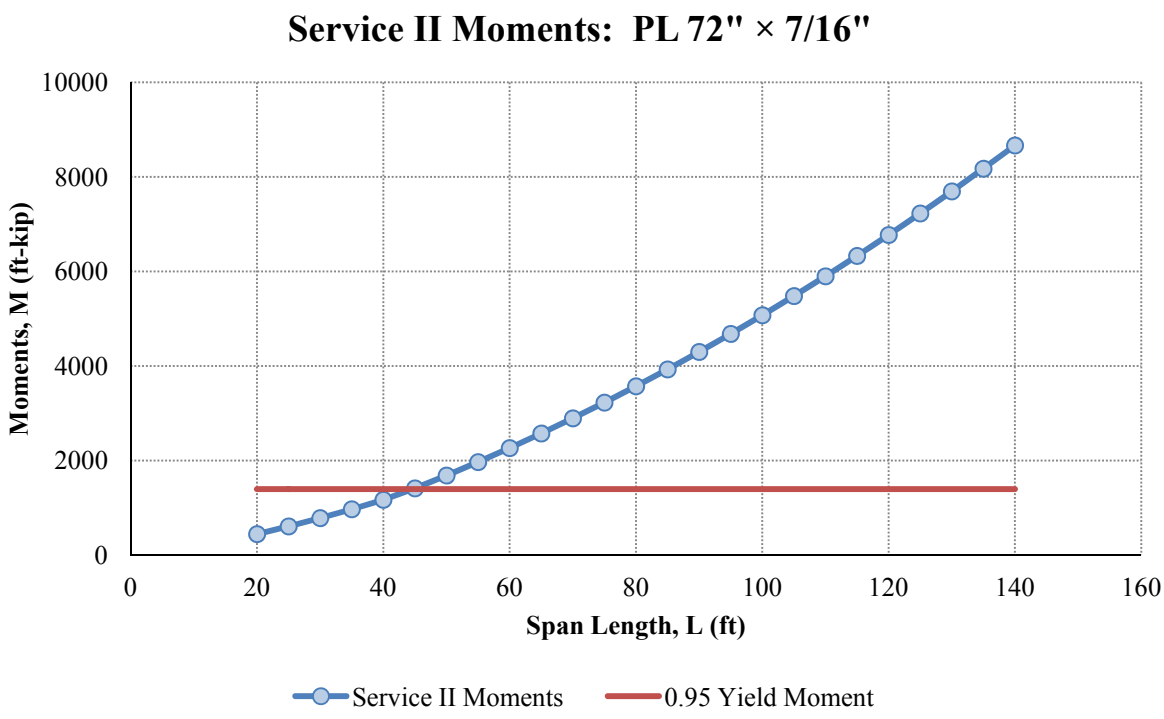
Service II Moments: PL 72" × 7/16"
Moments, M (ft-kip)
10000
8000
6000
4000
2000
0
0
20
40
60
80
100
120
140
160
Span Length, L (ft)
Service II Moments
0.95 Yield Moment

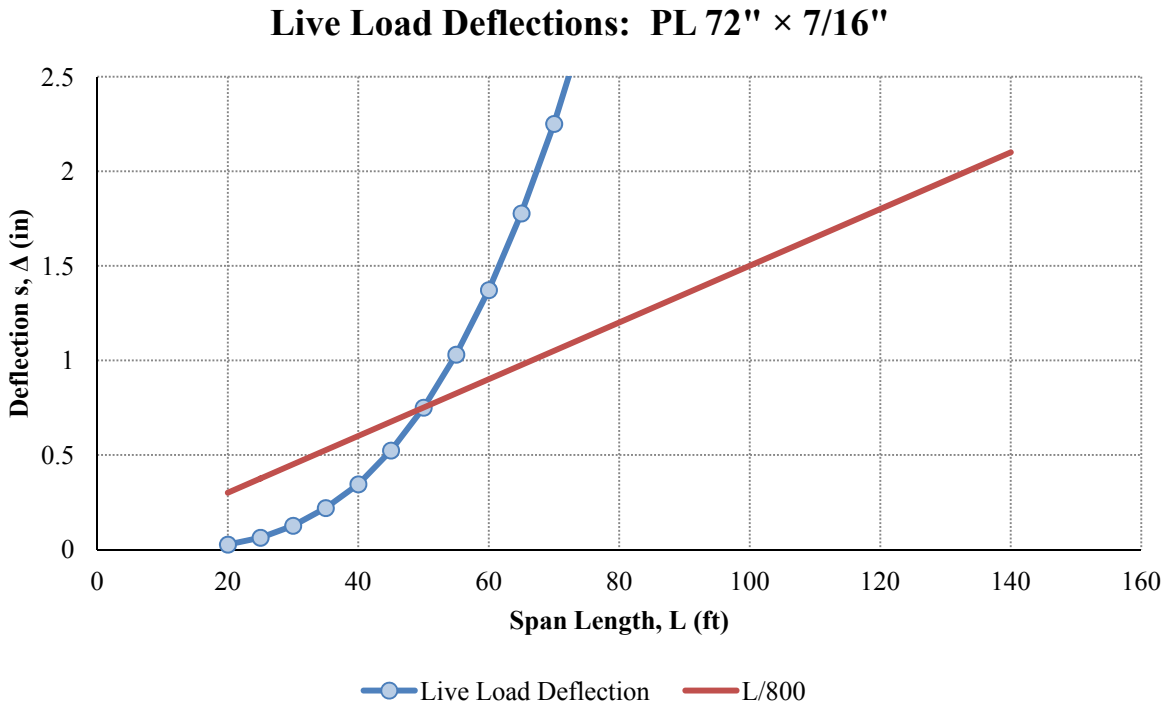
Live Load Deflections: PL 72" × 7/16"
Deflection s, Δ (in)
2.5
2
1.5
1
0.5
0
0
20
40
60
80
100
120
140
160
Span Length, L (ft)
Live Load Deflection
L/800

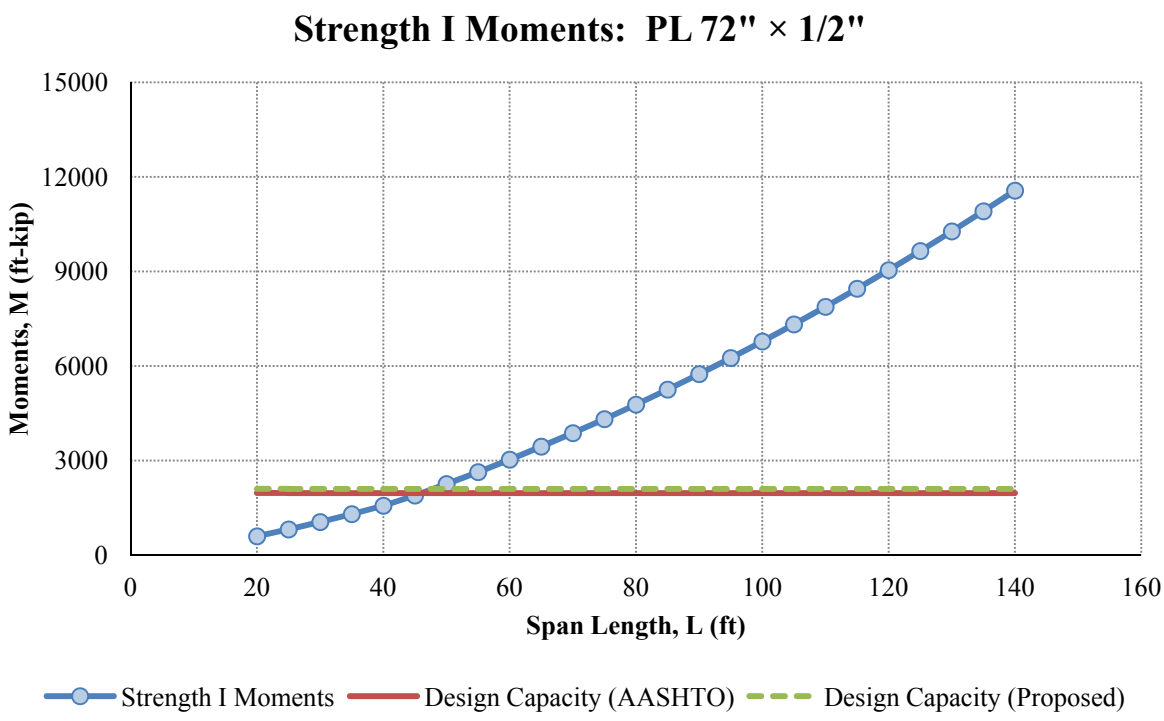
Strength I Moments: PL 72" × 1/2"
15000
12000
9000
6000
3000
0
Moments, M (ft-kip)
0
20
40
60
80
100
120
140
160
Span Length, L (ft)
Strength I Moments
Design Capacity (AASHTO)
Design Capacity (Proposed)

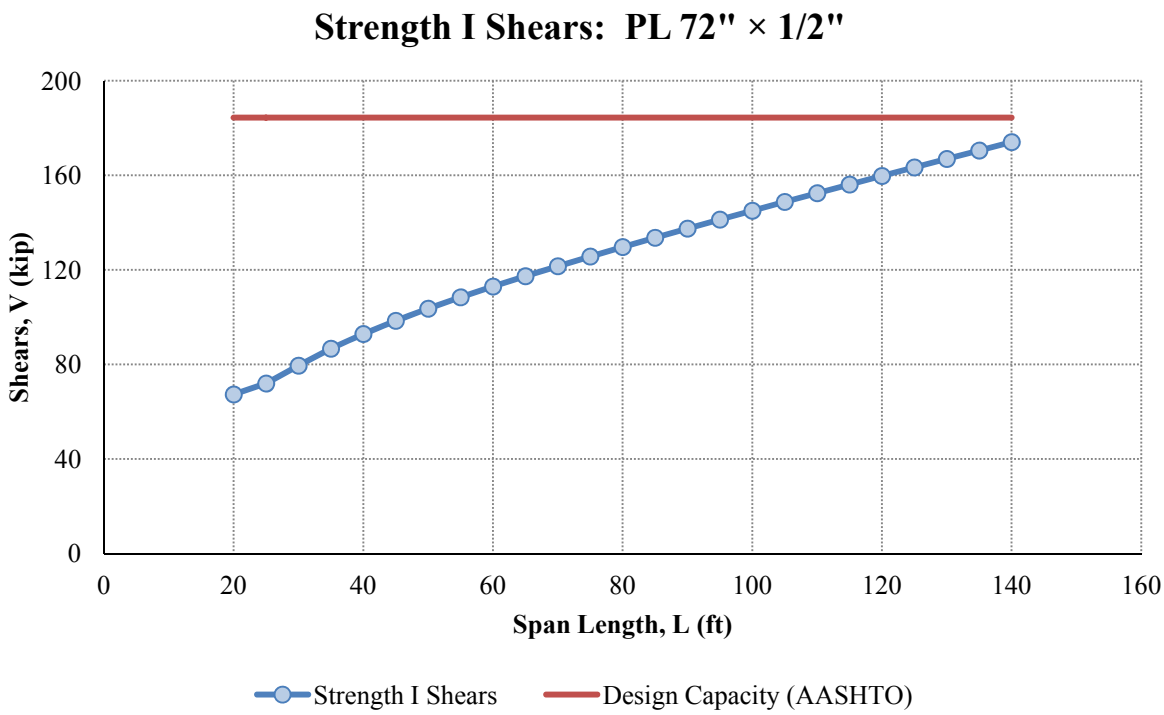
Strength I Shears: PL 72" × 1/2"
200
160
120
80
40
0
Shears, V (kip)
0
20
40
60
80
100
120
140
160
Span Length, L (ft)
Strength I Shears
Design Capacity (AASHTO)

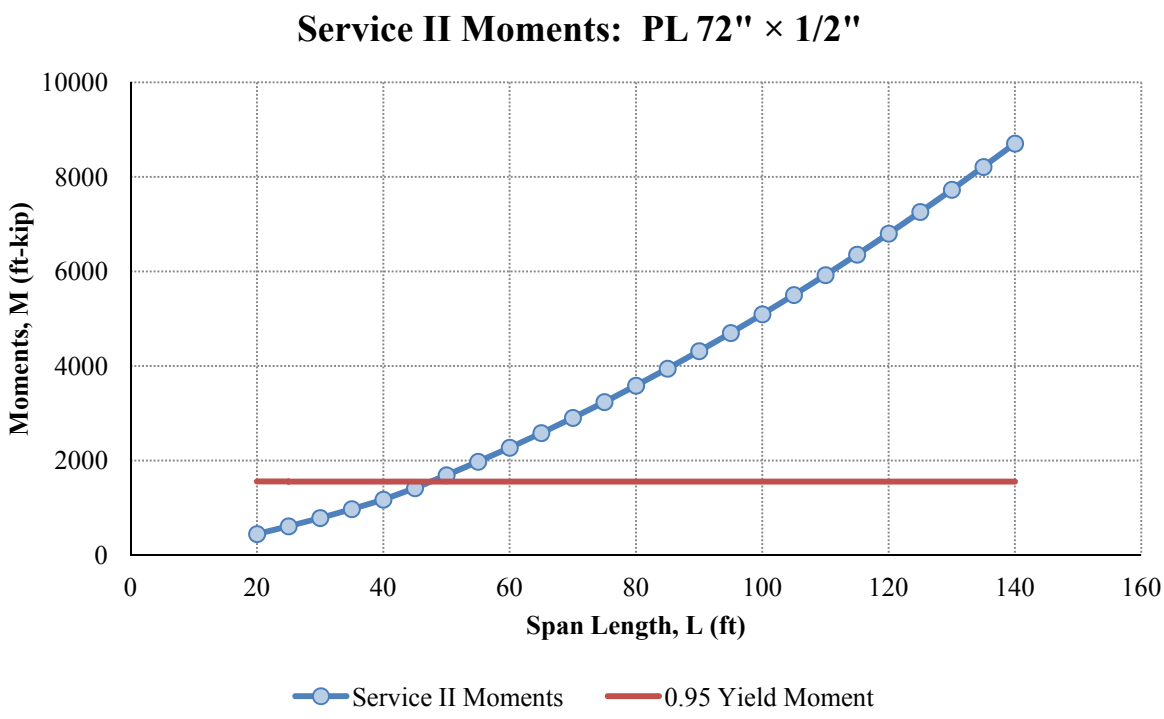
Service II Moments: PL 72" × 1/2"
Moments, M (ft-kip)
10000
8000
6000
4000
2000
0
0
20
40
60
80
100
120
140
160
Span Length, L (ft)
Service II Moments
0.95 Yield Moment

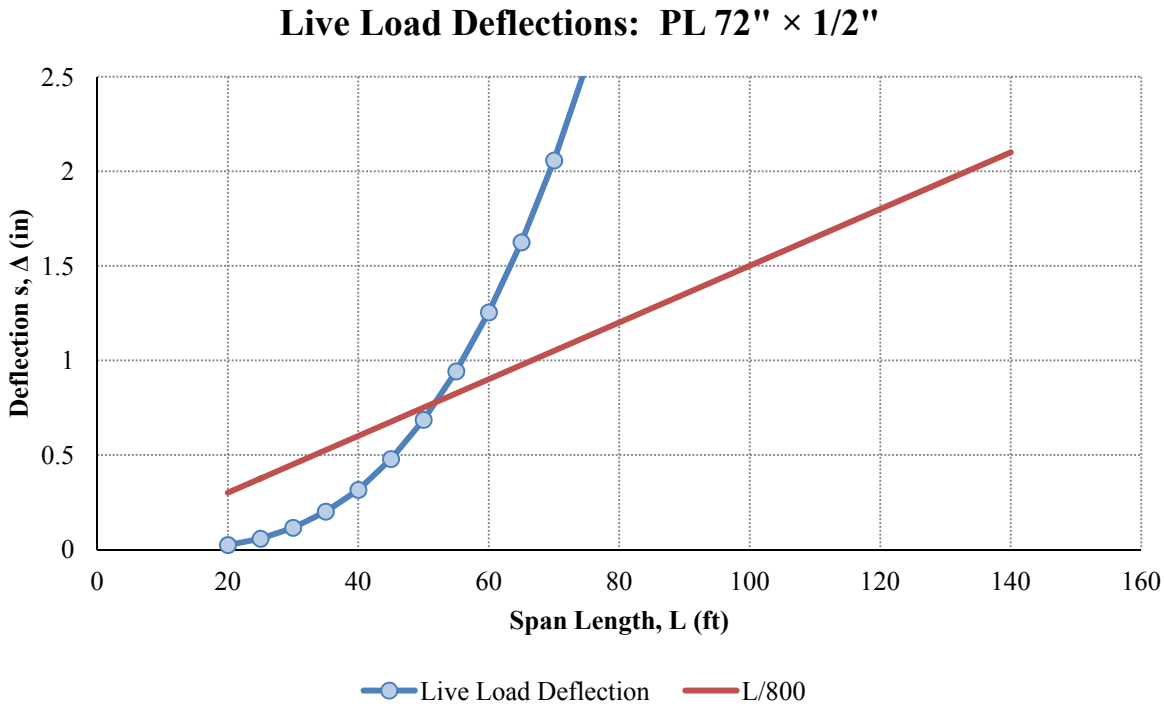
Live Load Deflections: PL 72" × 1/2"
Deflection s, Δ (in)
2.5
2
1.5
1
0.5
0
0
20
40
60
80
100
120
140
160
Span Length, L (ft)
Live Load Deflection
L/800

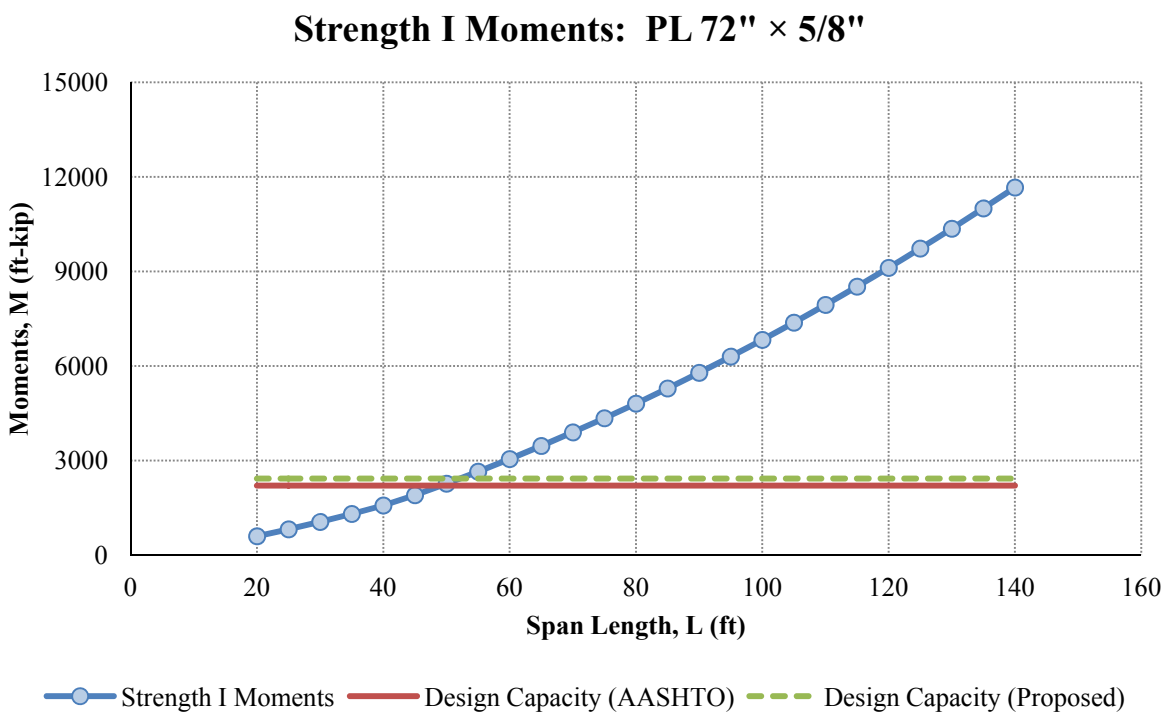
Strength I Moments: PL 72" × 5/8"
15000
12000
9000
6000
3000
0
Moments, M (ft-kip)
0
20
40
60
80
100
120
140
160
Span Length, L (ft)
Strength I Moments
Design Capacity (AASHTO)
Design Capacity (Proposed)

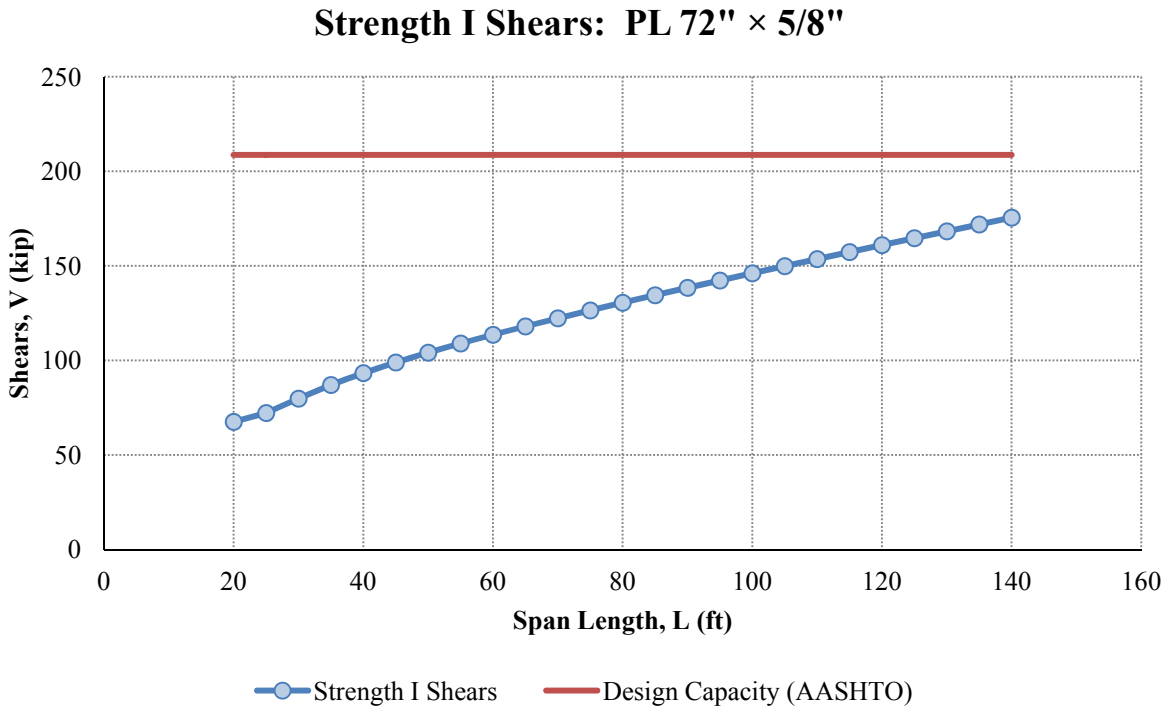
Strength I Shears: PL 72" × 5/8"
250
200
150
100
50
0
Shears, V (kip)
0
20
40
60
80
100
120
140
160
Span Length, L (ft)
Strength I Shears
Design Capacity (AASHTO)

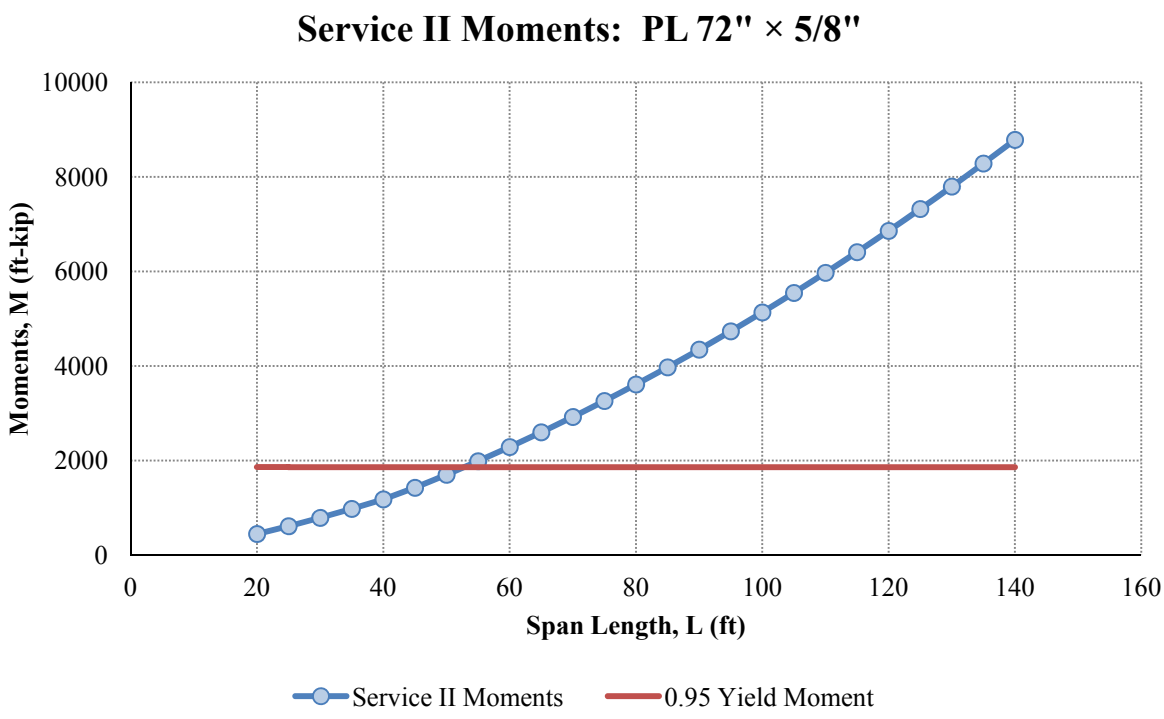
Service II Moments: PL 72" × 5/8"
Moments, M (ft-kip)
10000
8000
6000
4000
2000
0
0
20
40
60
80
100
120
140
160
Span Length, L (ft)
Service II Moments
0.95 Yield Moment

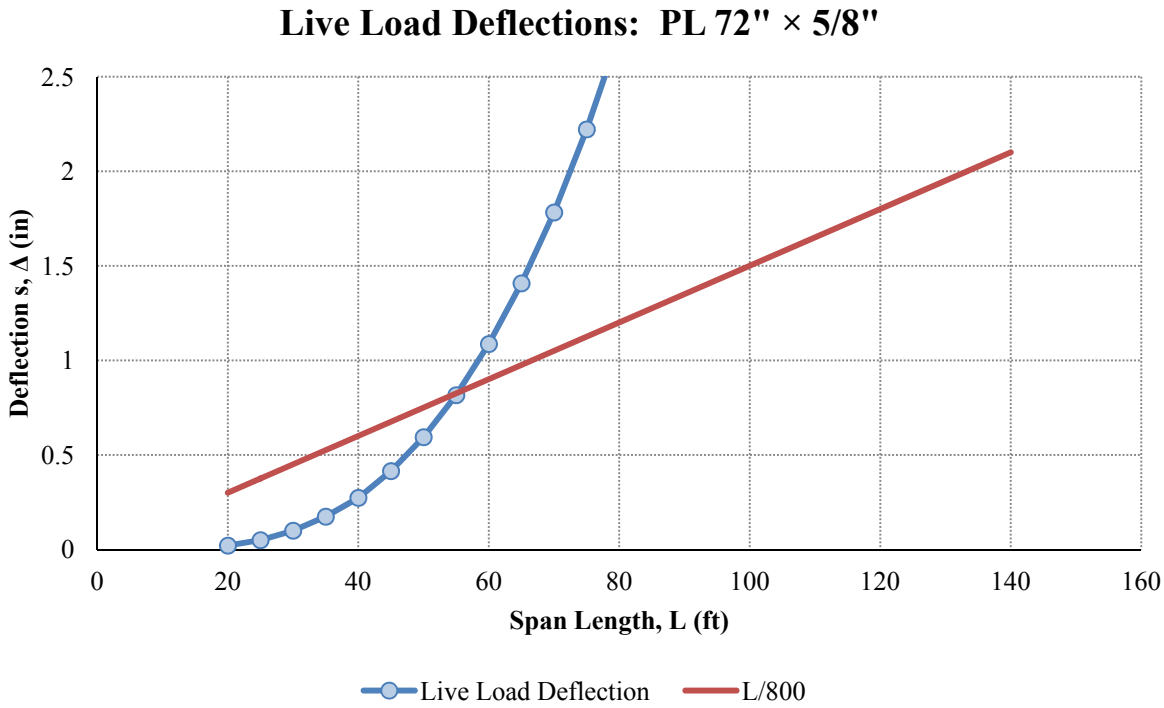
Live Load Deflections: PL 72" × 5/8"
Deflection s, Δ (in)
2.5
2
1.5
1
0.5
0
0
20
40
60
80
100
120
140
160
Span Length, L (ft)
Live Load Deflection
L/800

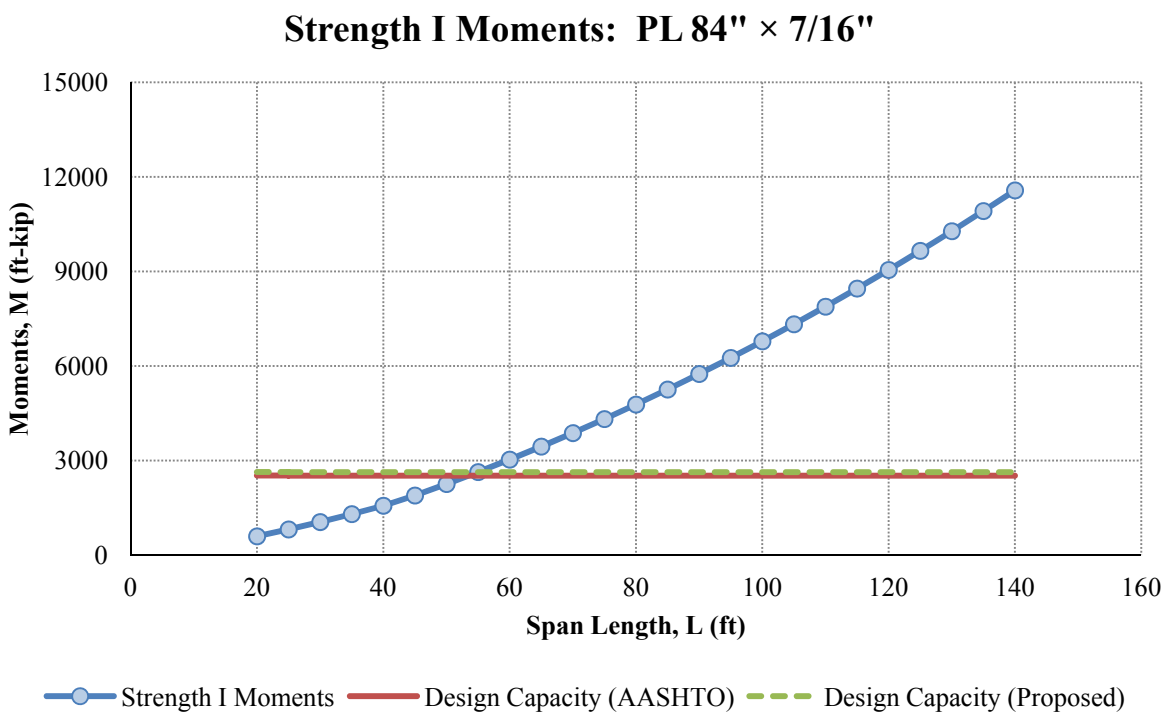
Strength I Moments: PL 84" × 7/16"
15000
12000
9000
6000
3000
0
Moments, M (ft-kip)
0
20
40
60
80
100
120
140
160
Span Length, L (ft)
Strength I Moments
Design Capacity (AASHTO)
Design Capacity (Proposed)

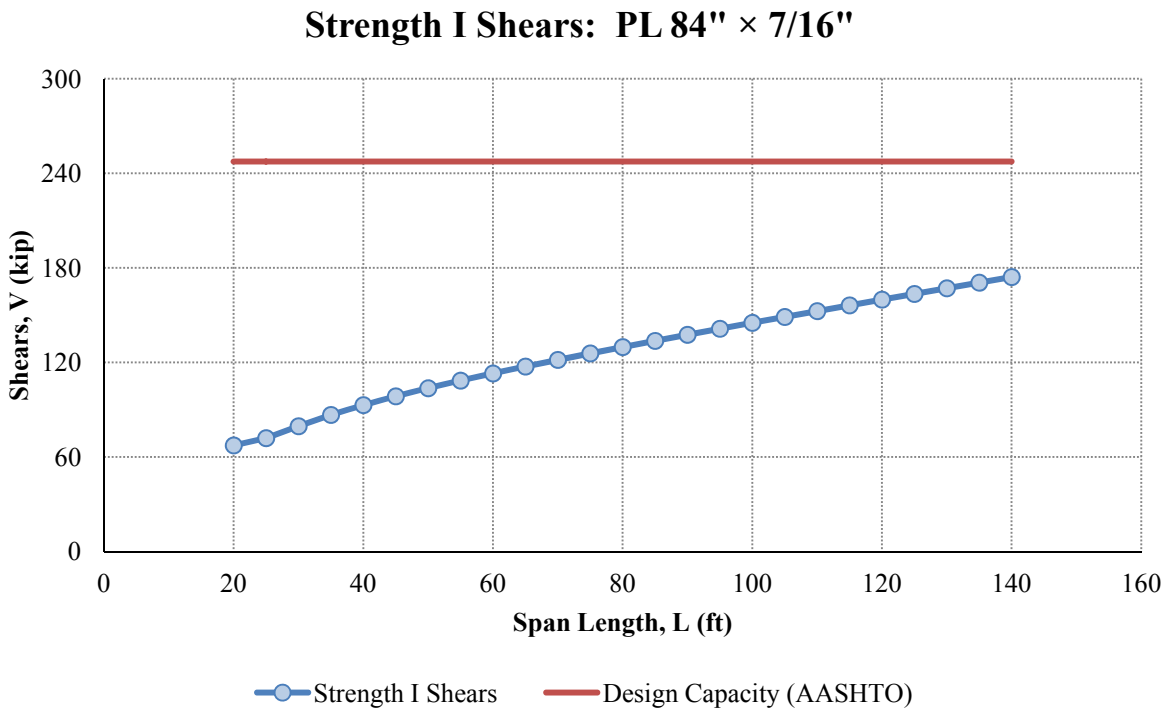
Strength I Shears: PL 84" × 7/16"
300
240
180
120
60
0
Shears, V (kip)
0
20
40
60
80
100
120
140
160
Span Length, L (ft)
Strength I Shears
Design Capacity (AASHTO)

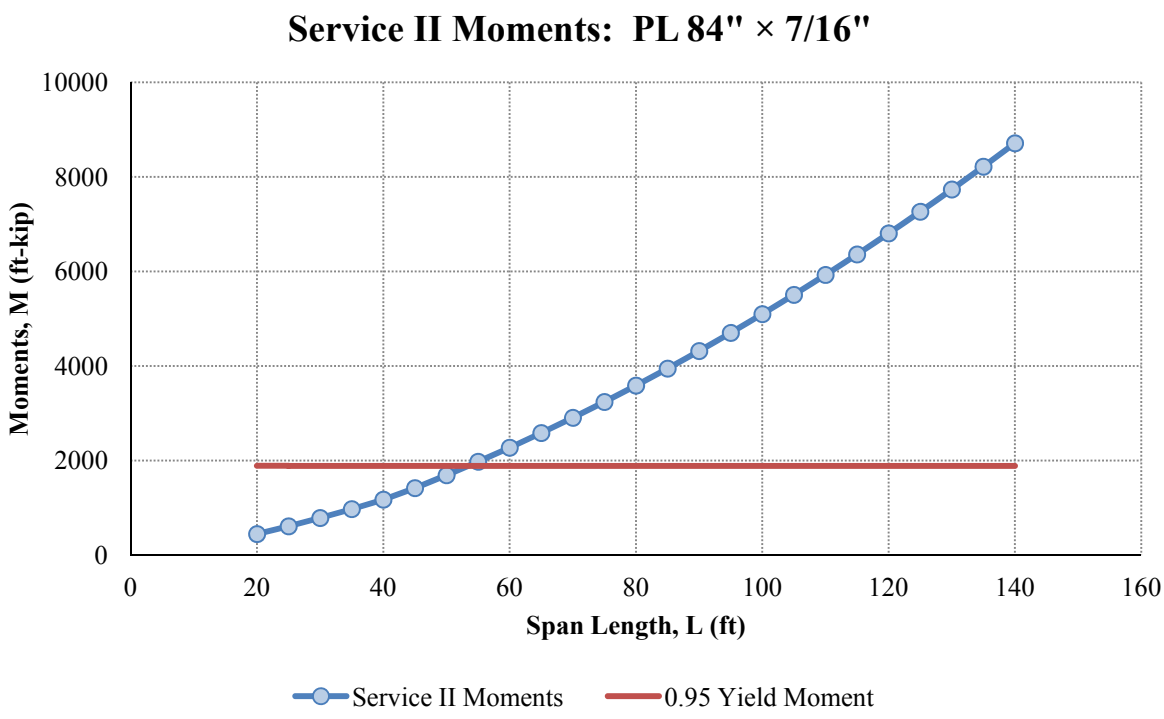
Service II Moments: PL 84" × 7/16"
Moments, M (ft-kip)
10000
8000
6000
4000
2000
0
0
20
40
60
80
100
120
140
160
Span Length, L (ft)
Service II Moments
0.95 Yield Moment

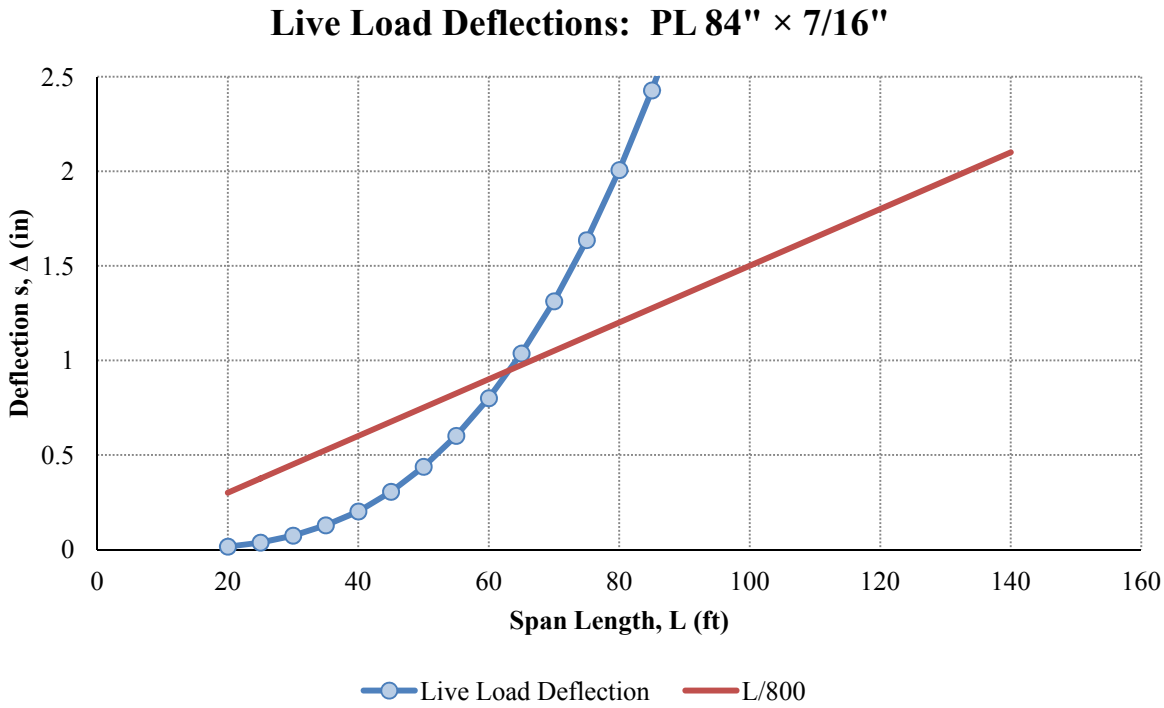
Live Load Deflections: PL 84" × 7/16"
Deflection s, Δ (in)
2.5
2
1.5
1
0.5
0
0
20
40
60
80
100
120
140
160
Span Length, L (ft)
Live Load Deflection
L/800

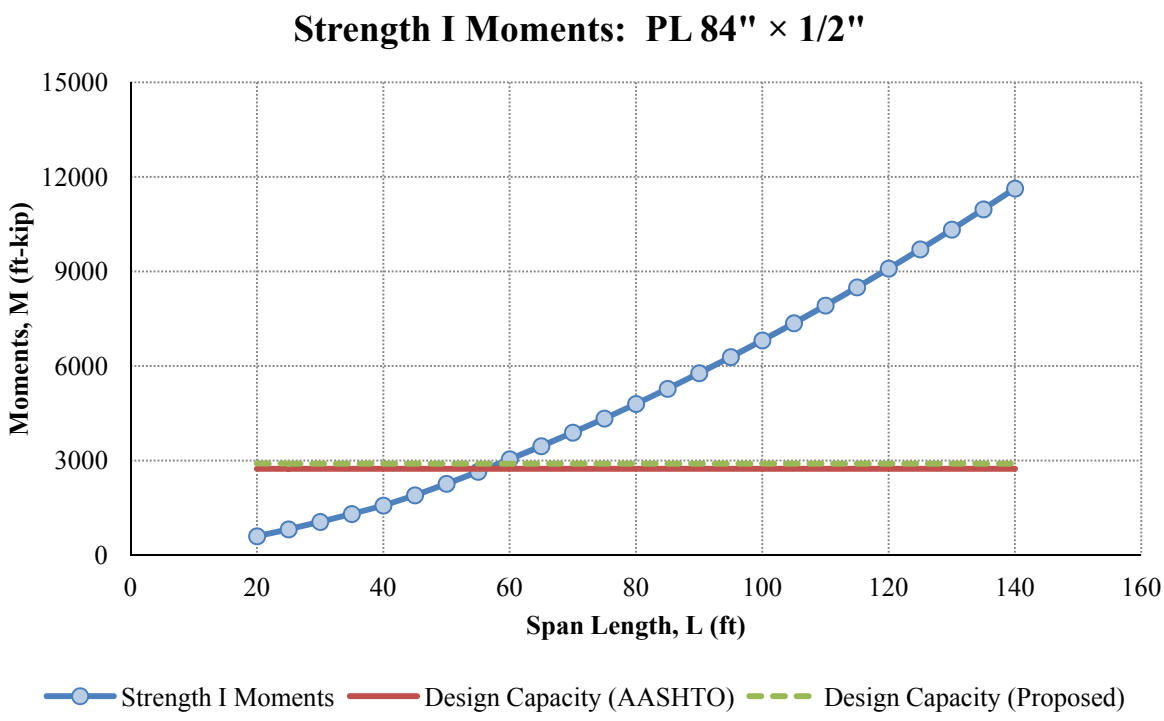
Strength I Moments: PL 84" × 1/2"
15000
12000
9000
6000
3000
0
Moments, M (ft-kip)
0
20
40
60
80
100
120
140
160
Span Length, L (ft)
Strength I Moments
Design Capacity (AASHTO)
Design Capacity (Proposed)

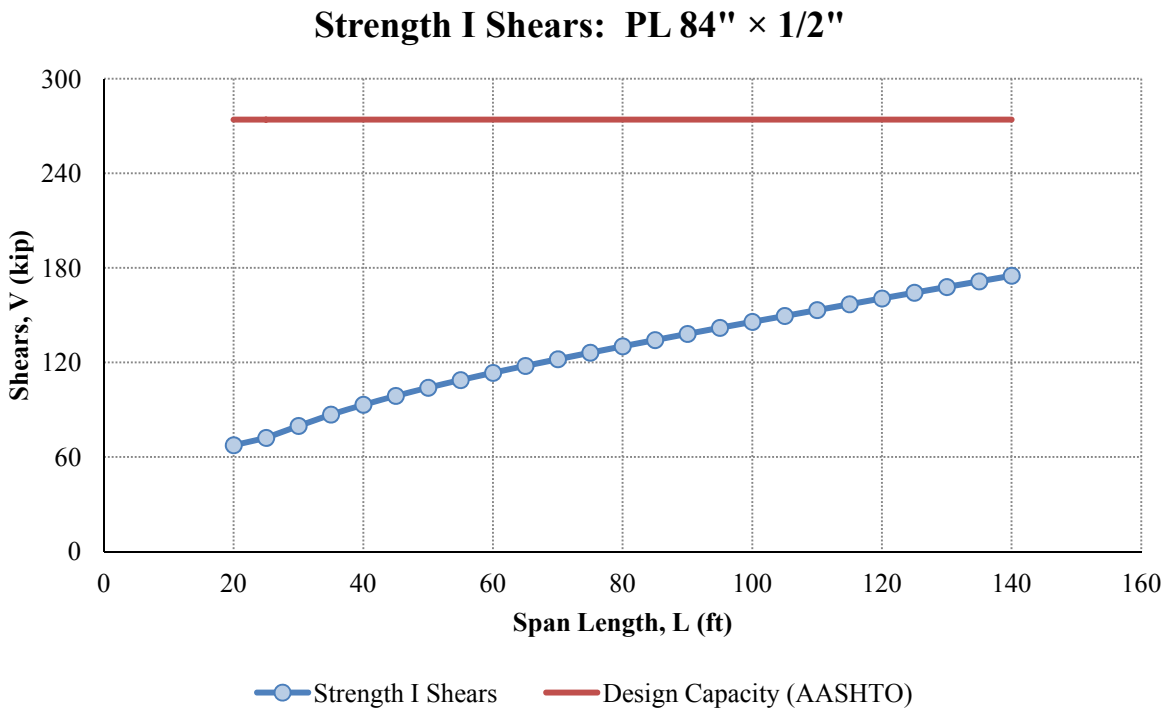
Strength I Shears: PL 84" × 1/2"
300
240
180
120
60
0
Shears, V (kip)
0
20
40
60
80
100
120
140
160
Span Length, L (ft)
Strength I Shears
Design Capacity (AASHTO)

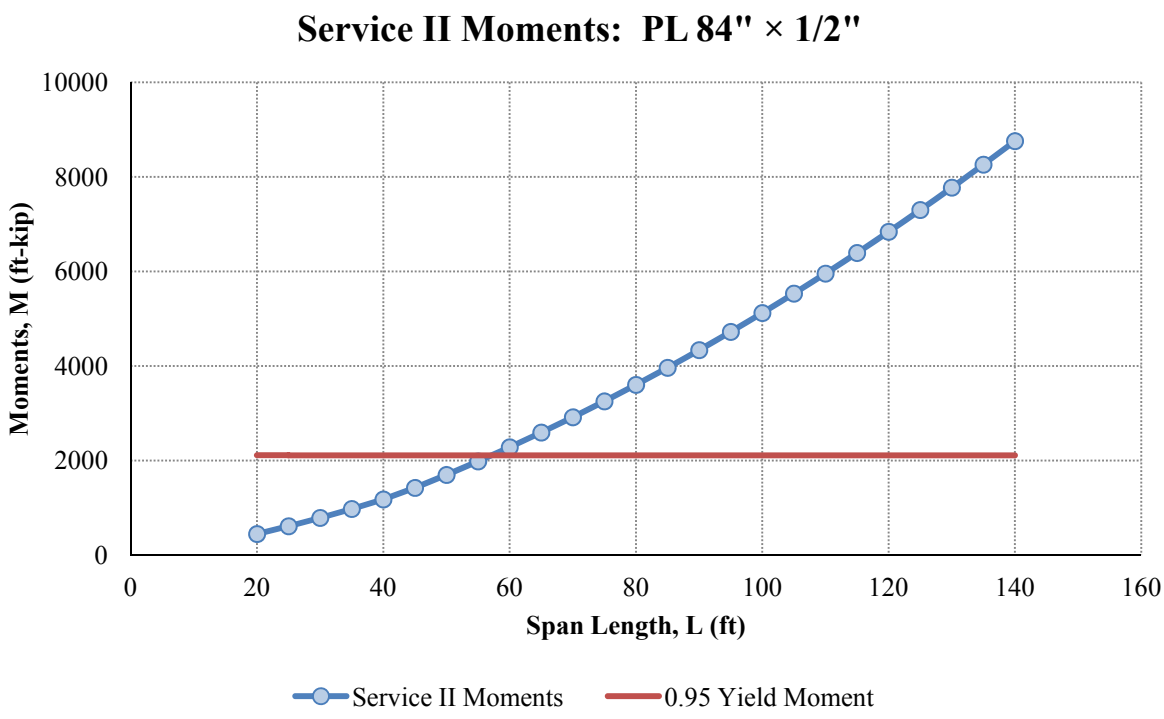
Service II Moments: PL 84" × 1/2"
Moments, M (ft-kip)
10000
8000
6000
4000
2000
0
0
20
40
60
80
100
120
140
160
Span Length, L (ft)
Service II Moments
0.95 Yield Moment

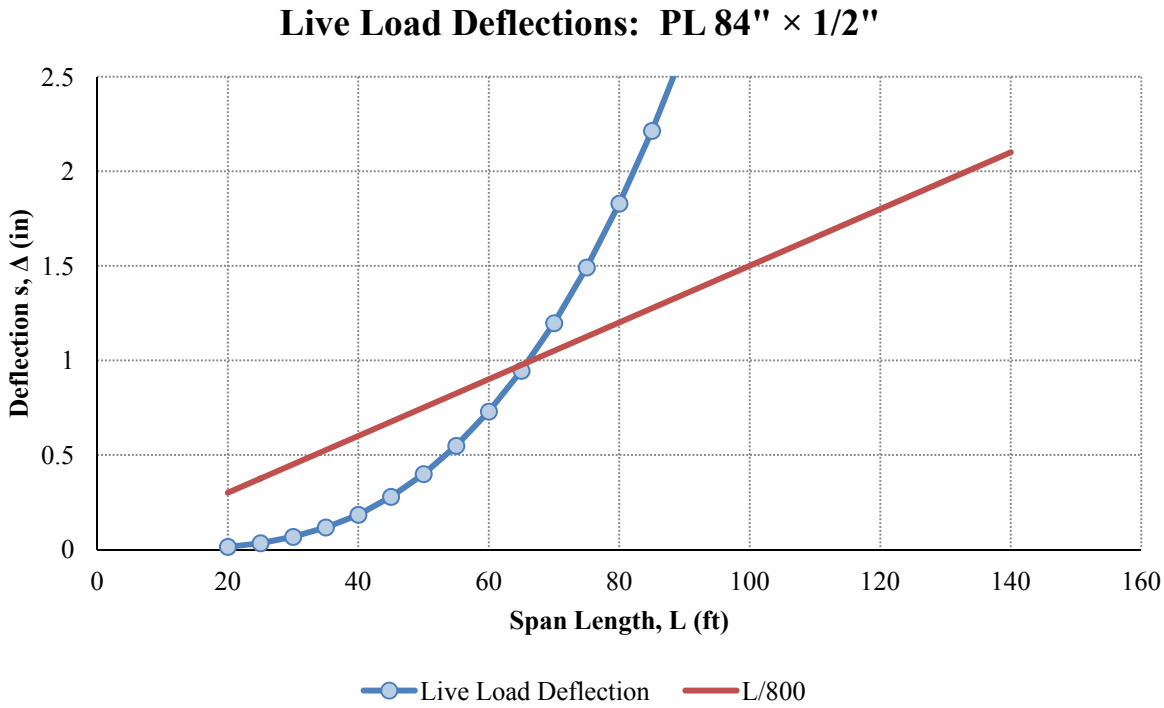
Live Load Deflections: PL 84" × 1/2"
Deflection s, Δ (in)
2.5
2
1.5
1
0.5
0
0
20
40
60
80
100
120
140
160
Span Length, L (ft)
Live Load Deflection
L/800

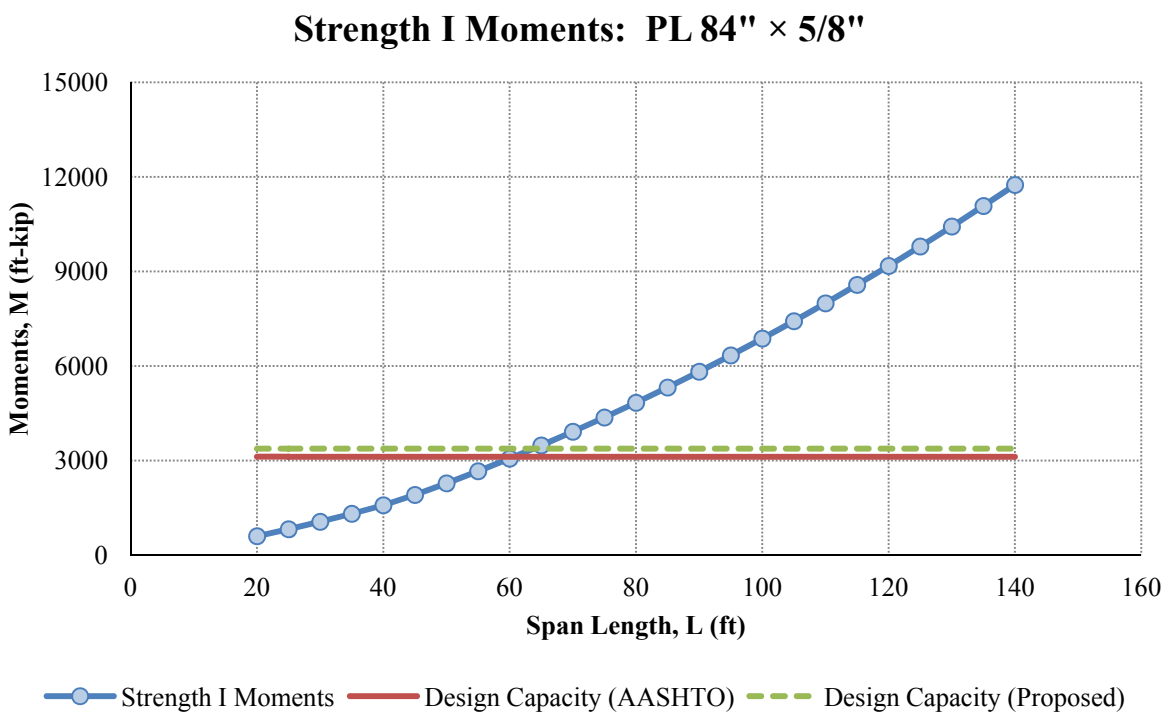
Strength I Moments: PL 84" × 5/8"
15000
12000
9000
6000
3000
0
Moments, M (ft-kip)
0
20
40
60
80
100
120
140
160
Span Length, L (ft)
Strength I Moments
Design Capacity (AASHTO)
Design Capacity (Proposed)

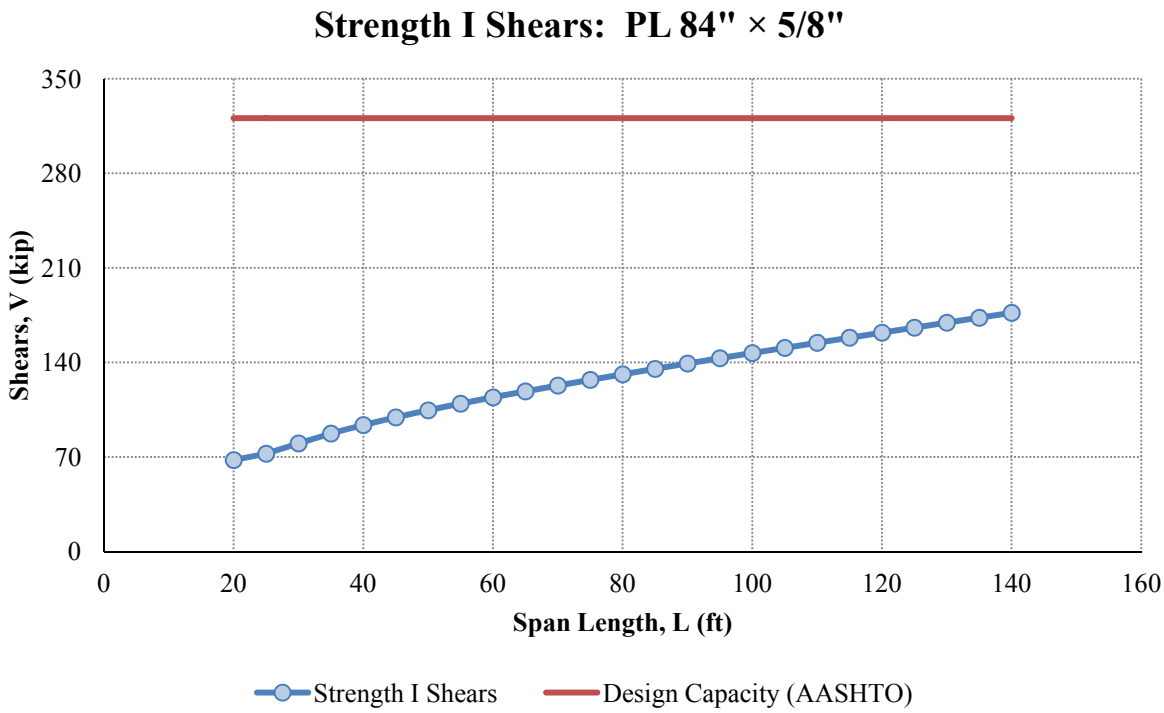
Strength I Shears: PL 84" × 5/8"
350
280
210
140
70
0
Shears, V (kip)
0
20
40
60
80
100
120
140
160
Span Length, L (ft)
Strength I Shears
Design Capacity (AASHTO)

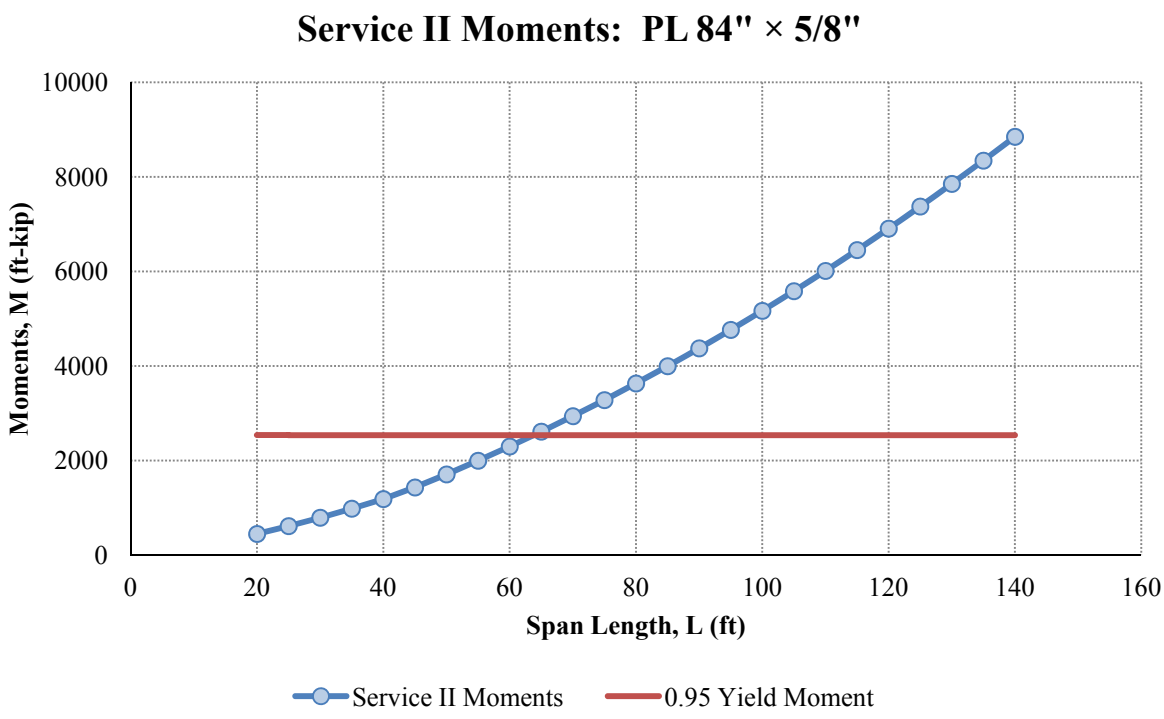
Service II Moments: PL 84" × 5/8"
Moments, M (ft-kip)
10000
8000
6000
4000
2000
0
0
20
40
60
80
100
120
140
160
Span Length, L (ft)
Service II Moments
0.95 Yield Moment

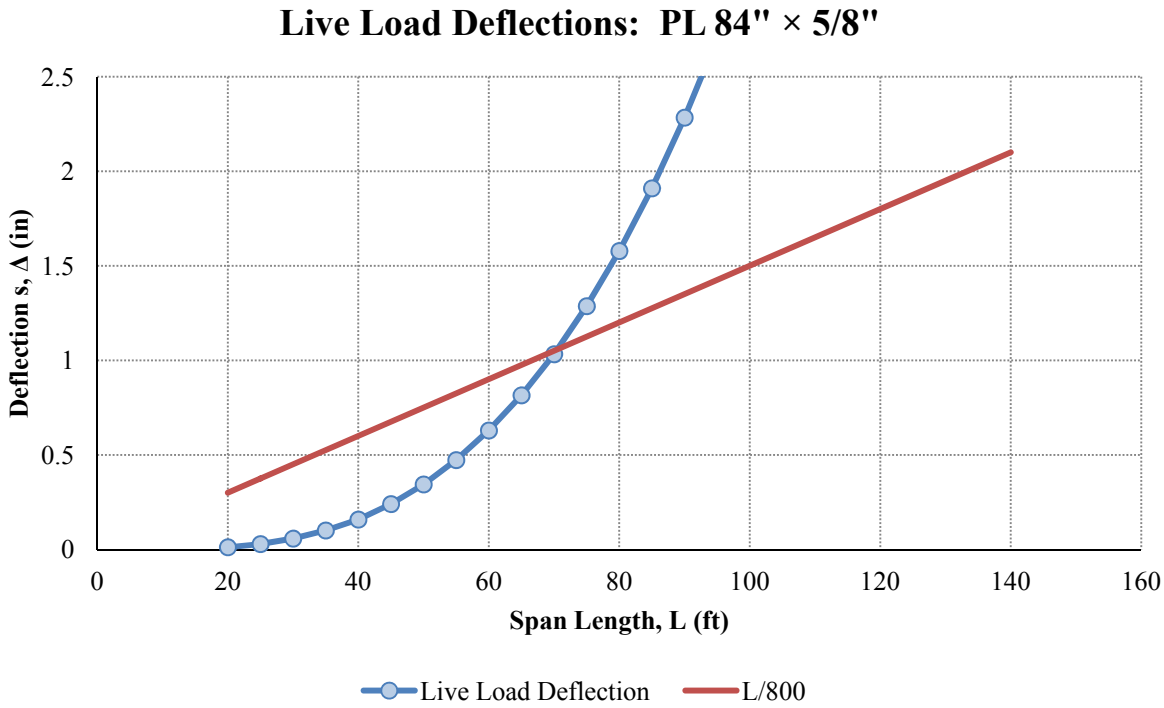
Live Load Deflections: PL 84" × 5/8"
Deflection s, Δ (in)
2.5
2
1.5
1
0.5
0
0
20
40
60
80
100
120
140
160
Span Length, L (ft)
Live Load Deflection
L/800

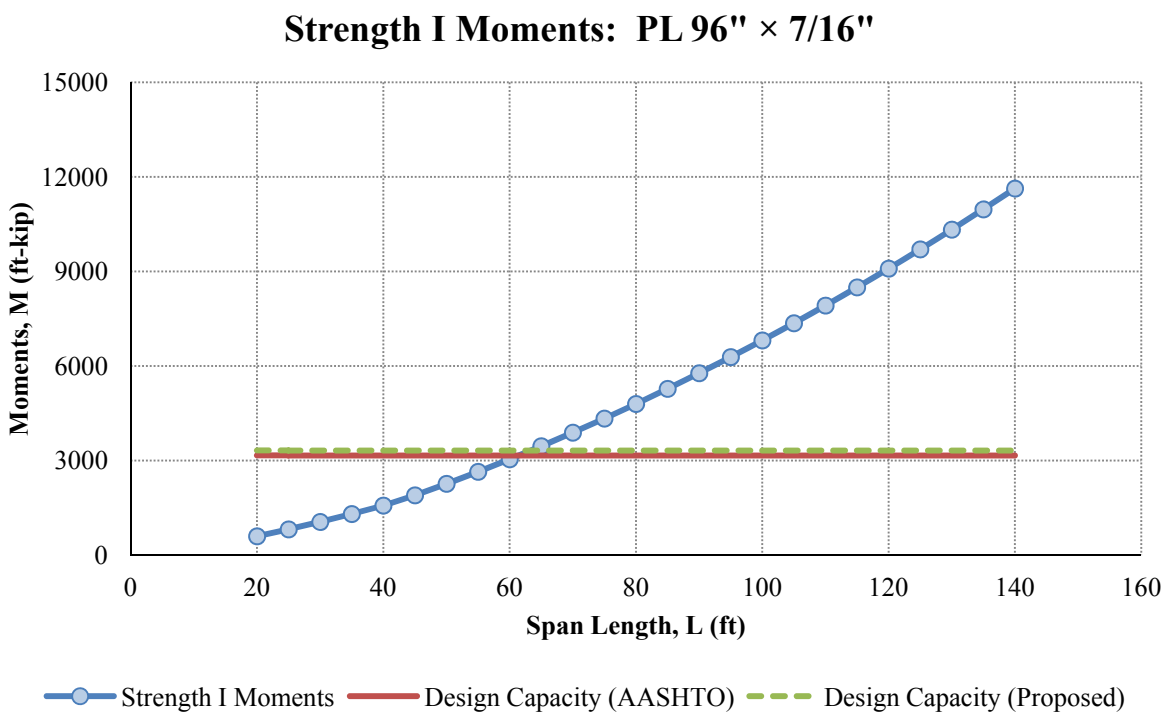
Strength I Moments: PL 96" × 7/16"
15000
12000
9000
6000
3000
0
Moments, M (ft-kip)
0
20
40
60
80
100
120
140
160
Span Length, L (ft)
Strength I Moments
Design Capacity (AASHTO)
Design Capacity (Proposed)

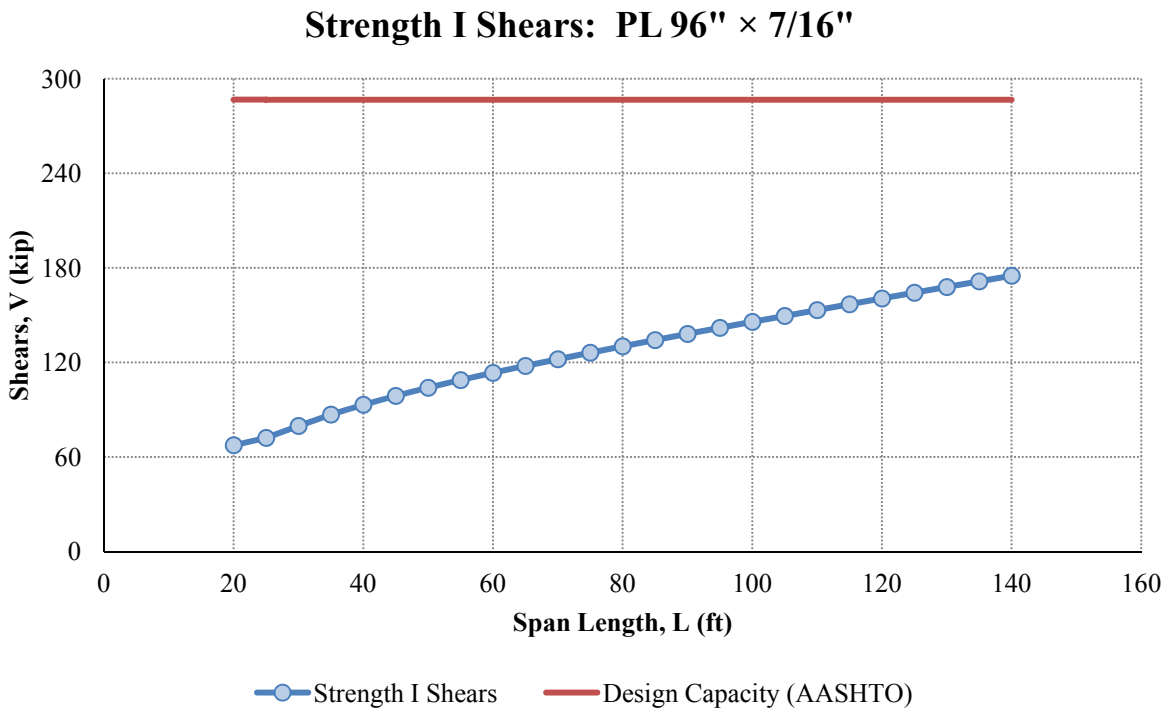
Strength I Shears: PL 96" × 7/16"
300
240
180
120
60
0
Shears, V (kip)
0
20
40
60
80
100
120
140
160
Span Length, L (ft)
Strength I Shears
Design Capacity (AASHTO)

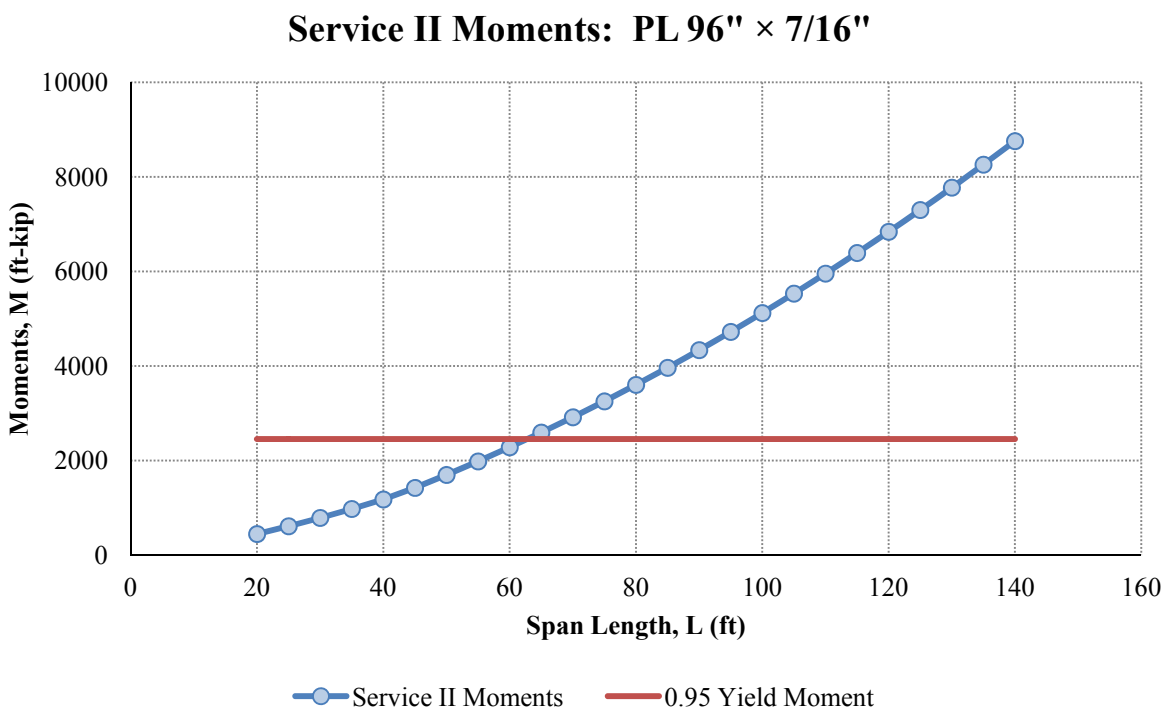
Service II Moments: PL 96" × 7/16"
Moments, M (ft-kip)
10000
8000
6000
4000
2000
0
0
20
40
60
80
100
120
140
160
Span Length, L (ft)
Service II Moments
0.95 Yield Moment

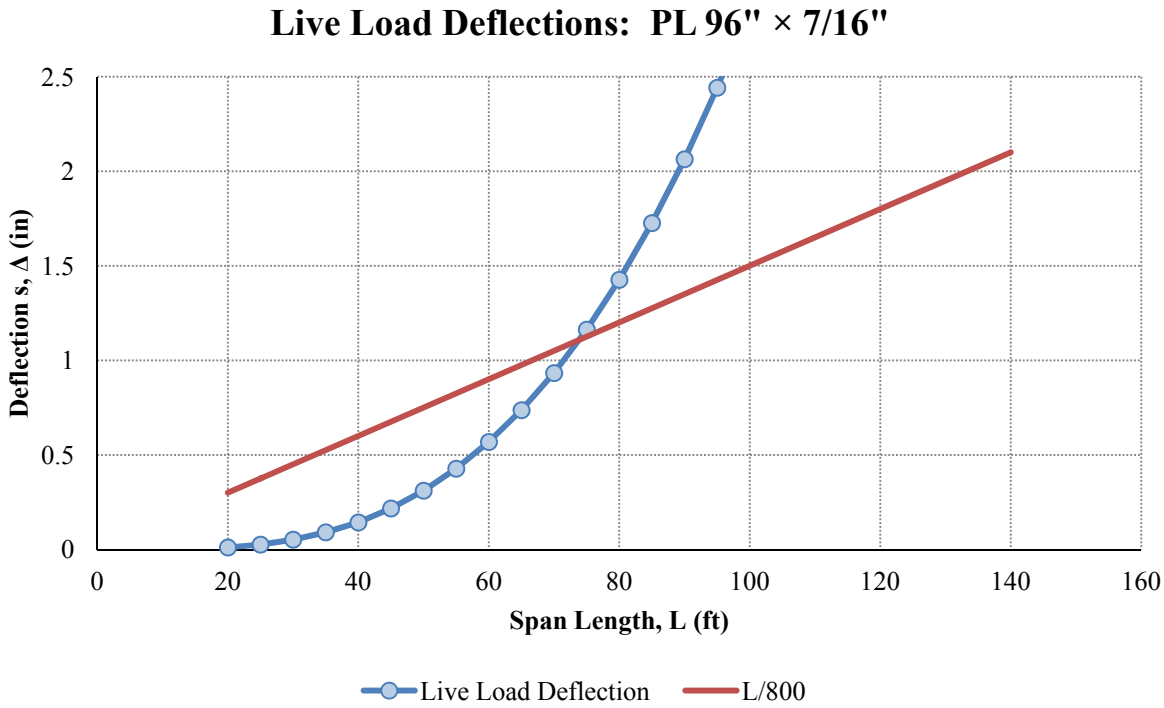
Live Load Deflections: PL 96" × 7/16"
Deflection s, Δ (in)
2.5
2
1.5
1
0.5
0
0
20
40
60
80
100
120
140
160
Span Length, L (ft)
Live Load Deflection
L/800

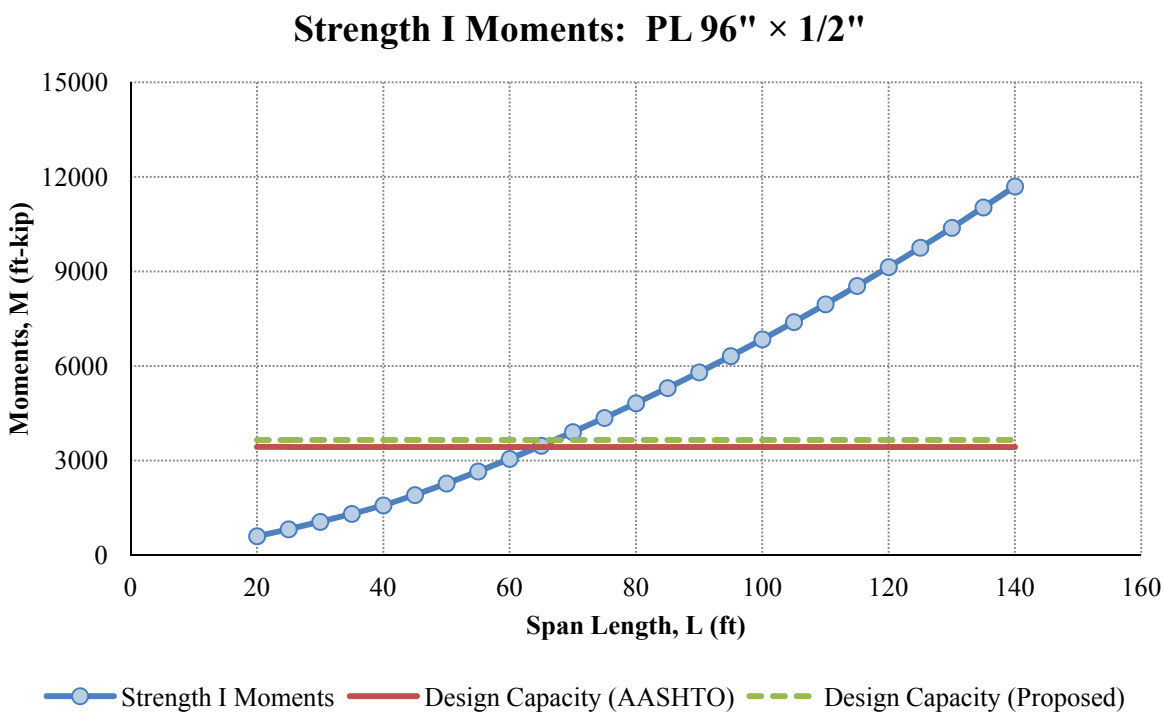
Strength I Moments: PL 96" × 1/2"
15000
12000
9000
6000
3000
0
Moments, M (ft-kip)
0
20
40
60
80
100
120
140
160
Span Length, L (ft)
Strength I Moments
Design Capacity (AASHTO)
Design Capacity (Proposed)

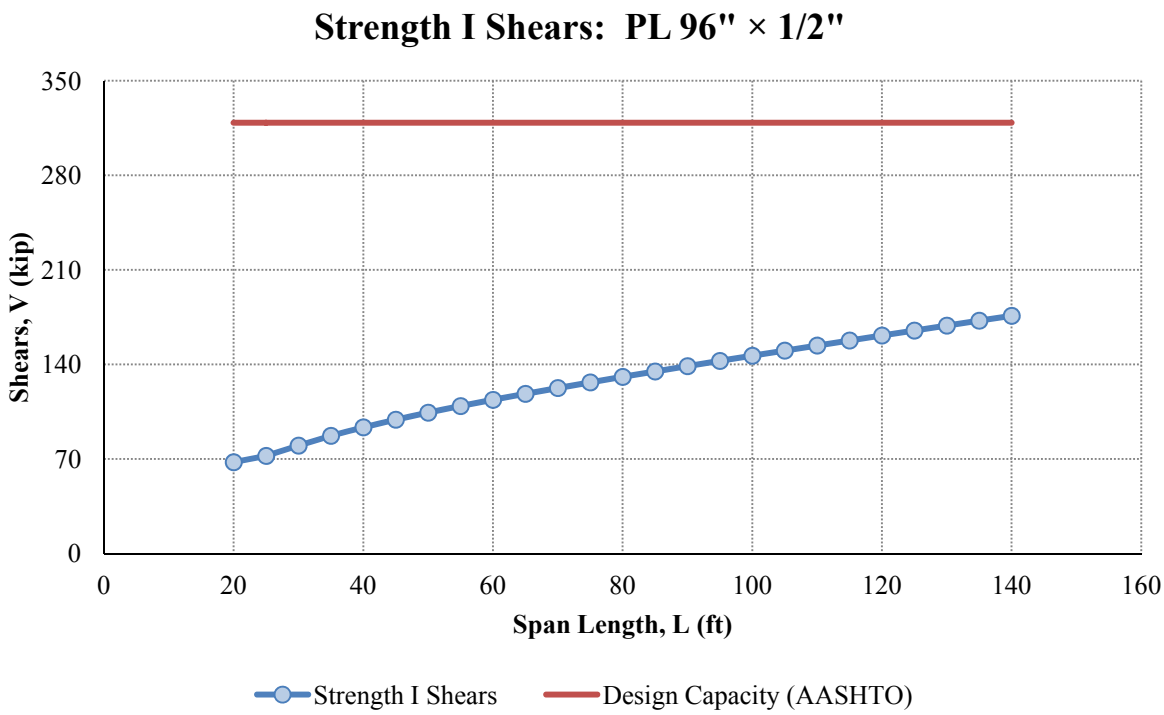
Strength I Shears: PL 96" × 1/2"
350
280
210
140
70
0
Shears, V (kip)
0
20
40
60
80
100
120
140
160
Span Length, L (ft)
Strength I Shears
Design Capacity (AASHTO)

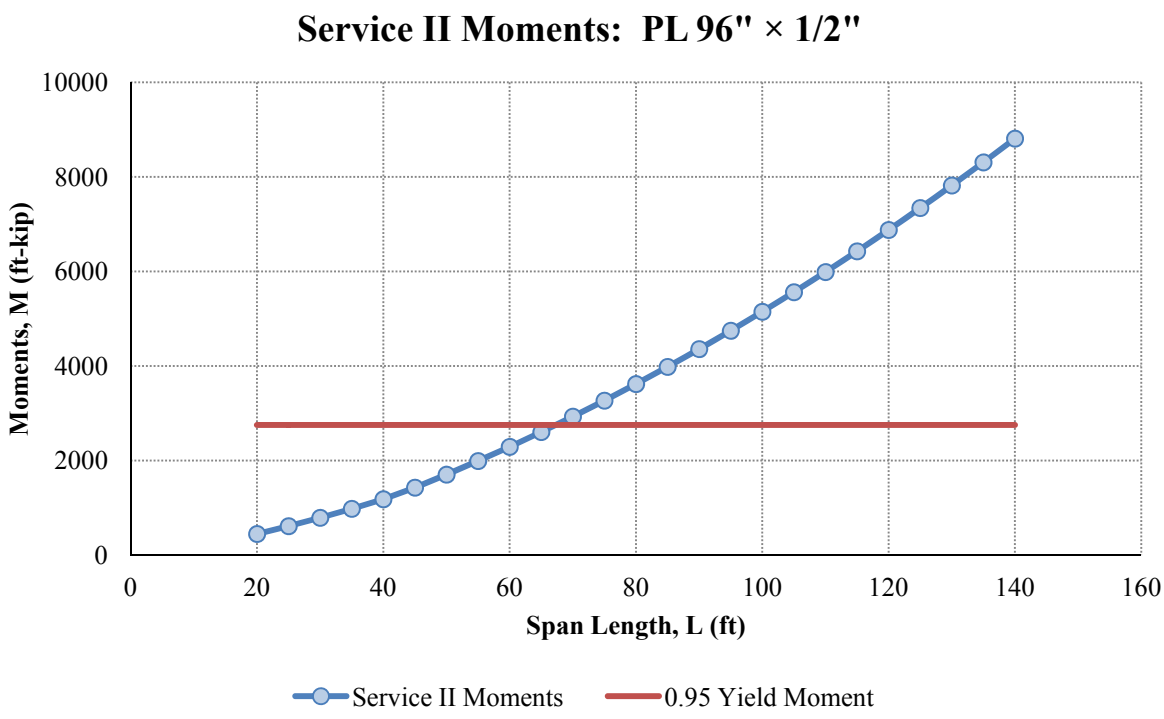
Service II Moments: PL 96" × 1/2"
Moments, M (ft-kip)
10000
8000
6000
4000
2000
0
0
20
40
60
80
100
120
140
160
Span Length, L (ft)
Service II Moments
0.95 Yield Moment

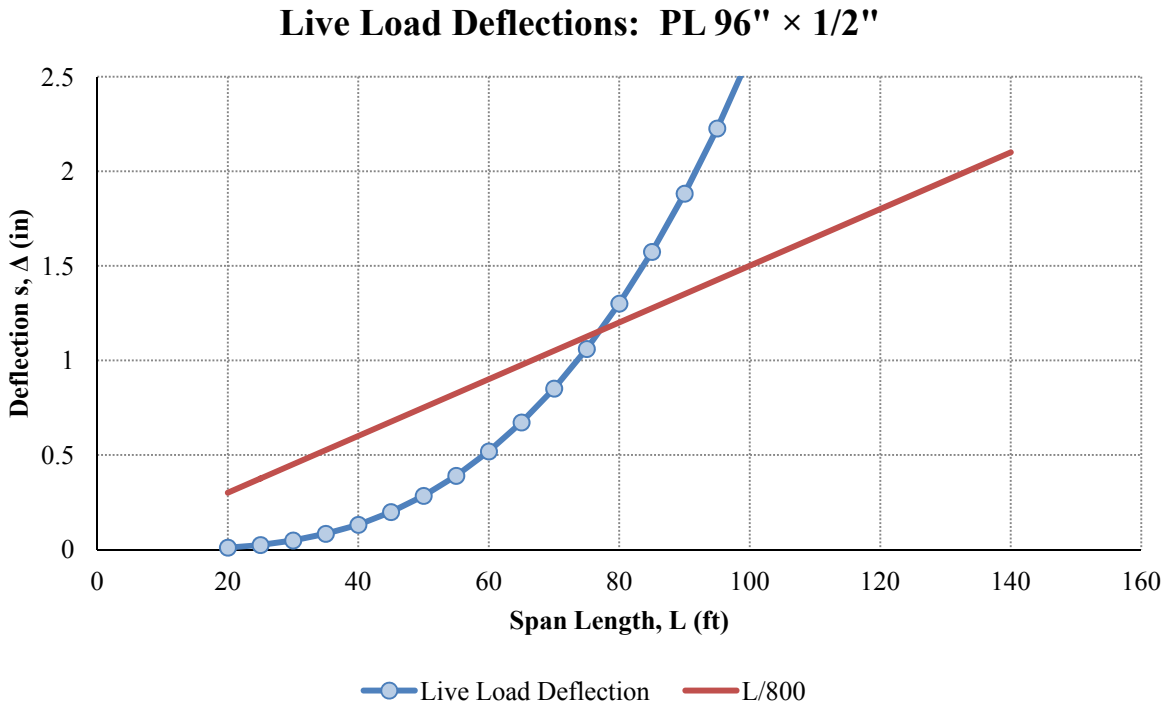
Live Load Deflections: PL 96" × 1/2"
Deflection s, Δ (in)
2.5
2
1.5
1
0.5
0
0
20
40
60
80
100
120
140
160
Span Length, L (ft)
Live Load Deflection
L/800

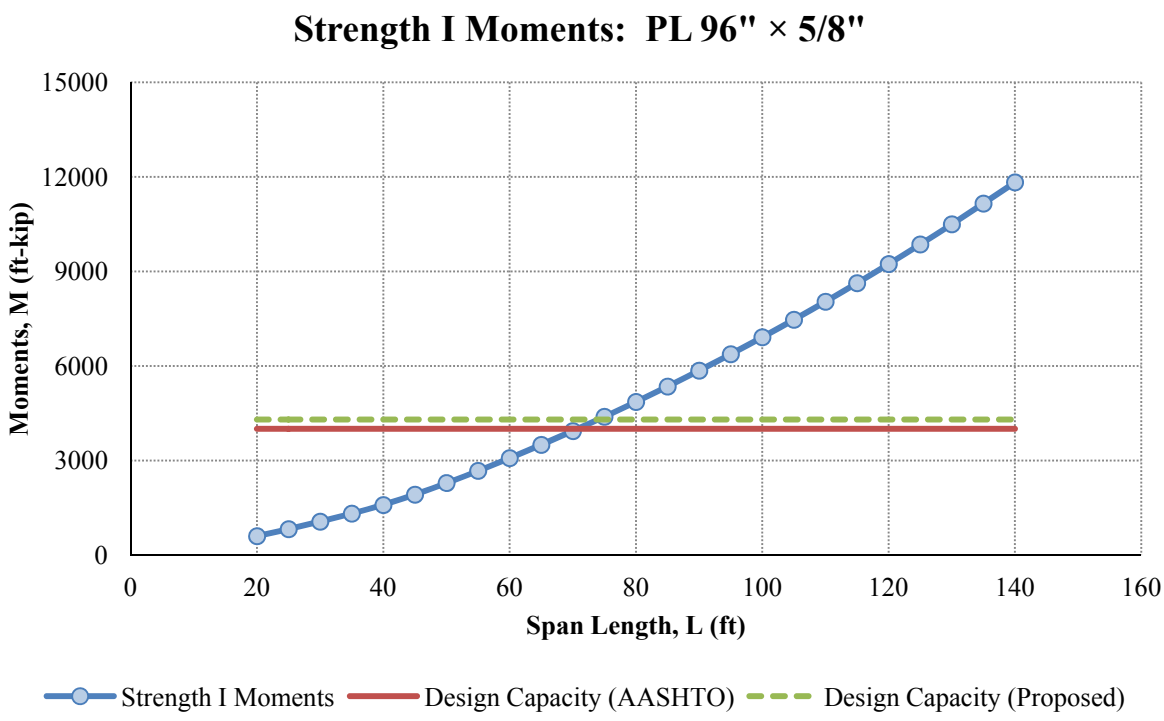
Strength I Moments: PL 96" × 5/8"
15000
12000
9000
6000
3000
0
Moments, M (ft-kip)
0
20
40
60
80
100
120
140
160
Span Length, L (ft)
Strength I Moments
Design Capacity (AASHTO)
Design Capacity (Proposed)

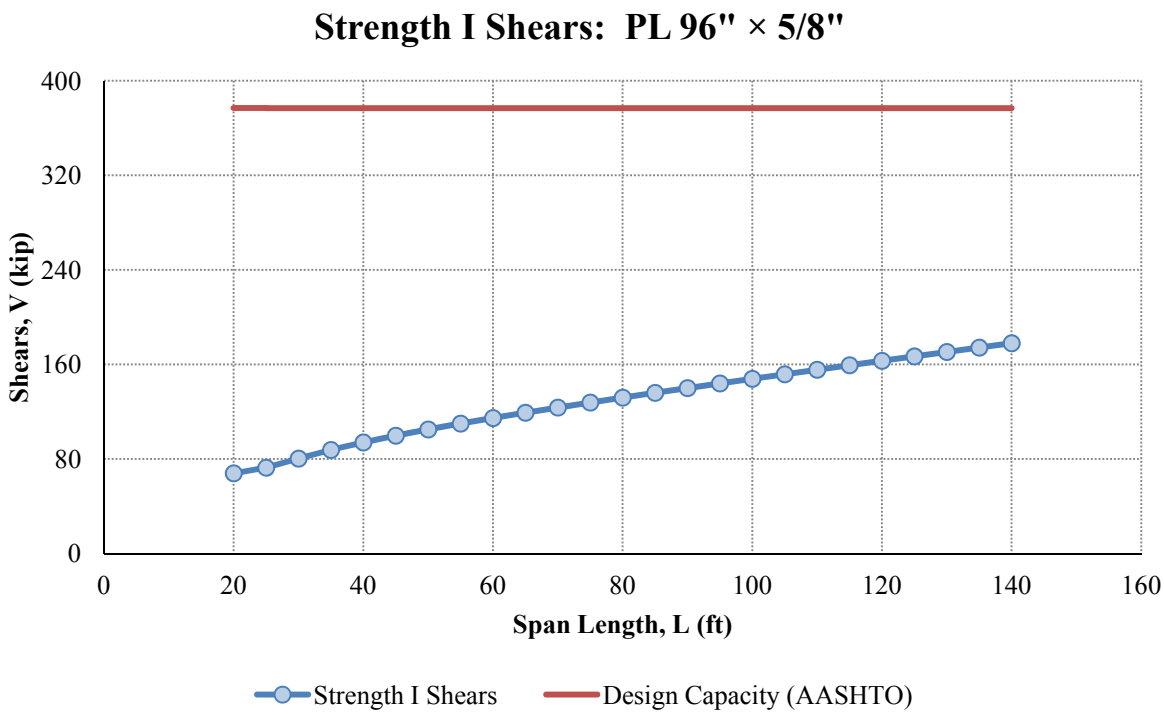
Strength I Shears: PL 96" × 5/8"
400
320
240
160
80
0
Shears, V (kip)
0
20
40
60
80
100
120
140
160
Span Length, L (ft)
Strength I Shears
Design Capacity (AASHTO)

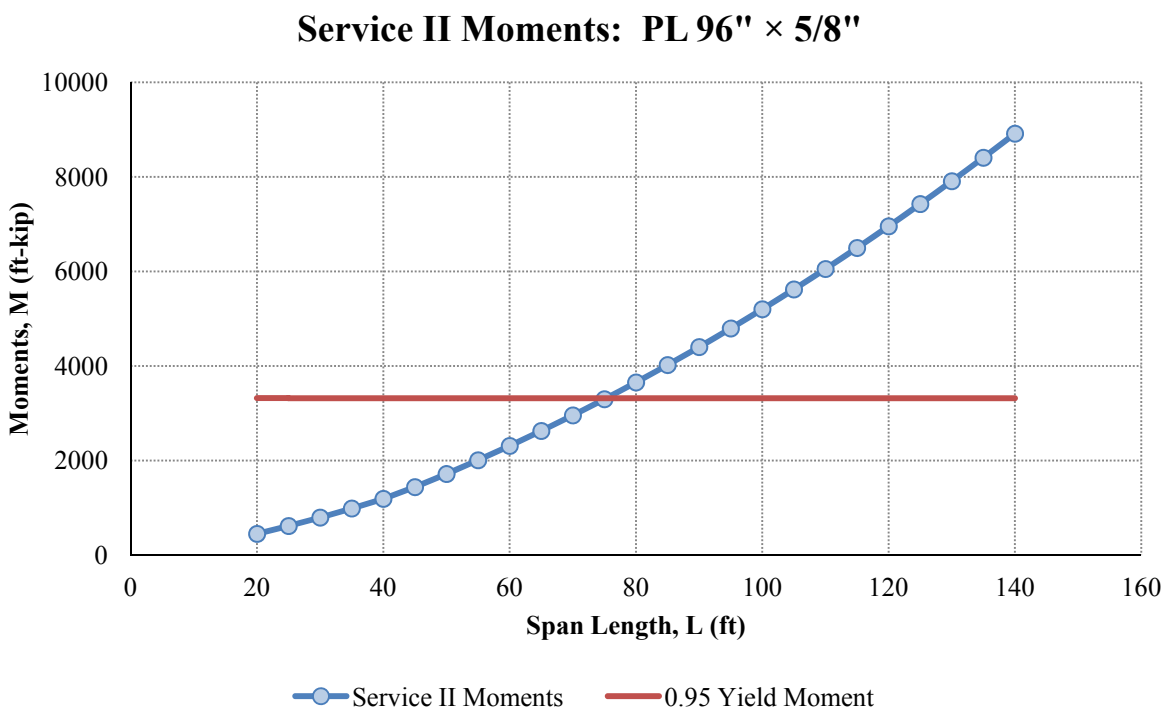
Service II Moments: PL 96" × 5/8"
Moments, M (ft-kip)
10000
8000
6000
4000
2000
0
0
20
40
60
80
100
120
140
160
Span Length, L (ft)
Service II Moments
0.95 Yield Moment

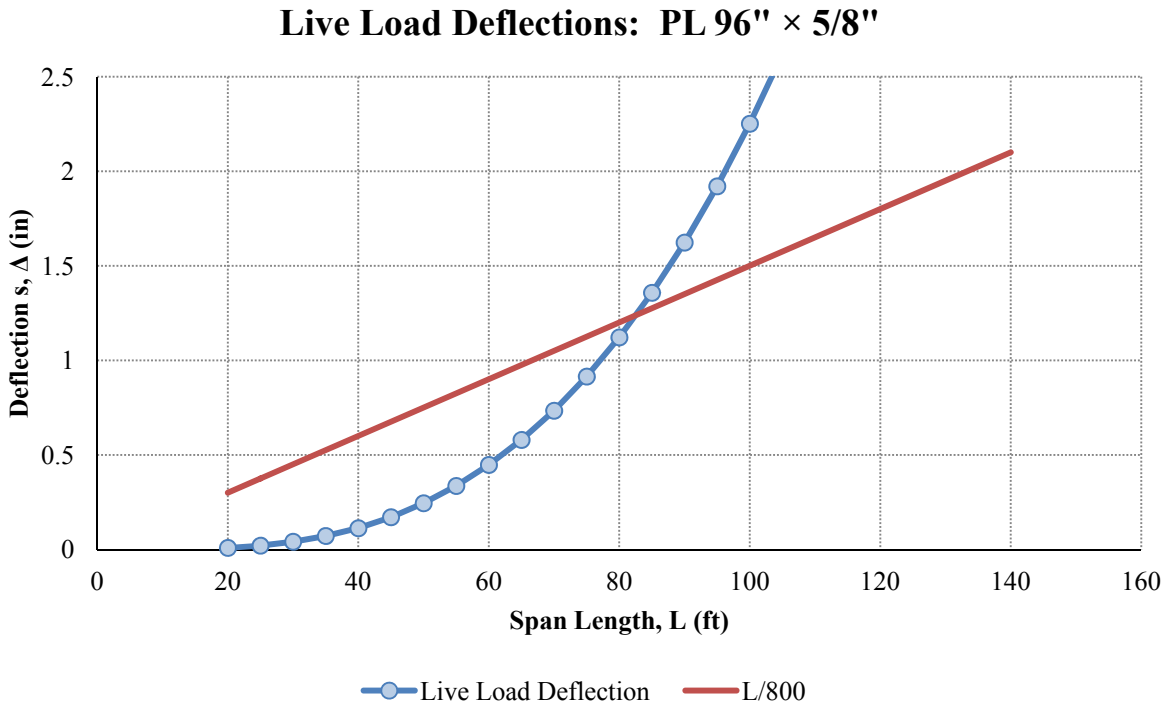
Live Load Deflections: PL 96" × 5/8"
Deflection s, Δ (in)
2.5
2
1.5
1
0.5
0
0
20
40
60
80
100
120
140
160
Span Length, L (ft)
Live Load Deflection
L/800

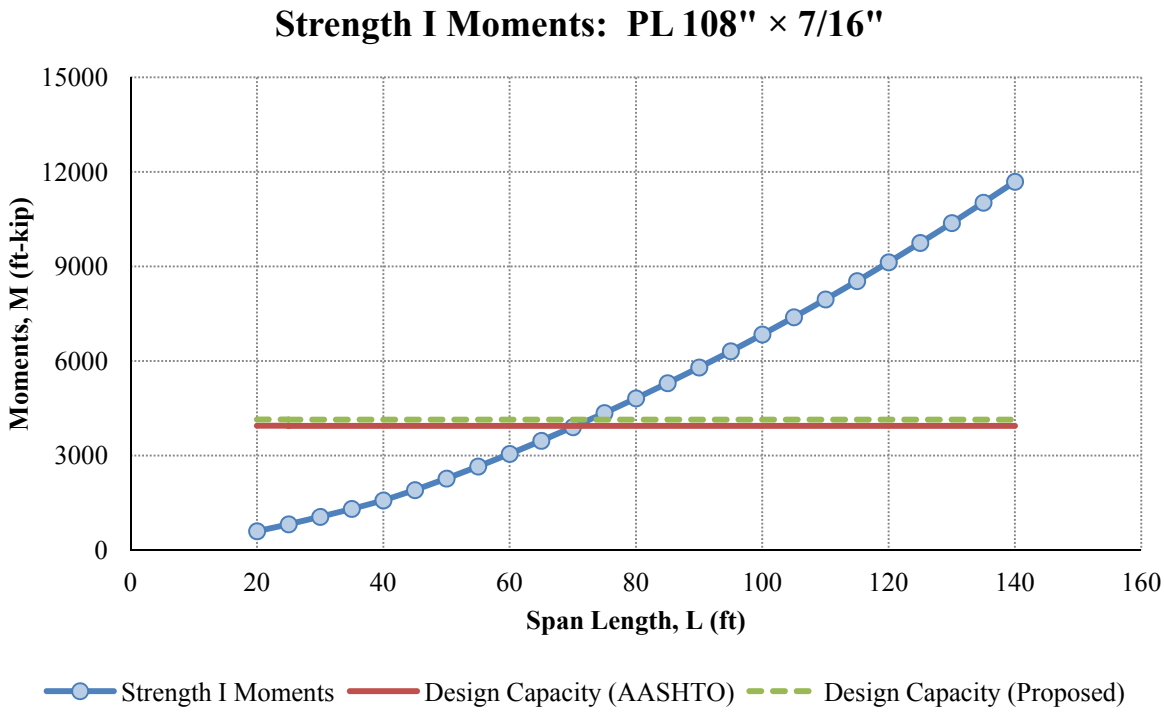
Strength I Moments: PL 108" × 7/16"
15000
12000
9000
6000
3000
0
Moments, M (ft-kip)
0
20
40
60
80
100
120
140
160
Span Length, L (ft)
Strength I Moments
Design Capacity (AASHTO)
Design Capacity (Proposed)

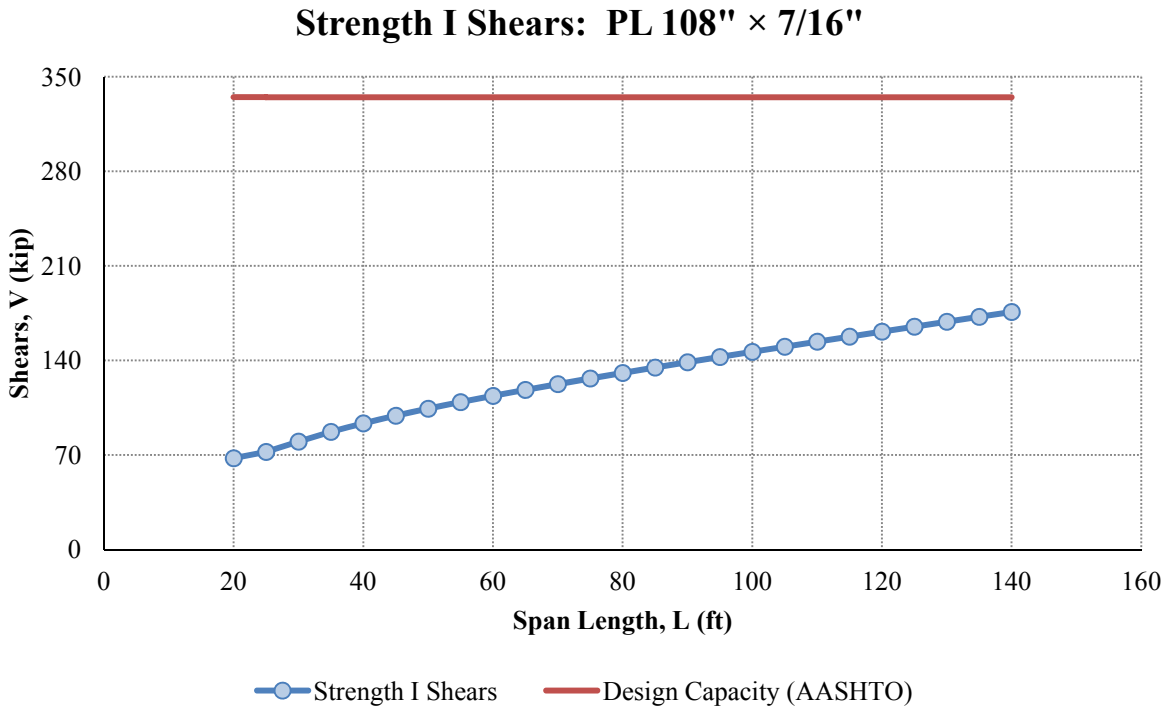
Strength I Shears: PL 108" × 7/16"
350
280
210
140
70
0
Shears, V (kip)
0
20
40
60
80
100
120
140
160
Span Length, L (ft)
Strength I Shears
Design Capacity (AASHTO)

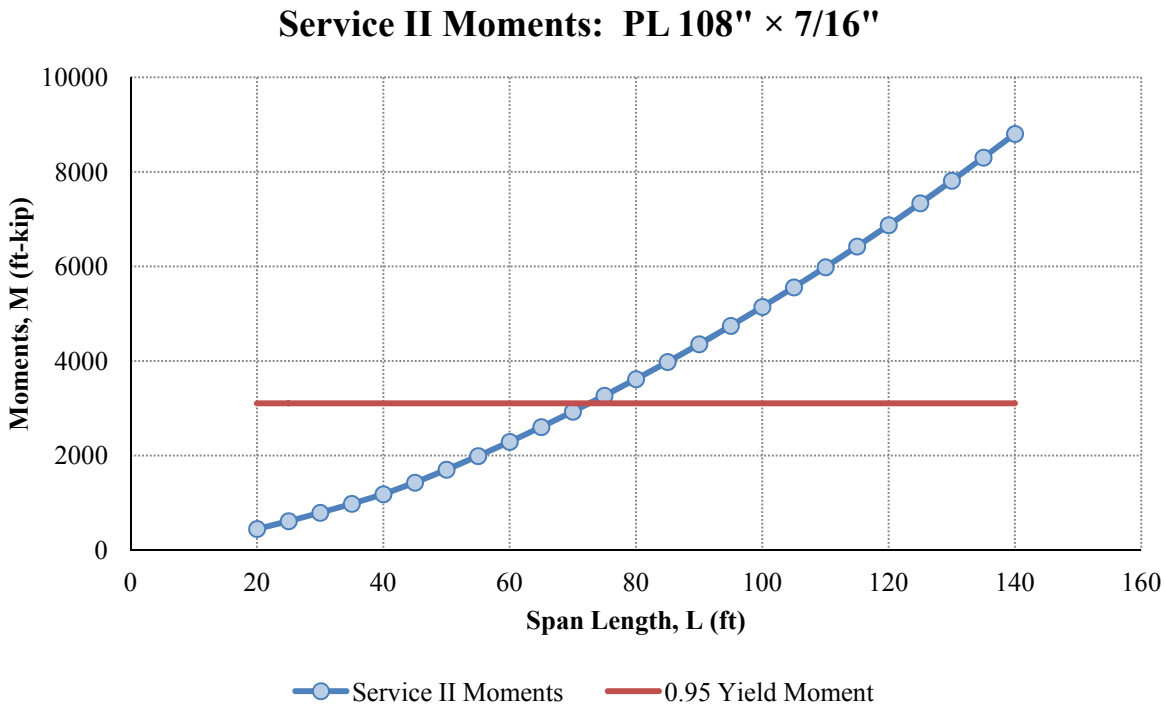
Service II Moments: PL 108" × 7/16"
Moments, M (ft-kip)
10000
8000
6000
4000
2000
0
0
20
40
60
80
100
120
140
160
Span Length, L (ft)
Service II Moments
0.95 Yield Moment

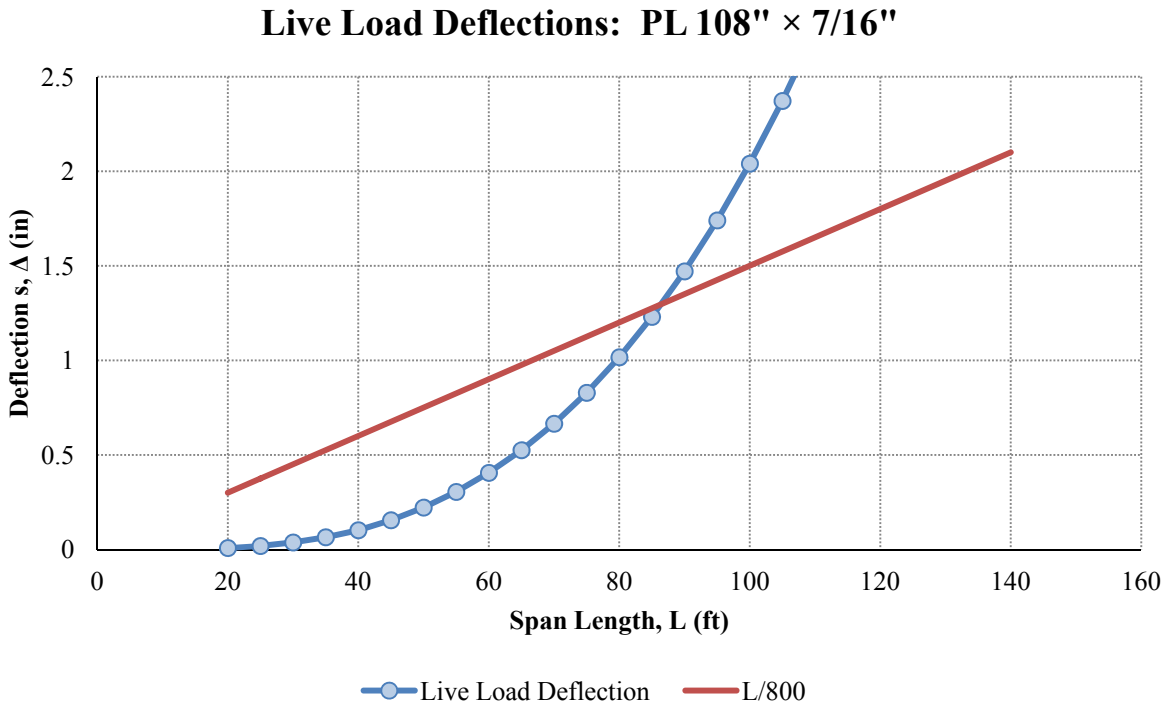
Live Load Deflections: PL 108" × 7/16"
Deflection s, Δ (in)
2.5
2
1.5
1
0.5
0
0
20
40
60
80
100
120
140
160
Span Length, L (ft)
Live Load Deflection
L/800

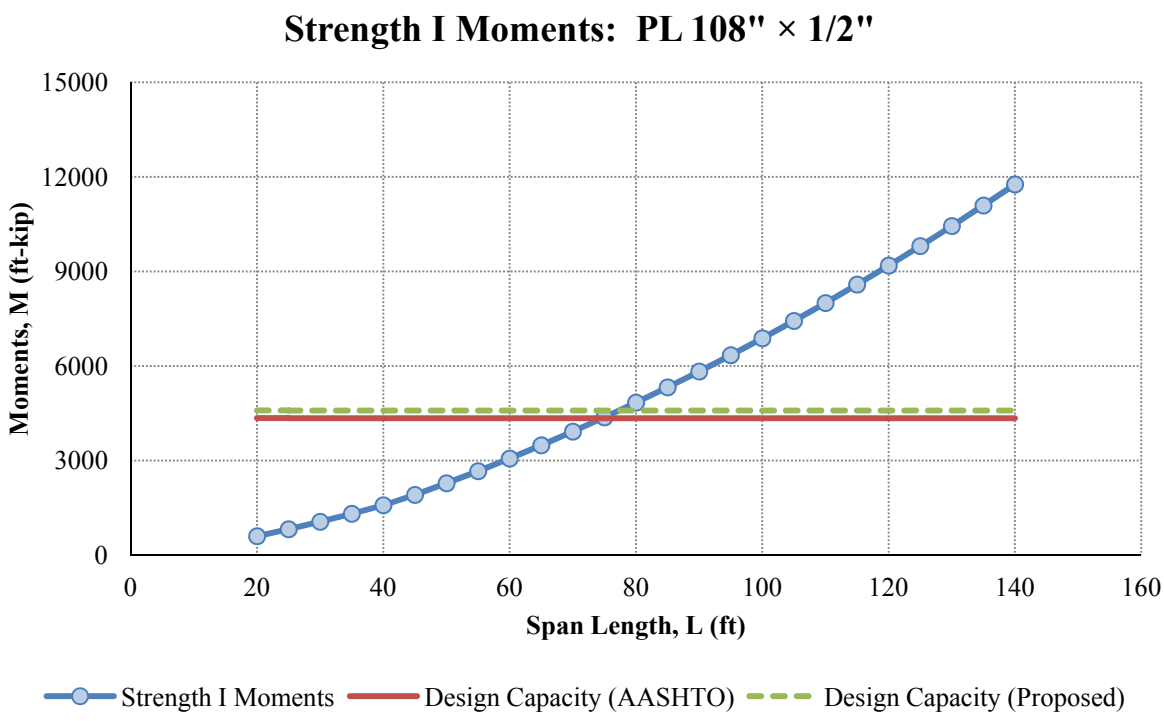
Strength I Moments: PL 108" × 1/2"
15000
12000
9000
6000
3000
0
Moments, M (ft-kip)
0
20
40
60
80
100
120
140
160
Span Length, L (ft)
Strength I Moments
Design Capacity (AASHTO)
Design Capacity (Proposed)

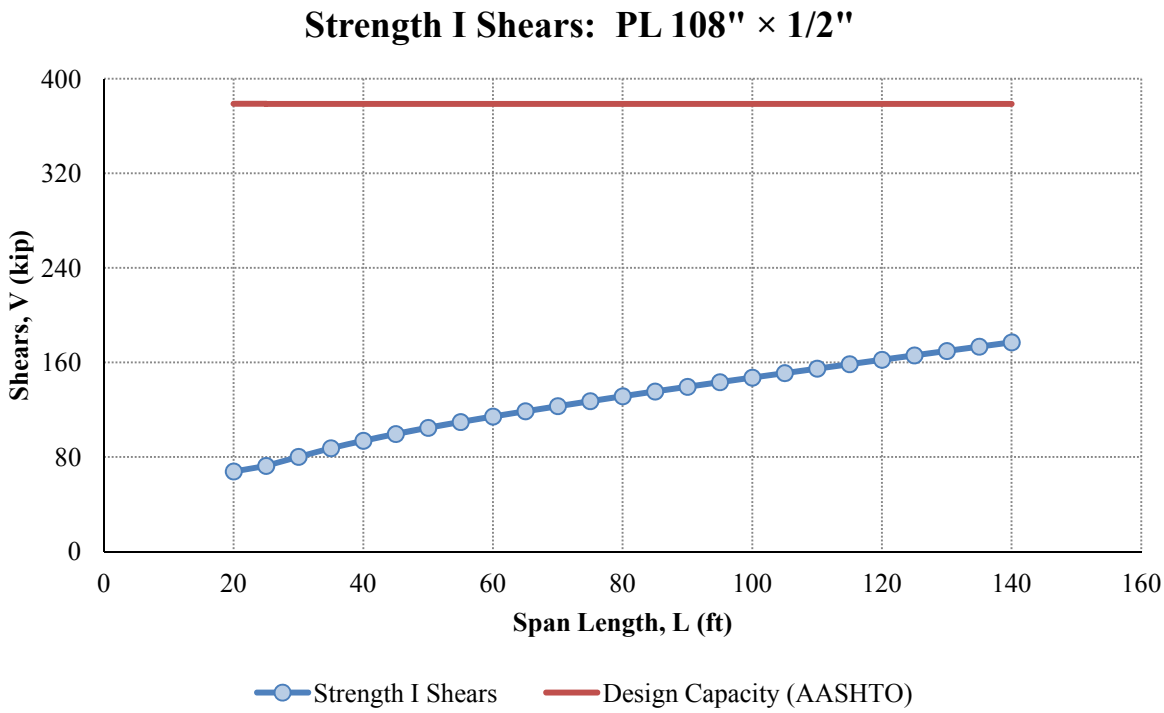
Strength I Shears: PL 108" × 1/2"
400
320
240
160
80
0
Shears, V (kip)
0
20
40
60
80
100
120
140
160
Span Length, L (ft)
Strength I Shears
Design Capacity (AASHTO)

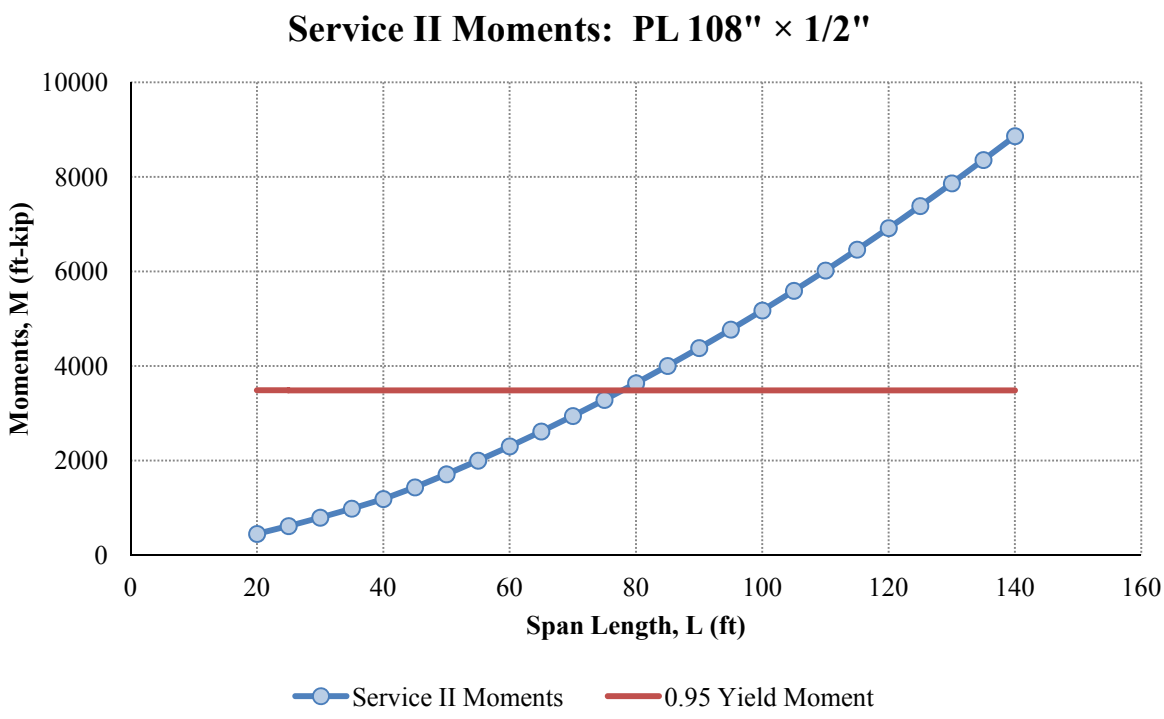
Service II Moments: PL 108" × 1/2"
Moments, M (ft-kip)
10000
8000
6000
4000
2000
0
0
20
40
60
80
100
120
140
160
Span Length, L (ft)
Service II Moments
0.95 Yield Moment

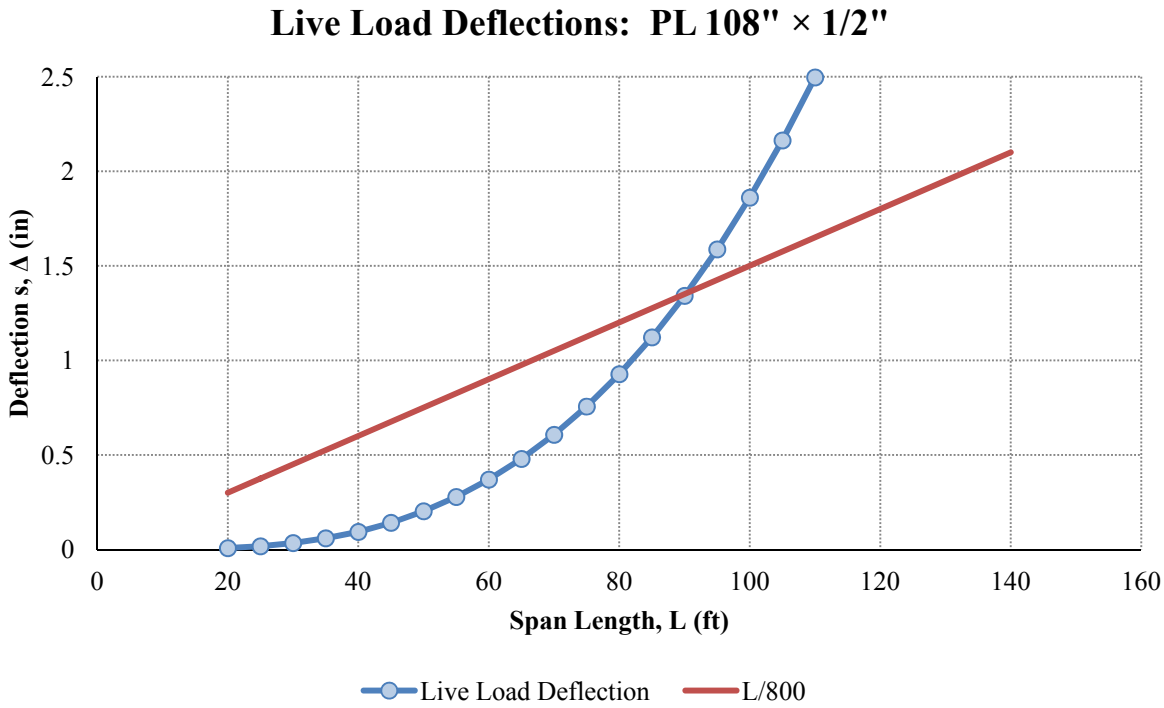
Live Load Deflections: PL 108" × 1/2"
Deflection s, Δ (in)
2.5
2
1.5
1
0.5
0
0
20
40
60
80
100
120
140
160
Span Length, L (ft)
Live Load Deflection
L/800

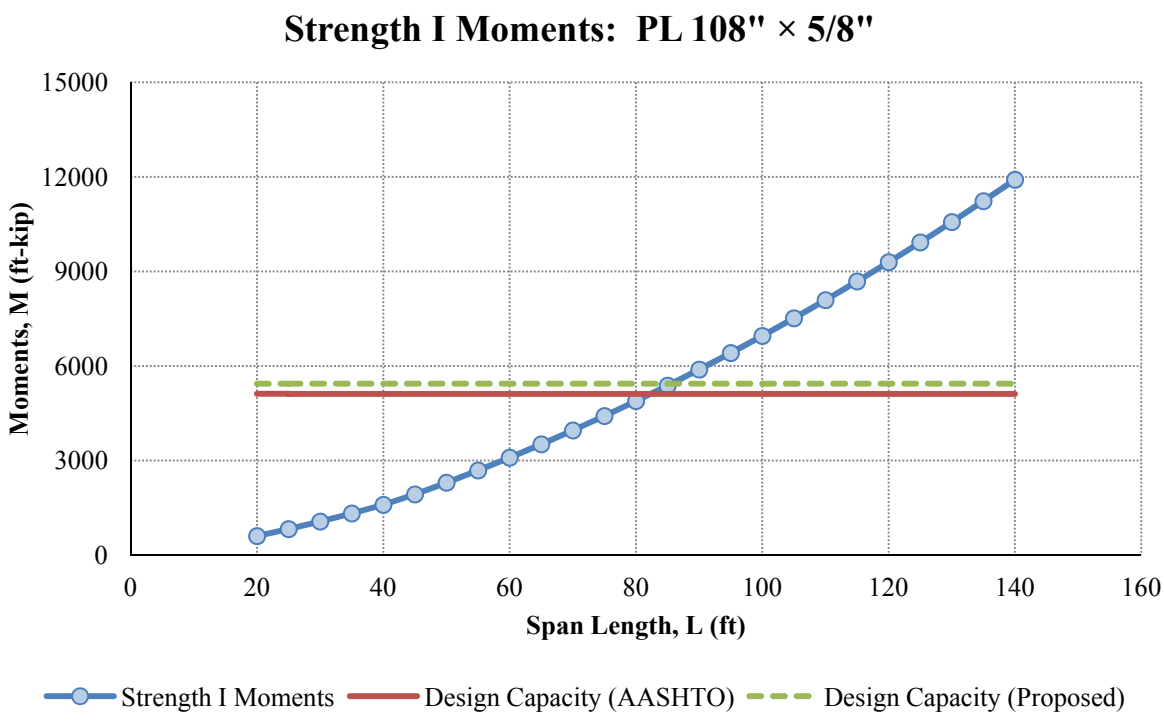
Strength I Moments: PL 108" × 5/8"
15000
12000
9000
6000
3000
0
Moments, M (ft-kip)
0
20
40
60
80
100
120
140
160
Span Length, L (ft)
Strength I Moments
Design Capacity (AASHTO)
Design Capacity (Proposed)

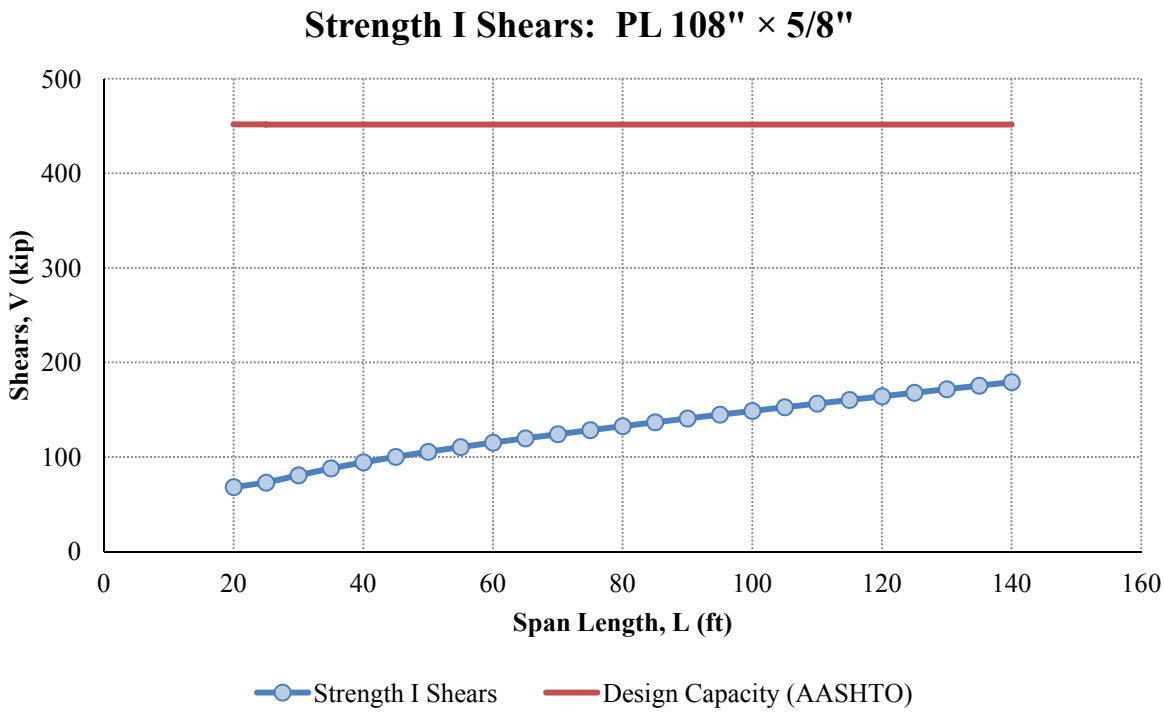
Strength I Shears: PL 108" × 5/8"
500
400
300
200
100
0
Shears, V (kip)
0
20
40
60
80
100
120
140
160
Span Length, L (ft)
Strength I Shears
Design Capacity (AASHTO)

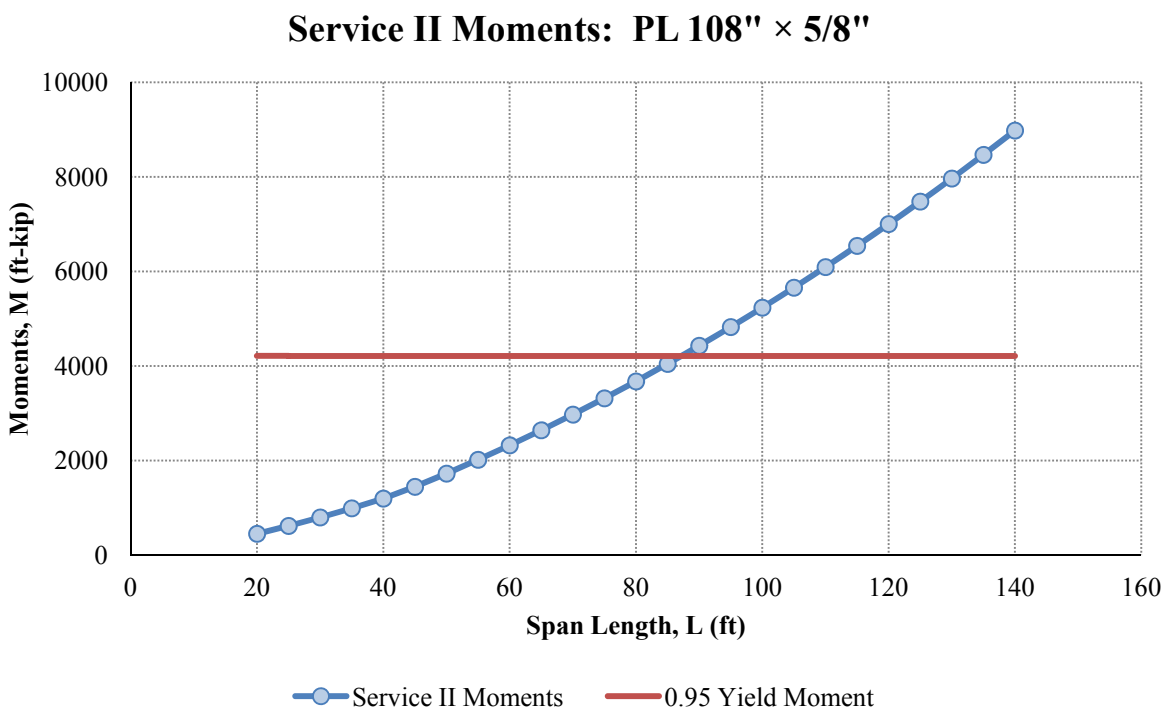
Service II Moments: PL 108" × 5/8"
Moments, M (ft-kip)
10000
8000
6000
4000
2000
0
0
20
40
60
80
100
120
140
160
Span Length, L (ft)
Service II Moments
0.95 Yield Moment

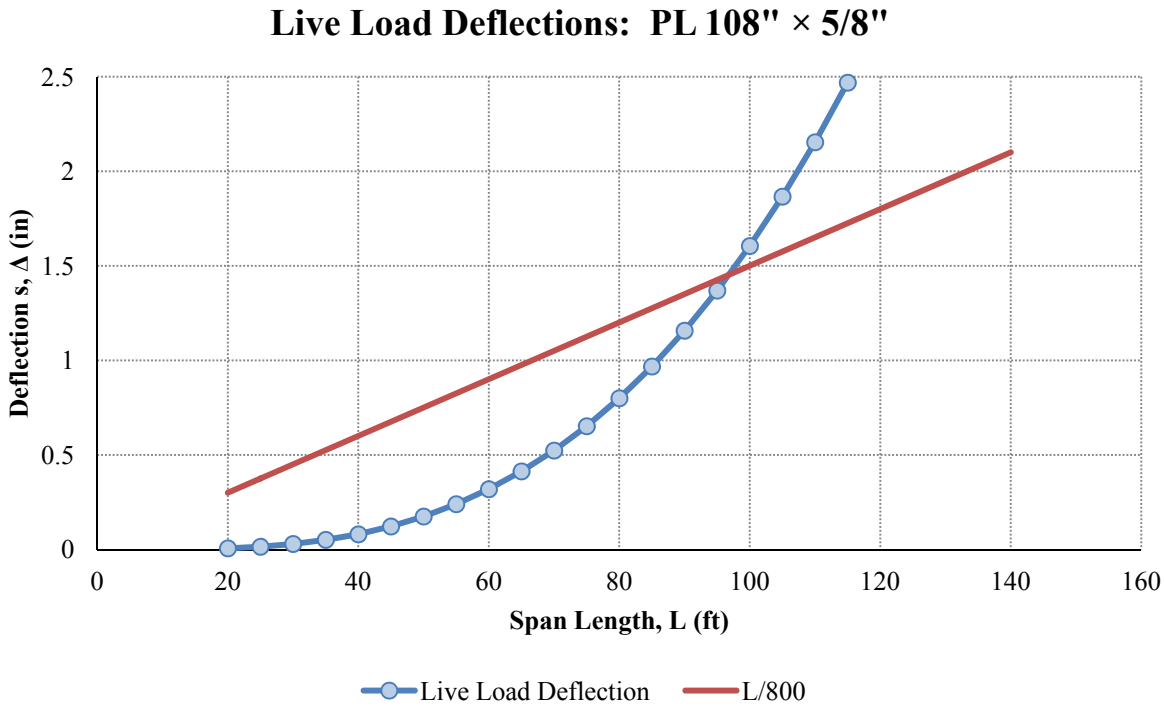
Live Load Deflections: PL 108" × 5/8"
Deflection s, Δ (in)
2.5
2
1.5
1
0.5
0
0
20
40
60
80
100
120
140
160
Span Length, L (ft)
Live Load Deflection
L/800

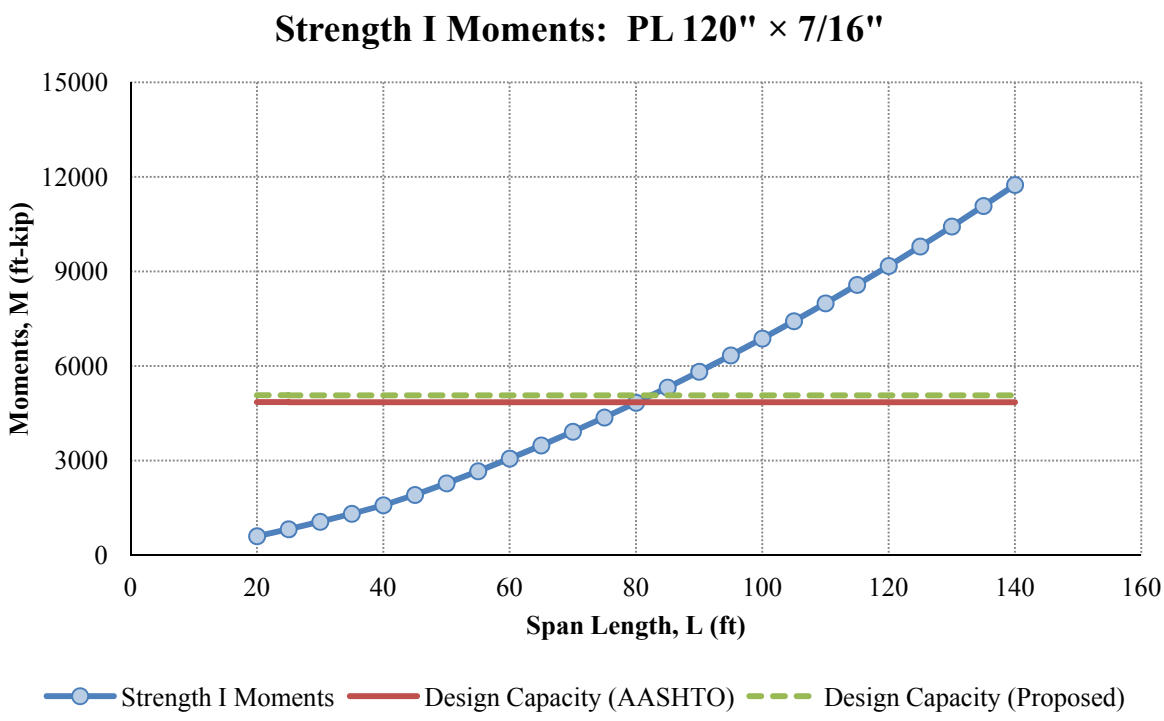
Strength I Moments: PL 120" × 7/16"
Moments, M (ft-kip)
15000
12000
9000
6000
3000
0
0
20
40
60
80
100
120
140
160
Span Length, L (ft)
Strength I Moments
Design Capacity (AASHTO)
Design Capacity (Proposed)

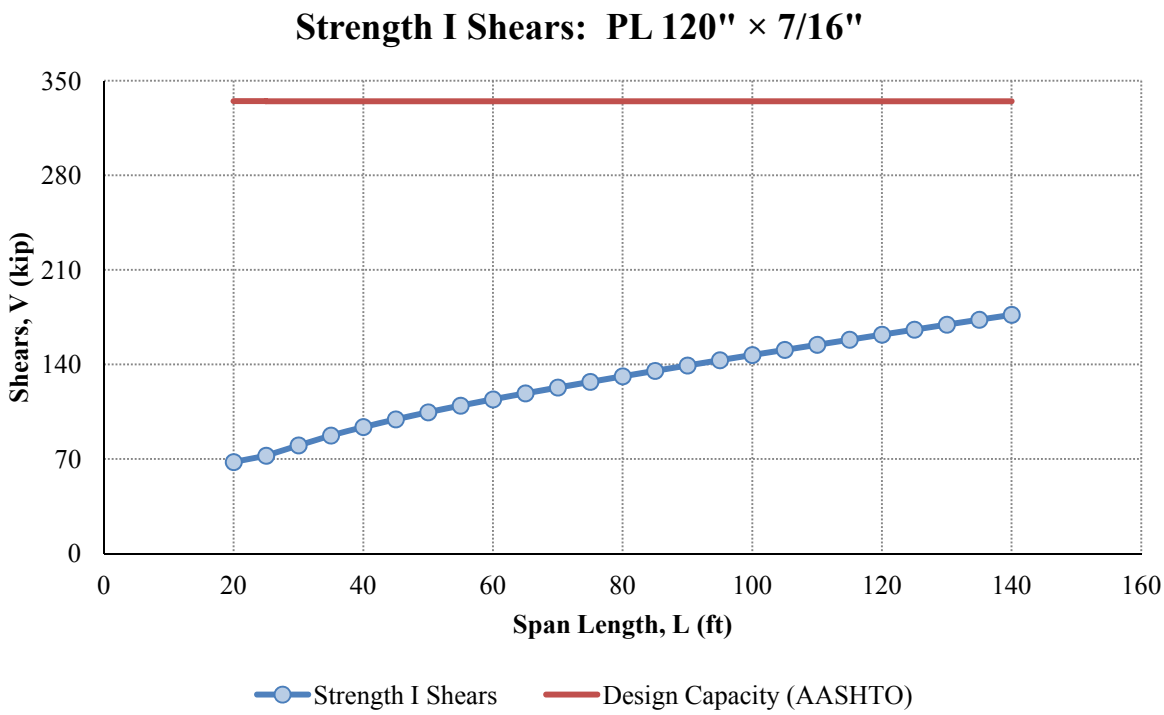
Strength I Shears: PL 120" × 7/16"
Shears, V (kip)
350
280
210
140
70
0
0
20
40
60
80
100
120
140
160
Span Length, L (ft)
Strength I Shears
Design Capacity (AASHTO)

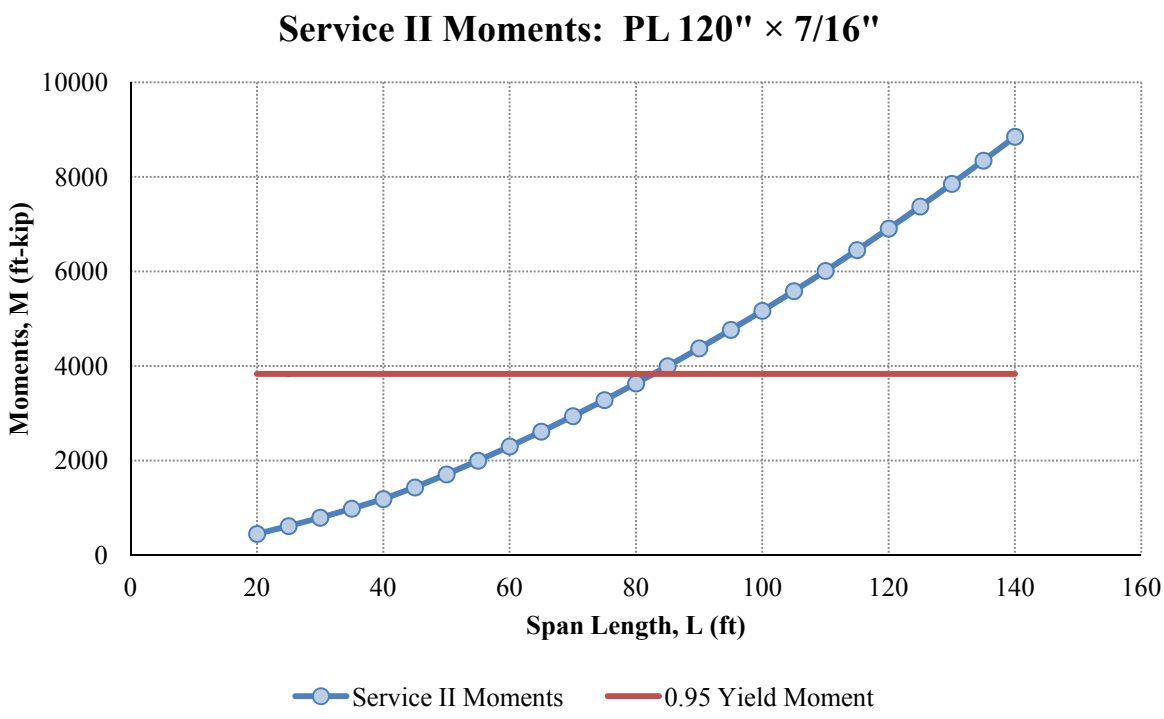
Service II Moments: PL 120" × 7/16"
Moments, M (ft-kip)
10000
8000
6000
4000
2000
0
0
20
40
60
80
100
120
140
160
Span Length, L (ft)
Service II Moments
0.95 Yield Moment

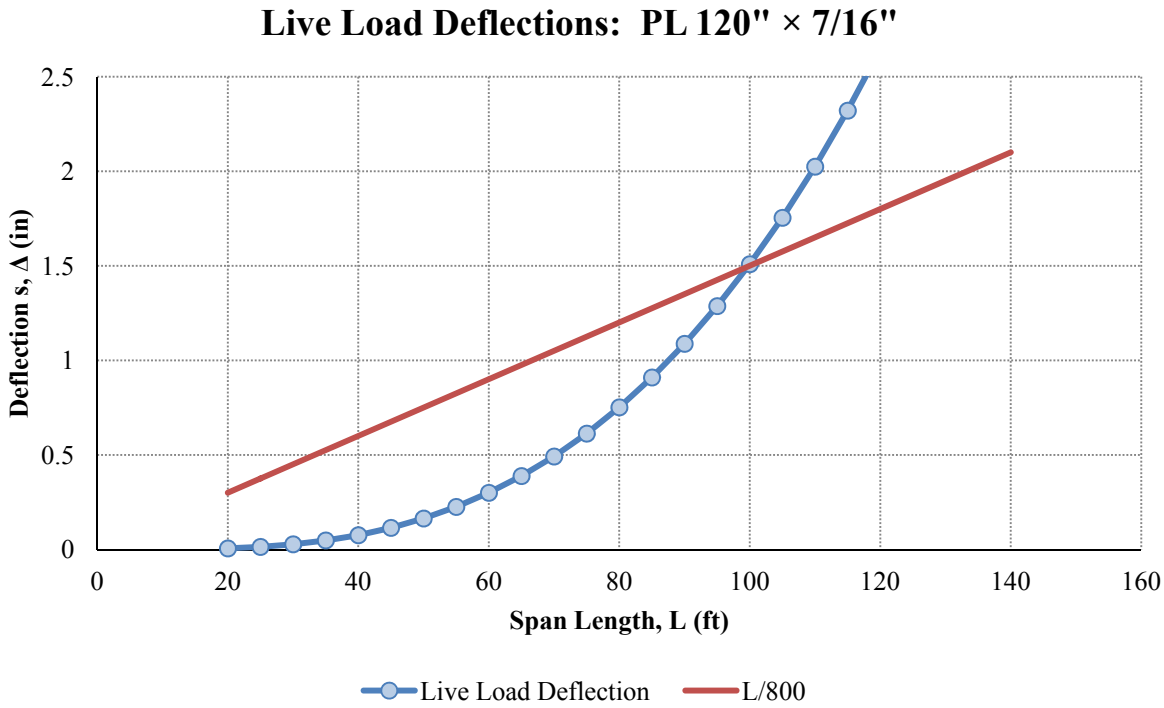
Live Load Deflections: PL 120" × 7/16"
Deflection s, Δ (in)
2.5
2
1.5
1
0.5
0
0
20
40
60
80
100
120
140
160
Span Length, L (ft)
Live Load Deflection
L/800

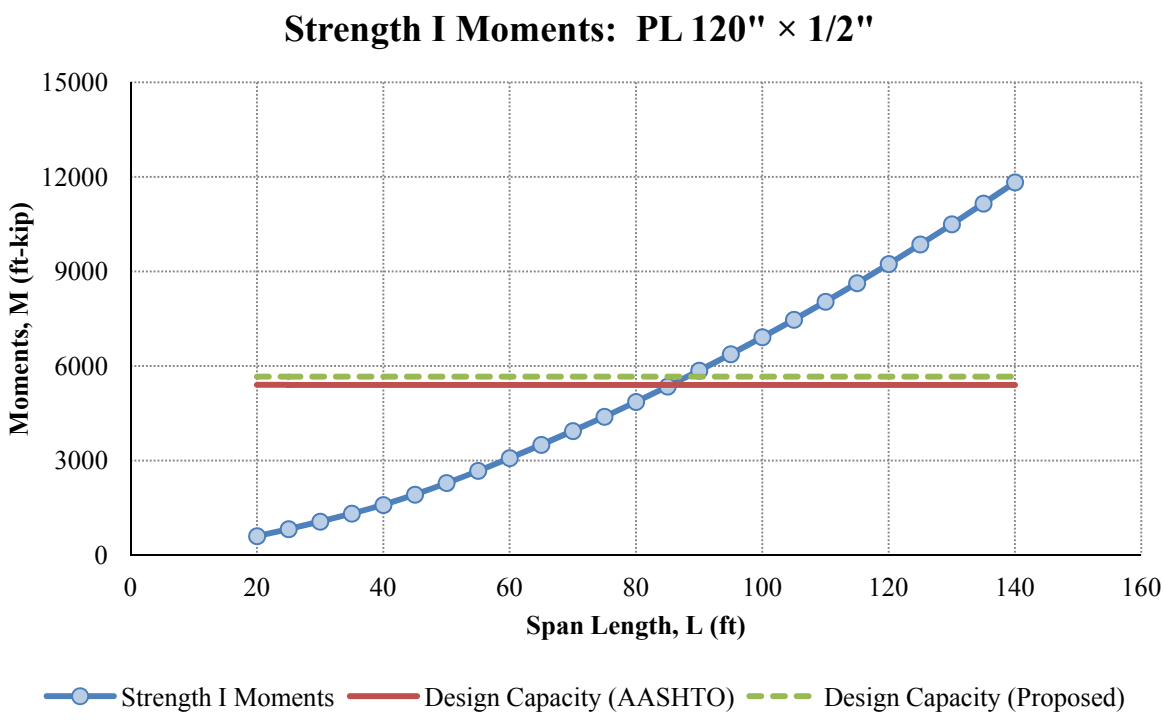
Strength I Moments: PL 120" × 1/2"
15000
12000
9000
6000
3000
0
Moments, M (ft-kip)
0
20
40
60
80
100
120
140
160
Span Length, L (ft)
Strength I Moments
Design Capacity (AASHTO)
Design Capacity (Proposed)

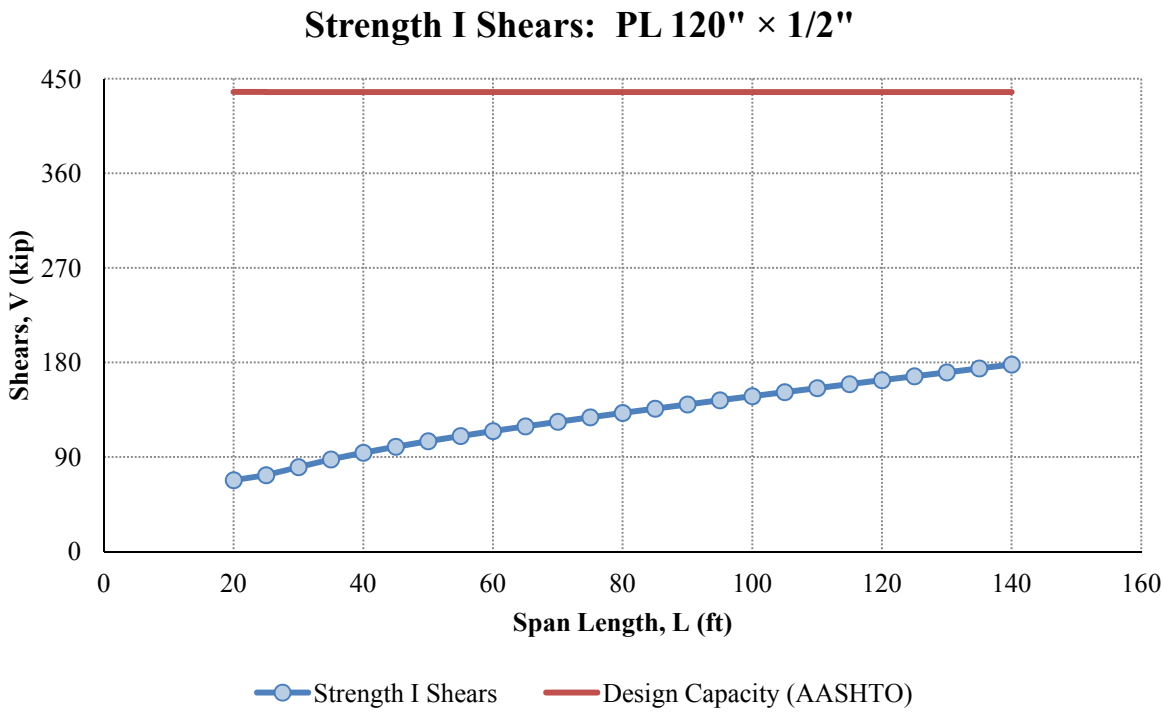
Strength I Shears: PL 120" × 1/2"
450
360
270
180
90
0
Shears, V (kip)
0
20
40
60
80
100
120
140
160
Span Length, L (ft)
Strength I Shears
Design Capacity (AASHTO)

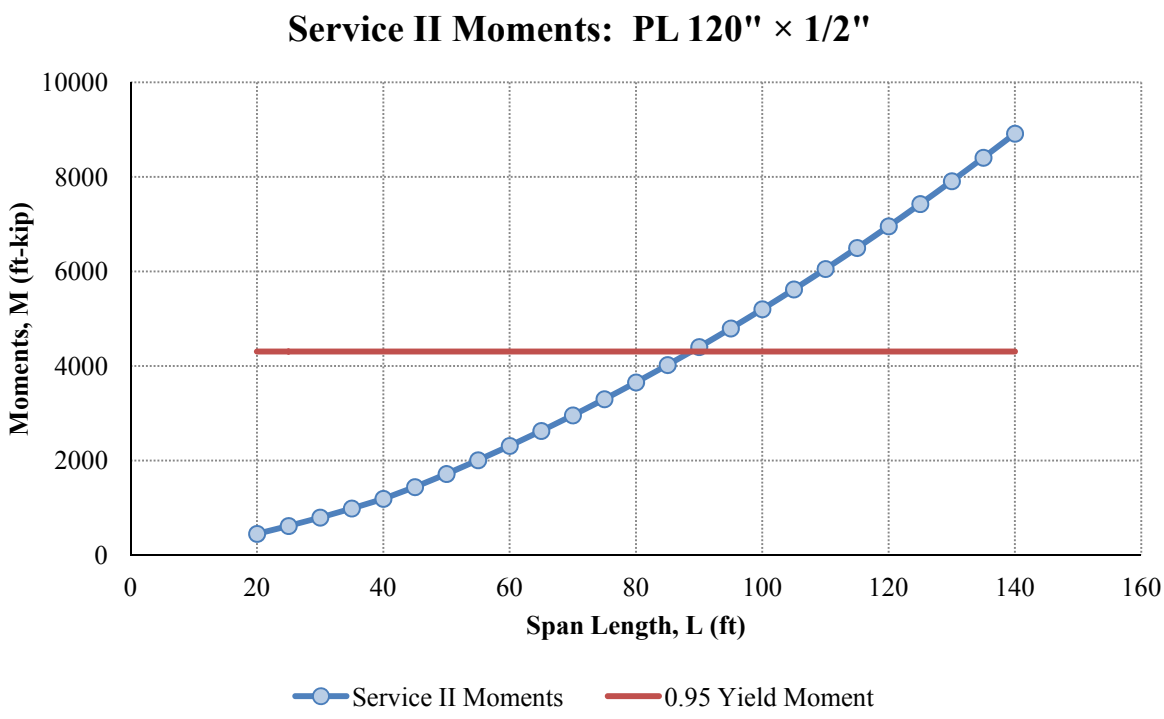
Service II Moments: PL 120" × 1/2"
Moments, M (ft-kip)
10000
8000
6000
4000
2000
0
0
20
40
60
80
100
120
140
160
Span Length, L (ft)
Service II Moments
0.95 Yield Moment

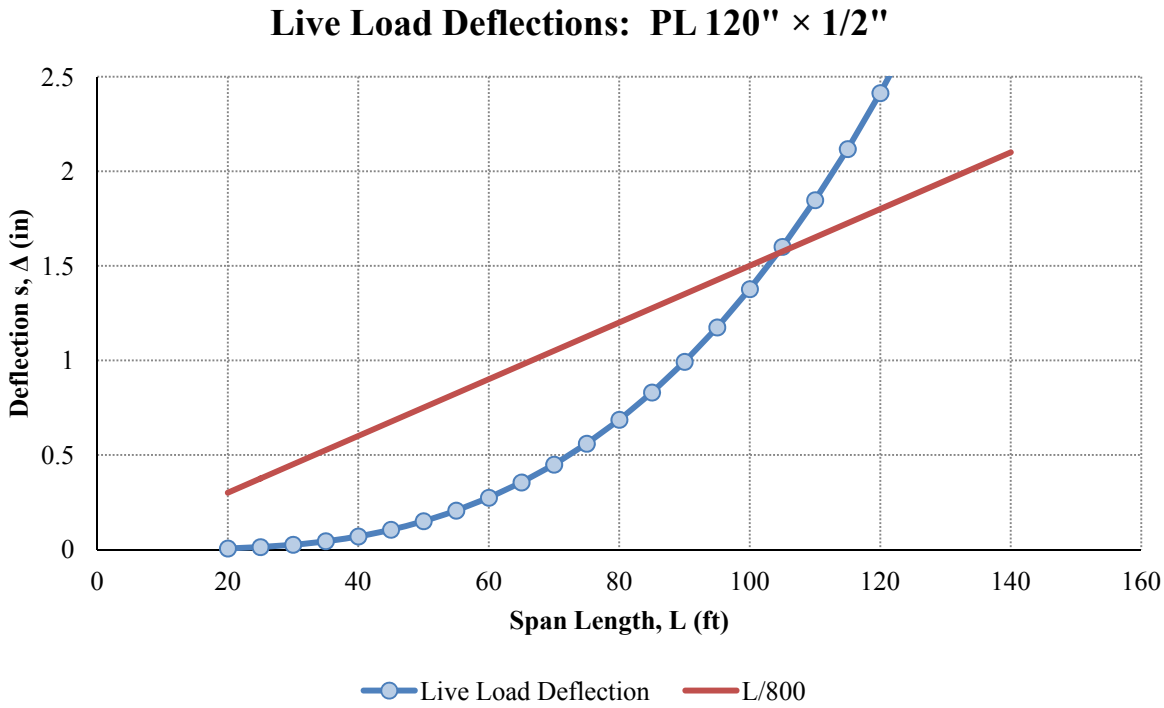
Live Load Deflections: PL 120" × 1/2"
Deflection s, Δ (in)
2.5
2
1.5
1
0.5
0
0
20
40
60
80
100
120
140
160
Span Length, L (ft)
Live Load Deflection
L/800

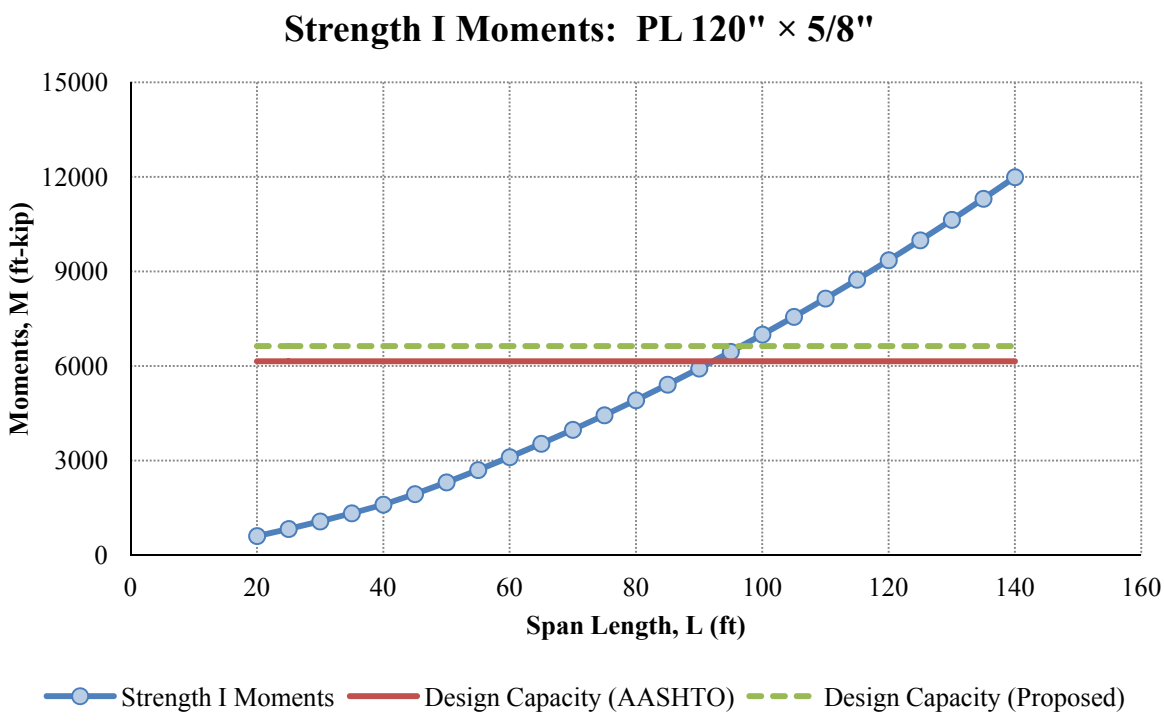
Strength I Moments: PL 120" × 5/8"
15000
12000
9000
6000
3000
0
Moments, M (ft-kip)
0
20
40
60
80
100
120
140
160
Span Length, L (ft)
Strength I Moments
Design Capacity (AASHTO)
Design Capacity (Proposed)

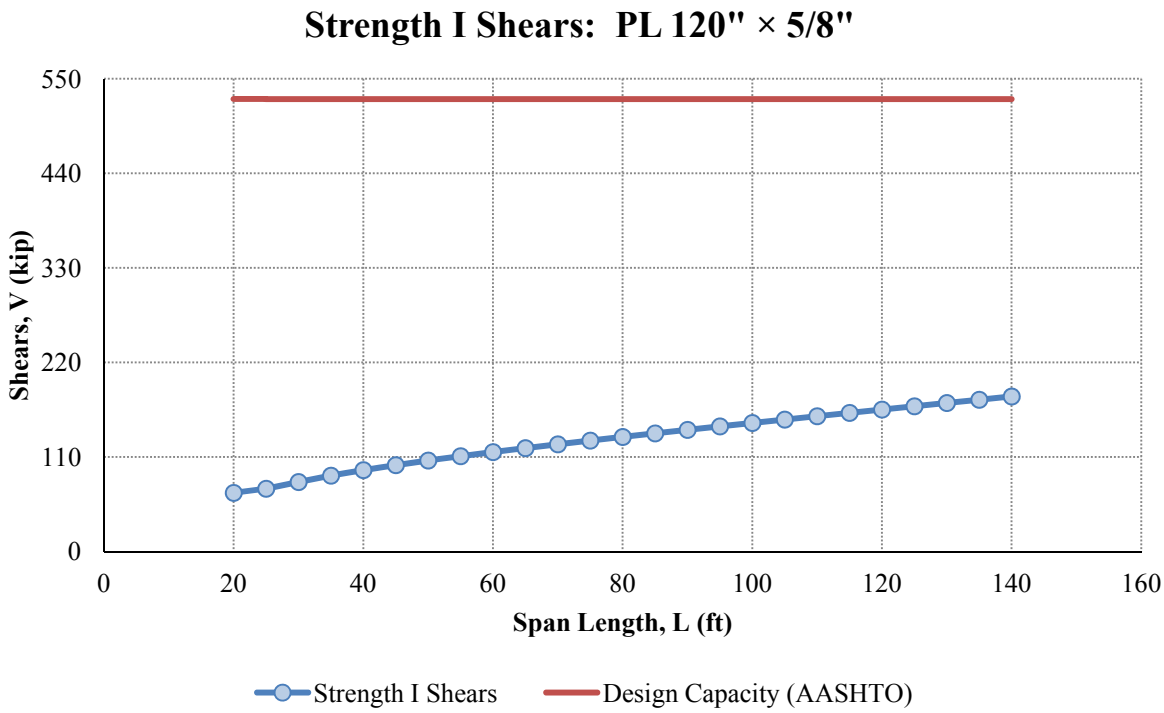
Strength I Shears: PL 120" × 5/8"
550
440
330
220
110
0
Shears, V (kip)
0
20
40
60
80
100
120
140
160
Span Length, L (ft)
Strength I Shears
Design Capacity (AASHTO)

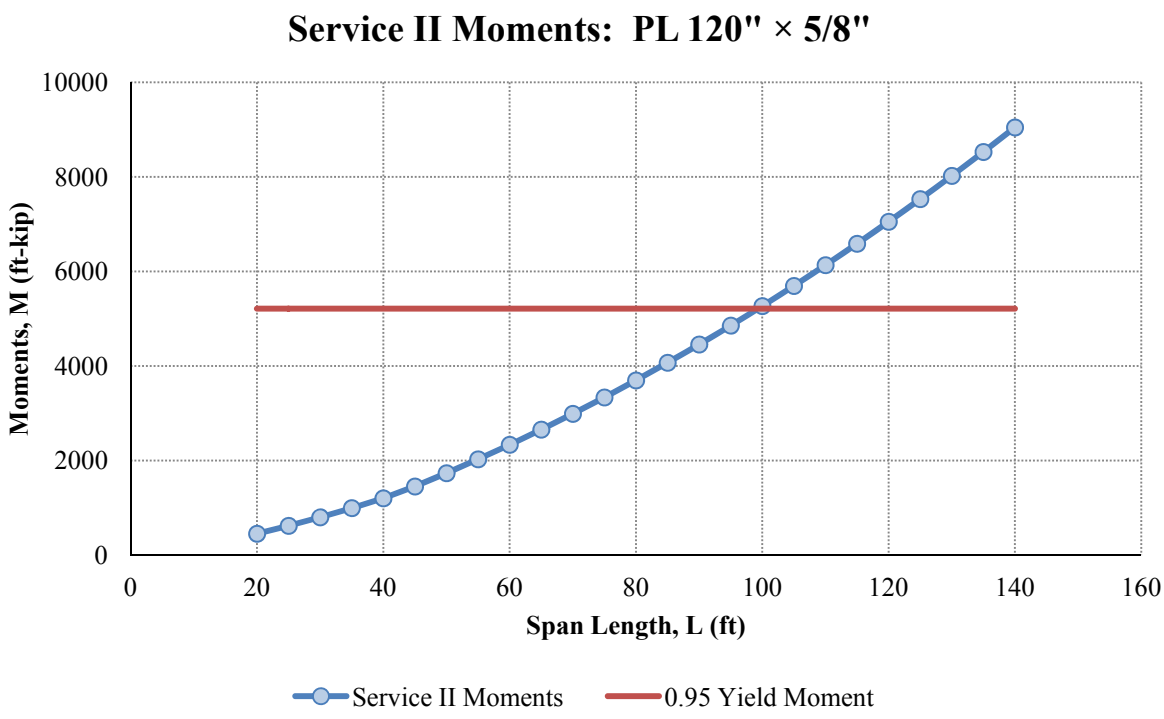
Service II Moments: PL 120" × 5/8"
Moments, M (ft-kip)
10000
8000
6000
4000
2000
0
0
20
40
60
80
100
120
140
160
Span Length, L (ft)
Service II Moments
0.95 Yield Moment

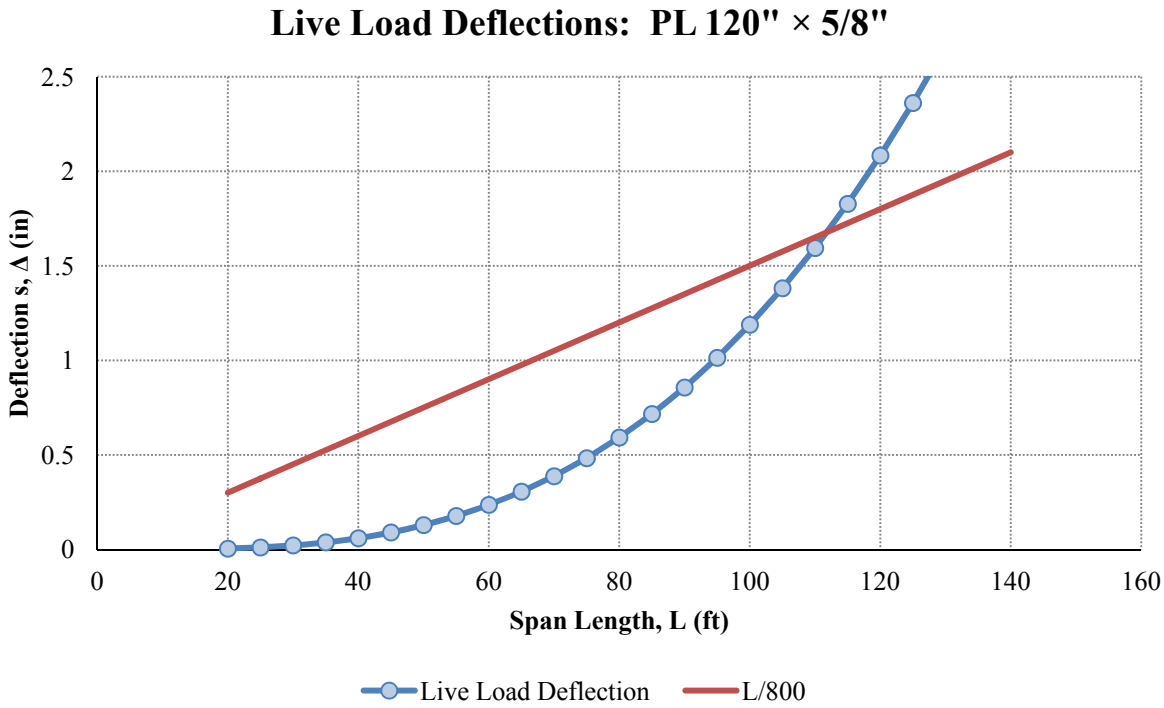
Live Load Deflections: PL 120" × 5/8"
Deflection s, Δ (in)
2.5
2
1.5
1
0.5
0
0
20
40
60
80
100
120
140
160
Span Length, L (ft)
Live Load Deflection
L/800

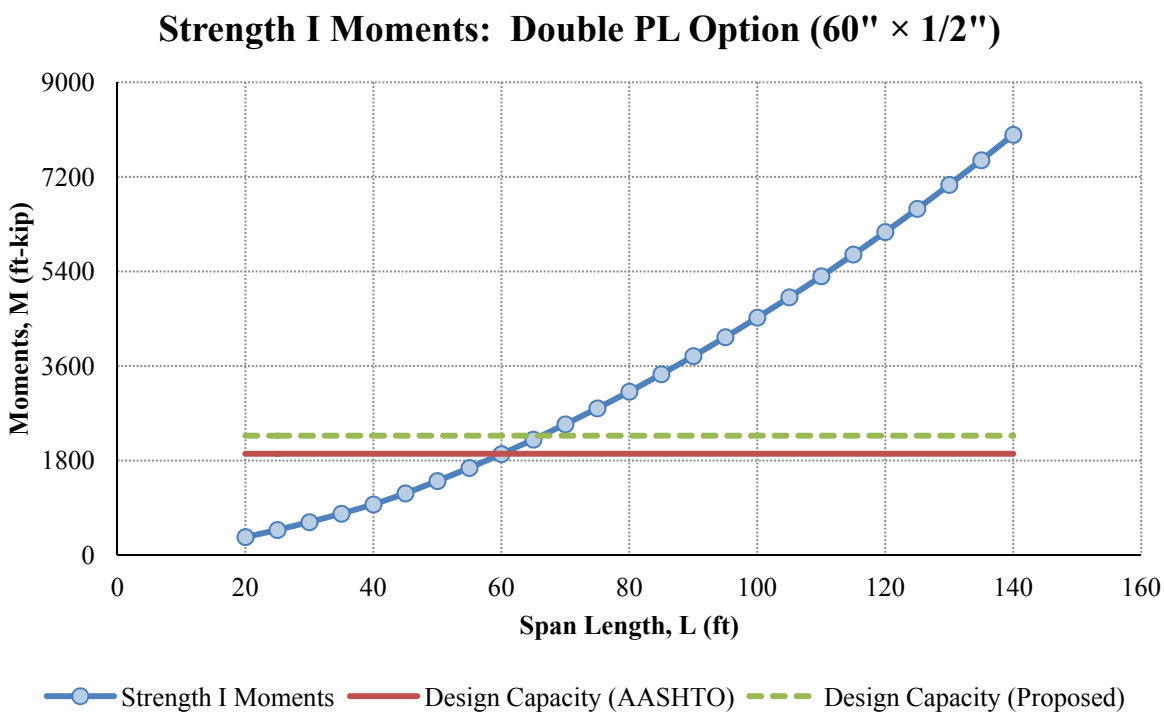
Strength I Moments: Double PL Option (60" × 1/2")
Moments, M (ft-kip)
9000
7200
5400
3600
1800
0
0
20
40
60
80
100
120
140
160
Span Length, L (ft)
Strength I Moments
Design Capacity (AASHTO)
Design Capacity (Proposed)

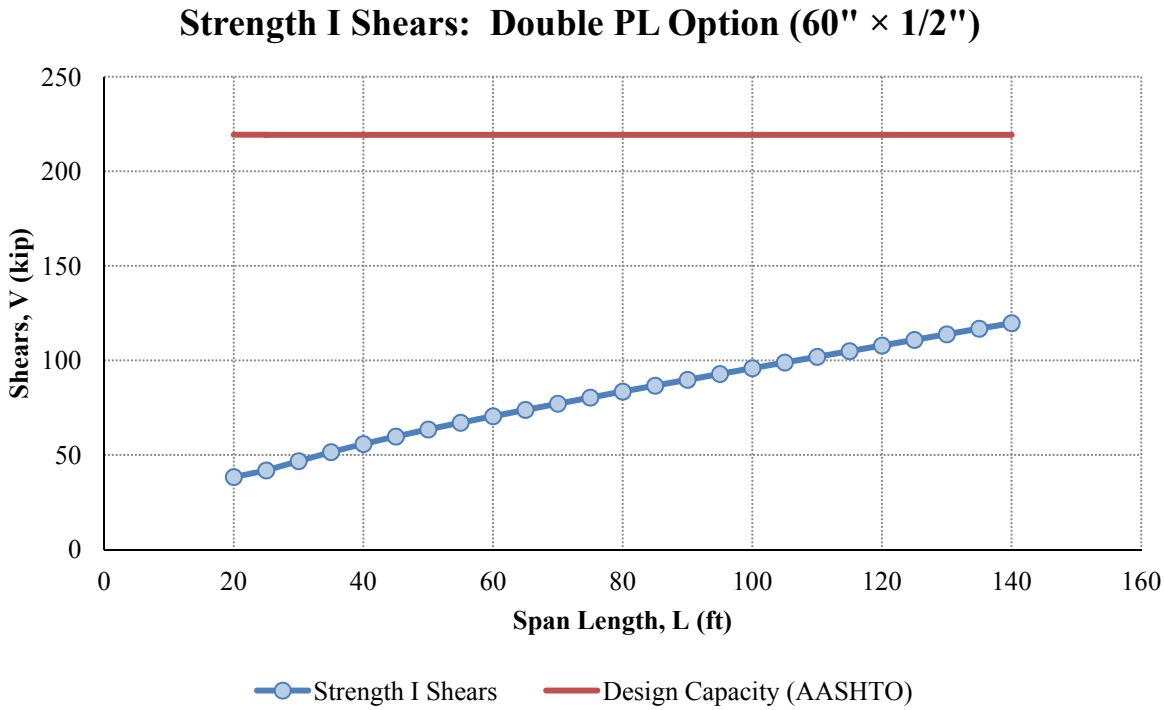
Strength I Shears: Double PL Option (60" × 1/2")
Shears, V (kip)
250
200
150
100
50
0
0
20
40
60
80
100
120
140
160
Span Length, L (ft)
Strength I Shears
Design Capacity (AASHTO)

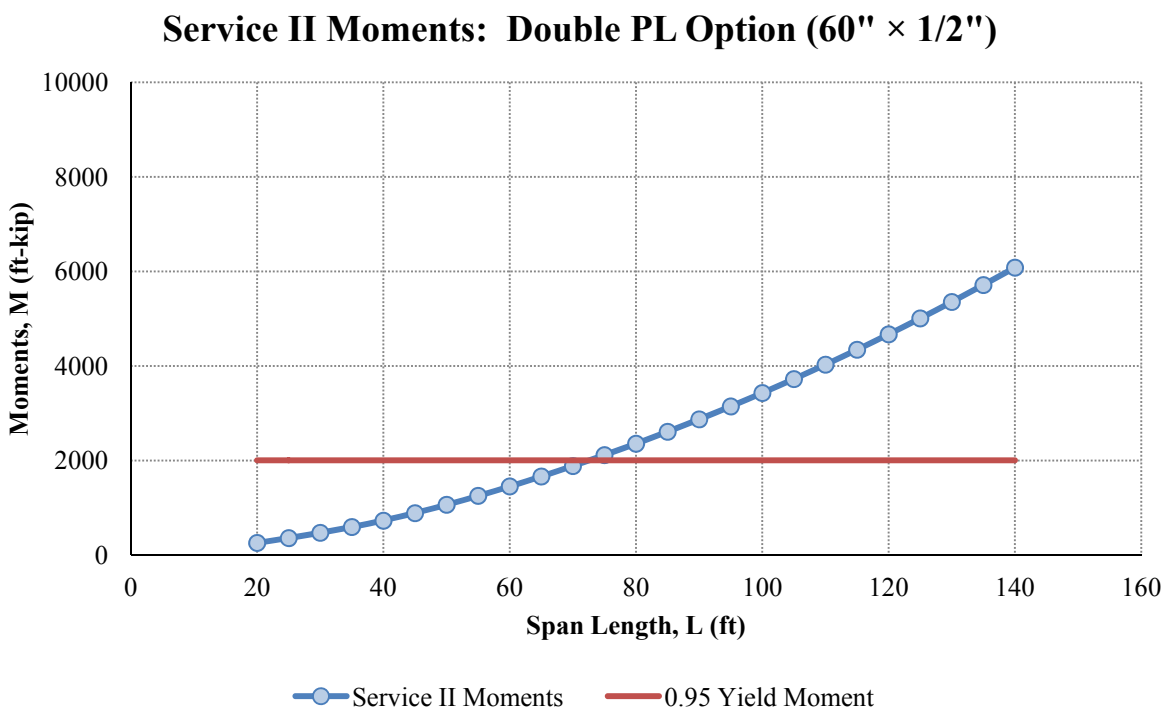
Service II Moments: Double PL Option (60" × 1/2")
Moments, M (ft-kip)
10000
8000
6000
4000
2000
0
0
20
40
60
80
100
120
140
160
Span Length, L (ft)
Service II Moments
0.95 Yield Moment

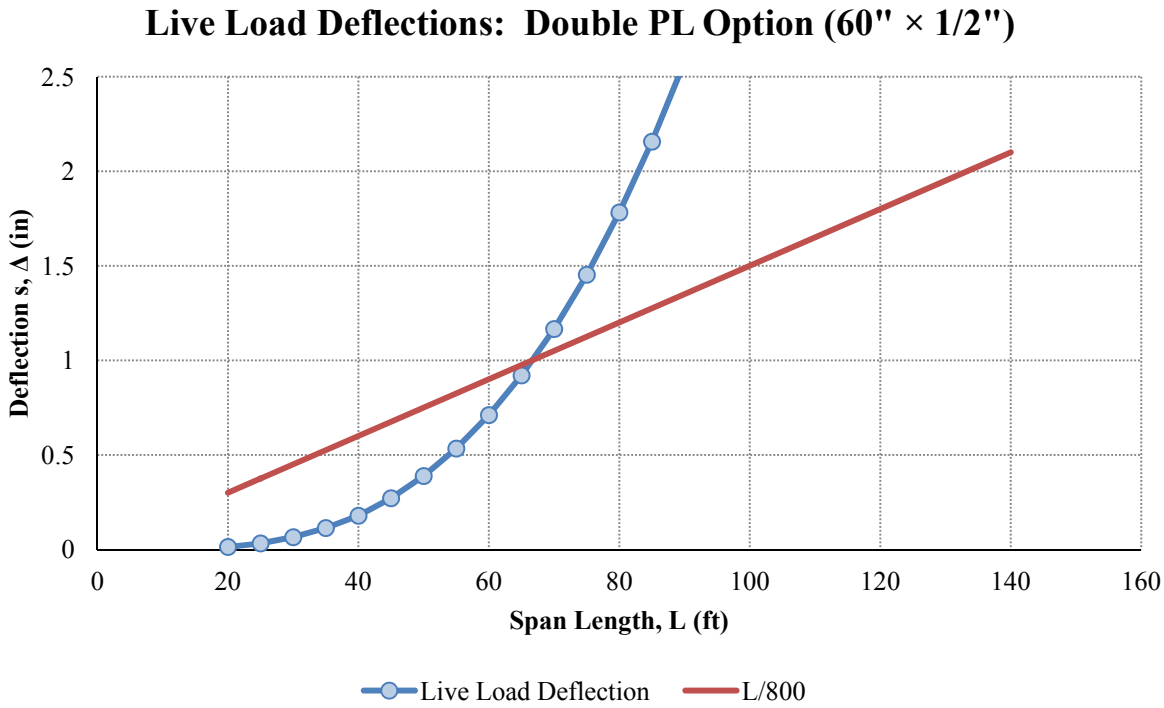
Live Load Deflections: Double PL Option (60" × 1/2")
Deflection s, Δ (in)
2.5
2
1.5
1
0.5
0
0
20
40
60
80
100
120
140
160
Span Length, L (ft)
Live Load Deflection
L/800

VITA

Gregory Kyle Michaelson received a Bachelor of Science degree from Bluefield State College in 2009 (where he was named co-valedictorian) and a Master of Science degree from West Virginia University in 2010, with an emphasis in structural engineering. He then began work towards his Doctor of Philosophy degree from West Virginia University in 2011. In that same year, he was named a recipient of the National Science Foundation's Graduate Research Fellowship (Grant No. DGE-1102689). His current research interests are focused in the area of structural engineering and include steel bridge design, nonlinear finite element modeling, structural stability, and experimental investigation of structural systems.